Dissertation

submitted to the
Combined Faculties for the Natural Sciences and for Mathematics
of the Ruperto-Carola University of Heidelberg, Germany
for the degree of
Doctor of Natural Sciences

presented by

Diplombiologe Mirko Singer
born im Mainz, Germany
Oral examination: 19.09.2017

Timed genome editing and sporozoite formation in *Plasmodium berghei*

Referees: Prof Dr. Michael Lanzer

Prof. Dr. Friedrich Frischknecht

... for Emma

and Paul...

Summary

Plasmodium species are unicellular eukaryotic parasites that are the causative agents of malaria. This disease places a high burden on most tropical countries due to the severity of its symptoms and high prevalence. The absence of sterile immunity under natural transmission conditions, rapidly evolving drug resistance and the lack of a protective vaccine intensify the problem. *Plasmodium* is a highly adapted intracellular parasite. *Plasmodium* sporozoites develop within oocysts in the mosquito midgut, enter the salivary glands and are injected into the skin of their mammalian host. Sporozoites reach the liver, develop intracellular within hepatocytes into merozoites and enter red blood cells. Multiplication of parasites in the blood causes the disease. If a mosquito takes a blood meal at this time, the parasites enter the midgut, causing an infection.

It has been shown in the past that parasites lacking genes required for liver stage development can be used as an experimental live-attenuated vaccine. Their arrest in the liver allows the host to launch a protective immune response, resulting in sterile protection from sporozoite challenge. Here I investigated if it is possible to exploit parts of the particular biology of *Plasmodium*, its haploid genome and the limitation of DNA repair to homologous recombination to generate a new generation of experimental vaccines. I generated parasites that express zinc finger nucleases causing a single well-timed double strand break within their own genome using stage specific promoters. This resulted in delayed death of the parasites as they failed to repair their split chromosome. I show that parasites arresting within the liver stage using this method can cause sterile protection from lethal sporozoite challenge. Additionally, rare breakthrough events resulting in blood stage infection were investigated. In these parasites I observed the genetic signature of DNA repair events by microhomology-mediated end joining with as little as four base pairs of homology.

The circumsporozoite protein (CSP) is the major surface protein of sporozoites, essential for their formation in the oocyst and despited extensive research its function at this stage is not understood. I used interdomain tagging with green fluorescent protein to study the function of the circumsporozoite protein (CSP). Using live cell microscopy of complete mosquito midguts, electron microscopy of midgut sections and analysis of protein extracts via western blotting I investigated the role of CSP during sporozoite formation. I could show that CSP undergoes previously unrecognized proteolytic processing at the C-terminus within the oocyst. Additionally my results suggest that extensive invagination of the plasma membrane has to occur prior to sporozoite formation and that

CSP plays a role in orchestration of these events. This work also highlighted the importance of a previously unappreciated membranous network, the labyrinthine structure, for sporozoite formation. In conclusion this part of my work focuses on sporozoite biology, on their formation in the oocyst and on how to block their development in the liver.

Zusammenfassung

Die Erreger der Malaria sind einzellige eukaryotische Parasiten vom Genus *Plasmodium*. Diese Krankheit betrifft die meisten tropischen Länder und verursacht eine hohe gesundheitliche und ökonomische Belastung. Das schnelle Auftreten von Resistenzen gegen Medikamente, die Fähigkeit des Parasiten Menschen wiederholt zu infizieren und das Fehlen eines verlässlichen Impfstoffes verstärken das Problem. Sporozoiten entwickeln sich innerhalb von Oozysten im Mitteldarm einer infizierten Stechmücke. Von dort gelangen sie in die Speicheldrüsen und werden bei einem Stich in die Haut gespuckt. Mit dem Blut begeben sie sich zur Leber und entwickeln sich innerhalb von Leberzellen zu Merozoiten. Diese gelangen in das Blut und vermehren sich innerhalb von Erythrozyten, dies führt zu den Symptomen der Malaria. Bei einer Blutmahlzeit werden die Parasiten mit aufgenommen und gelangen wieder in den Mitteldarm des Stechmücke.

Es konnte gezeigt werden, dass Parasiten denen essenzielle Gene für die Entwicklung des Leberstadiums fehlen als experimenteller Lebendimpfstoff genutzt werden können. Ihr Absterben in der Leber ermöglicht dem Wirt eine schützende Immunantwort aufzubauen die ihn komplett vor einer Infektion durch Sporozoiten schützt. In dieser Arbeit habe ich untersucht ob es möglich ist die biologischen Besonderheiten von *Plasmodium* auszunutzen um abgeschwächte Parasiten als experimentelle Impfstoffe herzustellen. Besonders sein haploides Genom und die Beschränkung der DNA-Reparatur auf homologe Rekombination machen ihn angreifbar. Ich habe Parasitenstämme hergestellt, die mit Hilfe von Stadium-spezifischen Promotoren zu einem gewünschten Zeitpunkt Zink Finger Nukleasen exprimieren. Ein einzelner so verursachter Doppelstrangbruch der Parasiten-DNA führt zu ihrem zeitverzögerten Absterben, da sie ihr zerschnittenes Chromosom nicht wieder reparieren können. Ich konnte zeigen, dass eine Immunisierung mit diesen Parasiten zu einem Impfschutz gegen Sporozoiten führt. Zusätzlich wurden selten vorkommende sogenannte Durchbruchinfektionen untersucht. In diesen Infektionen konnte ich anhand der genetische Signatur der Reparaturstelle die Existenz eines alternativen DNA-Reparaturweges nachweisen. Mikrohomologien von nur vier Basenpaaren weisen

darauf hin, dass *Plasmodium* zu der DNA-Reparaturmethode "microhomogy-mediated end joining" fähig ist.

Das "circumsporozoite protein" (CSP) ist das häufigste Oberflächenprotein der Sporozoiten. Es ist essentiell für die Bildung der Sporozoiten, doch seine Funktion in diesem Prozess ist trotz großer Anstrengungen noch nicht verstanden. Um seine Funktion zu untersuchen habe Ich Parasiten generiert bei denen zwischen den verschiedenen Proteindomänen von CSP das grüne fluoreszierende Protein eingefügt ist. Die Parasiten habe ich mit Lebendfluoreszenzmikroskopie infizierter Mitteldärme, Elektronenmikroskopie und mittels Western-Blotting untersucht. Ich konnte zeigen das CSP an seinem C-Terminus proteolytisch gespalten wird. Die Ergebnisse weisen außerdem darauf hin, dass einer erfolgreichen Sporozoitenbildung die vollständige Invagination der Plasmamembran vorrausgehen muss. CSP ist wichtig für die geordnete Abfolge dieser beiden Prozesse. Zusätzlich konnte ich zeigen, dass eine bisher vernachlässigtes Membrannetzwerk, die "labyrinthine structure", wichtig für die Bildung der Sporozoiten ist. Zusammenfassend beschäftigt sich diese Arbeit mit der Biologie der Sporozoiten, mit ihrer Entstehung in der Oozyste und damit, wie man ihre Weiterentwicklung in der Leber stoppen kann.

Contents

1 Introduction **1**

1.1 Plasmodium basics 1

1.1.1 Apicomplexa in the context of life 1

1.1.2 Phylogeny of Apicomplexa 3

1.1.3 *Plasmodium* life cycle 4

1.1.4 Malaria 8

1.1.5 Immunity 9

1.2 *Plasmodium* genetics 11

1.2.1 *Plasmodium* gene structure 12

1.2.2 *Plasmodium* DNA repair 13

1.2.3 Genetics in the context of the lifecycle 15

1.2.4 Genetics in the context of evolution 15

1.2.5 Generation of transgenic *Plasmodium* parasites 17

1.2.6 Tools used in *P. falciparum* genetics 20

1.3 Sporozoite biology 25

1.3.1 Sporozoite morphology 25

1.3.2 Sporogenesis 28

1.3.3 Gliding motility 30

1.3.4 The gliding motor model 31

1.3.5 Glycosylphosphatidylinositol-anchored proteins in Plasmodium . . 38

1.3.6 The circumsporozoite protein 39

2 Materials And Methods **47**

2.1 Materials 47

2.2 Methods . . . 52
2.2.1 Molecular biological methods . . . 52
2.2.2 Animal handling . . . 55
2.2.3 Injections . . . 55
2.2.4 Cervical dislocation . . . 55
2.2.5 Parasite handling . . . 56
2.2.6 Western blotting . . . 57
2.2.7 Fluorescence microscopy . . . 58
2.2.8 Electron microscopy . . . 59

3 Results **61**
3.1 Genetic manipulation of Plasmodium parasites . . . 61
3.1.1 Generation of basic transfection vectors . . . 61
3.1.2 Post transfection plasmid unfolding via Zinc finger nucleases in Plasmodium . . . 63
3.1.3 Attenuation by stage specific double stranded break using Zinc finger nucleases . . . 65
3.1.4 Self-excising selection marker through mosquito passage . . . 81
3.2 Visualization of proteins involved in gliding motility . . . 84
3.3 The role of the circumsporozoite protein on sporozoite formation . . . 85
3.3.1 Generation of CSP mutants . . . 86
3.3.2 Basic biology of CSP mutants . . . 89
3.3.3 Oocyst development of CSP mutants . . . 91
3.3.4 Processing of CSP . . . 122

4 Discussion **131**
4.1 Genetic manipulation of Plasmodium . . . 131
4.1.1 Plasmid unfolding . . . 131
4.1.2 Attenuation by double strand break . . . 132
4.1.3 Auto-recycling of selection marker during mosquito passage . . . 134
4.2 The circumsporozoite protein . . . 136
4.2.1 The processing of circumsporozoite protein within the oocyst . . . 137
4.2.2 Membrane dynamics during oocyst development . . . 145
4.2.3 The role of the circumsporozoite protein in salivary gland invasion 149
4.2.4 The circumsporozoite protein and gliding motility . . . 150

5 Appendix **195**

5.1 Species 195

5.2 Abbreviations 195

5.3 Primers 198

Chapter

1

Introduction

1.1 Plasmodium basics

1.1.1 Apicomplexa in the context of life

The most widely known members of the phylum Apicomplexa are the causative agents of malaria of genus *Plasmodium*. Apicomplexa are, together with ciliates and dinoflagellates, members of the Alveolata. Alveolates are defined by alveoli, flattened vesicles underlying the plasma membrane that are probably derived from the endoplasmatic reticulum (ER) [1]. The Alveolata are one of many members within the Chromalveolata, which itself are on of many within all Eukaryota (**Figure 1.1**).

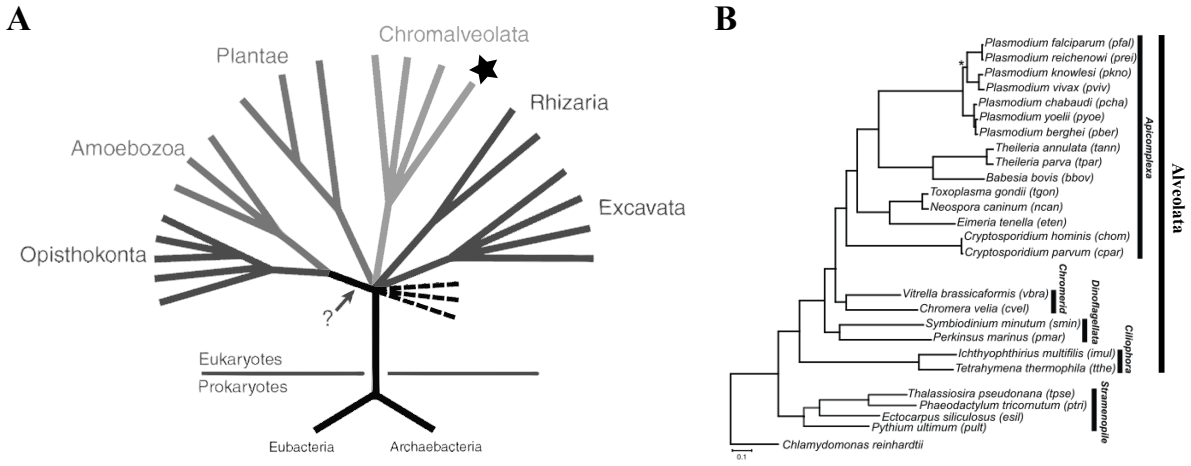

Figure 1.1: Phylogenetic placement of *Plasmodium*.
A Tree of life, showing the placement of Alveolata (indicated by the star) in the grant context of eukaryotic life. Figure modified and simplified from [2] **B** Phylogenetic placement of the Apicomplexa within the alveolates including outgroups. Figure slightly adjusted from [3]

All Apicomplexa employ a parasitic lifestyle, with the exception of the recently discovered *Chromeria velia*, which is the closest free-living ancestor of all parasitic Api-

complexa. Apicomplexa are estimated to be the most underdescribed group, with about 6000 described species and an estimated number of 1,2 -10 million [4]. Some scientists estimate that based on number of parasite species of well-studied hosts, most vertebrate and invertebrate species have their own Apicomplexan parasite [5].

As Apicomplexa are highly adapted to their hosts, they show a broad range of specializations and cellular adaptations. Diversification of Apicomplexa mainly occurs as they coevolve with their respective host species. The defining features of Apicomplexa are observable at least once over the course of their life cycle. Some have been lost in some groups. The typical Apicomplexan structures are present in the extracellular motile and invasive stages, whereas intracellular stages are highly diverse and might lack most Apicomplexan features.

Apicomplexa are unicellular organism with are highly polarized in the extracellular stage. The apical complex that gave rise to their name is a structure that is defined by polar rings and a conoid. The conoid is made of specialized microtubules whereas the apical polar rings function as the microtuble organizing center for subpellicular microtubules [6]. Specialized secretory vesicles are small micronemes and sack like rhoptries that are both apically secreted and most likely evolved from the endocytic pathway [7]. The inner membrane complex (IMC) are the alveoli of Apicomplexa and are underlined by the subpellicular network (SPN) and the subpellicular microtubules. All together give the extracellular stages their structure, shape and rigidity and their formation is involved in the final steps of cell division [8, 9]. The apicoplast, a secondary endosymbiotic organelle derived from a red algae is also present in all Apicomplexa except *Cryptosporidium* [10].

Most Apicomplexa show a relative high degree of host specificity, and many of them show a very long coevolution with their respective host species. This generally leads to a relatively low reproductive cost for the host species.

The origin of Apicomplexa was most likely a free-living single celled organism harboring a chloroplast. This was acquired by secondary endosymbiosis of a red algae. In the prototype-Apicomplexa *Chromeria velia* living today this chloroplast is still photosynthetically active [3]. All other Apicomplexa have reduced this organelle to the photosynthetic inactive apicoplast which is surrounded by four membranes or have even completely lost it [11].

It is assumed that ancestral Apicomplexa made a stepwise transition from a photosynthetic active free living organism to an ectoparasitic livestyle as the closed relatives Colpodellida employ today. This requires a polarized cell that performs both secretion

and phagocytosis at the apical end. The transition from transient interaction to permanent attachment to the host cell as in *Cryptosporidium* was followed by complete invasion. Coevolution with their hosts led to Apicomplexa following their hosts from marine to terrestric and limnic environments [12].

1.1.2 Phylogeny of Apicomplexa

Apicomplexa can be divided into three groups, gregarines, coccidians and Hematozoa with cryptosporidia being recently included into gregarines [13–15]. Gregarines are the most understudied group as they mainly parasitize annelids, atropods and molluscs. Some gregarines can reach sizes exceeding 1 mm, as a single cell.

Coccidia and cryptosporida are mainly parasites of vertebrates, and are often found in the digestive tract. They develop sporozoites within a stable oocyst wall within secondary cysts [14]. The best studied species are *Toxoplasma gondii*, *Cryptosporidium* species (*spec.*) and *Eimeria spec.*. Most coccidians parasitize only their respective host species and are transmitted via cysts. *T. gondii* is an expection to this rule as it can infect any nucleated cell while being restricted to members of the genus *Felidae* as its final host.

Haemosporidia and piroplasmorida belonging to the group Haematozoa alternate between the arthropod host and their vertebrate host. Haemosporidia are transmitted by dipteran hosts and reproduce asexually within erythrocytes of the vertebrate host preceded by an exo-erythrocytic reproduction cycle. Piroplasmorida are transmitted by ticks of the order Ixodidae and reproduce within circulatory cells. The best studied species are *Plasmodium*, *Theileria* and *Babesia*. Within Haemosporidia, previous phylogenetics used mitochondrial DNA to solve relationships between different species of *Plasmodium* implying multiple back and forth host switches. Recent reclassification using a multi gene approach gave rise to a more likely phylogeny with limited host switches [16]. It now seems likely that all members of the genus *Plasmodium* and *Hepatocystis* which is nested within *Plasmodium* share a common ancestor that is capable of blood schizogony. The rodent parasites *Plasmodium yoelii* and *Plasmodium berghei* group closely with the human parasites *P. vivax* and the closely related *P. knowlesi* whereas the recently sequenced parasites *P. ovale* and *P. malaria* are more distantly related and the laveranian parasites *P. falciparum* and *P. reichenowi* represent the outsiders of *Plasmodium* species. Recent sequencing of the whole laveranian subgenus revealed that *P. falciparum* separated from *P. praefalciparum*, which is infecting gorillas around

50.000 years ago with a starting population of *P. falciparum* which was not a single parasite [17]. The single parasite origin has been previously suggested due to imprints of a bottleneck into the *P. falciparum* genome, which is now attributed to an even more recent bottleneck around 5.000 years linked to the expansion of human agriculture [17]. These closed comparison between species genomes and host species indicate that the strongest determiner of host specificity is the capability for species specific red blood cell (RBC) invasion.

1.1.3 *Plasmodium* life cycle

In the cause of their life cycle, *Plasmodium* parasites infecting humans all switch between their insect and mammalian host (**Figure 1.2**). Their life cycle is almost identical with Plasmodium species infecting rodents, whereas the life cycle of Plasmodium species infecting bats and birds can be more diverse concerning life cycle stages and insect vectors.

Starting with the blood meal of an *Anopheles* mosquito, the insect takes up blood of the infected human. Of the parasites in the blood, only gametocytes are able to survive within the mosquito. Gametocytes are the dormant gamonts of both sexes that circulate in the blood within RBCs, residing within a parasite derived parasitophorous vacuole (PV). Gametocytes sense the drop in temperature, change in pH and the presence of xanturenic acid once ingested by the mosquito. This leads to an activation of mature gametocytes marked with a sharp increase of intracellular calcium only 10 seconds after external conditions change [18]. Male gametocytes undergo three nuclear divisions followed by egress of eight microgametes in a process termed exflagellation. At the same time, female gametocytes egress from their RBC and mature into female macrogametes. In both cases egress is initiated by secretion of the osmiophilic bodies which subsequently leads to the lysis of the parasitophorous vacuole membrane (PVM) and the RBC plasma membrane (PM) [19, 20]. About 10 minutes after activation, microgametes move within the blood meal utilizing flagellar motiliy and fuse with a macrogamete, forming a zygote [21].

The freshly formed zygote, after fusion of the haploid gametes, is the only stage of *Plasmodium* that is diploid. It directly undergoes meiosis, resulting in tetraploidity [22]. Within the next 20 hours, the zygote transforms into a motile ookinete, which traverses the periotrophic matrix of the mosquito midgut. Once in contact with the microvilli of the midgut epithelia, ookinetes traverse midgut cells resulting in their apoptosis to

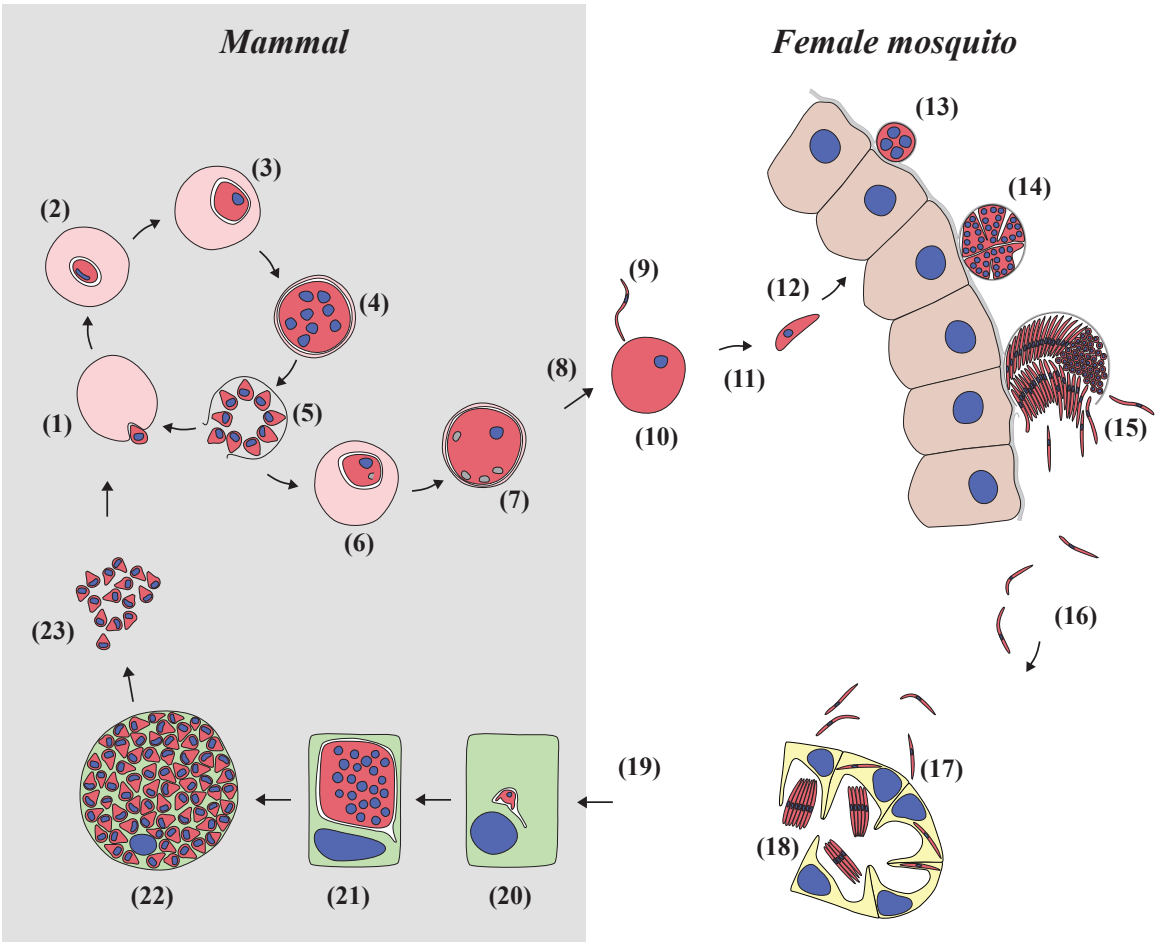

Figure 1.2: The lifecycle of *Plasmodium*.
The life cycle of mammalian *Plasmodium* parasites shown as it occurs in *P. berghei*. Parasites are shown in **red**, DNA in **blue**, RBCs in **light red**, mosquito midgut epithelia in **brown**, acinus cells of the salivary gland in **yellow**, hepatocytes in **green**. Free merozoites **(1)** bind and rapidly invade RBCs. Here they develop within the parasitophorous vacuole into the ring stage **(2)**, trophozoite stage **(3)**, schizont stage **(4)**, forming a segmenter **(5)** from which merozoites egress. These reinvade RBCs, repeating the cycle or develop into gametocytes **(6)** **(7)**. If taken up into the mosquito midgut, gametocytes egress and form male and female gametes **(8)** (not shown), male gametes **(9)** search for and fuse with female gametes **(10)**, forming a zygote **(11)** (not shown). This zygote transform into the motile ookinete **(12)**, which traverses the midgut epithelium and starts to form an oocyst **(13)** below the basal lamina. The developing oocysts grow in size **(14)**, and divide into hundreds of sporozoites during sporogony **(15)**. These midgut sporozoites egress the oocyst **(16)**, are passively transported with the mosquito hemolymph **(17)** and subsequently invade the salivary gland **(18)**. Here they rest in stacks within the salivary cavity after a transient intracellular phase **(19)** until they are injected into the skin of the mammal **(20)** (not shown). From here sporozoite enter capillaries, are passively transported into the liver, where they egress and invade hepatocytes after cell traversal. Within hepatocytes they develop from early liver stage **(21)** to liver schizont **(22)**, resulting in formation of merosomes **(23)** that are released into the bloodstream. Once the exoerythrocytic merozoites **(24)** are released, they close the life cycle with RBC invasion **(1)**.

finally reach the basal lamina, where they start to round up and begin to transform into an oocyst [23].

The oocyst slowly starts to grow over the next ten days, absorbing nutrients that are released from the freshly digested blood meal [24]. In the beginning, the oocyst forms an oocyst wall which is composed of a parasite derived inner layer and parts of the basal lamina of the mosquito. The growing oocyst undergoes mitotic divisions and generates membranes mainly in the form of endopasmatic reticulum (ER). Oocysts generally develop asynchronous in size and in developmental stage and some never successfully complete their development. Around 10 days after the blood meal the PM of the oocyst starts to separate from the oocyst wall and invaginates, resulting in a vast increase in surface area of the plasma membrane [25]. The nuclei, which are much smaller now, start to accumulate near the PM. Sporozoite formation is associated with a second order of invagination of the PM and coincides with the formation of the Golgi-derived flattened vesicles, the inner membrane complex (IMC), the underlying subpellicular microtubules and the single prerhoptry of every sporozoite [26, 27].

Sporozoites are fully formed within the oocyst and are surrounded by the plasma membrane and the two membranes of the IMC that is underlined by the SPN. Subpellicular microtubules of mature sporozoites originate at the apical polar ring and extend slightly behind the nucleus. Apical organelles are numerous micronemes and several rhoptries. If an oocyst is fully matured, sporozoites will eventually egress in a process that is not yet fully understood but does not require active gliding motility [28, 29]. Subsequently, sporozoites are passively transported within the mosquito hemolymph until they reach the salivary glands which they invade. Salivary gland invasion in detail has only been studied in *P. gallinaceum* by EM, but most likely involves an initial attachment step, basal lamina traversal, acinus cell invasion with the formation of a parasitophorous vacuole [30, 31]. Subsequently the vacuole is lysed and sporozoites egress with the host cell PM surrounding them. This membrane is ultimately lost and sporozoites accumulate into "stack-like" structures within the salivary gland lumen.

During a blood meal of the mosquito, sporozoites are released into the skin with the saliva during probing [32]. Once in the skin, sporozoites initiate rapid gliding motility in between cells and cell traversal [33–35]. While some sporozoites remain in the skin or end up in the lymphatics, many actively invade capillaries. With the blood flow they reach the liver, where they exit the blood via traversal of a liver resident Kupffer cell or an edothelial cell [36–39]. After cell traversal, they ultimately invade a suitable hepatocyte

forming a parasitophorous vacuole (PV) [40, 41].

Within the hepatocyte, sporozoites round up losing apical polarity and start to grow. In *P. vivax* and *P. ovale*, some of the invaded sporozoites arrest their development after invasion, forming a hypnozoite [42]. This hypnozoite can reactivate under conditions that are not well understood, initiating a new infection years after the infective bite. Liver stages that develop rapidly grow in size and ultimately give rise to thousands of liver stage derived merozoites. After PVM rupture, these merozoites reside within the host cell cytoplasm [43–45]. The host cell now rounds up forming a merosome that, in rodent species, leaves the liver intact and bursts during lung passage, releasing the enclosed merozoites [46].

Free merozoites immediately bind to and invade RBCs. Depending on the species, *Plasmodium* does or does not show a preference for reticulocyte or normocyte invasion [47]. Directly after invasion, merozoites reside as a ring stage within the PVM, develop into the trophozoite stage and subsequently the schizont stage that releases merozoites again. This blood stage replication cycle takes between one day in *Plasmodium* species infecting rodents and four days in *P. malaria* and is normally more or less synchronized (with the exception of *P. falciparum*) with the circadian rhythm of the host. During the blood stage cycle, *Plasmodium* parasites reach the highest biomass and numbers, up to half a kilogram in a human [48]. As soon as blood stage parasites reach a critical mass, the host experiences the symptoms of malaria (see **Malaria**), thus ending the asymptomatic phase of the infection. The onset of symptoms normally correlates with the phase the parasite is undetectable by blood smear, the prepatency.

Depending on external stress factors like parasite density, merozoites can be predisposed to develop into gametocytes [49]. In a male or female gametocyte, once mature, the parasite pauses development and awaits uptake by the mosquito vector. If this occurs, all asexually replicating and immature parasite stages die and mature gametocytes start the life cycle again.

Plasmodium organelles

Apicomplexan parasites possess several specialized organelles. During the *Plasmodium* lifecycle the parasite alternates between very polarized and organized extracellular stages and more unpolarized intracellular stages [9, 50]. Extracellular stages are generally surrounded by the IMC, an underlying SPN and apical microtubules that originate at the apical polar ring. Secretory organelles that are solely apically secreted are micronemes

and rhoptries, whereas dense granules are unclear [51]. Other secretory organelles like exonemes in merozoites and osmiophilic bodies in gametocytes have been described for single stages of the life cycle, indicating that secretion is highly organized and perfectly suited for the individual task required.

Generally micronemal proteins are involved in gliding motility and parasite attachment, rhoptry proteins are mainly involved in invasion and dense granule proteins are involved in PVM maintenance [52, 53]. Ookinetes lack rhoptries as well as invasive capacities, whereas sporozoites lack classical dense granules despite forming an extended PVM in the hepatocyte [54]. It is expected that sporozoite micronemes are comprised of several subsets, as this is also assumed for micronemes of *T. gondii* [55].

All Apicomplexa (with the exception of *Cryptosporidium*) possess a secondary endosymbiont termed apicoplast which is derived from a red algae [56, 57]. This organelle is enclosed by four membranes, contains its own circular DNA and possess four major metabolic pathways: isoprentenyl diposphate synthesis, fatty acid biosynthesis, iron sulphur complexes and partial synthesis of haem [58]. Plasmodium species also own a mitochondrion, which has the smallest known mitochondrial genome with only three encoded proteins [59, 60]. In the ookinete stage, *Plasmodium* also contains the crystalloid body, a structure that is reminiscent of virus-like particles found in other Apicomplexa [61]. While the function is not clear, several mutants lacking the crystalloid body have been shown to all arrest during oocyst development [62].

1.1.4 Malaria

Malaria is the disease caused by *Plasmodium* parasites in their human hosts. More than a billion people are at risk of infection, with around 200 million cases occurring annually and around 430.000 deaths [63]. The most severe form of malaria, malaria tropica is caused by *P. falciparum*, followed by *P. vivax*. *P. ovale* and *P. malaria* cause more long lasting chronic infections. *P. knowlesi* has gained recent interest as it is originally a *Plasmodium* species infecting macaque monkeys in Asia and has recently caused more human cases [64]. While the liver stage is asymptomatic, during the replication of the parasites in the blood (**Figure 1.2**) infected individuals suffer from fever. Fever chills occur regularly in species where merozoite egress is synchronized, every two days in *P. vivax* and *P. ovale*, every three days in *P. malaria* and irregular in *P. falciparum*. In severe malaria, which mainly occurs in young children and malaria naive adults, cytoadhesion can lead to coma and death which is caused by brain swelling (cerebral malaria)

or organ failure [65]. Prolonged infections can cause splenomegaly, hepatomegaly and severe anemia [66].

1.1.5 Immunity

In the field under natural conditions, humans develop a semi-immunity against *Plasmodium* over the time of several years. The higher the transmission rate the faster semi-immunity is aquired [67]. This protection is mainly mediated by antibodies [68]. However, sterile immunity is never achieved and the number of malaria episodes does not decrease with age, only disease severity. In brief, the vast diversity of variant surface antigens is believed to be responsible for the life-long struggle with blood stage parasites. Additionally, the immune-suppressing properties of blood stage parasites against liver stage immunity, accompanied with functionally exhausted T-cells is most likely the primary reason for this phenomenon [69–75].

Studies on *Plasmodium* immunity in humans which includes direct manipulation of the host or parasite is very limited due to ethical reasons, thus a lot of studies are performed in rodents. Immunity against blood stages is possible to archive in mice using blood stage attenuated strains, even cross-species protection has been achieved several times [76–78]. The number of strains where this has been possible and the fact that this list includes parasites lacking metabolic enzymes suggests that these strains do not all lack regulation of the host immune system but rather general fitness. However, it is not clear if these findings are transferable to humans. So far studies on blood stage attenuated parasites in human models have have shown unclear results, and even results in different mouse strains are highly variable [79–81].

Liver stage attenuated parasites

It was discovered decades ago that immunisation of γ-radiated sporozoites or infected mosquitoes resulted in protection from sporozoite challenge but not blood stage challenge [82, 83]. In contrast, immunisation with heat killed sporozoites resulted in no protection [84]. Sporozoites that are γ-radiated with the right dose are still motile, invade hepatocytes but stop development in early liver stage [85]. It is assumed that this is mainly due to double strand breaks (DSB) and results in failure to replicate the genome that has been shown to be the lethal damage of γ-radiation in other systems [86]. The direct measurement of damage caused by γ-radiation in sporozoites has not been performed. DSB rate relative to irradiation dose and genome size can be measured fairly precise.

Using data from other systems, the DSB rate after protective irradiation can be estimated to be an average of 17 per sporozoite for 150 Gy [87, 88]. However, radiation can also damage mRNA, and many mRNAs are stored in sporozoites to be expressed during early liver stage development [89] and impact on their expression levels has not directly been tested.

Repeated imunisation with radiation attenuated sporozoites (RAS) has been shown to protect both humans and mice from wild type (WT) challenge in a CD8 T-cell dependent fashion [82, 90–92]. These liver resident T-cells recognize infected hepatocytes via specific parasite peptides presented on the major histocompatibility complex (MHC) class I [93–95]. While these CD8 T-cells are also primed in a natural infection, the following blood stage infection blocks them to mature into liver resident CD8 T-cells [69–71].

It has also been shown that protective immunity can be achieved by immunizing with WT sporozoites under drug cover [96, 97]. This works with drugs targeting the developing liver stages directly like primaquine and pyrimethamine, targeting the formation of infective merozoites by blocking apicoplast division with azitromycin and clindamycin or by targeting only blood stages with chloroquine or piperaquine [98–101].

This implies that the developmental block of parasites during liver stage development is not required for protective immunity and priming of CD8 T-cells can occur during normal development. Liver stage numbers are reduced about 50% during liver stage development in vitro and even stronger in vivo [54]. Parasites are living a risky life as they seem to utilize nutrients from the hepatocyte via the autophagy pathway and develop better during host cell starvation but be eliminated via autophagy and possibly actin [54, 102, 103]. It has not been shown if T-cell priming occurs only from hepatocytes which manage to eliminate their respective liver stage or commit to apoptosis [104], a process that is later blocked by the developing parasite [105]. However, during WT challenge of protected animals every single developing liver stage is eliminated, suggesting that every single infected hepatocyte presents sufficient parasites peptides via MHC class I in order to be detected and eliminated. While priming of CD8 T-cells still occured in mice that lack the TAP-mediated processing of antigens, these mice are not protected against sporozoite challenge as CD8 T-cells are not reactivated [106].

CD8 positive T-cells specific for the major sporozoite protein, the circumsporozoite protein (CSP) (see **The circumsporozoite protein**) and the main micronemal protein, the thrombospondin related anonymous protein (TRAP) (see **Thrombospondin**

related anonymous protein family) are protective against challenge with WT parasites [107]. However, other proteins are also involved in protection [108, 109]. In the related parasite *T. gondii* MHC class I presented peptides have been sequenced and show that a multitude of proteins are presented from the host cell, with a slight enrichment for dense granules (DG) and cytoplasmic proteins [110].

Genetically attenuated parasites (GAP) have been generated with the deletion of genes that are essential in the liver stage but result in no growth arrest during the blood stage and the mosquito stage. The first GAPs resulted from the deletion of genes localized to the PVM [111–113]. Later, an early master regulator of early liver stage genes [114] as well as genes essential for later liver stage development were identified [115, 116].

Comparing the different modes of attenuation shows that late attenuated parasites generally result in better protection from WT challenge than immunization with early arresting parasites [117–119]. It is expected that this is due to the increased amount of and increased breath of immune response, but this has not formally been shown. Targets of CD8 T cells that are only expressed in late liver stages are not identified yet. Simply the increased time window an individual immunized with a late-attenuated liver stage has to eliminate liver stages could explain the higher protectivity.

1.2 *Plasmodium* genetics

Plasmodium parasites are, as all Apicomplexa, haploid organisms throughout the majority of the life cycle. This might be beneficial to allow for smaller cell size, help with schizogony and monoallelic expression of variant surface antigens, but the only trait that is common to all Apicomplexa is the strong selective pressure to co-adapt with the respective host [120, 121]. Apicomplexa harboring a mitochondrion with the smallest know mitochondrial genome that is linear and encodes only three genes of less than 6 kilo bases (KB) [122] and an apicoplast derived from the secondary endosymbiosis of a red algae with a circular genome of around 35 KB [123]. The nuclear genome of *Plasmodium* is around 23 mega bases (MB) in *P. falciparum*, up to 30 MB in *P. vivax*, 33,5 MB in *P. malaria* and *P. ovale*, about 24 MB in *P. gallinaceum* and around 20 MB in *P. berghei* [124–128]. Within the *P. falciparum* genome, roughly over 50% are protein coding, with a mean gene length of 2,3 KB and about half of these containing introns.

Unlike with other Apicomplexa, the genomes of different *Plasmodium* species are

quite conserved and the central parts of the chromosomes with the syntheny between different species representing their phylogenetic relationship [129]. Sequences in the subtelomeric regions are highly diverse within different *Plasmodium* species and encode most of the species specific genes, many of them part of big multi gene families expressed during the blood stage [128]. *Plasmodium* species also differ in the AT content of the genome, which is highest in *P. falciparum* reaching 80% and lowest in *P. vivax* with about 50%. It has been proposed that base excision repair (BER) was lost in the *Laverania* [130] resulting in a shift in AT content. With the recent realization that the AT content of the avian species *P. relictum* and *P. gallinaceum* is equally high, a simple loss of function would not explain the higher AT content of other mammalian *Plasmodium* species [127]. As in other extreme AT biased genomes, intergenic regions of *P. falciparum* are more AT rich than coding regions [131]. Nevertheless, the impact of the AT content in codon bias is strong, favoring AT rich codons in most *Plasmodium* species and also shifting the amino acid usage [132].

1.2.1 *Plasmodium* gene structure

In *Plasmodium* genes, many features are not clearly understood. Experimental evidence has shown that many genes are controlled in expression by less than 1000 bp of their 5' upstream region. However this is not necessarily true for all genes, and genes showing strong expression and / or tight regulation of expression tend to have very long 5' untranslated regions. Is has been discussed that cis-regulatory elements, small DNA motifs of 6 -10 bp are enriched in specific subsets of genes and many or these are bound by an family of transcription factors normally found in plants, the Apicomplexan apetala2 transcription factors (ApiAP2) [133, 134]. Transcription start sites (TSS) are poorly mapped in *Plasmodium* species, but some have recently been sequenced in blood stages [135, 136]. The following Kozak like consensus sequence preceding the start codon is strongly influenced by the codon bias in *Plasmodium* and reads 'taaAAA**ATG**Aan' [137], but there are plenty of exceptions. The presence of introns is rare but frequently occurs in gene families with conserved regions like the Plasmodium interspersed repeat genes (*pir*) gene family [17] and has been implicated in gene regulation in the *var* gene family [138].

1.2.2 *Plasmodium* DNA repair

DNA repair in *Plasmodium* has a direct impact on *Plasmodium* evolution as well as on its genetic accessibility. In almost all eukaryotic cells, DNA repair is extremely important. Bigger genomes generally require more efficient DNA repair and also lower mutation rates caused by DNA replication. The newly sequenced genomes of *P. relictum* and *P. gallinaceum* are the only Plasmodium genomes so far that contain a copy of Ku70, but lack Ku80. Also they contain retrotranspons in their genomes, and it is quite likely that the DNA damage resulting from active retrotransposons permitted their existence in other *Plasmodium* species [127].

In most eukaryotic cells, a DNA DSB is repaired with homologous repair (HR) or non-homologous end joining (NHEJ). The favored DNA repair pathway is vastly different in different species, cell types and cell cycle stages. Some DNA repair occurs with microhomology-mediated end joining (MMEJ), which seems to be universally present in all eukaryotic cells as a low level backup pathway that is only activated if other repair pathways fail [139]. In most experimental settings, DNA repair pathways are identified by the characteristic of the repair products observed and not directly observed "in action" [140].

Additionally to DSBs, it is possible that single base pairs are miss-matched or bases are chemically modified. There are base excision repair (BER), nucleotide excision repair (NER) and DNA mismatch repair (MMR). In BER small base lesions are removed resulting in a single strand break and between one and 10 nucleotides are synthesized. During NER a bulky helix distorting base lesion results in a short strand of single stranded DNA is being removed and then repaired by DNA polymerase and DNA ligase. During MMR the cell normally identifies the newly synthesized strand which is specifically repaired. This strand is nicked, processed by an exonuclease and refilled by DNA polymerase [141, 142].

Homologous recombination

HR is a DNA repair pathway that allows for the error free repair of a DSB. It requires a second copy of the damaged region that is used as a template during the repair process, which can be the other allele in diploid organisms or a second copy of the genome. During this repair process crossover between the broken DNA strand and the template can occur.

Plasmodium possesses a fully functioning HR machinery, and all repair products

observed during blood stage growth so far result from HR with a few notable exceptions noted below. Repair of DSB from HR can not be identified by the characteristics of the repair product unless the template differs from the repaired DNA strand, as repair products are error free.

The DSB is recognized by the MRX complex, composed of Mre11, Rad50 and Xrs2 [143]. This initiates DNA resection in 5' to 3' orientation, resulting in 3' overhangs. The initial resection is the rate limiting step of the reaction and also occurs during MMEJ. in HR, this process is followed by extensive resection, formation of a Rad51 decorated DNA single strand and subsequent strand invasion, leading to activity of polymerase δ [144].

Non homologous end joining

NHEJ is a fast DSB repair pathway that is the major repair pathway in most mammalian cells as well as in *T. gondii* [145]. It does not require any homology as a template and can, in the case of multiple DSBs, result in the joining of the wrong ends. After the DSB the ends are stabilized by a heterodimer of Ku70 / Ku80 and a few bases can be recessed or gaps are filled by specialized polymerases. Following this process DNA Ligase IV ligates the DSB. In *Plasmodium* species, which lacks all known genes involved in NHEJ, this process has not been observed [146].

Microhomology-mediated end joining

Considered as an ancient backup mechanism, MMEJ is normally observed if other DSB repair pathways are inhibited [147, 148]. During MMEJ, both sides of the DSB undergo 5 prime recession until a microhomology between both sides is exposed. These pair, excess bases are cleaved and the DSB is joined by DNA ligase III. Recently the requirement for polymerase θ activity in joining the microhomology overhang has been shown [149]. MMEJ has been reconstituted *in vitro* using only six proteins [150]. Of these, three are present in *P. falciparum* [144]. In *P. falciparum*, following DSB induces by a endonuclease, DNA repair was shown at a very low level and termed alternative homologous end joining. Repair products included insertions of several bases and microhomology of three bases within the endonuclease recognition site [151]. In *T. cruzi*, MMEJ repair products are the main DNA repair products observed and micro-homologies flanking DSB sites can be used to predict repair products of targeted DSBs [152].

1.2.3 Genetics in the context of the lifecycle

With their small and condensed haploid genome, *Plasmodium* species can replicate extremely fast, allowing for a fast mutation rate to outcompete the evolution of their respective host. The haploid nature of their genome further promotes this, making *Plasmodium* exceptionally well suited to switch traits, both on a epigenetic and genetic level. *Plasmodium* performs asexual division in the liver and blood via schizogony and in the mosquito via sporogony, which is a specialized form of schizogony. These involve multiple rounds of closed nuclear divisions that are considered to be unsynchronized [153], followed by a synchronized nuclear division coinciding with cytokinesis [9, 50, 154]. The ookinete of *Plasmodium* is tetraploid as meiosis without cytokinesis is followed by the formation of the oocyst [22, 155]. If individual nuclei with the oocyst are tetraploid, diploid or haploid is not known, but it is known that haploid sporozoites generated within the oocyst can have the genotype of either gamete or are a crossover-product of the two [155, 156]. This needs to be considered if sporozoites of fresh genetic crosses are characterized directly, as individual sporozoites can lack a gene, but still possess the protein due to carry over of protein and mRNA from the oocyst.

1.2.4 Genetics in the context of evolution

In its recent evolution, *Plasmodium* species have reacted to various evolutionary pressures. It is assumed that the ancestral host of *Plasmodium* is the insect, as this is the place where sexual reproduction takes place within the midgut. The life cycle was probably more similar to that of other Apicomplexan parasites having only one host today, like *Eimeria*, *Cryptosporidium* or *Gregarina*. To avoid the immune response in the secondary amniote host, *Plasmodium* species changed host cells to the immune privileged liver and the denucleated erythrocyte in mammals that does not express MHC class I.

The main adaptation to sustain prolonged blood stages in their respective hosts are the subtelomeric species specific multi gene families. The multigene familiy that occurs in varying copy numbers in all *P. falciparum* species and is the least understood, is the pir family (termed *bir, yir, vir, cir* in *P. berghei, P yoelii, P. vivax and P. chabaudi* respectively, and *rifin* and *stevor* in *P. falciparum* [128, 157, 158]. Recently the multi families *fal-l* and *fal-m* have been described in *P. malariae*, which seem to occur and evolve in pairs and potentially form heterodimers on the RBC surface [126]. *P. falciparum* also posesses the *var* gene family, which is expressed in a mono allelic fashion during the blood stage [138]. All contain regions with high homology that are suggested

to be involved in gene duplication events. Also, in *P. falciparum* the var genes found in the field are expected to be extremely numerous due to recombination events in contrast to the 60 var genes found in any parasite strain [159]. Most of these processes are expected to occur during meiosis resulting from crossover events powered by homologous recombination. It has been suggested that in case of a double infection and sufficient strain crossing within the mosquito, individual sporozoites have a high genetic diversity [160]. In the case of hypnozoite formation, this would allow the developing hypnozoite to develop a new infection as it is sufficiently different from those parasites that developed directly into blood stages.

One additional very recent evolutionary process, the development of drug resistance, has been extensively studied in *P. falciparum*. While the parasite has the advantage that parasite numbers are huge during the blood stage (up to 10^{12}), additional gene duplication events are frequently observed preceding the occurrence of resistance mutations [161, 162]. These have been observed to be flanked by long AT repeats that are found in the intergenic regions of *P. falciparum*. It is assumed that the repair of a random DSB within such an AT repeat can result in the duplication of all genetic information in between two of those AT repeats via homologous recombination. This duplicated set of genes can now further increase in copy number via homologous recombination following a random DSB anywhere within the duplication. This can lead to duplication events up to 30 copies and up to 100 KB in length. This increases the chance of a protective mutation to occur dramatically while at the same time allowing for mutations to occur that interfere with normal gene function. At the same time, an increased amount of the target protein can already significantly increase resistance to the drug. After protective mutations are manifested, the inverse process will slowly reduce copy numbers back to one or two, reducing the translational costs for the parasite. These events also gave some insights to genes that result in a dominant negative phenotypes. If resistant selection is performed in the lab, some neighboring genes are always excluded from gene duplication events. These are considered to be deleterious for the parasite if expressed at a higher level.

Another feature of the genomes of *Plasmodium* parasites is the high occurrence of variable number of tandem repeats (VNTR) within coding regions [163, 164]. These are generally highly conserved internally and also code for amino acid repeats but can vary in repeat length. They tend to be different within the same gene of different species, both on a copy number level and length and sequence of the repeat itself. This

can be exemplary observed in the repeat region of the circumsporozoite protein [163] (**Figure 1.6**), but is abundantly observed in many genes.

1.2.5 Generation of transgenic *Plasmodium* parasites

Transfection of *Plasmodium* parasites can be performed with circular or linear DNA. The transfection efficiency is low in *P. berghei* [165] and even far lower in *P. falciparum* [166–168]. Additionally, in *P. falciparum*, intracellular parasites or uninfected RBCs are transfected, requiring the DNA uptake by the parasite post-transfection through unknown mechanisms. There is evidence that only circular DNA survives this process [165]. Transfection of free *P. falciparum* merozoites is also possible, but technically challenging [169]. This also allows for transfection of linear DNA. Recently, integration efficiency has been greatly improved in *P. falciparum* using the clustered regularly interspaced short palindromic repeats (CRISPR) and the CRISPR associated protein 9 (Cas9) (see **CRISPR/Cas9**) transfection system [170, 171]. This has also improved transfection in virtually every other system such as *P. yoelii* and *T. gondii* [172, 173] and allows for selection marker free integration. In theory, *Plasmodium* species should allow exceptionally high numbers of observed selection marker free integration events using a nuclease as the DSB itself represents a second selection process on its own as parasites failing to repair the DSB using the template will never survive.

Transfection

The first transgenenic *Plasmodium* parasites were generated in the rodent parasite *P. berghei* [174]. The first major hurdle was the electroporation of DNA into the parasite itself. The transfection rate of *Plasmodium* is extremely low compared to other systems. The parasite can be electroporated directly if in the free merozoites or mature schizonts stage. It is expected that mature schizonts rupture during electroporation, resulting in effectively merozoites being transfected. Mature *P. berghei* schizonts are blocked in egress during in vitro culture and remain viable, in contrast to *P. yoelii* or *P. falciparum* schizonts [169]. Depending on the species, viability of free merozoites varies between a few minutes in *P. falciparum* to around 15 minutes in *P. berghei* [175]. This time window is further reduced if parasites are stressed during electroporation, making the whole process very time sensitive [176]. Even today, for *P. falciparum* transfection, electroporation of DNA is still routinely performed into uninfected RBCs, which maintain circular DNA reliably. After invasion, circular plasmids are taken up probably via the

food vacuole through an unknown pathway [177]. This seems to work only with circular DNA, classical linear DNA is degraded, but can now be modified at the 5' ends to protect the DNA from hydrolyzation.

Episomal maintenance

Post transfection, circular DNA is replicated and divided reliably under drug selection. The mechanism of how the parasite performs this is unknown, but it is speculated that for DNA replication, origins of replication selection is not very stringent and plasmid segregation during schizogony is random. This is supported by the fact that circular plasmids are maintained easily under selection independent of the amount of parasite sequences within the plasmid but easily lost without drug pressure. Depending on the combination of drug and selection marker used it can be beneficial for the parasite to carry multiple copies of the episome which are assumed to be present as a concatamer [178, 179]. Plasmids containing a centromere are divided very faithfully in every daughter cell without drug selection throughout the whole life cycle, further indicating that plasmids are copied reliably during DNA replication [180].

Episomal transfection has several disadvantages, mainly unstable copy numbers down to zero without selection and the inability to modify the parasite genome actively.

Stable integration of foreign DNA

Stable integration of plasmid DNA in *Plasmodium* works quite efficiently under certain conditions, once the DNA enters the parasite cytoplasm. Stable integration requires at least one region of homology between the foreign DNA and the chromosomal target site. Homologies of several hundred base pairs are required for efficient integration, but integration efficiency increases with longer homology [181].

Single crossover integration

A circular plasmid can integrate into the genome by single crossover integration. There are several possible ways how this can be initiated. If a circular plasmid is present within the parasite, a DSB within the plasmid or the genome can occur. There is no experimental evidence about the frequency of DSBs in *Plasmodium* and whether this is different between plasmid or genomic DNA. If the DSB occurs in a sequence that has homology between the plasmid and the genome, the only potential template for HR is the respective other piece of DNA if the parasite is in a truly haploid stage of the life cycle.

If the DSB occurred in the plasmid and is not repaired the plasmid is linearized and subsequently lost, if the DSB occurred within the genome and is not repaired the parasite will loose one part of the chromosome during the next schizogony and subsequently die. If the DSB is repaired via HR, the result is a duplication of the homology region flanking the entire remaining sequence of the plasmid within the genome. The repair can also occur via synthesis dependent strand annealing (SSA), resulting in the recreation of the original genetic state [144]. Integration can be forced immediately by transfection of a linear plasmid that is cut within the homology region itself, thus skipping the time consuming step of random DSB.

Integration of plasmid DNA via single homology integration is reversible, as a random DSB within one of the two homology regions can initiate repair, resulting in excision and recircularisation of the original plasmid. This is the reason why today gene deletions via single crossover integration are not used any more. Functionally, single crossover integration allows tagging, expression of additional genes as well as gene deletions by splitting long coding regions into two untranscribed fragments using a short homology in the center of the coding region.

Double crossover integration

If a circular plasmid is designed correctly, it can also result in the stable replacement of some chromosomal DNA with a foreign piece of DNA inserted. In order to achieve this, two homology regions are required surrounding a positive selection marker and a negative selection marker on the remaining plasmid. Random double strand breaks in some parasites lead to the integration of the plasmid via single crossover utilizing any of the two homology regions. The majority of parasites retains the plasmid as an episome. To enrich integrated parasites, positive selection is removed for several growth cycles, which results in the loss of the majority of episomally maintained plasmids but not the integrated plasmids. Subsequent reintroduction of the positive selection marker enriches the single crossover parasite population. This parasite population can now be selected with the negative selection marker. This will result in the selection of those parasites that first integrated via one homology region and looped the negative selection marker out via the other homology, resulting in the integration of the DNA in between the two homology regions of the plasmid while replacing the sequence in between the two homology regions of the chromosome. Since these parasites still possess the positive marker in between the two homology regions, they can be selected against all other

possible events. The resulting parasites do not contain any duplicated homology regions, the genetic modification is thus not reversible.

If parasites are tranfected directly, it is highly beneficial to use linear DNA. This is routinely used in the rodent *Plasmodium* species but has only rarely been reported for *P. falciparum*. In this case integration does not rely on a random DSB within the homology regions, but the ends of the plasmid are directly recognized as a DSB. Integration will only be successful if two homology regions exist in correct orientation to each other on the target chromosome. In this case, the transfected linear DNA replaces the DNA in between the two homology regions on the chromosome. Independent from the origin (circular or linear DNA), replacement of a chromosomal DNA sequence in between two homology regions is termed double-crossover.

Recently, it was shown that the targeted integration of circular DNA can be sped up by generating using a targeted DSB within the genome using a nuclease [146, 170, 171]. In contrast to transfection of linear DNA, here the DSB occurs within the chromosome. This has the advantage that parasites that do not incorporate the homologous sequence from the plasmid die as they cannot repair the double strand break. This allows for the selection of only the circular plasmid for a few days and not necessarily the integrated DNA, thus making marker free insertions become possible. This implies that also short fragments of DNA can be changed without changing the genetic environment [170, 172]. For these strategies it is crucial that the homology of the plasmid DNA is protected from the DSB by silent shielding mutations.

1.2.6 Tools used in *P. falciparum* genetics

Generally, all versatile tools in general cell biology are copied and adopted into *Plasmodium* research with some delay in time. While due to its unique biology *Plasmodium* genetics is generally very tedious, its unique genetics makes some methods even more powerful that in other systems and opens new possibilities not feasible in standard model systems.

Zinc finger nucleases

Zinc finger nucleases (ZFNs) are artificial fusion proteins of several zinc finger DNA binding domains and the endonuklease FokI from *Flavobacterium okeanokoutes* [182, 183]. Each zinc finger domain binds a three base pair DNA sequence and typically three to five of these are combined to bind a unique sequence of 9 to 15 bp. As FokI is required

to dimerize in oder to induce a DSB, a second ZFN has to bind a suitable DNA motive on the complimentary DNA strand. Generally there is a spacer of 6-8 bp in between the two recognition motifs. Binding of both ZFNs results in dimer formation of the FokI, resulting in a DSB break within the spacer region. While there are zinc finger domains know to bind each possible DNA triplet on its own, multiple zinc fingers result in unpredictable crosstalk in between neighboring DNA binding specificity. This means that the generation of a single pair of ZFNs requires the production and screening of multiple zinc finger combinations that have to be validated before they can be used.

To increase specificity, newer ZFNs are design as an a and b form that can only form heterodimers with each other [184]. Additionally, increased numbers of ZFN domains increase the specificity of a specific ZFN pair. Off target effects can still occur in many systems, but are only relevant if individual clones are generated where the phenotype observed can potentially be caused by a off-target-DSB and following frameshift mutation caused by NHEJ repair. Direct quantification of bulk populations are not affected by off target effects as these are always semi-random and only occurs in a minority of individual cells. The same is true for all *Plasmodium* species. Due to the lack of NHEJ, off target DSBs will either be repaired via HR or the single parasite dies and disappears from the population.

CRISPR/Cas9

Clustered regularly interspaced short palindromic repeats are short repeats found in many bacterial species and most archaea that function as a adaptive immune response against phages [185]. This system is used by bacteria to keep a genetic record of short fragments of phage DNA sequences (a spacer) they have encountered, each one flanked by the repeat. The repeat is responsible for the three dimensional structure of the guide RNA (gRNA) that is generated from one repeat and one spacer. This gRNA is bound by a nuclease like Cas9 and together they scan DNA sequences for the spacer sequence. Once an appropriate target is bound, Cas9 induces a double strand break, thus destroying the phage DNA.

This system has quickly been adopted as a tool to generate sequence specific DSBs. Their location within the genome can simply be encoded by a 20 bp sequence within the gRNA. The only limitation is the nuclease specific protospacer adjacent motif (PAM) sequence, that has to occur directly next to the spacer sequence in the target sequence. The PAM is not part of the spacer sequence but specific to each CRISPR/Cas9 system

and ensures that the bacteria does not cut its own DNA within the CRISPR region.

CRISPR/Cas9 has already been successfully implemented in Plasmodium in multiple instances and is currently being used in most labs working on *P. falciparum* [170, 172]. Recently, in *T. gondii* a whole genome wide Cas9 screen has been performed, exploiting the NHEJ repair pathway, so that targeted DSBs within target genes led to frameshift mutations, eliminating the need for specific repair templates at all [186]. In Plasmodium, Cas9 requires a homologous DNA to repair the DSB via HR, otherwise all parasites with successful DSB die due to lack of NHEJ. However, using 5' modified primers, also short linear PCR products are sufficient to deliver the DNA required for repair. Cas9 based systems have so far worked in every system tested and can also be employed as gene drive systems [187, 188].

TALENs

Transcription activator-like effector nucleases (TALEN) are fusion proteins of naturally occurring TALEs that are fused to a FokI nuclease as it is the case in ZFNs [189, 190]. The TALE DNA-binding domains of TALEs have been identified in *Xanthomonas* bacteria that are frequently used to transform plant species [191]. These bacteria use TALEs which they export into the plant cells they infect to change gene expression. The DNA binding domain consists of highly conserved repeats of 33-34 amino acids that differ only in two positions that are highly variable. TALENs have the advantage over ZFNs that individual repeats do not influence the binding affinity of the neighboring repeats. However, as every repeat encodes only the binding to a single nucleic acid, about 20 repeats have to combined for a single TALEN. Since these repeats are almost identical, design and sequencing are technically challenging. Much promise was put on TALENs as they are cheaper to produce that ZFNs, but since CRISPR/Cas9 was published few labs still use TALENs. So far no use of TALENs in *Plasmodium* has been published.

Cre recombinase

Cre recombinase is an enzyme of the P1 Bacteriophage that can recognize two 34 bp DNA sequences, termed loxP sites, and depending on their orientation, flip or excise the sequence in between the loxP sites [192]. This Cre recombinase was first transferred to Apicomplexa in *T. gondii*, as a constitutively active enzyme [193]. This limits the use Cre combinase. Induction of a gene flanked with loxP sites lead to rapid removal of the respective gene sequence. Another 13 years later, it was shown that Cre recombinase

is inducible as a split enzyme, termed DiCre [194, 195]. Here two inactive fragments of Cre were fused with the FRB domain of mTOR and the FK506 binding protein (FKBP12) respectively, which dimerize in the presence of rapamycin. This makes it possible to probe gene function of essential genes by deleting them in all parasites at once independent of transfection efficiency. By activating the expression of a fluorescent protein upon gene excision, gene deletion can be monitored on a single cell level. This system was also adapted to *P. falciparum* [196].

In contrast to the nucleases mentioned above, Cre will only target the loxP site, and thus always requires the correct placing of these prior to activation. Recently it has been shown that loxP sites can be "hidden" in artificial introns, dramatically increasing the freedom for loxP placement thus reducing the chance for unwanted side-effects [197].

Flippase

The recombinase flippase (FLP) is a recombinase from a plasmid of *Saccharomyces cerevisiae* that recognized two flippase recognition target (FRT) DNA sequences and flips or excises the DNA sequence in between the two FRT sites [198]. This system has been shown to work in *P. berghei* during the mosquito stage and was later used to probe the function of the blood stage essential gene MSP1 in the liver stage [199, 200]. As the original FLP gene from yeast is thermolabile and had to be optimized for activity at 37 °C, the original version has been used, possibly resulting in low activity. Even further optimization in expression timing still resulted in incomplete excision on a population level, a common problem also in the DiCre system [201, 202].

Selection markers

Multiple selection markers have been used in the past for *Plasmodium* species [168]. Only those that are applicable to rodent parasites will be discussed here. The first selection marker that was used routinely was pyrimethamine, and it is still the standard selection marker today for rodent *Plasmodium* parasites, due to its convenient application via the drinking water [203]. Pyrimethamine inhibits the dehydrofolat reductase (DHFR) of the parasite, which exists as a fusion enzyme of DHFR and thymidylate synthase (DHFR-TS) [204], a gene fusion that is conserved in all bikonts. As resistant parasites to pyrimethamine appeared long before transfection methods became available [205], the identification of the drug target and resistant mutations were already known. Later also the gene of resistant *T. gondii* (*Tgdhfr-ts*) was used to reduce unwanted homology and

also the human dehydrofolat reductase (*hdhfr*) was used to further reduce size of the coding region [167]. Another inhibitor of the dehydrofolate reductase, which has to be injected subcutaneously in mice is the drug WR 99120 [203]. Resistant *Tgdhfr-ts* results in resistance to pyrimethamine but not to WR, while *hdhfr* confers resistance against both drugs [206]. In mammals DHFR has been shown to autoregulate its own translation via binding to its respective mRNA if not bound to its substrate. This autoregulation occurs via the substrate binding sites in human DHFR thus being responsive to presence of substrate or inhibitor but via non-substrate binding sites in *Plasmodium* DHFR-TS [207], thus only responding to enzyme presence. This causes active translation of *hdhfr* upon drug inhibition but not of *Plasmodium dhfr-ts*. The effective resistance of *hdhfr* against WR-99210 both in humans as well as in *Plasmodium* thus results from increased translation upon drug inhibition.

To facilitate selection marker recycling, in the last years a positive-negative selection marker has been used in *P. berghei* [208]. This special selection marker cassette makes use of the reversibility of single crossover integration. The whole selection marker within the plasmid is flanked by 500 bp of homology which allows the parasites to loop out the entire selection cassette at a low frequency. The selection marker itself is a fusion of *hdhfr* with the fusion of the coding regions of yeast cytosine deaminase and uridyl phosporibosyl transferase (*yfcu*). After positive selection with pyrimethamine and subsequent cloning, single parasites that lost the whole selection marker cassette via homology based excision are selected for with 5-fluorocytosine (5-FC), a prodrug which is metabolized to 5-fluorocytosine triphosphate via *yfcu*. The only disadvantage is the requirement to clone the parasites after both the positive and negative selection. This can be avoided using the gene insertion marker out (GIMO) system, where a recipient line is generated that carries the *hdhfr-yfcu* gene within the target locus that is not flanked by homology regions [209]. Only parasites that integrate the selection marker-free transfected DNA via double crossover and loose the *hdhfr-yfcu* gene in the process are able to survive the following negative selection after transfection.

Additionally fluorescent activated cell sorting (FACS) can be used to select for fluorescent parasites expressing a selection marker in the blood stage [210]. This allows not only to generate selection marker free parasites, but to generate non-clonal isogenenic parasite populations. This limits the effects of possible random mutations within a single clone that produce a phenotype not connected with the genetic manipulation itself [211].

1.3 Sporozoite biology

Sporozoites have a unique and fascinating biology that is vastly understudied, especially their *in vivo* behavior. There are big gaps in our knowledge. Open questions include sporozoite formation within and egress from the oocyst, salivary gland invasion, capillary egress as well as the precise differences between sporozoites of the different stages. While sporozoites are formed within the oocyst, they still change their morphology slightly until they finally reach the salivary gland [212]. Salivary gland sporozoites seem to be passively waiting, storing multiple mRNAs by binding them with Pumilio-2 (Puf-2) to have them ready for the first hours after hepatocyte invasion [89]. Additionally protein synthesis is blocked via phosphorylation of eukaryotic initiation factor 2α (eIF2α) by upregulated in infective sporozoites 1 (UIS1), which is later dephosphorylated by the phosphatase UIS2, as soon as it's translation is no longer repressed by Puf2 [213]. On the other hand it has been shown for CSP that it is actively translated in salivary gland sporozoites at least *ex vivo* [214], as is also true for TRAP [215].

These differences between sporozoites isolated from different organs are also represented by their motility *in vitro*, which increases from low levels in midgut derived sporozoites (MGS), is higher in hemolymph sporozoites (HLS) and highest in salivary gland derived sporozoites (SGS) [216]. In vivo infectivity after intravenous (IV) injection is extremely low for MGS and almost as high for HLS as for SGS but intradermal (ID) injection requires SGS to be effective [28, 217–220].

1.3.1 Sporozoite morphology

Sporozoites have a highly organized and apical polarized morphology (**Figure 1.3 A** and **B**). They are highly elongated cells that are about 12 µm in length and about 1 µm in diameter at the widest area which is at the nucleus [212, 221, 222]. They are slightly curved (more pronounced in SGS) and chiral, meaning they have a defined apical and basal side, a convex and a concave side, as well as a dorsal and ventral side. The latter is implied from their preferred direction of motility, which is clockwise on a two-dimensional surface or a right handed helix in a three dimensional environment [34, 223–225].

Sporozoites are surrounded by a uniform plasma membrane that is covert mainly with the glycosylphosphatidylinositol (GPI) anchored major sporozoite surface protein, the circumsporozoite protein (CSP) [226]. The plasma membrane shows no visible perturbations and a uniform distance of about 25 nm to the underlying inner membrane complex (IMC) [212]. The space in between is termed the subpellicular space and the

uniform

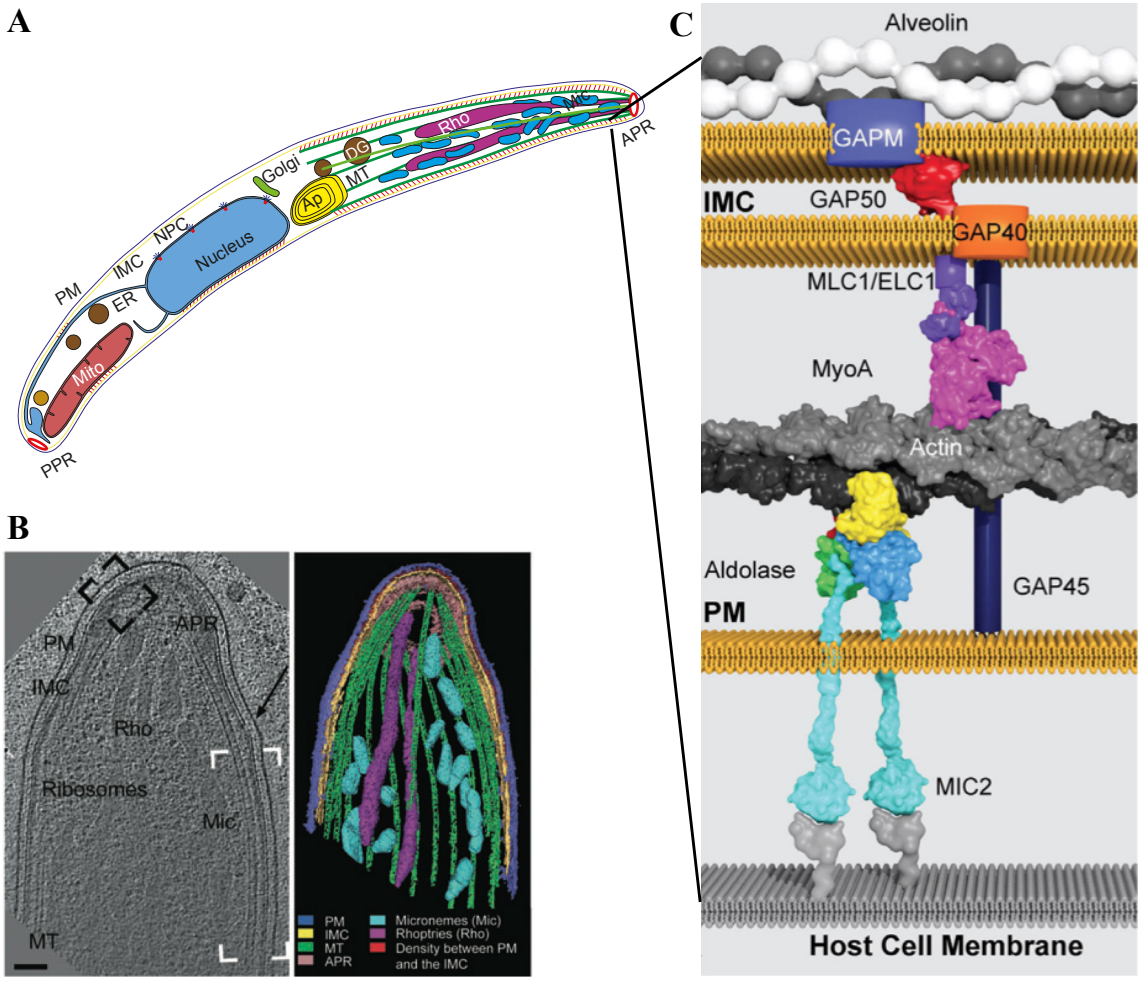

Figure 1.3: Gliding motility of sporozoites
A Model of a sporozoite. Inner membrane complex (IMC) and apicoplast (Ap) shown in **yellow**, plasma membrane (PM), endoplasmatic reticulum (ER), nucleus and micronemes (Mic) in **blue**, microtubules and Golgi in **green**, apical polar rings (APR) and proximal polar ring (PPR) and mitochondrion (Mito) in **red**, rhoptries (Rho) in **violet**, dense granules (DG) in **dark green**. **B** Apical tip of a sporozoite, shown as an slice (left) and volume rendering (right) from a cryo-tomogram. **C** Current model of the motor, mostly derived from data of *T. gondii* data. Location of the motor in A is depicted. The involvement of aldolase has been disproved and the new linker between actin in adheins (here MIC2 is shown) is suggested but not yet verified [227, 228]. Figure A and B are from [222], Figure C is from [229].

distance is assumed to be maintained via the protein glidosome associated protein 45 (GAP45) which is anchored both into the plasma membrane and the IMC [230–232]. The IMC is presumably derived from the endoplasmatic reticulum (ER) and exists as a system of flattened vesicles that surround the entire surface of the sporozoite except openings within the apical and basal polar rings. In other parasites like *T. gondii* and *P. falciparum* gametocytes, separate IMC plates connected via surtures have been described [233–236]. It is expected that these also exist in sporozoites, as a family of IMC sub-

compartment proteins (ISPs) define separate subcompartements and show hierarchical sub-IMC localization in both *Plasmodium* sporozoites and *T. gondii* tachyzoites [237, 238].

The IMC is possibly given its shape and structure by the subpellicular network (SPN) that contains a large set of intermediate filament like proteins that a conserved among all Alveolata and are termed alveolins [236, 239, 240]. The SPN matures during the transition from midgut to salivary gland sporozoite in respect to its density by cryo-electron-tomography [212]. Alveolins are believed to be highly interconnected via their repeats and are linked to the IMC [239]. They give zoites a high degree of stiffness and resistance to osmotic rupture [241] but at the same time a degree of elasticity. Other proteins within the SPN have only a strong impact on shape while tensile strength in their absence is unchanged, this might be due to a successive assembly of the SPN [242].

Indirectly linked to the IMC are also the 14-15 + 1 subpellicular microtubules. The inter-microtubular distance is homogenous at the apical tip and separates towards to the nucleus of the sporozoites into the 14-15 + 1 organization [212, 221]. Apical microtubules are stable, formed during sporogenesis (see **Sporogenesis**) and are believed to persist until the sporozoite transforms after invasion of the hepatocyte. They originate from the apical polar ring which serves as the microtubules organizing center (MTOC) and end at the position of the nucleus with their plus end [243–245]. The subpellicular microtubules are believed to give sporozoites further stability and have been suggested to guide micronemes for apical secretion [246, 247]. However most micronemes are not associated directly with microtubules [222].

The apical polar rings in sporozoites are tilted about 60 degrees in respect to the apical-basal axis and together with the microtubules defines the top and bottom side of sporozoites. All apical secretion is expected to occur through the apical polar ring [248]. Sporozoites possess the secretory organelles, micronemes and rhoptries but presence of dense granules found in *T. gondii* and *Plasmodium* merozoites is not clear. These might be only present after sporozoites invade [30], whereas UIS4 present in the PVM of liver stages is translated just in time after invasion [249, 250].

Sporozoites generally contain four rhoptries that are very long and slender and appear to be closely anchored to the apical tip of the sporozoite with the rhoptry neck. Micronemes fill most of the space between the apical tip and the nucleus and fuse with the plasma membrane within the apical polar ring [222, 246, 248].

Sporozoites contain some ER which is mostly the nuclear envelope and extends to-

wards the apical and basal end of the sporozoite [222]. The Golgi is on the apical side of the nucleus, directly above the single ER exit site at the nuclear envelope. [40, 251]. A single copy of the apicoplast and the mitochondrion are mostly basal in respect to the nucleus and are often in close connection [222]. The basal polar ring is closely associated with the IMC and the SPN and defines the basal end of the sporozoite [9, 154, 222].

In some studies and species, a micropore has been described in sporozoites, a single structure roughly in the middle of the sporozoite that could be involved in direct secretion or endocytosis [252]. However, endocytosis has not been shown for sporozoites and also not for *T. gondii* tachyzoites, where structures identical to the micropore are present during dense granule secretion [248].

1.3.2 Sporogenesis

Sporozoites are generated within the oocysts that grow between the mosquito midgut epithelia and the surrounding basal membrane. Depending on the species, it can take about 8-15 days from the arrival of the ookinete until sporozoites leave the oocyst.

If the ookinete has traversed the midgut epithelia, it will start rounding up [253]. Initial interaction occurs via the ookinete surface proteins SOAP, P25, P28 and CTRP with components of the basal lamina [254–256]. Also, the expression of the major oocyst capsule protein CAP380 will ultimately result in a thick capsule protecting the oocyst [257]. On the basal site, the oocyst capsule is directly associated with the basal lamina itself [26]. However, also oocyst developing without contact to the basal lamina are observed [258].

During the beginning of oocyst development, the oocyst is rapidly growing. It is assumed that the oocyst takes up nutrients that are released from the blood meal the mosquito ingested together with the parasites [259]. The main sink of fatty acids and protein from the blood meal are the developing eggs, which can take as little as three days to develop [260, 261]. How exactly the parasite takes up nutrients at this stage is not know. Until the oocyst reaches its maximum diameter of about 30-40 µm, the ER is rapidly expanding, mitochondria and apicoplast are increasing in size and nuclear division takes place [26, 221]. While the original nucleus is tetraploid in the ookinete, the relationship between genome duplication and nuclear division is unclear, nor if it is regular at all [155].

One of the earliest signs that sporozoite formation is about to be initiated is the expression of CSP, which can start as early as day six post blood meal [262]. However

development of oocysts is intrinsically asynchronous [263]. At time of CSP expression, nuclear division results in nuclei becoming smaller and associating closer to the plasma membrane [264]. The plasma membrane, before in thigh association with the oocyst wall, now starts to retract slightly and invaginations of plasma membrane occur [25, 264]. The nuclei follow the plasma membrane of the invaginations, so that eventually multiple cell bodies, termed sporoblasts, are formed within a single oocyst [27, 265]. On the whole surface of the plasma membrane, sporozoite formation occurs almost simultaneously (**Figure 1.4**). Above each nucleus, a single big vesicle, the prerhoptry appears [27, 266]. Directly underlying the plasma membrane, the first signs of an IMC appear [25, 267]. Now the plasma membrane invaginates surrounding this initiation of the apical tip, while at the same time the IMC and the underlying microtubules are formed [27]. At this time also the striated rootlet fibre becomes visible [268]. During sporozoite formation, the nucleus is elongated while the sporozoite forms around it.

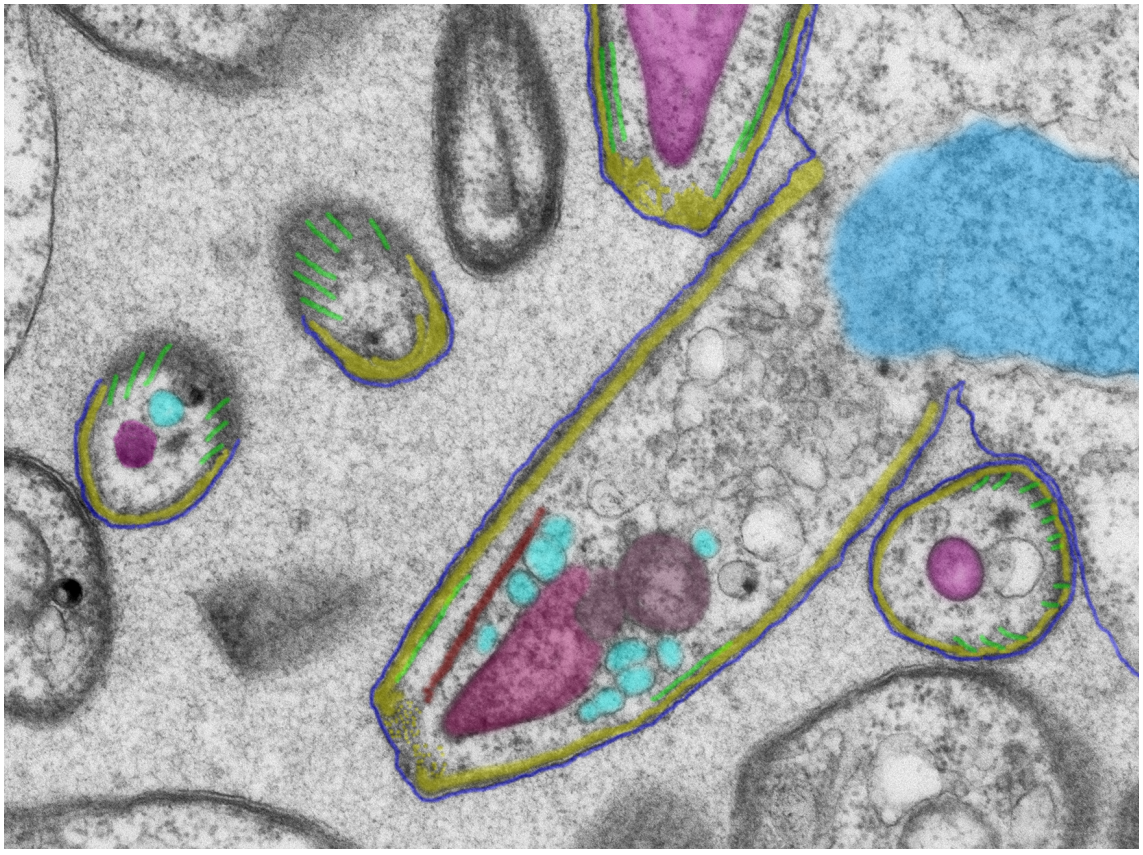

Figure 1.4: Sporozoite formation within the oocyst
Colorized transmission electron-tomography image of sporozoites forming within an oocyst. Structures are color coded: plasma membrane and nucleus in **blue**, microtubules in **green**, inner membrane complex in **yellow**, striated rootlet fible in **dark red**, forming rhoptries in **violet** and micronemes in **turquoise**. Coloration by Friedrich Frischknecht [269].

In *T. gondii* division, microtubules are an essential driver for cell division [270] and

drive nuclear division [271]. The fact that both the IMC and the forming microtubules colocalize exactly with the plasma membrane invagination during sporozoite formation strongly suggest that they are equally important for sporozoite formation. It is not known how sporozoite formation is finalized, but eventually sporozoites loose contact from the residual body, the remaining part of the sporoblast. This can occur while oocysts are still intact, as complete oocysts are observed where sporozoites lost the parallel arrangement towards each other [29].

The process of sporozoite egress from the oocyst is a very obscure process. It is not know if this event is triggered intrinsically or extrinsically, if sporozoites leave the oocyst all together or in multiple batches, if there is a preformed opening within a oocyst wall as has been observed for other Apicomplexan cysts or there are multiple simultaneous exit sites [263, 272]. In the *T. gondii* oocysts wall a thin structure termed the micropyle has been described, possibly allowing gas exchange or being involved in stimulation of excystation, and excystation occurs in between plates of the oocyst wall [273]. Several mutants that do not egress *Plasmodium* oocysts have been described in the literature, from protease deletions, four amino acid mutations of the CSP C-terminus and deletion of a small TRAP-related protein [29, 274, 275]. Of these, the protease SERA5 and the thrombospondin related protein 1 (TRP1) have been shown to result in mature sporozoites that move within the oocyst but fail to egress. For the C-terminal mutation of the CSP C-terminus motility within the oocyst was not studied, but egress was blocked without obvious differences in CSP cleavage and expression.

1.3.3 Gliding motility

The term gliding motility describes a special kind of motility that is substrate dependent, does not involve obvious changes in shape and does not involve flagella or microvilli [229, 276]. It is used simultaneously to describe motility of certain bacteria as well as Apicomplexans, and only the latter will be described here.

Male gametocytes of Apicomplexan parasites drive their fast swimming locomotion by a flagellum in a microtubule dependent manner, with a special role proposed for α-tubulin II [21, 277, 278]. This motile stage is devoid of an IMC but motility depends also on actin II [279]. All other motile stages of Apicomplexa utilize gliding motility as their only form of active locomotion. This process seems to be fundamentally the same for both the giant cells of some gregarines which exceed 1 mm in length down to merozoites which are slightly longer than 1 µm, although it is debated if *Plasmodium*

merozoites are motile at all and gregarines can also move substrate-independent in vivo [280, 281]. Most Apicomplexa have in common that only non-replicative extracellular stages show gliding motility which is always correlated with a highly polarized cell and a structured subcellular organization. Different stages and different species show vastly different speeds and requirements for gliding motility, from *P. berghei* sporozoites that show prolonged gliding motility of 1,5-2 μm/s for almost an hour and some forms of gregarines that show prolonged motility of up to 20 μm/s to *Plasmodium* merozoites where the motile phase is limited to the 1 μm to invade the RBC [280, 282, 283].

Gliding motility of Apicomplexa has mainly been studied in *P. berghei* sporozoites and *T. gondii* tachyzoites [216, 284–286]. In the past the differentiation between invasion and gliding motility has slightly changed. Many proteins implicated in gliding motility are essential for invasion and or cell traversal [28, 219], but the process is not the same from the parasites point of view, which has recently been illustrated with several *T. gondii* mutants that barely glide but still show normal invasion rates [195, 287]. Sporozoites are mainly motile in the skin after the mosquito bite and in the liver, preceding hepatocyte invasion [34, 35, 41, 288]. The ability to invade the salivary glands, which consists of attachment to and traversal of the basal lamina and traversal of the acinus cells (which in itself might be a functional invasion followed by evasion) correlates with the ability for gliding motility in vitro for many genes [28, 289]. In some cases, like for the putative pathothenate transporter (PAT) the motility phenotype is dominant [290], in others like S6 and MAEBL the salivary gland invasion phenotype is dominates [217, 291]. Apart from TRAP, which is essential for all of these processes, and partly for CSP, gliding motility and hepatocyte invasion have not been connected by the function of individual proteins [28, 275, 292].

1.3.4 The gliding motor model

The gliding motor model has over time be developed from results of multiple studies investigating single aspects of gliding motility and has not been formally challenged in it's complete entity [229, 230, 293–295] (**Figure 1.3 C**). While it offers a base to investigate gliding motility it might also restrict the researcher in a mental corset that limits the understanding of a process with a much higher degree of complexity. A good example is the recent realization that the supposed linker of adhesins and the actin motor, aldolase, is completely dispersible for gliding motiliy [227].

Here I will attempt to minimize the model to those results that have been confirmed

at least in two species, mostly *P. berghei* sporozoites and *T. gondii* tachyzoites.

Actin

Overwhelming evidence exists that the formation of actin filaments is involved in efficient gliding motility [216, 270, 296]. This has been shown with the inhibiting effects of the actin polymerizing drug jasplakinolide (Jas) and the actin destabilizing drug cytocalasin D (Cyto D) which both completely block motility of sporozoites and tachyzoites in the μM range [286, 297]. It is noteworthy to mention that Jas initially and at low doses increases gliding motility and that pretreatment with Cyto D blocks attachment whereas block with Cyto D during gliding results in firm substrate attachment [285, 298]. This suggests that Cyto D has other targets than actin involved in gliding motility [286], potentially affecting secretion and rhomboid cleavage. Actin filaments have not been visualized in motile tachyzoites or sporozoites, and biochemical data suggests that actin filaments are extremely short and unstable [299]. Recently an actin deletion mutant has been generated in *T. gondii* which shows a phenotype on intracellular development and some residual gliding motility with reduced speed [286]. Also, actin filaments have been visualized in intracellular tachyzoites which appear to stabilize cytoplasmic connections of tachyzoites within a PV [300].

Myosin A

All myosins in *Plasmodium* and *T. gondii* involved in gliding are members of the class XIV myosins [270]. Important for gliding motility in *Plasmodium* is myosin A, in *T. gondii* myosin A, B and C are involved in gliding motility, with myosin A being the main myosin for gliding and invasion [286, 301, 302]. These myosins localize to the subpellicular space, where they are in a complex with a myosin light chain and GAP45 [230, 287, 303, 304]. This complex is linked to the IMC via binding to glidosome associated protein 50 (GAP50) which is an integral membrane protein [305]. GAP50 itself is also associated with the glidosome associated protein 40 (GAP40) which is also an integral membrane protein of the IMC [8].

GAP45

GAP45, the glidosome associated protein 45 is associated with the plasma membrane (PM) via N-terminal palmitoylation and myristylation and with the IMC via its C-terminal binding to GAP50 [8, 303, 306]. In this way it indirectly links the PM and the

IMC and it is assumed that this is responsible to keep the distance between these two membranes constant. GAP45, as well as the associated GAP50, are essential in both *Plasmodium* and *T. gondii* [8, 186, 307].

Inner membrane complex

The IMC is a membranous compartment that is most likely Golgi-derived [308]. It consists of flattened membranous vesicles termed alveoli that surround all of the parasite but the very apical and basal tip in all extracellular motile stages [222, 270] and *P. falciparum* gametocytes. In *T. gondii* tachyzoites the IMC consists of multiple plates that form three rows that are tightly joined to each other via surtures [234]. In *Plasmodium* merozoites, ookinetes and sporozoites the IMC consists of a single vesicle which might be joined be a single longitudinal surture in sporozoites [236, 309]. The protein family of IMC subcompartement proteins (ISP) defines these three rows in *T. gondii* but curiously shows a similar localisation pattern in *Plasmodium* [237, 238]. Also, four proteins localized to surtures in *T. gondii* are present in all *Plasmodium* species [234, 235]. Also, IMC subcompartment proteins (ISPs) identified in *T. gondii* show comparable localization in *P. berghei* [237, 238].

The assembly of the IMC and the underlying SPN and microtubules seems to be crucial for cell division and the shape of the parasites [8, 306]. The assembly of the IMC is tightly organized in a spatial and temporal manner and is initiated at the apical polar ring which acts as the microtubules organising center (MTOC) and then extended via microtubules polymerization [50]. During extention the basal polar ring or basal complex extends towards the back of the cell and is marked by membrane occupation and recognition nexus protein (MORN1), which is also localized to the apical polar ring [310–312]. The basal complex ultimately colocalizes with the invaginating plasma membrane preceding cell division [9].

Subpellicular network

The IMC is tightly linked via multiple multi-pass-transmembrane domain proteins with the underlying subpellicular network, which consists of intermediate filament like proteins [313]. The most prominent member of the SPN are the alveolins which are characterized by tandem repeats of a 12 amino acid motif [240]. Many of these are essential for parasite formation or shape [314–316]. Other unrelated proteins also localize to the SPN, such as PHIL1 [317].

Subpellicular microtubules

Subpellicular microtubules are tightly associated with the SPN and are very conserved in shape in numbers in motile stage, from 0-4 in merozoites, 15-16 in sporozoites and 22 in tachyzoites [270, 294]. Without them IMC assembly is amorphic, but their impact on gliding motility, cell shape and pellicle stability could not been tested yet as they are extremely stable. There a no drugs know to depolymerize subpellicular microtubules, they are stable at low temperatures and they are stable after cell extraction, which has been associated with the subpellicular microtubule binding protein 1 (SPM1) [318]. Proteins are suggested to be localized within subpellicular microtubules or are associated with SPM1 [244, 319]. Recently, more microtubule associated proteins have been identified [245]. Subpellicular microtubules have also been implicated to be important for the positioning of micronemes [247].

Micronemes

Micronemes and their protein content are believed to be an integral part of parasite egress, motility and attachment [320]. Different subpopulations of micronemes have been proposed to co-exist [55]. besides micronemes, the rhoptries are involved in parasite invasion and the dense granules, as well as exonemes, which are believed to be a special form of dense ganules are involved in merozoite egress [321]. Protein trafficking to various organelles is better studied in *T.gondii* [322–324].

In sporozoites, micronemes are formed within the oocyst during sporozoite formation and are slowly disassembled during late liver stages [325]. The turnover of micronemes is not well studied, but some proteins suggested to be localized to the micronemes are only expressed within the salivary gland (TLP for example) and metabolic labeling of TRAP within salivary gland sporozoites is possible [215, 326].

Proteins are assumed to be targeted via a signal peptide and a tyrosine containing micronemal targeting motif which is localized directly after the last transmembrane domain [327]. However, proteins lacking transmembrane domains can also be targeted to the micronemes, as the ookinete specific protein SOAP [254].

Thrombospondin related anonymous protein family

Several micronemal proteins are considered to be adhesins, proteins involved in cell adhesion and force transmission during motility. The best characterized micronemal proteins of sporozoites is TRAP, which is essential for salivary gland invasion, gliding

motility and liver cell invasion [28]. The binding partner of TRAP on the mosquito salivary gland is saglin [328], whereas the direct binding partner of TRAP in the skin and hepatocyte are unknown but expected to be a rather unspecific interaction.

TRAP contains a signal peptide, a von-Willebrandt factor like A-domain and a thrombospondin type repeat (TSR) followed by an uncharacterized repeat region which is not important for TRAP function [215]. The following transmembrane domain contains the cleavage site for a rhomboid protease (see **Rhomboid proteases**). The C-terminus of TRAP contains a tryptophan and is quite acidic [329]. The homolog of TRAP in *T.gondii* is the micronemal protein 2 (MIC2), and both share the general orientation with signal peptide, A-domain, TSR-domain (MIC2 contains 5), transmembrane domain with the rhomboid cleavage site, and the C-terminus with the micronemal targeting motif and the conserved tryptophan [327, 330, 331].

Several other proteins are also considered to belong to the TRAP family of proteins and share some of the features of TRAP. These are the merozoite TRAP-like protein (MTRAP) which has recently been shown to important for gametocyte egress rather than merozoites in *P.berghei* [20], the circumsporozoite and TRAP-related protein (CTRP) expressed in ookinetes [332] and both the S6 protein and TRAP-like protein (TLP) also expressed in sporozoites [217, 326]. All of them have one transmembrane domain and the C-terminal tail with the conserved tryptophan but show different numbers and orientation of A- and TSR-domains [29]. CTRP is functionally most similar with TRAP as ookinetes lacking CTRP are non-motile and are not infectious to mosquitoes unless injected directly into the hemolymph bypassing midgut epithelium traversal [333].

Rhomboid proteases

Rhomboid proteases are transmembrane proteins that are capable of cleaving specific motifs of transmembrane domains of other proteins [334]. They have long been postulated to be responsible for the fast cleavage of micronemal proteins after these have been translocated to the back of the motile cell [335, 336]. Several micronemal proteins have been assessed in a mammalian cell line for their cleavage by rhomboid proteases [337]. Recently work has been done in *T. gondii* describing rhomboid protease 4 (ROM4) to be responsible for cleavage of most micronemal proteins, which had previously been shown for *P. berghei* sporozoites [215, 338].

For sporozoites, the cleavage of micronemal proteins after secretion has been suggested to be a stochastic process, assuming equal transmembrane localization of ROM4

[215]. If cleavage is not occurring efficiently, and assuming the cell travels one cell length within less than ten seconds, equal amounts of adhesion proteins should be bound to the motor machinery producing forward force and at the basal end of the cell holding the cell back. Thus it is expected that rhomboid proteases have to be almost constantly active during motility.

The gliding motility motor

In the attempt to unify the various components of gliding motility of Apicomplexan parasites several assumptions have been made in the past which have been carried along without experimental evidence. Here I will discuss what is known and not know about gliding motility with the example of sporozoites:

Sporozoites are mostly non-motile when they are localized within the salivary gland duct, and have been shown to associate in stacks with each other [30, 223]. Once injected into the skin by the mosquito or activated in vitro with bovine serum albumin (BSA) sporozoites rapidly start productive gliding motility in their three-dimensional or two-dimensional substrates [40, 229, 284, 288]. What is completely unknown is how sporozoites are initially activated, only that the activation cascade involves Ca^{2+} signaling later on. Unactivated sporozoites have very little TRAP on their surface suggesting no or very low micronemal secretion before activation. The F-actin binding protein coronin relocalizes from a peripheral to a basal localization upon activation of sporozoites in a actin-binding-dependent fashion [289]. This suggest that F-actin is ether relocalized upon activation via myosin and / or that the amount of F-actin increases upon activation.

Once activated, sporozoites move quite continuously with up to 2 μm/s, traversing their own cell length as fast as every five seconds [285]. The micronemal protein TRAP which is essential for gliding motility is secreted during gliding motility at the apical tip of the sporozoite and can be found on the surface of activated sporozoites as well as on the substrate, marking the "trail" of the sporozoites. Assuming that TRAP is mainly moved by the intracellular motor machinery and that it cannot detach from the substrate once bound, micronemal proteins need to be secreted at least once every few seconds. This process has not been visualized directly so far. Thus it is not know if the content of a complete microneme is secreted at once. If the rhomboid cleavage site of TRAP is mutated reducing cleave efficiency, sporozoites are moving slower, suggesting that they are held back by excess amounts of TRAP at the basal end of the sporozoite

[215].

The force generation and force transmission to the adhesins are not well understood. It is assumed that gliding motility is F-actin dependent, as motile Apicomplexans are quite sensitive to the actin modulating drugs Cyto D and Jas [285, 286]. It is assumed that short actin filaments are moved rearward by myosin A which is known to be tightly associated to the IMC via MLC1 and GAP45 [287, 339]. They are also assumed to be depolymerized at the back of the parasite. Myosin A has not been characterized in sporozoites, but tachyzoites lacking myosin A show only very slow movement [286, 287]. Until recently the force transmission from the actin filament to the adhesins was believed to be mediated by aldolase, but this has been shown to be wrong [227]. New data suggests that an armadillo repeat protein might play a role as a linker [228], however unpublished results in *P. berhei* suggest that this might not be universally true for all Apicomplexa. The fact that tachyzoites lacking essential components of the gliding motility motor still show residual motility could be due to the fact the many *T.gondii* proteins have multiple orthologs which are usually expressed in the *T.gondii* sporozoite stage that can partially compensate the function. However, recent inducible deletion parasites [286] should not suffer from this effect since they lack the time for the parasite to adapt. Yet it could be assumed that diffusion of adhesins after apical secretion alone allows for slow motility in vitro. This process could also play a role in invasion, along with the possible mechanism of local changes in host cell PM tension and actin cytoskeleton induced by rhoptry discharge [340].

Several components that have not been discussed yet have also been shown to be important for gliding motility. However, the minimal model for gliding motility consists of the stabilized IMC, myosin A, some F-actin and a single adhesins that is apically secreted and cleaved by rhomboid proteases at the basal part of the PM. The actin binding proteins that are normally implicated in F-actin turnover are not well characterized. However it is assumed that the essential formin 1 and formin 2 are involved in actin polymerization at the apical part of the sporozoite and that actin depolymerizing factor (ADF) and profilin are involved in actin depolymerization and monomer stabilization [341–343]. Both the actin capping protein CPβ and coronin influence actin filaments and are important for gliding motility and salivary gland invasion [289, 344]. What has not been shown experimentally is if and how myosin A is oriented in the IMC as well as the local dynamics of actin polymerization and depolymerization. Sporozoites can produce patch gliding, a motile behavior where they move up to one sporozoite length

over a single adhesion site or gliding motility which is always forward. It might be possible that the direction of forward motility is only determined by the apical secretion of adhesins together with the stochastic or even basal associated cleavage by rhomboid proteases and myosin A is also the motor driving patch gliding, a form of motility where sporozoites move back and forth over a single adhesion site [285].

1.3.5 Glycosylphosphatidylinositol-anchored proteins in Plasmodium

GPI-anchored proteins play a big role in many unicellular parasites, variant surface glycoprotein (VSG) in *Trypanosoma brucei* [345], SAG1 in *T.gondii* [346], gp34 in *Theileria* [347], the merozoite surface protein 1 (MSP1) in the *Plasmodium* merozoites [348], and CSP in the *Plasmodium* sporozoite [349]. Also less prominent examples, like *Trypanosoma* and *Plasmodium* insect stages have GPI-anchored proteins or free GPI-anchors on their surface [255, 350, 351]. While GPI-anchored proteins also exist in metazoa, their numbers and especially abundance is much lower [352]. It is generally assumed that GPI-anchored proteins allow for denser packing of proteins on the membrane [353, 354], result in higher stability within the membrane [349] as well as specific trafficking [355–357] and allow for a separate mode of regulation of protein turnover at the PM by selective cleavage [350, 358, 359]. What has been less studied is the impact of high numbers of GPI-anchors on the properties of the plasma membrane itself [360].

The proteins that are GPI-anchored contain a C-terminal GPI-anchor signal which is cleaved at the ω-site within the ER and covalently bound to the phosphoethanolamine of the GPI-anchor [361]. The GPI-anchored protein is then trafficked to the plasma membrane [357].

The GPI-anchor of Plasmodium is structurally different from the mammalian GPI-anchor [362, 363] and it has been suggested that this is detected by the immune system during blood stage disease [364–366]. Also the signals used in Apicomplexa are not identical to those in mammalian cells [367]. It has also been suggested that GPI-anchored proteins cluster within the membrane in so called lipid rafts, regions with lower membrane fluidity and enriched in specific transmembrane proteins, cholesterol and sphingolipids [360]. Also it has been shown that GPI-anchored proteins can "jump" from one cell to another via direct cell contact, nanotubes and exosomes. These have been suggested to spread of prions throughout the brain during bovine spongiform encephalopathy (BSE) [368–371].

1.3.6 The circumsporozoite protein

The major surface protein of *Plasmodium* sporozoites is the circumsporozoite protein (CSP). It is estimated to account for about 10% of the total protein and is by far the most abundant protein observed in sporozoites [372, 373]. CSP is expressed during oocyst development, localized on the plasma membrane of the sporozoite as well as the liver stage [25, 262, 374]. It is assumed that CSP is GPI-anchored, although this has not been experimentally validated [349, 375].

The CSP proteins is conserved among all *Plasmodium* species as a single copy gene. It consist of an N-terminal signal sequence, a rather uncharacterized N-terminus, a conserved Region I (RI), a central repeat region and a C-terminal a-TSR domain followed by the GPI-anchor. The repeat region is present in all species on both the amino acid and the nucleotide level and varies between 4-12 amino acids in length which are repeated 8-37 times [226, 376]. While initial attempts to generate *Plasmodium* species swaps of CSP resulted in a phenotype [292, 377], recent experiments suggest that some CSPs can functionally complement for each other [378]. The CSPs protein of *P. gallinaceum* and *P. relictum* might be an exception to this rule, with their modified Region I and different host cells of sporozoites in the avian host than in the mammal [377, 379].

The N-terminus

The N-terminus is the most elusive part of CSP. It is the only part which has been not structurally resolved. The N-terminus of CSP (**Figure 1.5**) has been shown to contain two Plasmodium export elements (PEXEL) motifs [374], which have been mainly a subject of research during the RBC stages of the parasite life cycle. There, cleavage of the PEXEL motif by Plasmepsin V results in export into the RBC cytoplasm via the Plasmodium translocon of exported proteins (PTEX) which is located within the PVM [380, 381]. Sporozoites expressing CSP without PEXEL showed normal development including hepatocyte invasion, but lower numbers and size after 48 h [374]. It was suggested that the PEXEL motif is responsible for export into the host cytoplasm and subsequent nuclear import via an nuclear localization signal (NLS) in the C-terminus of CSP, a finding that has been questioned by others and is challenged by the low conservation of the NLS and by the lack of HSP101 expression during the liver stage, an essential component of PTEX [382]. However in *T. gondii*, export of dense granule protein 16 (GRA16) and dense granule protein 24 into the host cytoplasm is dependent on cleavage by aspartyl protease 5 (ASP5), the homolog of Plasmepsin V and myc

regulation 1 (MYR1) while the translocon itself has not been identified and is expected to be structurally different from *Plasmodium* PTEX [383, 384]. The homolog in *T. gondii* of the pore formin protein of PTEX, exported protein 2 (EXP2) is dense granule protein 17 (GRA17), which together with dense granule protein 23 (GRA23), rather forms a unspecific pore to facility diffusion of small molecules [385]. This suggests that both alternative export pathways besides PTEX might exist also in Plasmodium and parts of PTEX might facilitate different functions during other stages than the blood stage.

The main body of experiments focusing on the N-terminus are focusing on it's cleavage and are discussed below (see **Processing of CSP**).

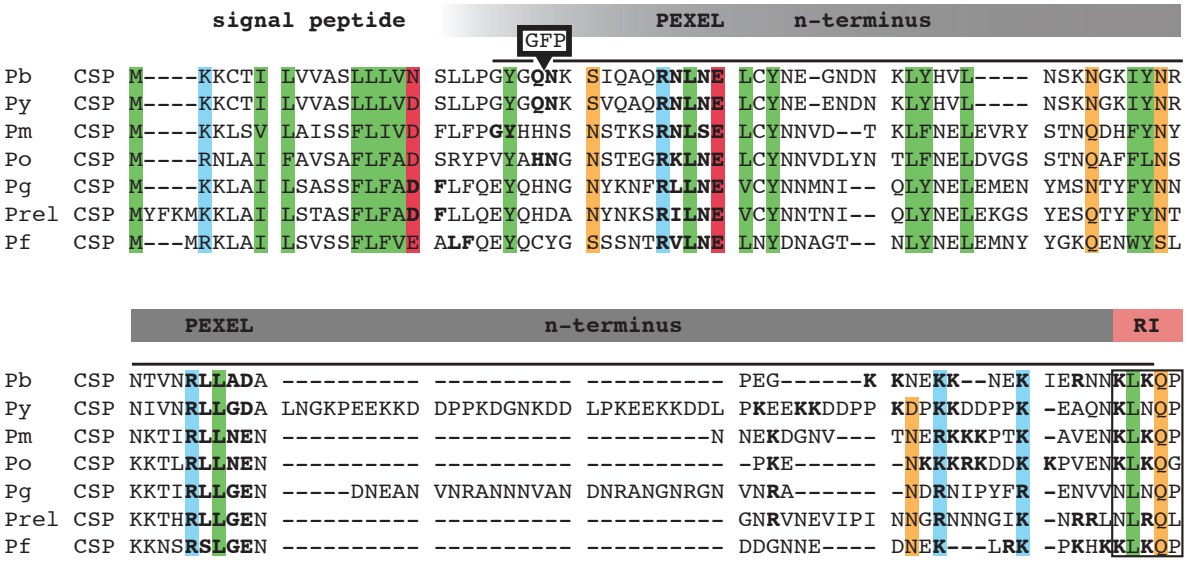

Figure 1.5: N-terminus of CSP of different species.
Alignment of amino acids was manually curated to condense in size and highlight conserved features of CSP. Conserved residues are colored according to type, **green** = hydrophobic, **red** = acidic, **blue** = basic, **orange** = charged, **pink** = prolin and glycin, **yellow** = cystein. The predicted N-terminus after signal peptide cleavage was predicted with SignalP and is highlighted in **bold** [386]. The site where GFP is inserted in the mutant CS I including a linker of four and eight glycins is indicated. This shifts the predicted signal cleavage site by one base to GQG - GG, whereas the latter two glycin are from the linker sequence. The two five amino acid PEXEL motif are highlighted in **bold** [374]. Region I is emphasized with a box. Basic residues implicated in hepatocyte invasion adjacent to Region I are highlighted in **bold**. The peptide used to generate the N-terminal antibody is highlighted by a black line on top of the alignment [387].

The repeat region

It has been suggested that the repeat region of CSP (**Figure 1.6**) is functionally exchangeable between different *Plasmodium* species [388, 389]. Only recently if was shown that the repeat region is essential for sporozoite formation. The repeats are fairly conserved not just on an amino acid level but also on the codon usage. They tend to contain

one or more core repeats flanked by partial or imperfect repeats and the copy number of the repeat is flexible in between species [390].

Parasites lacking the repeat region arrest during sporozoite budding, an effect that is exacerbated if the N-terminus is also missing, which on its own enhances sporozoite formation [27, 214] (**Figure 1.7**). The fact that parasites lacking the repeat initiate sporogenesis but then stop and subsequently die could suggest that repeat increases the stability of CSP on the sporozoite surface [27].

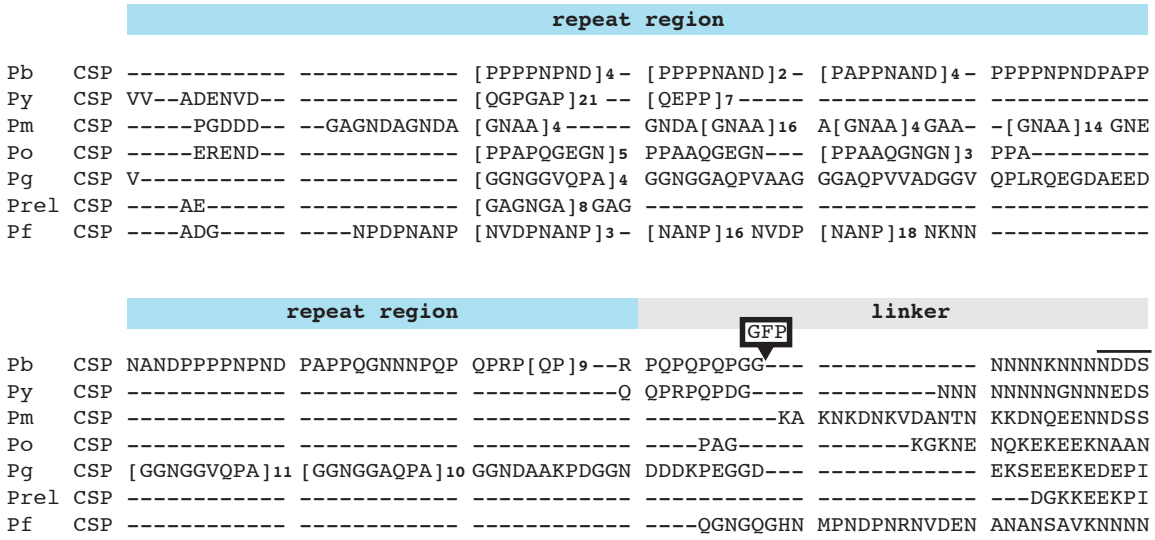

Figure 1.6: Repeat region of CSP of different species.
Alignment of amino acids was manually curated to condense in size and highlight conserved features of CSP. Perfect repeats are shown only once and copy number is indicated. The linker regions joins the α-helix of the repeat region with the α-helix of Region III. The site where GFP is inserted in the mutant CS II (including two linkers of eight glycine) is indicated. The beginning of the peptide used to generate the C-terminal antibody is highlighted by a black line on top of the alignment [387].

The C-terminus

The C-terminus (**Figure 1.8**) folds into an α-TSR domain, a single unit consisting of the conserved Region III and the TSR domain (containing the conserved Region II+ [391]). This structure contains an unusual hydrophobic pocket normally not present in TSR domains and the N-terminus of the α-TSR domain is unusually closed to the C-terminus. This suggests that the repeat region, which has been postulated to fold into a stem-like superhelix composed of β-turns (see **The structure of CSP**), might orient parallel to the PM, allowing for intermolecular interaction with the hydrophobic pocket, resulting in masking of the C-terminus by the repeat region.

Within the α-TSR domain is the glycosylation motif WXXC which results in the

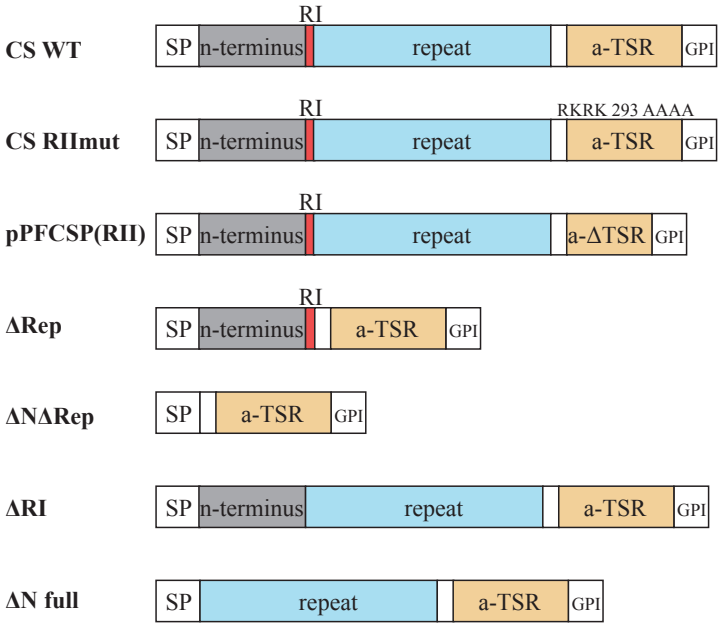

Figure 1.7: CSP published mutants
A structural summary of the most important published CSP mutants. **CS RIImut** [275] **CSPFCSP(RII)** [292] **ΔRep, ΔNΔRep** [27] **ΔRI, ΔN full** [214].

partial glycosylation of the nearby threonine with a O-fucose or O-glucosylfucose disaccharide [373]. Structurally this is expected to results in shielding of the cysteine-cysteine disulfide bond by the sugar group.

Deletion of the GPI-anchor addition sequence or replacement with the transmembrane domain of TRAP resulted in no sporozoite formation [349]. Despite the problems that in these experiments rhomboid cleave could occur and potential micronemal targeting as the transmembrane domain used in the experiments was that of TRAP, sporozoite formation was completely blocked with the protein localized to the PM of the oocyst as in WT. This suggests that the GPI-anchor itself might be crucial for CSP function during sporozoite formation [303, 360], possibly via raft formation anchoring the forming IMC (potentially via the internal proteins GAP45) or by tight packing [353] and increased stability on the surface [349].

The mutation of only four base pairs in the conserved Region II+ within the α-TSR domain results in a block of sporozoite egress from the oocyst but has no impact on sporozoite formation [275]. Deletion of the core 20 amino acids of the α-TSR domain in another study resulted in sporozoites that do not enter salivary glands or hepatocytes, but oocyst egress was not assessed in this study making it likely that the phenotypes are similar [292]. Additionally, both mutants, when injected as midgut derived sporozoites IV into mice, failed to cause an infection, in contrast to midgut sporozoites from wild type.

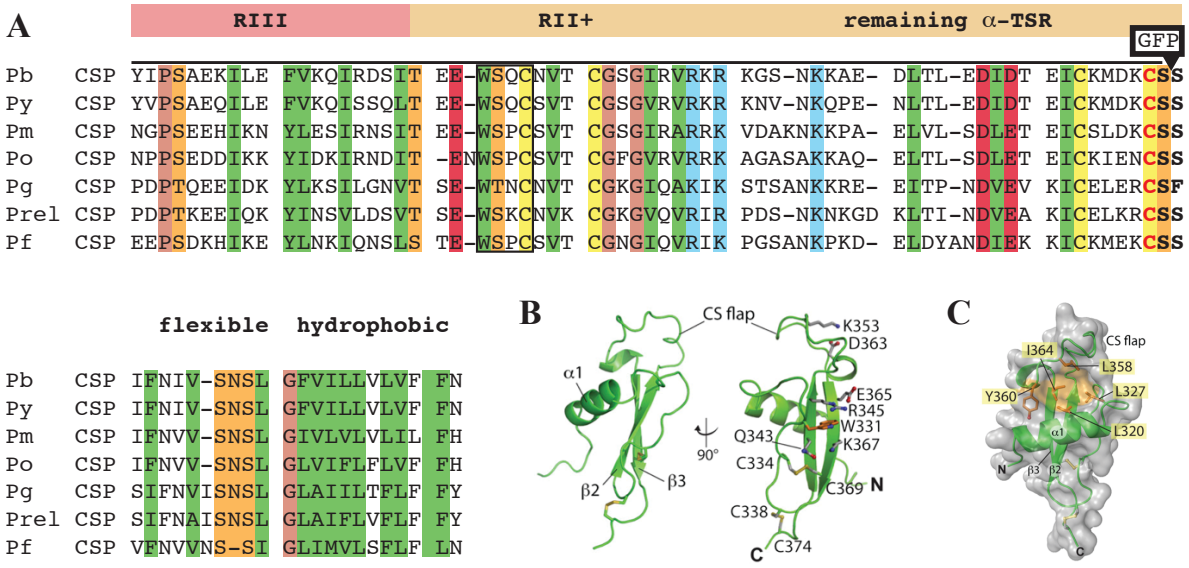

Figure 1.8: C-terminus of CSP of different species.
A Alignment of amino acids was manually curated to condense in size and highlight conserved features of CSP. Conserved residues are colored according to type, green = hydrophobic, red = acidic, blue = basic, orange = charged, pink = prolin and glycine, yellow = cysteine. Region III and Region II+ are both part of the α-TSR domain. The glycosylation motif WXXC is highlighted with a box [373]. The amino acid that is GPI-anchored, the ω-site, is indicated in **bold red**, followed by the residues ω+1 and ω+2, highlighted in **bold** (prediction with PredGPI [392]). The GPI-anchor additions signal also consists of the flexible and the hydrophobic region, which are cleaved upon GPI-anchor addition. The site where GFP is inserted in the mutant CS III (including two linkers of eight glycine) is indicated. This results in a modified ω-site DELYK**GAG**GGGGG, resulting in GPI-anchor addition to the second last C-terminal amino acid of the GFP. The sequence of the peptide used to generate the C-terminal antibody is highlighted by a black line on top of the alignment [387]. **B** Structure of α-TSR **C** Structure of α-TSR in surface representation, the hydrophobic pocket is shown in orange. Both **B** and **C** are from [391].

Processing of CSP

A field with many believes and very little reliable data is the processing of CSP which has been intensively debated. There are speculations about the potentially different forms of CSP, proteins involved in the processing and biological processes that are regulated by CSP processing. The biggest evidence today about the state of CSP is the recent data that has been generated via mass spectrometry of sporozoites and the surface proteome of sporozoites [373, 393]. This data suggests that CSP is mainly present from the last two amino acids of Region I, suggesting that **QP** (of **KLKQP**) might be the effective N-terminus of CSP. Direct N-terminal protein sequencing has so far been unsuccessful (personal communications - Photini Sinnis). The central part of the repeat is poorly resolved via mass spectrometry due to its repetitive nature and the last amino acids of the C-terminus detectable are the sequence **KICKMEK** directly preceding the ω-site cysteine.

The first evidence of CSP itself showed evidence that several processing states are

present on sporozoites, 44 kDa, 52 kDa and 54 kDa in size for *P. berghei* [372]. It was shown that the N-terminus of CSP is cleaved upon hepatocyte contact by an until today uncharacterized cystein protease [387]. This process depends mainly on Region I, precedes cell invasion and is suggested to occurs in front of Region I. This cleavage is a requirement for cell invasion. Sporozoites lacking the complete N-terminus adhere unspecifically to all mosquito tissues thus reducing salivary gland invasion [214]. It has also been shown that a CSP binding protein is localized to the salivary glands that binds CSP, much like the proposed relationship between saglin and TRAP [394]. In the mammal, sporozoites lacking the N-terminus invade cells directly at the inoculation site in the skin but efficiently invade hepatocytes after IV injection. Sporozoites that only lack Region I show reduced CSP cleavage, resulting in reduced invasion of hepatocytes [214]. Similar experiments with *P. falciparum* CSP in the *P. berghei* parasite background observed no phenotype in the Region I deletion [292]. The effect in this study might have been masked by the reduced infectivity of the *P. berghei* sporozoites with *P. falciparum* CSP, which might result from reduced protein levels, reducing the necessity for efficient protein cleavage. Also it has been shown that the C-terminus of *P. falciparum* CSP on *P. berghei* sporozoites is accessible in contrast to that of WT parasites, negating the necessity for cleavage.

It was recently suggested that the initial binding of CSP to hepatocytes which has been linked to Region II+ of the C-terminus [395] is mediated by a lysine-rich site located just before the Region I within the N-terminus [396]. It is unclear how this binding triggers CSP cleavage on the surface of sporozoites, but it is clear that presence of hepatocyte triggers cleavage of the N-terminus [387]. These results indicate that CSP is involved in the transition from a migratory to an adhesive state and that this process is highly regulated to avoid premature adhesion. The current model is that the N-terminus of CSP masks the adhesive C-terminus prior to cleavage, thus CSP processing is regulating invasion of sporozoites. It has been previously shown that a small peptide of the lysine-rich site of *P. falciparum* including Region I could block invasion of sporozoites into the salivary gland, while the same region of *P. yoelii* CSP did not [397]. This is not surprising given that the lysine-rich region of *P. yoelii* CSP lies further upstream of Region I and was not included into the peptide (**Figure 1.5**). The fact that sporozoite expressing CSP lacking the entire N-terminus show lower invasion of the salivary gland but not of hepatocytes [214] suggest that for salivary gland invasion actual binding of the N-terminus might be more important, while for hepatocyte invasion processing is

crucial, and this might be initially triggered by N-terminal binding.

The structure of CSP

The complete crystal structure of CSP has not been resolved. Studies performed on small peptides of the repeat region of *P. falciparum* using nuclear magnetic resonance (NMR) suggested that the NANP repeat stabilizes into a type I β-turn [398]. Expression of the entire protein and analysis via atomic force microscopy as well as modelling of the entire repeat suggested that CSP is a flexible and highly extended protein and the repeat forms a long thin rod-like structure [399]. If the repeat region of other *Plasmodium* species takes up a similar fold has not been tested. It is expected that the conservation of the CSP repeat, especially on a genetic level, is due to its evolutionary expansion and has not been selected for to be repetitive in nature.

CSP and sporozoite biology

The first gene deletion generated in *Plasmodium* was the deletion of CSP in *P. berghei* [400]. This resulted in complete block of sporozoite formation within the oocyst [25]. So far, complete deletion studies post sporozoite formation have not been attempted, but it is generally assumed that CSP is essential for all sporozoite biology due to its extremely high expression level. Oocysts lacking CSP rapidly assemble the IMC and subpellicular microtubules underlying the entire PM before PM invagination in contrast to WT oocysts, which invaginate and then only initiate IMC formation at apical tip initiation of sporozoites [25].

Motile sporozoites leave CSP on the substrate when they glide, a process which has been termed trail formation or CSP shedding and is also observed in *T. gondii* tachyzoites with the major surface protein SAG1 [284, 297, 401]. Electron microscpy studies show the presence of tiny vesicular structures that are deposited on the surface and strongly increase in numbers if the surface has been coated with antibodies against CSP [401]. If the structure of the trail is vesicular in its native state or only after processing for electron microscopy and if a trail is formed in vivo is unclear. From experiments using antibodies binding CSP on live sporozoites the term circumsporozoite reaction or shedding of CSP has been termed [284, 372]. It was suggested that this is triggered by the crosslinking of CSP via antibodies. Judging from electron microscopy data [401] it is highly likely that the cross-linking results in the formation a small vesicles mainly consisting of PM with CSP and small volumes of cytoplasm. There is no evidence that proteins are solitarily

deposited on the surface without plasma membrane and CSP (with the exception of CELTOS [402]), and the fact that a multitude of other proteins have been detected in trails supports this [402]. It has also been suggested that CSP is secreted at the apical side of sporozoites, translocated to the rear end and subsequently forms the trail [403], however these results have been produced under artificial conditions and not reproduced.

It has been suggested that CSP is released into cells that are traversed within the liver [404] and that CSP manipulates traversed cells and not all of the traversed cells survive cell traversal [405]. On the parasite side hepatocyte traversal is most likely the strongest trigger for CSP processing and to switch into an invasive state [406].

The speculation of involvement of CSP into gliding motility has been based only on association [403] and has been hampered by the essentiality of high level CSP expression during sporozoite formation [25, 400]. It has been suggested that CSP produces a physical and immunological 'cover' for the essential players of sporozoite biology and liver cell invasion [407] but has also been shown to be crucial for salivary gland and hepatocyte invasion itself [214, 387], although this function might be more of a passive nature.

Chapter

2

Materials And Methods

2.1 Materials

Equipment

10x Apoplan objective (NA 0.25, water)	Carl Zeiss, Jena, Germany
25x Objective (NA 0.8, water)	Carl Zeiss, Jena, Germany
4x Laemmli Sample Buffer	Bio-Rad Laboratories GmbH, München, Germany
40x CP-Acromat (NA 0.65 Ph2)	Carl Zeiss, Jena, Germany
60x Apochromat TIRF (NA 1.49, oil)	Nikon, Tokyo, Japan
63x Objective (NA 1.4, oil)	Carl Zeiss, Jena, Germany
100x A-Plan (NA 1.25, oil)	Carl Zeiss, Jena, Germany
100x Apoplan objective (NA 1.25, oil)	Carl Zeiss, Jena, Germany
100x Plan Apo VC objective (NA 1.4 oil)	Nikon, Tokyo, Japan
Amaxa Nucleofector II	Lonza, Köln, Germany
Analytic scale TE1245-OCE	Satorius, Göttingen, Germany
Autoclave	Holzner, Nußloch, Germany
Axiostar plus	Carl Zeiss, Jena, Germany
Axiovert 200 with XL-3 incubator	Carl Zeiss, Jena, Germany
Binocular Nikon SMZ 1500	Nikon, Tokyo, Japan
Cabinet dryer	Heraeus, Hanau, Germany
CCD camera EASY 440 K	Herolab, Wiesloch, Germany
Centrifuge 5417 R (cooled)	Eppendorf, Hamburg, Germany
Centrifuge Galaxy Mini	VWR, Darmstadt, Germany
Centrifuge Heraeus BioFuge pico	DJB Labcare, Buckinghamshire, UK
Centrifuge Heraeus Laborfuge 400e	ThermoScientific, Waltham, USA
Centrifuge J2-21M/E	Beckman, Krefeld, Germany
Centrifuge Heraeus Multifuge 1 S-R	DBJ Labcare, Buckinghamshire, UK
Counter DeskTally mechanical 4 Gang	TRUMETER, Manchester, UK
DAPI filter set 01 (365/395)	Carl Zeiss, Jena, Germany
Eppendorf tube 1.5 ml	Sarstedt, Nürnbrecht, Germany
Film developer Curix 60	Agfa, Mortsel, Belgium

Freezer -80 °C	New Brunswick Scientific, Edison, USA
Freezers	Liebherr, Ochsenhausen, Germany
GFP filter set 37 (450/510)	Carl Zeiss, Jena, Germany
GFP/RFP filter set 61 (474/527; 585/645)	Carl Zeiss, Jena, Germany
Heating block neoBlock 1	neoLab, Heidelberg, Germany
Heating block Thermomixer compact	Eppendorf, Hamburg, Germany
Incubator CO_2 Ihnova CO-170	New Brunswick scientific, Edison, USA
Incubator CO_2 MCO-17AI	Sanyo, München, Germany
Incubator Innova 400 shaker	New Brunswick scientific, Edison, USA
Incubator Multitron 2	Infors Incubator, Bottmingen, Switzerland
Liquid Nitrogen tank ARPEGE 170	Air liquide, Düsseldorf, Germnany
MAC5000 stage control	Ludl Electronics, Hawthorne, USA
magnetic stirrer	Carl-Roth, Karlsruhe, Germany
Microsoft Office 2004 software	Microsoft, Unterschleißheim, Germany
Microwave oven Micromaxx	Medion, Essen, Germany
Mini-PROTEAN Electrophoresis Cell	Bio-Rad Laboratories GmbH, München, Germany
Mini-PROTEAN TGX precast gels 4-15%	Bio-Rad Laboratories GmbH, München, Germany
motorized stage DC 120 x 100	Märzhäuser, Wetzlar, Germany
Restraining tube	custom build
Neubauer improved	Brand, Wertheim, Germany
Nikon coolpix 5400	Nikon, Tokyo, Japan
Nikon TE2000 inverted microscope	Nikon, Tokyo, Japan
Optical table	Newport, Irvine, USA
Orca ER EMD-CCD camera	Hamamatsu, Hamamatsu, Japan
Piezo driven stage	Physik Instrumente, Karlsruhe, Germany
Pipette Gilson (P2, P10, P200, P1000)	Gilson, Middleton, USA
Pipette Pipet lite 2-20 µl	Rainin, Oakland, USA
Pipettus SWIFTPET	ABIMED, Langenfeld, Germany
PH-Meter	Hanna Instruments, Kehl, Germany
Power supply (Electrophoresis) EV231	Consort, Turnhout, Belgium
Power supply (Electrophoresis) EV831	Consort, Turnhout, Belgium
Precision Plus Protein Dual Color	Bio-Rad Laboratories GmbH, München, Germany
RFP filter set 20 (546/575-640)	Carl Zeiss, Jena, Germany
Rotor Type Ja 10	Beckman, Krefeld, Germany
Safety cabinet FWF 90	Düperthal, Kleinostheim, Germany
Scale EW600-2M	Kern, Balingen, Germany
Silica cuvettes	Hellma Optik, Jena, Germany
Spectrophotometer SmartSpec plus	Bio-rad, München, Germany
Spinning disc confocal ERS-FRET	Perkin Elmer, Waltham, USA
Sterile Workbench Herasafe	Thermo, Waltham, USA
Sterile Workbench BSB 6	Gelaire, Sydney, Australia
Thermocycler Mastercycler ep gradient	Eppendorf, Hamburg, Germany
Timer	Oregon scientific, Neu-Isenburg, Germany
Transmogrifier	Simone's, Heidelberg, Germany
UV-table UVT-28 L	Herolab, Wiesloch, Germany
Vortex-Genie 2	Scientific Industries, Bohemia, USA
Waterbath Isotemp 210	Fischer Scientific, Swerte, Germany
Zeiss Axiocam HRm	Carl Zeiss, Jena, Germany

Disposables and chemicals

1 kb Plus DNA ladder	Invitrogen, Karlsruhe, Germany
10x Taq Buffer with $(NH_4)_2SO_4$	Fermentas, Burlington, USA
24 well culture plates	Greiner bio-one, Frickenhausen, Germany
384 well Assay plates	Corning, Corning, USA
5x Phusion GC & HF buffer	Thermo Fisher Scientific, Waltham, USA
96 well optical bottom plates	nunc, Rochester, USA
Acetic acid CH_3COOH	Zentrallager, Heidelberg, Germany
Agarose Serva research grade	SERVA, Heidelberg, Germany
Alsever's solution	Sigma Aldrich, München, Germany
Amaxa human T cell Nucleofector Kit	Lonza, Köln, Germany
Ampicillin sodium salt	Carl Roth, Karlsruhe, Germany
Anti-anti Antibiotic-Antimycotic	Gibco, Thermo Fisher Scientific, Waltham
Bacto-Yeast extract	Sigma-Aldrich, München, Germany
Bovine Serum Albumine, BSA fraction V	Carl Roth, Karlsruhe, Germany
Calcium chloride $(CaCl_2) \cdot 2H_2O$	Merck, Darmstadt, Germany
Cell culture flask Cellstar 250ml	Greiner bio-one, Frickenhausen, Germany
CIP Alkaline Phosphatase	New England Biolabs, Ipswich, USA
Cover slips 24x60 mm	Carl Roth, Karlsruhe, Germany
Cryovials CRYO.S	Greiner bio-one, Frickenhausen, Germany
D(+)-Glucose	Merck, Darmstadt, Germany
Diethyl ether	Sigma Aldrich, München, Germany
Dimethylsulfoxide (DMSO) HYBRI-MAX	Sigma Aldrich, München, Germany
dNTP Mix 2 mM each	Fermentas, Burlington, USA
Erlenmeyer flask 100 ml - 5 l	Schott, Mainz, Germany
Ethanol 100 %	Sigma Aldrich, München, Germany
Ethanol 96 %	Zentrallager, Heidelberg, Germany
Ethidium bromide 1 %	Carl Roth, Karlsruhe, Germany
Falcon tubes (15 ml, 50 ml)	Nerbe plus, Winsen, Germany
FBS 16000 Origin:US, GIBCO	Invitrogen, Karlsruhe, Germany
FCS	c.c.pro, Oberdorla, Germany
5-Fluorocytosine (5-FC)	Sigma-Aldrich, München, Germany
Gentamycin (10 mg/ml)	PAA, Pasching, Austria
Giemsa stain solution	VWR, Poole, UK
Glass-Bottom dish 10mm	MatTek, Ashland, USA
Glass-Bottom dish 14mm	MatTek, Ashland, USA
Glass-Bottom dish 24 well	MatTek, Ashland, USA
Gloves nitril	VWR, Darmstadt, Germany
Gloves peha soft satin	Hartmann, Heidenheim, Germany
Glycerol 99% waterfree	Zentrallager, Heidelberg, Germany
Heparin-Natrium 25000 U	Ratiopharm, Ulm, Germany
High Pure PCR Product Purification Kit	Roche, Mannheim, Germany
Imersion oil, ne = 1.482	Chroma, Münster, Germany
Immersol 518F, ne = 1.518	Carl Zeiss, Jena, Germany
Immersol W, ne = 1.334	Carl Zeiss, Jena, Germany
Insulin syringe U-100 1 ml	Bran, Melsung, Germany
Jaspakinolide	CalBiochem, La Jolla, USA
Kanamycin	Sigma-Aldrich, München, Germany
Ketamine hydrochloride solution	Sigma Aldrich, München, Germany

Methanol 100%	J.T. Baker, Phillipsburg, USA
Microscope slide	Menzel, Braunschweig, Germany
Midori Green	Nippon Genetics Europe, Düren, Germany
$MgCl_2$, Reaction Buffer	Fermentas, Burlington, USA
Needles	BD GmbH, Heidelberg, Germany
Nycodenz	Axis-shield, Heidelberg, Germany
Parafilm	Pechiney plastic packaging, Menasha, USA
Paraformaldehyd, PFA	Riedel-de Haën, Seelze, Germany
Pasteur capillary pipettes	WU, Mainz, Germany
PCR tubes Quali, 8-strips	G.Kisker GbR, Steinfurt, Germany
Penicillin/Streptomycin 100x	PAA, Pasching, Austria
Petri dish	Greiner bio-one Frickenhausen, Germany
pGEM-T Easy Vector Systems	Promega, Madison, USA
PBS with Ca & Mg	PAA, Pasching, Austria
Phusion polymerase	Thermo Fisher Scientific, Waltham, USA
Plastic Pipettes (5 ml, 10 ml, 25 ml)	Greiner bio-one Frickenhausen, Germany
Platinum Taq DNA Polymerase	Invitrogen, Karlsruhe, Germany
Pipette tips	Gilson, Middleton, USA
Plastic pistil	Greiner bio-one Frickenhausen, Germany
Potassium chloride	Merck, Darmstadt, Germany
ProLong Gold antifade reagent	Invitrogen, Karlsruhe, Germany
Protease Inhibitor	Roche, Mannheim, Germany
Pyrimethamine	Sigma Aldrich, München, Germany
QIAamp gDNA Blood Mini Kit	Qiagen, Hilden, Germany
QIAprep Spin Miniprep Kit	Qiagen, Hilden, Germany
QIAquick PCR Purification Kit	Qiagen, Hilden, Germany
QPCR SEAL optical clear film	VWR, Darmstadt, Germany
Restriction Enzymes	New England Biolabs, Ipswich, USA
Restriction Enzymes	Fermentas, Burlington, USA
Restriction buffers (buffer 1, 2, 3, CutSmart)	New England Biolabs, Ipswich, USA
Restriction buffers	MBI Fermentas, Burlington, USA
RPMI 1640 + L-Glutamine - Phenol Red	PAA, Pasching, Austria
Saponin from Quillaja bark	Sigma Aldrich, München, Germany
Sea salt, NaCl	Alnatura, Bickenbach, Germany
SIR-Tubulin	Spirochrome, tebu-bio, Offenbach, Germany
Sodium acetat, $Na(CH_3COO) \cdot 3H_2O$	Merck, Darmstadt, Germany
Sodium cloride, NaCl	J.T. Baker, Phillipsburg, USA
Sodium dihydrogen phosphate, NaH_2PO_4	J.T. Baker, Phillipsburg, USA
Sodium hydroxide, NaOH	Sigma-Aldrich, München, Germany
Sterile filter	Merck, Darmstadt, Germany
Sterile Filter Unit 1000 ml	Nalgene, Rochester, USA
SuperSignal West Pico Chemiluminescent	Thermo Fisher Scientific, Waltham, Substrate USA
SuperSignal West Femto Maximum	Thermo Fisher Scientific, Waltham, Sensitivity Substrate USA
Syringe cannula Microlance 3 (20G, 27G)	BD, Heidelberg, Germany
Syringe Plastipak (1 ml, 5 ml)	BD, Heidelberg, Germany
T4 DNA Ligase	Fermentas, Burlington, USA
T4 DNA Ligase Buffer	Fermentas, Burlington, USA
Taq DNA Polymerase	Fermentas, Burlington, USA
Trans-Blot Turbo Mini 0,2 µm Nitrocellulose	Bio-Rad Laboratories GmbH, München, Germany
Transfer Packs	Bio-Rad Laboratories GmbH, München, Germany

TRIS	Carl Roth, Karlsruhe, Germany
Triton X-100	Merck, Darmstadt, Germany
Trypsin / EDTA 10x	c.c.pro, Oberdorla, Germany
Tween 20	Carl Roth, Karlsruhe, Germany
X-Gal	Neolab, Heidelberg, Germany
XL1-Blue competent cells (*E.coli*)	Stratagene, La Jolla, USA
Xylazine hydrochloride solution	Sigma Aldrich, München, Germany

Software and webservices

ApE v2.0.45	Biologlabs, Utah, USA
Axiovision 4.6 software	Carl Zeiss, Jena, Germany
CLC Main Workbench 7.9.1	CLC bio, Qiagen bioinformatics, USA
FIJI is just imageJ	LOCI, Wisconsin-Madison, USA
Prism 5	GraphPad Software, CA, USA
Illustrator CS5.1 software	Adobe, München, Germany
Photoshop CS 5.1 software	Adobe, München, Germany
Texshop 3.75	Rochard Hoch
Volocity 6.1.1.	Perkin Elmer, Waltham, USA

clustal Omega	www.ebi.ac.uk/Tooks/msa/clustalo/
GeneDB	www.genedb.org/Homepage
OPTIMIZER	http://genomes.urv.es/OPTIMIZER
PlasmoDB	plasmodb.org/plasmo/
PredGPI	gpcr.biocomp.unibo.it/predgpi/pred.htm
SignalIP 4.1	www.cbs.dtu.dk/services/SignalP/
SMART	smart.embl-heidelberg.de
STRING	https://string.db.org
TREE OF LIFE web project	http://tolweb.org/tree/phylogeny.html

Antibodies

α-PbHSP 70 antibody	[408]
α-CSP repeat - mAB 3D11	[409]
α-Uis4 polyclonal antibody	(Julia Sattler, unpublished)
α-c-terminus CSP	kind gift of Photini Sinnis [387]
α-GFP antibody 13.1 + 7.1	Roche, Merck, Darmstadt, Germany
α-GFP antibody, ABfinity	ThermoScientific, Waltham, USA
Alexa Fluor 488 goat anti-mouse IgG antibody	Invitrogen, Karlsruhe, Germany
Alexa Fluor 488 goat anti-rabbit IgG antibody	Invitrogen, Karlsruhe, Germany
Alexa Fluor 594 goat anti-mouse IgG antibody	Invitrogen, Karlsruhe, Germany
Alexa Fluor 594 goat anti-rabbit IgG antibody	Invitrogen, Karlsruhe, Germany
Cy5 goat anti-rabbit IgG antibody	Abcam, Cambridge, UK
Alexa Fluor 647 goat anti-rabbit IgG antibody	Invitrogen, Karlsruhe, Germany
goat anti rabbit HRP	Bio-Rad Laboratories GmbH, München, Germany
goat anti-mouse HRP	GE healthcare, ThermoScientific, Waltham, USA

Media

Agar-LB Medium	15 g/l Agarose in LB-Medium
Ampicillin 1000x	100 mg/ml Ampicillin in dd H_2O
Freezing solution	10% (v/v) Glycerol in Alsever's solution
KX solution	PBS 10% (v/v) Ketamine 2% (v/v) Xylazine
LB-Medium	H_2O 10 g/l NaCl 10 g/l Bacto-Tryptone (Peptone) 5 g/l Bacto-Yeast extract
Nycodenz stock	500ml pH 7.5 0.394 g Tris/HCl 0.112 g KCL 0.056 g Na_2EDTA 138 g Nycodenz add DI H_2O
PBS	dd H_2O 137 mM NaCl 2.7 mM KCl 8 mM dd Na_2HPO_4 1.8 mM dd KH_2PO_4 pH = 7.4
Pyrimethamin drinking water	tap water 280 µM Pyrimethamin from stock pH = 3.5-5.5 (prefereably pH 5) with HCl
Pyrimethamin stock	28 mM Pyrimethamin in DMSO
T-Medium	RPMI 1640 20% (v/v) FCS (US!) heat inactivated 56 °C 0,03% Gentamycin
TAE 50x	242 g Tris 100 ml 0.5 M Na_2EDTA (pH 8.0) 57.1 ml CH_3COOH add 500 ml dd H_2O

2.2 Methods

2.2.1 Molecular biological methods

DNA purification

Plasmids were isolated from *E. coli* using ether the QIAprep Spin Miniprep Kit or the AccuPrep Plasmid Mini Extraction Kit. For purification of DNA from restriction enzyme digest or gels the high pure PCR product purification kit was used according to the manual. Genomic DNA of parasites was extracted with the DNAeasy Blood and Tissue Kit. If parasites DNA was purified from blood, the blood was diluted in PBS to a final volume

of 14 ml with 0.2 % (w/v) saponin, centrifuged for 8 min at 2800 rpm at 4 °C with brake. The pellet was resuspended in 1 ml PBS, centrifuged for 2 min at 7000 rpm at 4 °C, then the pellet was resuspended in 200 µl PBS. At this time the pellet was stored at -20 °C or directly proccssed with the DNAeasy Blood and Tissue Kit.

Restriction enzyme digestion

Digestion of DNA with restriction endunucleases was done to specifically cut vector and insert DNA for cloning procedures or control digests. For all restriction enzymes, provided buffers were used in the appropriate concentrations. Reaction time was between one hour and over night, depending on stability of the enzyme and quality of the digestion. Triple digest were avoided by sequential digests.

Ligation

The insert and the desired vector, both digested with the appropriate restriction enzymes (the vector was also digested with CIP alkaline phosphatase), were incubated for 3 h at room temperature (or 16 °C over night) under the following conditions:

	L1	*L2*	*L3*
vector	1 µl	1 µl	1 µl
insert	7 µl	3 µl	0 µl
buffer	1 µl	1 µl	1 µl
ligase	1 µl	1 µl	1 µl

If a PCR-product was used as insert and cloning proved troublesome, one extra subcloning step was included. Without restriction enzyme digestion, the PCR-product was directly cloned into the pGem-T easy vector using the pGEM-T Easy Vector Systems cloning kit.

Polymerase chain reaction

Polymerase chain reaction (PCR) was used for gene amplification of a specific piece of DNA. Preparative PCR with hifi Taq (high fidelity Taq polymerase) or Phusion Taq was used for genomic DNA (gDNA) or a plasmid as template. Analytic PCR with Taq polymerase was used for colony PCR or to analyze gDNA for integration or knockout of a specific sequence. Assembly PCR was used to fuse two PCR products with a small linker region. To do this the internal primers produces an internal overlapping product with a melting temperature of 68 °C. After 5 reaction cycles the outer primers were added and the fused product was amplified. Small mutagenesis PCR was also performed in an assembly PCR style.

In all cases the lowest melting temperature of the primers was used as the annealing temperature. The reaction temperature for the polymerase was reduced from 68 °C to 60°C in case of *Plasmodium berghei* sequences, since this increases the synthesis of the AT-rich DNA. Following reaction mixes where used:

Reaction mix Taq		*PCR program*		
0.25 µl	Primer 1	94 °C	5’	
0.25 µl	Primer 2	94 °C	30”	⎤
2.5 µl	10 x buffer	var. °C	30”	⎥ 25x
1.5 µl	$MgCl_2$ (25 mM)	60 °C	1’ per 1000 bp	⎦
			+ 30”	
2.5 µl	dNTPs	60 °C	10’	
0.25 µl	Taq	4 °C	pause	
1 µl	Plasmid or gDNA			
ad 25 µl	dd H_2O			

Reaction Mix hifi		*PCR program*		
0.25 µl	Primer 1	94 °C	5’	
0.25 µl	Primer 2	94 °C	30”	⎤
5 µl	10 x buffer hifi	var. °C	30”	⎥ 25x
1.5 µl	$MgSO_4$	60 °C	1’ per 1000 bp	⎦
			+ 30”	
5 µl	dNTPs	60 °C	10’	
0.2 µl	Taq-hifi	4 °C	pause	
1 µl	Plasmid or gDNA			
ad 50 µl	dd H_2O			

Reaction Mix	Phusion	*PCR program*		
0.5 µl	Primer 1	98 °C	5’	
0.5 µl	Primer 2	98 °C	15”	⎤
10 µl	5x Phusion buffer	var. °C	30”	⎥ 25x
5 µl	dNTPs	60 °C	1’ per 2000 bp	⎦
			+ 30”	
0.5 µl	Phusion	72 °C	10’	
1 µl	Plasmid or gDNA	4 °C	pause	
ad 50 µl	dd H_2O			

quantitative PCR

Quantitative PCR was performed on genomic parasite DNA. Primers were designed to generate products of around 150 bps. qPCR was performed using SYBR Green PCR master mix with an ABI7500 thermo cycler. Reaction was 40 cycles with 15 s denaturation at 95 °C and 1 min elongation at 60 °C. Reaction volumes were 12,5 µl per technical duplicate. Data analysis was performed using the $D^{\Delta\Delta CT}$ method.

Electrophoresis of DNA

Separation of DNA fragments by size was performed by electrophoresis in agarose gels. Gels were prepared from 0.8% - 2% agarose solution in TAE buffer stored at 60 °C depending on the size of the DNA fragment. In order to visualize DNA after the electroporation, 3 µl of Ethidium bromide solution (1%) was added to 35 ml of agarose solution (10 µl / 150 ml) prior to polymerization or 1 µl / 1 ml of mindory green was added to the loading dye. Gel pockets were loaded with DNA with 1/5 (v/v) of 5x DNA loading buffer and electrophoresis was performed in TAE buffer at 80 -300 V for 7 - 45 min. Visualization of gels was performed on the UV table and images captured with CCD camera EASY 440 K.

Sequencing

From a standard miniprep, 10 µl of plasmid were diluted with 25 µl of dd H_2O. If non-standard primers are necessary, they were diluted 1:10 in dd H_2O. Direct sequencing of PCR products was performed on purified and undiluted DNA. Probes were placed in the GATC drop box at DKFZ Heidelberg and sequenced by GATC, Konstanz, Germany. Sequences were checked for mutations by comparison with database sequences using the web-application clustalW (http://www.ebi.ac.uk/Tools/clustalw2/index.html).

Transformation

After thawing of 35 µl of XL1-Blue competent cells, 0.68 µl of ß-mercaptoethanol were added and the cells were incubated for 10 min on ice. Then 2 µl of the ligation product or 1 µl of a 1:1000 dilution of the plasmid were added and the cells were incubated for 30 min on ice. A heating block was prewarmed to 42 °C, the bacteria were incubated for 46 s on 42 °C, then stored on ice for 2 more minutes. In case of ampicillin resistance, 200 µl of prewarmed (37 °C) LB-medium was added and the bacteria were plated onto a petri dish with LB-agar containing 100 µg/ml ampicillin. If the transformation was done with the pGem-T easy vector, 20 µl XGal and 100 µl IPTG were added instead of LB-Medium to allow for blue/white selection.

2.2.2 Animal handling

While conduction of animal experiments, great care has to be taken to avoid or reduce stress and pain for the animals. Also, animal numbers should be kept as low as possible. One of the most important ways to reduce stress is to be experienced in your handling techniques, so the procedure is applied calm and fast.

2.2.3 Injections

Different injection types were used for different applications.

i.p. Intraperitoneal injections were used to inject stabilates of infected blood, fresh infected blood, KX solution or WR solution with a 27G cannula. The mouse was pulled slightly to the back so it stretches, then fixed with forefinger and thumb in the neck, placed on the folded middle and ring finger and fixed with the little finger at the base of the tail. The mouse was held inclined with the head as the lowest part, so guts slide towards the head. Now, the cannula was injected into the lower abdomen in a ≈ 45 ° angle and the sample, not more than 300 µl, was injected.

i.v. Intravenous injections were used to inject freshly transfected schizonts, sporozoites or infected blood. The mouse was placed into the restraining tube, and the tail was warmed in warm water to dilate the veins. The volume to inject loaded into an insulin syringe. Then not more then 200 µl were injected into one of the lateral veins of the tail.

Cardiac puncture

If higher volumes of blood were required, blood was withdrawn by cardiac puncture. This is a final procedure which always ends with killing of the mouse. A 1 ml syringe was prepared by coating it with heparin, then the mouse was anesthetized with diethyl ether. After checking for reflexes, the blood was withdrawn from the atrium. After that, the mouse was killed by cervical dislocation.

2.2.4 Cervical dislocation

To kill an animal fast while reducing the stress during the procedure, mice were killed by snatching the neck so the carotid arteries rupture and the spinal cord becomes separated. After the mouse is anesthetized, the head was fixed while pulling the base of the tail in a ≈ 45 ° angle to the back.

2.2.5 Parasite handling

Stabilates of infected blood

Whenever necessary, stabilates of infected blood were prepared. The desired number of cryovials were prepared with 200 µl of freezing solution, labeled and stored on ice. The blood was drawn by cardiac puncture, then 100 µl of blood was added to each cryovail, which were stored directly in liquid nitrogen.

Transfection and selection

Transfection was essentially performed as described before [203]. In order to gain synchronized schizonts for transfection of *Plasmodium berghei*, infected mouse blood was cultured over night. One ml blood with 5 % parasitemia is sufficient for 5-10 transfections. The following procedure is described for blood from one mouse (2-3 mice regarding numbers in brackets).

Under a sterile workbench 75 ml (200 ml) of T-medium was prepared, sterile filtered and stored at 37°C. A cell culture flask was prepared with 20 ml (100 ml) of T-Medium and stored at 37°C. Also, a 15 ml (50 ml) falcon tube was filled with 10 ml T-Medium and 250 µl Heparin and stored at 37°C.

The infected blood was gained by cardiac puncture from the infected mouse, added to the prepared falcon tube and centrifuged 8 min at 1000 rpm. 10 ml (20 ml) of T-Medium were added to the pellet and added to the prepared cell culture flask. The falcon tube was flushed with 4 ml (15 ml) of T-Medium twice, and added to the cell culture flask as before. The cell culture flask was placed in the incubator at 37 °C, 90 % N_2, 5 % O_2 and 5 % CO_2. After 15 min, the culture was agitated at 77 rpm and incubated for 16-18 h. Incubation without agitation provided identical results.

The selection for *Plasmodium berghei* transfectants was performed after transfection or to reselect a non-clonal strain. In the normal case, selection was done with pyrimethamine, which was administered with the drinking water until the parasitemia reached 2-5 % (normally $\approx$ 7-10 days post transfection).

Counting of blood parasitemia by bloodsmear

A sterile cannula was used to pierce a little hole in the skin of the tip of the mouse tail. One drop of blood was collected onto a glass slide and distributed with the border of a second glass slide to obtain a single layer of erythrocytes. The smear was fixed in 100% methanol for 1 min and then transferred into a 10% Giemsa staining solution. After 20 minutes the slides were washed with tap water and air dried.

After addition of one drop of immersion oil, the bloodsmear was examined under a microscope with an 100x Apoplan objective (NA 1.25, oil). In a region with similar distribution of erythrocytes, the number of erythrocytes in one field of view was counted. Then, infected erythrocytes were counted in 12 fields and parasitemia was calculated.

Determination of exflagellation

With a sterile cannula a little hole was pierced into the skin of the tip of the tail. One drop of blood was collected onto a glass slide and covered with a cover slip. The sample was stored for 10 minutes at 20 °C, then checked for exflagellation events under a microscope with an 40x objective. In a single layer of erythrocytes, 1-3 exflagellation events per field of view were considered acceptable for mosquito infection, more than 3 as good.

Rearing of *Plasmodium berghei* infected mosquitoes

Mosquitoes of *Anopheles stephensi* (Strain Sda 500) were reared in the insectary of the department of parasitology in Heidelberg under standard conditions at 28°C. Ideally, about 3 days before hatching of the mosquitoes, the desired strain of *Plasmodium berghei* was chosen and a stabilat of infected blood was injected i.v. in one mouse. In the case of normal bloodstage development the parasitemia ranged between 1-5 % after 4 days. Then, 2 mice were infected with i.p injection of 20 million infected erytrocytes. After 3 days, both mice were tested for exflagellation. Mosquitoes, now 3-11 days post hatching, were starved over night or at least 4 hours, then an infected mouse with good exflagellation was anesthetized with 110 µl of KX solution. The mouse was placed on

top of the mosquito cage on its back, ears flipped so they are easily accessible by the mosquitoes. After 40-60 minutes, if most mosquitoes completed their bloodmeal, they were transferred into the incubator at 21 °C. After one day with only 1 % sea salt solution and no sucrose, to kill off most of the undesired male mosquitoes, they were fed with 1 % sea salt and 10 % sucrose pads.

Sporozoite preparation

Mosquitoes infected with *Plasmodium berghei* were usually used 17-30 days post infection. From day 17 on, most sporozoites reached the salivary glands and could be harvested by dissection. The desired number of mosquitoes was taken from the cage and stored on ice for a few minutes. Mosquitoes were washed in 70 % Ethanol to reduce hydrophobicity of the cuticle and stored in PBS. Now mosquitoes were dissected in PBS under a Binocular Nikon SMZ 1500 with GFP illumination using two G27 cannula on 1 ml syringes. The abdomen was removed pulling at the last two segments with a cullula. The emerging midgut was collected in a seperate eppendorf tube filled with 50 µl of PBS. The head was pulled of the thorax, salivary glands were taken up with one cannula, and transferred into 50 µl of PBS or RPMI on ice. Still in the intact salivary glands, sporozoites can be stored for a few hours on ice. To release sporozoites midguts or salivary glands were homogenized with a plastic pistil prior to usage.

For hemolymph preparation hand modified pasteur capillary pipettes were used. The last two segments of the abdomen were removed, then the tip of the pipette was inserted into the spiracle of the mesothorax. Carefully pressure was applied to rinse the hemolymph with the desired medium, then 1-3 drops of liquid were collected from the end of the abdomen. For comparative countings haemolymph, midgut and salivary glands were prepared from the same mosquitoes in this order.

Purification of sporozoites

Sporozoites from midgut or salivary glands were purified using a 17% (w/v) Accudenz solution [410]. Sporozoites were released by hmogenization with a plastic pistil, diluted in 1,5 ml was PBS and transferred into a 15 ml falcon tube. 3 ml of Accudenz solution was underlayered below the sporozoite solution and centrifugation was performed at RT at 2500 g for 20 min. The upper- and interphase was removed with a pipet, mixed and pelleted for 1 min. The pellet was then resuspended in the desired buffer.

Cultivation of mammalian cells

Huh7, HepG2 and Hela cells were cultured in tissue culture flasks. For continuous cultivation cells were grown to a confluent cell layer and then split 1:10. To split adherent cells, the cells were washed with 10 ml of pre-warmed PBS, then incubated with 3 ml of trypsin solution for 10-30 minutes. As soon as the cells were rounded up and floating in the medium, 7 ml of PBS was added. The suspension was homogenized by pipetting up and down, then all but 1:10th of the volume was removed. 15 ml of complete medium was added and the cells were incubated at 5 % CO_2 and 37 °C. If cells were cultivated in 24 well labTek slides, volumes were adjusted to 1 ml complete medium and 200 µl Trypsin.

Sporozoite infection of Huh7 and HepG2 cells

Liver cells were infected with freshly dissected sporozoites. For this purpose mosquitoes were washed 3 times in 70 % EtOH and 3 times in H_2O. Sporozoites were directly dissected in cell culture media containing 10% FBS. Cells were washed once with PBS, and then 20.000 sporozoites were added in a volume of 200 µl per well for a 24 well plate or adjusted volumes for other containers. Sporozoites were incubated for 2 h at 37 °C, then cells were washed with PBS and liver stages were cultured in cell culture media supplemented with Anti-anti. Medium was changed every 24 h.

2.2.6 Western blotting

Samples for western blotting were isolated and prepared on ice. Sample was lysed in fresh ice-cold RIPA buffer with protease inhibitor at least one hour on ice. Sample was then resuspended by flicking the tube and aliquots

stored at -80°C at this timepoint. The desired volume was mixed with 4X Laemmli Sample Buffer, incubated for 5 min at 95 °C, briefly cooled on ice and centrifuged for 1 min at 13.000 rpm. The supernatant was loaded on 4-15% precast gels with marker a separated by electrophoresis. Sampes were semi-dry transferred using the BioRad Transblot turbo system. All following incubation steps were performed in PBS-T (PBS with 0,1% Tween 20. The membrane was blocked with 5% milk powder for one hour. Primary antibody was incubated ON (over night) at 4°C with gentle agitation. Sample was washed at least 3 times and incubated with the secondary antibody 1:10 000 for one hour. Sample was washed at least 3 times, incubated with SuperSignal West Pico Chemiluminescent solution and developed. If samples were reprobed with a separate antibody, the HRP bound to the blot was exhausted by incubation with 30% H_2O_2 for 30 minutes, washed extensively and reprobed with the second primary antibody.

2.2.7 Fluorescence microscopy

Imaging was performed at an inverted Axiovert 200 M microscope from Zeiss, at a spinning disc confocal from PerkinElmer using a Nikon inverted microsocope or a TIRF setup Axiovert 200 M microscope from Zeiss.

Gliding assay

Gliding assays were performed with salivary gland sporozoites or haemolymph sporozoites in RPMI with 3% BSA or with purified midgut sporozoites in RPMI with 3% BSA unless stated otherwise. Sporozoites we settled in a 96-well plate with optical bottom by centrifugation at 800 rpm for 3 minutes. Sporozoites were imaged for 180 second with 1 fps.

Immunofluorescence analysis

Immunofluorescence analysis was performed a various samples under varying conditions. In brief, the sample was fixed as rapid as possible in 4% paraformaldehyde (PFA) solution for 1 hour till overnight. Sample was washed 3 times with PBS for 5 minutes, blocked and permeabilized with PBS with 3% BSA and 0,5% Triton-X-100. Subsequent washing steps were performed with PBS with 3% BSA and 0,2% Triton-X-100. Incubation of primary antibodies was performed for 1 hour or overnight. Following the sample was washed three times and incubated with the secondary antibody supplemented with Hoechst 33342 (1:1000 of a 10 mg/ml stock solution in DMSO) for 1 hour. The sample was washed at least three times and mounted with ProLong Gold Antifade Reagent.

Microscopy of midguts and oocysts

Live cell microscopy of midguts was performed in PRMI with 3% BSA. If desired, a staining was performed prior to microscopy. To do so midguts were directly dissected into PRMI with 3% BSA supplemented with SIR-Tubulin [411] staining and Hoechst 33342 (1:1000 of a 10 mg/ml stock solution in DMSO) and incubated for 10 minutes. Then the medium was briefly exchanged against PRMI with 3% BSA, the sample covered and sealed with a 1:2:1 mixture of lanolin:parraffin:vaseline.

FRAP

Fluorescence recovery after photobleaching (FRAP) microscopy was performed using the PerkinElmer Nikon spinning disc confocal with the Volocity FRAP software using the UltraVIEW FRAP unit. FRAP was performed during imaging with 4 or 5 pfs, and an area of 20 x 20 or 25 x 25 pixels was bleached. Settings used were: PK cycles = 5, PK step size = 1, Spot period = 50, PK Spot Cycles = 15-20, PK spot size = small. Bleaching laser intensity was set to 100% for 405 nm, 440 nm, 488 nm, 514 nm, 561 nm and 640 nm. Prior to imaging FRAP calibration was performed using a glass cover slide painted with edding marker. Comparative imaging was always performed within the same calibration using the same settings. For analysis, the fluorescent intensity was determined for area frame for the bleached area (b), a control area (c) within the same sporozoite and a background area (n), all of identical size. The mean fluorescent intensity was determined for every frame. Corrected bleached values were calculated ($f = (b - n)/(c - n)$) and minimum (mi) and maximum (ma) intensity after the bleaching was

determined. From this the half recovery value was calculated ($t1/2 = (ma - mi)/2$). The second time point (to avoid premature apparent recovery due to quantification errors) (t1/2 was exceeded was used to calculate the time of half recovery.

Deconvolution and Image analysis

Deconvolution was performed using the Autoquant X3 software. In cases where localization of fluorescence is displayed to give structural information and no quantification is performed, background substraction was performed and image intensities were adjusted using the sqareroot. If image intensities were measured, image modifications required for efficient thresholding performed to generate a thresholding mask. This was then applied on the raw data and fluorescent intensities were measured. General image handling was performed with imageJ and Adobe Photoshop. Figures were prepared in Adobe Illustrator.

2.2.8 Electron microscopy

Electron microscopy was performed with the Electron Microscopy Core Faciility (EMCF) of the Heidelberg university. Midguts were dissected directly into the fixation buffer and sample preparation was performed by the core facility (Steffi Gold), using classical chemical fixation. Primary fixation was performed in 2%Glutaraldehyd with 2% PFA in 100 mM Caco buffer at 4 °C ON. Sample was washed 3 times with 100 mM Caco buffer and secondary fixation was performed with 1% Osmium in 100 MM Caco buffer for 60 min at RT. Sample was washed twice in Caco buffer, twice in dd H_2O and contrasted in 1% Uranylacetat in dd H_2O at 4 °C ON. Sample was washed in dd H_2O twice and dehydrated in 30%, 50%, 70%, 90%, 100% and 100% Aceton for 10 minutes each. Sample was then embedded in Spurr resis and for this incubed in 25%, 50% and 75% 45 min at RT each and in 100% at 4 °C ON. Embedding was finalized in BEEM capsules ON at 60 °C. Electron microscopy was performed at a Joel JEM-1400 transmission microscope with a bottom mount 4k digital camera (F416) with the assistance of Dr. Stefan Hillmer.

Chapter

3

Results

The following work presented was performed by myself unless stated otherwise. Students working under my supervision contributed to the following projects. Catherine Moreau (cloning first CS mutants), Carmen Bayly (Formin), Olivia Ramsey (Zinc finger nucleases), Ulrike Amelung (Tubulin and Formin), Jennifer Marshall (Zinc finger nucleases), Jannik Traut (Oocyst microscopy of CSP mutants).

3.1 Genetic manipulation of Plasmodium parasites

3.1.1 Generation of basic transfection vectors

In order to facilitate all cloning requirements, a set of basic vectors was generated which were used as backbones in the individual projects. These are described here briefly in design and how they have been generated. As transcription start sites (TSS) are poorly mapped and promoters are poorly understood [249, 412], I will only refer to 5' untranslated regions (5'UTRs) in the following work, which generally are a region starting between 1500 bp to 500 bp upstream off and ending directly upstream of the start codon, unless stated otherwise. The term promoter is used synonymously.

The original vector used to generate Pb237 was derived from b3D+ with the *Pb* heat shock protein 70 (*hsp70*) 5'UTR, *Pb* dehydrofolat synthase (*dhfr*) 3'UTR and two homologous regions within chromosome 12, termed chr12a (bp 846483-846980) and chr12b (bp 847281-847711), all from [279]. The chromosomal site has been further characterized recently [413].

To generate Pb238, the *hDHFR* gene was amplified from human cDNA with P241 and P99 and cloned with AgeI and NheI into Pb237. Next, the *ef1α* 5'UTR was amplified

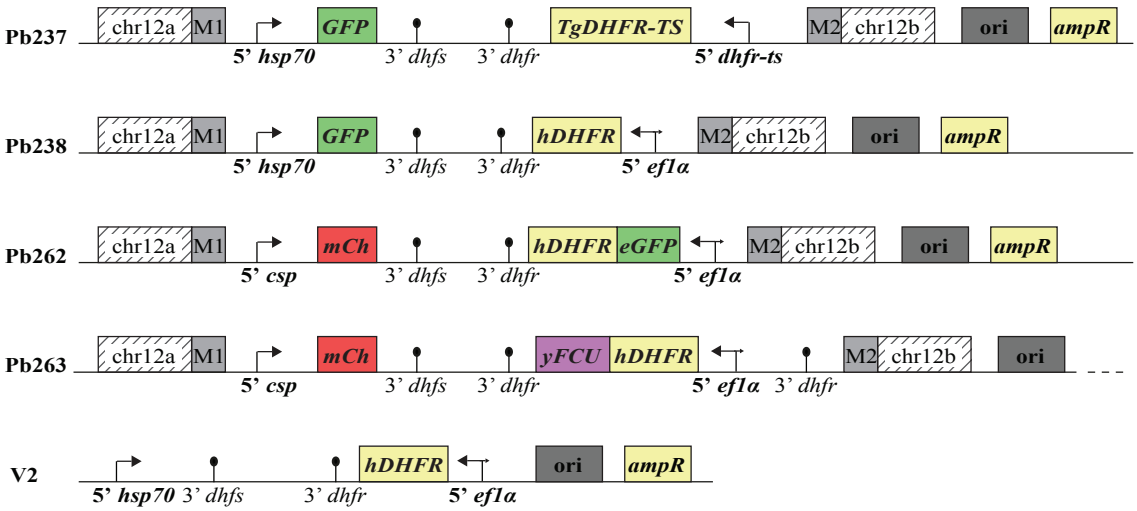

Figure 3.1: Basic vectors
Design of basic vectors used in this study. **Pb237**: Original vector design with homology arms into chromosome 12 and constitutive cytoplasmic *GFP* expression. 9784bp. **Pb238**: Optimized selection marker, using the much smaller human dehydrofolat reductase *hDHFR* gene under the control of the ef1α 5' untranslated region (5'UTR) which shows some bidirectional promoter activity. 7611 bp. **Pb262**: Strong cytoplasmic *mCherry* expression under the control of the 5'UTR of *CSP* and constitutive expression of a enhanced GFP (*eGFP*) as a fusion product with hDHFR under the control of *ef1α* 5'UTR. 7587bp. **Pb263**: This vector utilizes a *Plasmodium* selection marker that is a fusion of hDHFR with the yeast cytosin deaminase and uridyl phosphoribosyl transferase (yFCU), resulting in negative selection after addition of 5-fluorocytosine (5-FC). The whole selection marker can excise via single crossover recombination, resulting in loss of both positive and negative selection marker. 8434bp. **V2**: Minimum cloning vector with empty expression cassette and small selection marker. 4981bp.

from *Pb* genomic DNA (gDNA) with primers P233 and P234 and inserted with ApaI and AgeI, resulting in Pb238.

To generate vector Pb262, the 5'UTR of *CSP* was amplified from *P. berghei* gDNA with primers P207 and P208 and cloned into Pb238 with EcoRI and NdeI. The open reading frame of *mCherry* was amplified with primers P238 and Pb232 and inserted into the vector with NdeI BamHI. Next *eGFP* was amplified with P242 and P243 and inserted with AgeI, resulting in Pb262.

The generate vector Pb263, the whole selection cassette *dhfr* 3'UTR - *ef1α* 5'UTR - *hDHFR* - *yFCU* - *dhfr* 3'UTR [208] was amplified from a PlasmoGEM transfection vector [181] with P600 and P601, and cloned with EcoRV HindIII into Pb262, resulting in Pb263.

To generate V2, the bacterial backbone of the pBAT vector [414] was amplified with P847 and P848 and combined with the minimal selection marker *ef1α* 5'UTR - *hDHFR* - *dhfr* 3'UTR - *dhfs* 3'UTR of Pb238 [279] using primers P849 and P850 with EcoRI and KpnI. With P851 and P852, the 5'UTR of *HSP70* was amplified from *Pb* gDNA and inserted with HindIII and XhoI, resulting in V2.

3.1.2 Post transfection plasmid unfolding via Zinc finger nucleases in Plasmodium

The aim of the following experiments was twofold: 1. To test the activity of ZFNs and TALENs in *Plasmodium* parasites. 2. Test if it is possible to transfect a circular plasmid which, post transfection, transcribes a nuclease targeting the plasmid itself. Can this in vivo linearized plasmid integrate efficiently using double crossover integration using two homology regions previously flanking the nuclease target site (**Figure 3.2**)?

Starting with V2, the homology sites chr12a and chr12b were amplified from *Pb* gDNA using primers P853, P854 and P855, P856 respectively and joined via assembly PCR in a Chr12b - TALEN binding site - Ch12a orientation using primers P854 and P855. The homology box was cloned into V2 using HindIII and KpnI yielding V3-Tt. In parallel, chr12a and chr12b were amplified from *Pb* gDNA with primers P893, P854 and P855, P894 and PCR products were fused with P854 and P855 and cloned into V2 using HindIII and KpnI, yielding V3-Zt. In both of these vectors the TALEN targeting *samd4* was cloned using XhoI and AflII from the vector pcDNA-samd4 (gift of Mhlanga lab [415] resulting in V4TALEN-Zt and V4TALENTt. The *ZFN* pair *ZFNa* - 2A - *ZFNb* was amplified with P891 and P892 from the vector LsZFN (see **(Figure 3.6**) and cloned using AflII resulting in V4ZFN-Zt and V4ZFN-Tt.

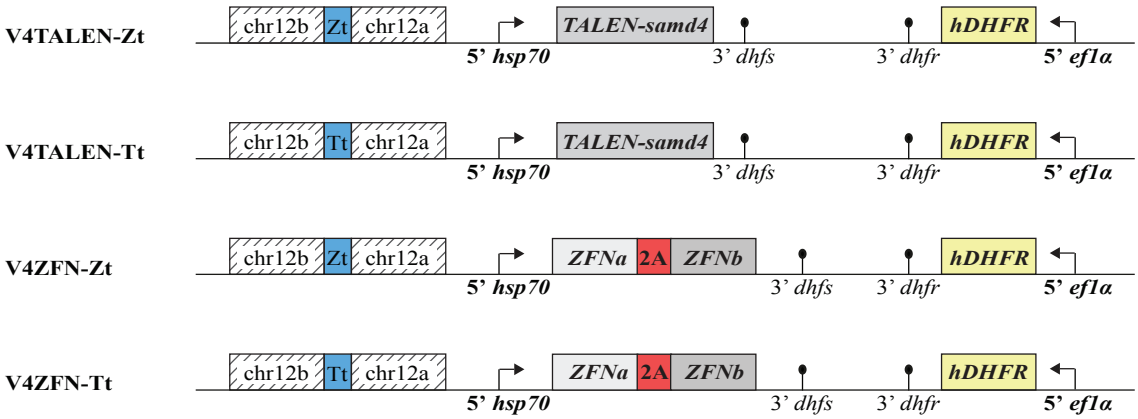

Figure 3.2: Vector design of unfolding vectors
The arrangement of the DNA fragments present in the circular vector is shown. Homology regions used for integration into Chromosome 12 integration site are depicted as striped boxes and separated by the nuclease target site shown in blue. The **T**ALEN samd4 **t**arget site is abbreviated as **Tt**, the **Z**FN **t**arget site as **Zt**. Coding regions are shown with boxes, promoter regions (5') and 3'UTRs (3') are indicated. Sequences required for bacterial replications are not shown.

Of these four plasmids, two (V4TALEN-Tt and V4ZFN-Zt) are expected to self linearize and integrate into the chr12 locus (**Figure 3.3**), while the other two (V4TALEN-Zt and V4ZFN-Tt) are expected to stay circular or integrate via single crossover at a low level. In case of the TALEN, a single TALEN is targeting a targeting site that

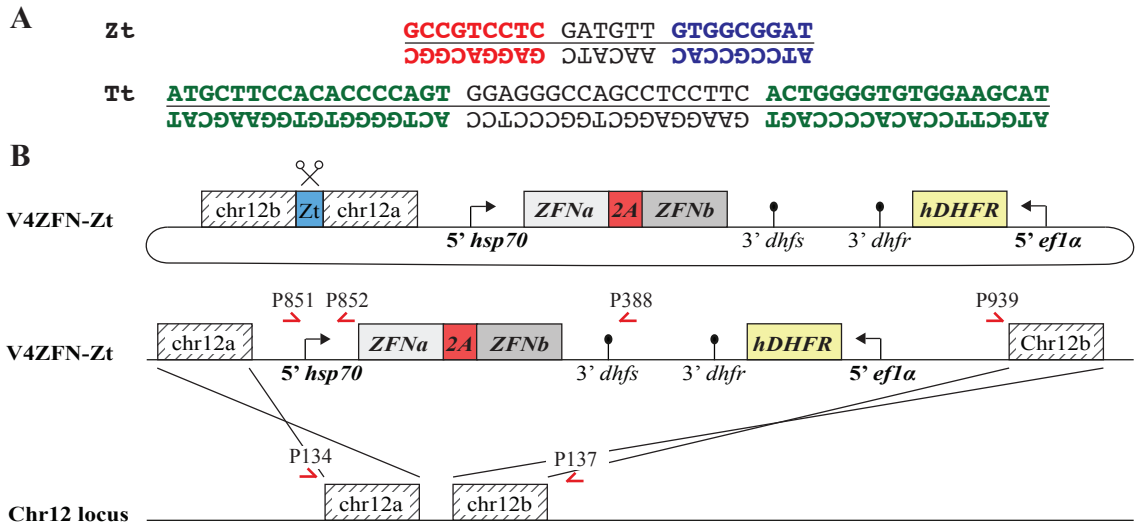

Figure 3.3: Integration of unfolding vectors
A The basepair composition of the ZFN target site **Zt** and TALEN target site **Tt** are shown. **Zt** consists of the binding site of ZFNa shown in **dark violet** and the binding site of ZFNb on the opposite strand shown in **dark red**. DSB occurs in the central area of the 6 bp spacer. **Tt** consists of two identical binding sites of the TALEN targeting *samd4* shown in **dark green** on opposite strands. DSB occurs in the central area of the 18 bp spacer. **B** Planned integration of unfolding vectors into chromosome 12 locus is shown with the example of V4ZFN-Zt, the vector encoding ZFNs and the target site Zt in between the two homology regions chr12b and chr12a. After transfection of the circular vector the *ZFNs* are expressed under a constitutive promoter and induce a DSB at the ZFN target site Zt. The circular vector unfolds, resulting in a linear vector flanked by the homology sites chr12a and chr12b in the correct orientation. Primers used are indicated.

consists of a duplicated binding region that is once inverted, separated by a 18 bp spacer in between (**Figure 3.3 A**). DSB break occurs upon homodimerization of two TALEN molecules. In the case of the ZFNs, two *ZFNs* are expressed from a single mRNA and the protein is separated via a self cleaving 2A skip peptide [416]. The targeting region is well characterized and occurs within the *eGFP* gene [417], and is defined by the binding regions of ZFNa and ZFNb separated by a 6 bp spacer (**Figure 3.3 A**). It requires heterodimer formation of both ZFNa and ZFNb for DSB to occur [184].

All four vectors were transfected uncut in a single transfection into NMRI mice. Parasites transfected with V4TALEN-Tt and V4TALEN-Zt were harvested 12 days post transfection, V4ZFN-Zt was harvested 17 days post transfection. Parasites transfected with V4ZFN-Tt transiently appeared 15 days post transfection, but the mouse cleared parasitemia on the following days. From the parental populations gDNA was prepared and analyzed via PCR (**Figure 3.4**). For both vectors expressing *TALENs*, no targeted integration events could be observed. In contrast, parasites transfected with V4ZFN-Zt showed 5' and 3' integration into the Chromosome 12 target locus. The episomal vector was still present as expected in a parental population. The nuclease-expression cassette

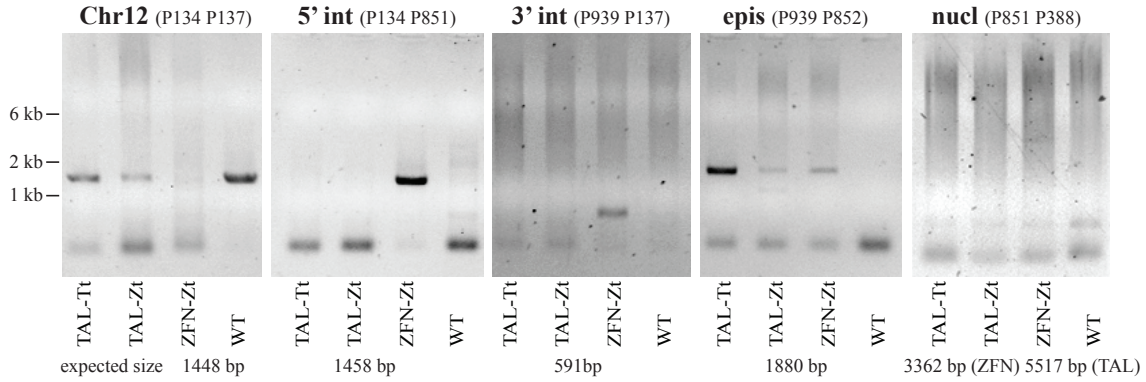

Figure 3.4: Genotyping of unfolding vectors
Parental parasite populations after transfections were used to generate gDNA and analyzed by PCR. PCR was performed for whole locus of Chromosome 12, 5' and 3' integration, episomal control and amplification of the nuclease expression cassette. Primers used were indicated, binding sites of primers are shown in (**Figure 3.3**).

was faintly visible for ZFN-Zt.

3.1.3 Attenuation by stage specific double stranded break using Zinc finger nucleases

In the following experiments, stage specific expression of *ZFNs* was used to assess the parasite responses to targeted DSB depending on DSB timing and homologies surrounding the DSB site. Parasites showing arrest after IV injection of sporozoites were used to immunize mice for challenge by wt sporozoites.Most of this work was published [418].

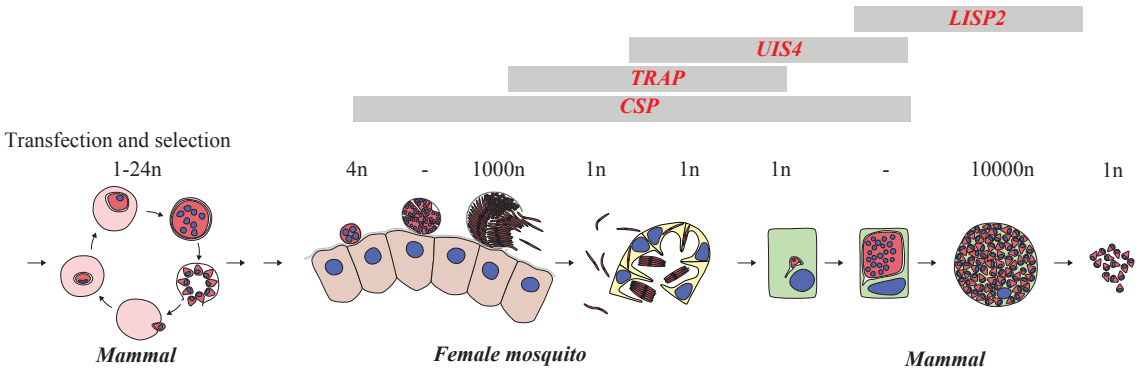

Figure 3.5: Genome copy number throughout the *Plasmodium* life cycle
Depicted is an excerpt of the life cycle of *Plasmodium*. Activity of promoter sequences used in this study are illustrated above. The genome copy number of the haploid parasite genome is indicated. It is not known to which stages homologous recombination is limited, except stages with N=1. The nuclei are shown in **blue**, parasite cytoplasm in **red**, host cell cytoplasm **light red** for the erythrocyte, **brown** for the midgut, **yellow** for the salivary gland and **green** for the hepatocyte. Figure modified from [418].

Vector generation

All vectors used for transfection were based on Pb238. To generate the *ZFN* expression cassette, cloning was performed in pGEM. The 5'UTR of *CSP* was amplified from *Pb*

gDNA with P377 and P378 and cloned into pGEM. *ZFNa* was amplified with P379 P380 from a vector (gift from the lab of Toni Cathomen) and inserted with KpnI PshAI. The 3'UTR of *CSP* was amplified from *Pb* gDNA with P381 P382 and inserted with PshAI SwaI. In parallel the 3'UTR of *DHFS* was amplified from *Pb* gDNA with P387 P388 and cloned into a second pGEM vector. *ZFNb* was amplified with P385 P386 from a vector and inserted with KpnI PshAI. The 5'UTR of *TRAP* as amplified with P383 P384 from *Pb* gDNA and inserted with SwaI PshAI. The entire second pGEM insert was inserted into the first pGEM vector using EcoRV SwaI. The entire fragment was cloned with NotI EcoRV into Pb238, resulting in the vector SpZFN (**Figure 3.6**).

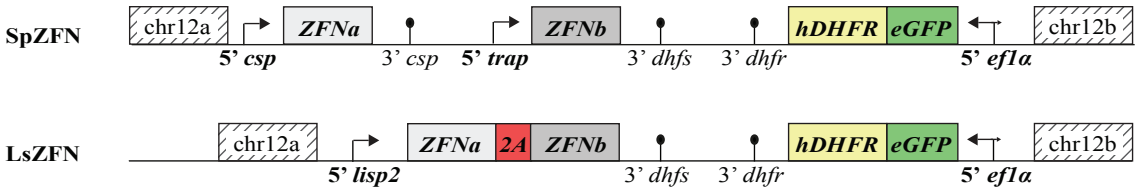

Figure 3.6: Vector design of SpZFN and LsZFN
The arrangement of DNA fragments integrated is shown. The binding site of the dimer of ZFNa and ZFNb is located within the *eGFP* coding region. Chr12a and chr12b indicate the left and right homology arm. Coding regions are shown with boxes, 5'UTRs and 3'UTRs are indicated. Figure modified from [418].

To generate LsZFN (expression of *ZFNs* in the liver stage), the 5'UTR of *LISP2* was amplified from *Pb* gDNA with P685 P686. *ZFNa* was amplified using P687 P688, introducing a 2A skip peptide. Both PCR products were fused via overlap extension PCR using primers P658 P688 and cloned into SpZFN with NotI PshAI, resulting in LsZFN (**Figure 3.6**).

The silently mutated *eGFP* (*mGFP*), harbouring a C465A mutation in the coding region of *eGFP* and thus producing a single mismatch in the 6 bp homology of GCCGAC on position 462-468 and 537-543 within the coding region was generated by overlap extension PCR. To do this two fragments of *eGFP* were amplified with P1168, P1169 and P1170, P1171, fused with primers P1168 and P1171 and cloned with SwaI PstI into LsZFN. Additionally the coding region of *ZFNa* was codon optimized for *Pb* [419] with the help of OPTIMIZER [420] and then manually optimized to be as codon-missmatching as possible with *ZFNb*. The resulting sequence, *ZFNacm*, was, including the 2A skip peptide, ordered from GeneArt (Regensburg). The 5'UTR of *CSP* was amplified with P377 P1173, the 5'UTR of *LISP2* was amplified with P685 P1172 and each cloned separately into the *ZFNacm* vector with NotI HindIII and each together with *mGFP* cloned into LsZFN with NotI PshAI, resulting in Sp2ZFN and Ls2ZFN respectively

(**Figure 3.13**).

The 5'UTRs of *TRAP* and *UIS4* were amplified with P1260 P1261 and P1259 P1262 respectively and cloned with NotI NdeI into Sp2ZFN, resulting in TrapZFN and Uis4ZFN (**Figure 3.13**).

For transfection, all vectors were linearized with PvuI prior to transfection. Genotyping after transfection and limiting dilution was performed with P134 P137 for the whole locus. The outer primer for 5' integration was P134 for all parasites, the inner primer was P378 for SpZFN and P207 for Sp2ZFN, P686 for LsZFN and Ls2ZFN, P384 for TrapZFN and P1262 for Uis4ZFN. The outer primer for 3' integration was P137, the inner primer P243 for SpZFN, SP2ZFN, LsZFN and Ls2ZFN and P99 for TrapZFN and Uis4ZFN.

For further genotyping, the *ZFN* locus was amplified with forward primers P377, P685, P1259, P1260 for Sp, Ls, Uis4 and Trap respectively and reverse primer P388. The locus of *eGFP / mGFP* was amplified with P242 P243.

Quantitative qPCR was performed on gDNA with primers P1134 P1135 for amplification over the cutting site C1, L2: P1136 P1137 upstream of the chromosome 12 site (8133 bp upstream of C1), R2: P1138 P1139 (8240 bp downstream of C1), L1: P1174 P1175 (upstream of C1, 97,7 kb away from telomere), R1: P1176 P1177 (downstream of C1, 99 kb away from telomere), N1: P1140 P1141 (1,404 mb downstream of start) N2: P1142 P1143 (27120 bp downstream of N1), N3: PP1144 P1145 (1778 downstream if N2).

Breakthrough events after sporozoite challenge

Parasites were designed in a way that transfection and selection of clonal lines was possible in the BS without expression of *ZFNs*. These parasites then start expressing *ZFNs* under the control of different 5'UTRs in stages with varying genome copy numbers (**Figure 3.5**). The first set of parasites was designed to express *ZFNa* under the control of 5'UTR of *CSP* and *ZFNb* under the control of the 5'UTR of *TRAP* and was termed SpZFN (sporozoite expression of *ZFNs*). The second parasite expressed both *ZFNa* and *ZFNb* under the control of the 5'UTR of the liver stage specific *LISP2* and termed LsZFN for liver stage expression. In this case both proteins were fused into a single ORF separated by a self-cleaving 2A skip peptide (**Figure 3.6**). For both parasite lines the target of the ZFNs pair was integrated into the chromosome with the same transfection vector within the *eGFP* gene. Successful DSB within *eGFP* is expected

to split the chromosome 12 within the integration site. Parasites have the potential to restore the chromosome by HR, repair the DSB with MMEJ introducing small deletions (and thus most likely loosing fluorescence), or fail to repair the DSB, resulting in cell death (**Figure 3.7**).

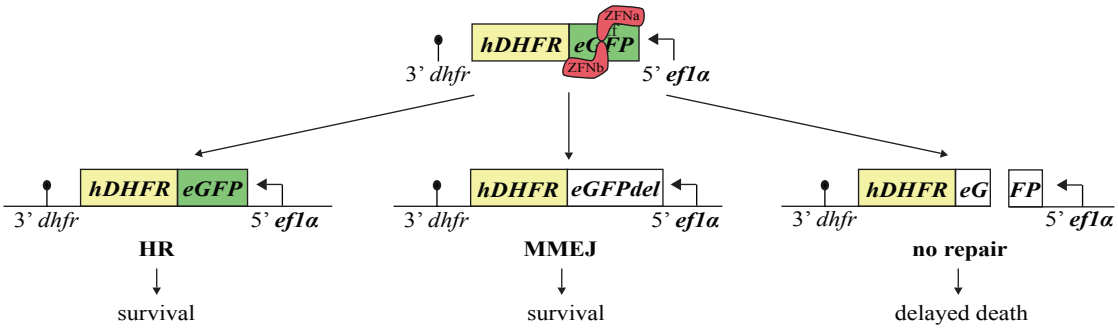

Figure 3.7: Possible genetic responses following a genomic DSB
Shown are the three possible ways a single cell could react to a DSB. NHEJ is not shown due to its absence in *Plasmodium*. Figure taken from [418].

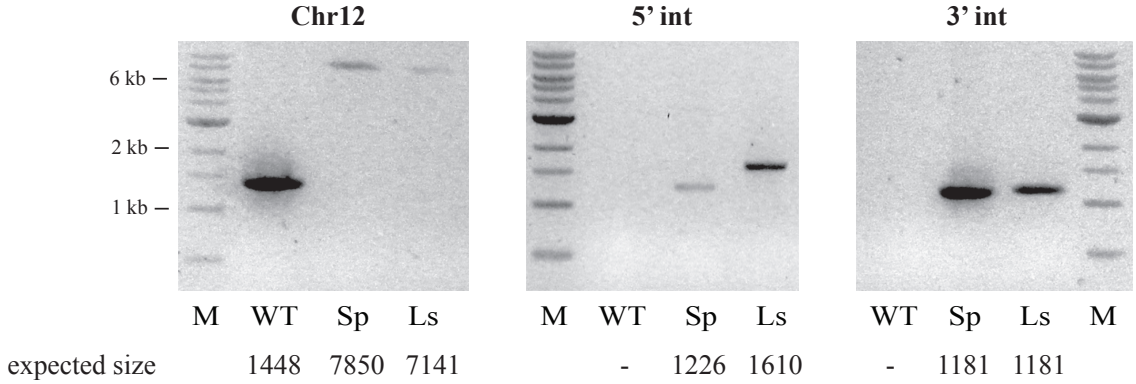

Figure 3.8: Genotyping of SpZFN and LsZFN
Genotyping of the clone used in all following experiments is shown for both SpZFN and LsZFN. Expected size of PCR products is indicated. Figure take from [418].

Parasites were generated via transfection and the generated clones were genotyped (**Figure 3.8**). Mosquitoes were feed with both parasite strains and parasite development was assessed (**Table 3.1**). Both parasite lines showed numbers of sporozoites in midgut and salivary glands comparable to WT. Sporozoites were injected IV into C57BL/6 mice with escalating doses from multiple infected mosquito cages (**Table 3.2**). All parasites that caused BS infections in mice after sporozoite challenge were labeled as sporozoite induced (SI) and numbered according to appearance. Parasites were isolated and gDNA was prepared. Genotyping of breakthrough parasites via PCR showed that for SpZFN, the *ZFN* expression cassette had been severely reduced in size in SpZFN SI 5-11 which was also detectable in the parental clone c1 (**Figure 3.9**). SpZFN appeared to be a mixed population for both the *ZFN* expression cassette as well as the *eGFP* gene.

Table 3.1: Infectivity of parasite strains in *Anopheles stephensi*

Parasite line	*Midgut sporozoites / mosquito*	*Salivary gland sporozoites / mosquito*	*Salivary gland sporozoites / midgut sporozoites*	*Number of infected mosquitoes analyzed*
WT	111.000	21.000	0,19	30
SpZFN	84.000	12.000	0,14	18
LsZFN	157.000	29.000	0,18	22
Sp2ZFN	50.000	2.500	0,05	30
Ls2ZFN	181.000	22.000	0,12	30
TrapZFN	55.000	25.000	0,46	11
Uis4ZFN	5.300	1.700	0,32	14
SpZFN SI 2	17.000	8.300	0,49	30

Table taken from [418].

SpZFN SI 1-4 appeared to have a *eGFP* slightly reduced in size. For LsZFN, LsZFN SI 1, 3 and 4 also had a reduced size of the *ZFN* expression cassette, and none of the clones showed any apparent change in size of the *eGFP* gene.

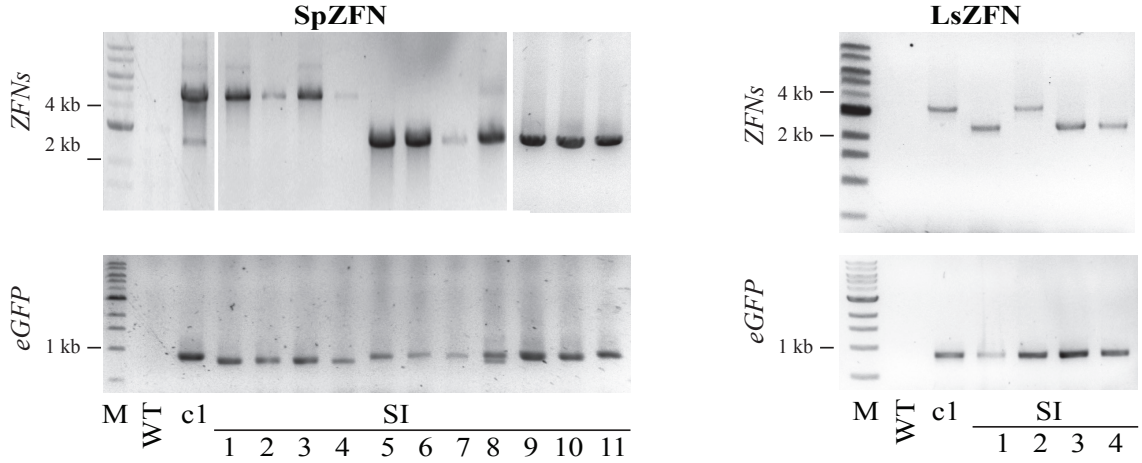

Figure 3.9: Genotyping of sporozoite induced (SI) clones after breakthrough of SpZFN and LsZFN.
Primers used are shown in **Figure 3.12**. Figure taken from [418].

All PCR products of breakthrough parasites were sequenced and closely analyzed. For the *ZFN* expression cassette, alignments had to be manually corrected as *ZFNa* and *ZFNb* display multiple stretches of perfect homology (**Figure 3.10**). All parasites that had reduced their *ZFN* copy number to one displayed products of homologous recombination between the homology regions of both *ZFNs*. Three clones, SpZFN SI 6, SpZFN SI 10 and LsZFN SI 1 were unique and had used homology regions of 57 bp, 114 bp and 130 bp respectively. All other clones, SpZFN SI 5,7-9,11 and LsZFN SI 3-4 had used a bigger homology region of 332 bp in size.

The *eGFP* coding regions of all breakthrough parasites were sequenced and aligned

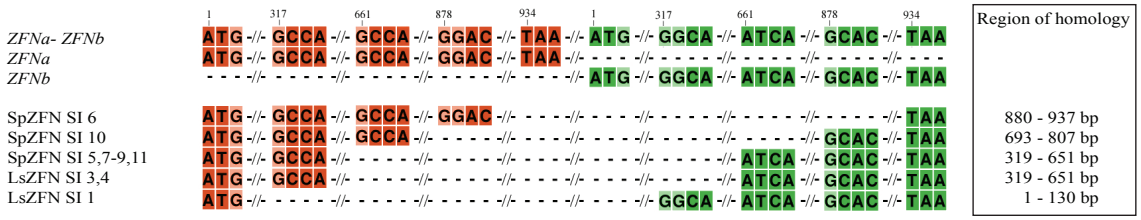

Figure 3.10: Copy number reduction of *ZFNs* in SI of SpZFN and LsZFN
Homology regions used for HR involved are mapped using alignment of the *ZFNs* locus after breakthrough to the unmodified *ZFNs* locus. Size of the regions of homology used are indicated on the right. Figure taken from [418].

(**Figure 3.11**). SpZFN SI 1-4 were genetically identical and showed the same 75 bp deletion which was originally flanked by the 6 bp microhomology GCCGAC. Sequencing reads of SpZFN SI 8 were manually split into c1 and c2, of which c1 showed a 81 bp deletion originally flanked by AGCAGAA. Both deletions resulted in complete removal of the binding sites of both ZFNs. Expression and lack of expression of eGFP in blood stages in all SI parasite lines corresponded to the *eGFP* gene sequenced, also for the mixed breakthrough infection of SpZFN SI 8.

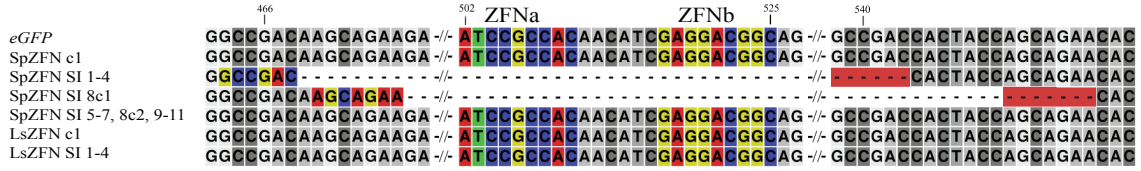

Figure 3.11: Genomic locus of the *egfp* gene of sporozoite induced clones of SpZFN and LsZFN
ZFN target sites (ZFNa; ZFNb) and microhomologies used for repair are shown in color. Figure taken from [418].

Schematics of genomic loci of all sporozoite induced parasites are shown (**Figure 3.12**). Only LsZFN SI 2 survived the mosquito passage with no genetic modification. Both the possibility that ZFNs did not induce a DSB in a single parasites or that repair of DSB occurred via HR cannot be distinguished experimentally.

In order to reduce the breakthrough rates of the *ZFNs* expressing parasites two optimizations of the vector were performed. The first is the introduction of a single silent point mutation in the 6 bp microhomology region which was observed in 4 out of 5 repaired DSBs within the *eGFP* gene. The second modification was the reduction of internal homology within the two *ZFNs*. As both *ZFNs* were codon optimized for mammalian expression, optimization of *ZFNa* for *Pb* codon usage already introduced most potential changes in codon usage. After alignment of both *ZFNs*, all codons that could be possibly changed without changing the amino acid sequence were changed,

Table 3.2: Summary of all mice challenged with sporozoites.

Parasite line	*sporozoite dose injected IV*	*infected mice / total mice*	*sporozoite induced breakthrough parasites*
WT	10.000	4/4	
WT	10.000	4/4	
WT	10.000	4/4	
SpZFN	10.000	0/4	
SpZFN	25.000	1/10	SpZFN SI 1
SpZFN	25.000	3/9	SpZFN SI 2-4
SpZFN	500.000	4/4	SpZFN SI 5-8
SpZFN	25.000	3/16	SpZFN SI 9-11
LsZFN	10.000	4/4	LsZFN SI 1-4
Sp2ZFN	25.000	0/4	
Sp2ZFN	10.000	0/4	
Ls2ZFN	25.000	5/12	Ls2ZFN SI 1-5
Ls2ZFN	250.000	4/8	Ls2ZFN SI 6-9
Ls2ZFN	1.000.000	2/4	ND
TrapZFN	25.000	2/4	TrapZFN SI 1-2
TrapZFN	250.000	0/4	
Uis4ZFN	25.000	0/8	
Uis4ZFN	250.000	3/8	Uis4ZFN SI 1-3
SpZFN SI 2	10.000	8/8	ND

Table taken from [418].

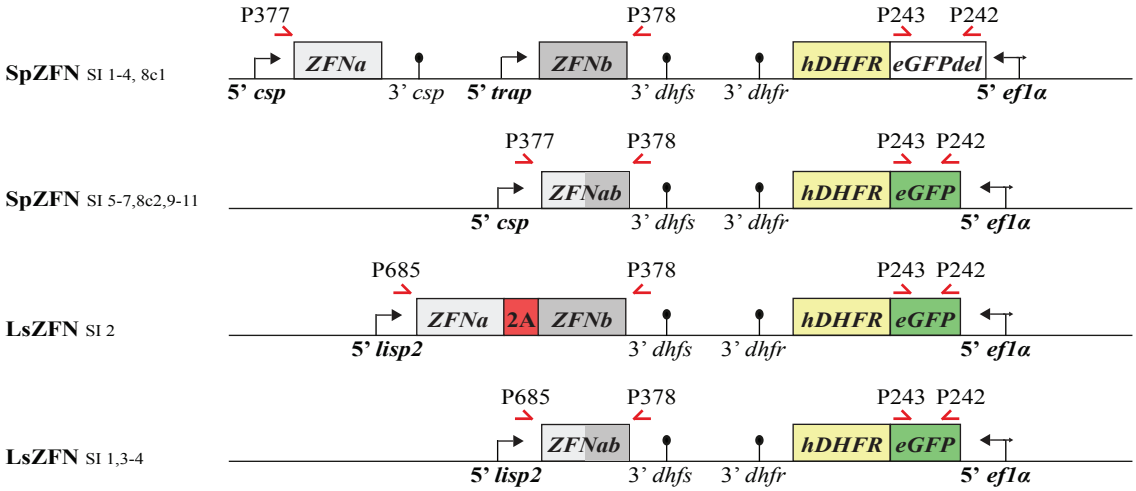

Figure 3.12: Genomic loci after breakthrough
Overview of the plasmid integration site of all sporozoite induced clones. Primers used for genotyping are indicated. Figure taken from [418].

resulting in very limited homology between *ZFNb* and the new codon modified *ZFNacm*. For both sporozoite specific and liver stage specific expression constructs were redesigned to express both *ZFNacm* and *ZFNb* linked with a 2A skip peptide from a singe 5'UTR (**Figure 3.13**). In total three parasite lines were generated for sporozoite

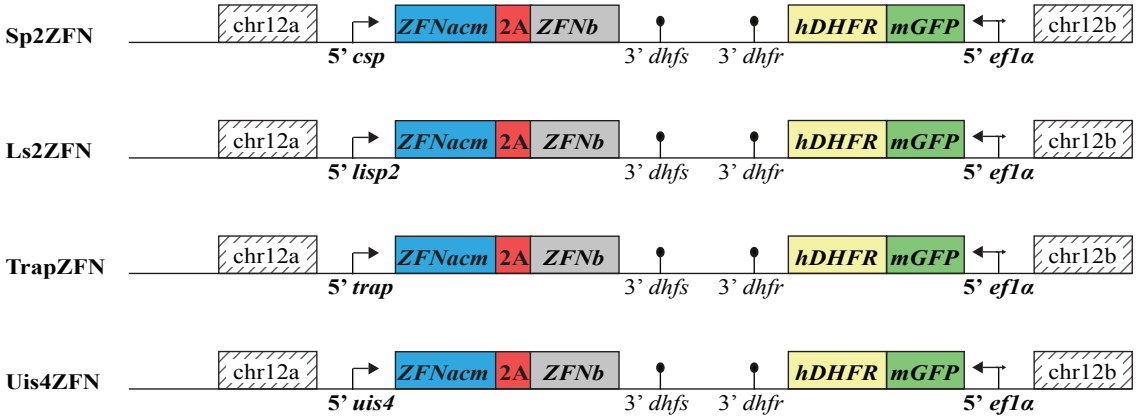

Figure 3.13: Gene models for Sp2ZFN, Ls2ZFN, TrapZFN and Uis4ZFN. Figure modified from [418].

specific expression, ranging from 5'UTR of *CSP* which is active from day 6 post infection (Sp2ZFN) [349] two late oocyst expression using 5'UTR of *TRAP* (TrapZFN) [own observations] to salivary gland specific expression using 5'UTR of *UIS4* (Uis4ZFN) [249]. Genotyping of clonal lines was performed (**Figure 3.14**).

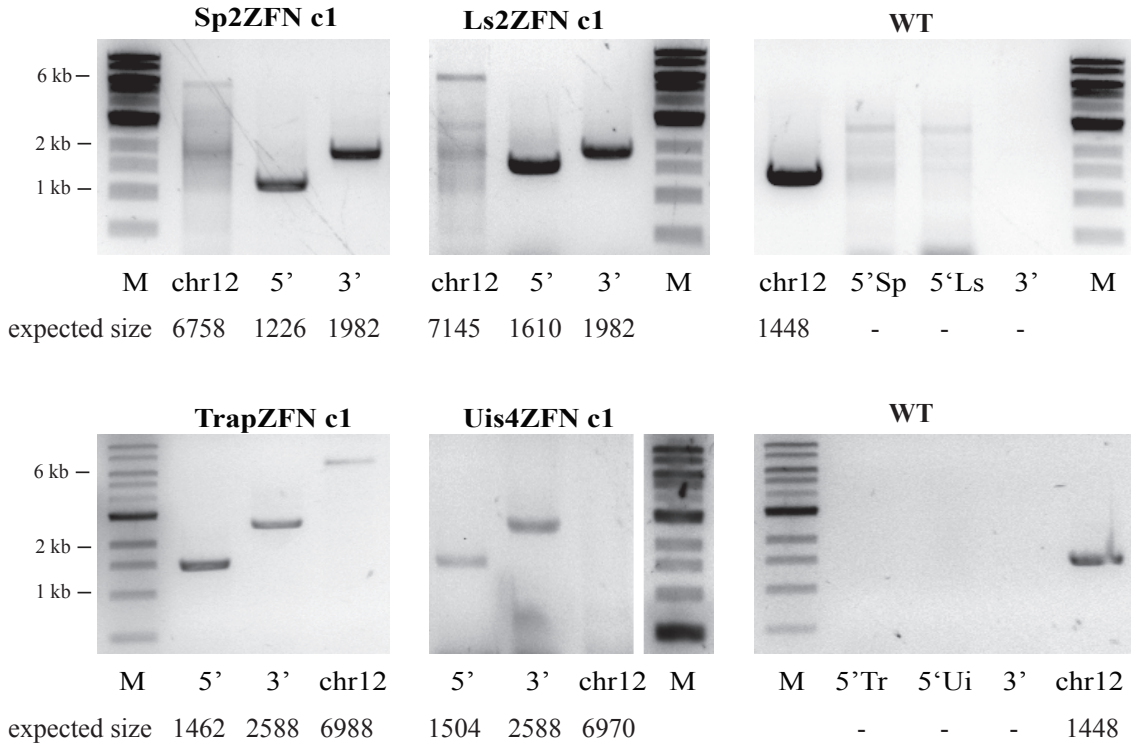

Figure 3.14: Genotyping of Sp2ZFN, Ls2ZFN TrapZFN and Uis4ZFN. Figure taken from [418].

Mice were infected IV with parasites of all four strains (**Table 3.1**) and breakthrough parasites were analyzed by PCR (**Figure 3.15**) and sequencing (**Figure 3.16**). The *ZFN* expression site was stable in all sporozoite induced clones. In case of the *eGFP*

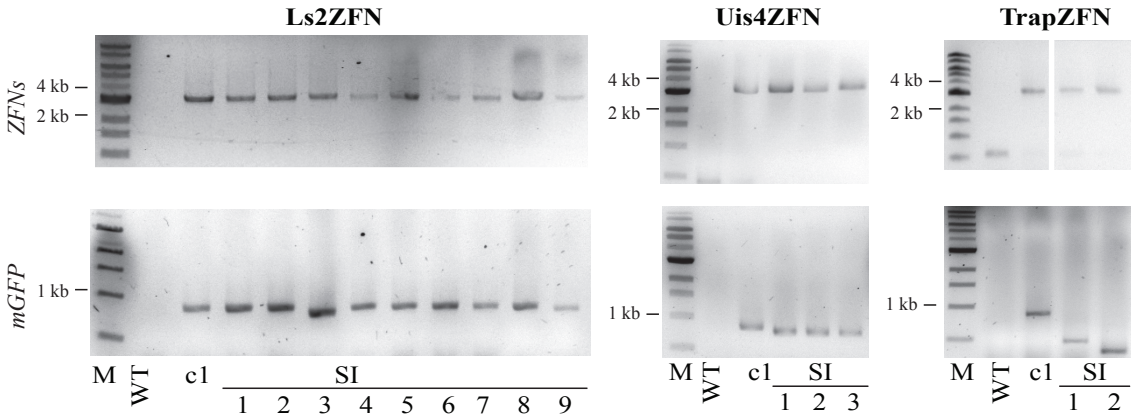

Figure 3.15: PCR analysis of sporozoite induced parasites of Ls2ZFN, TrapZFN and Uis4ZFN.
Primers used are indicated in **Figure 3.17**. Figure taken from [418].

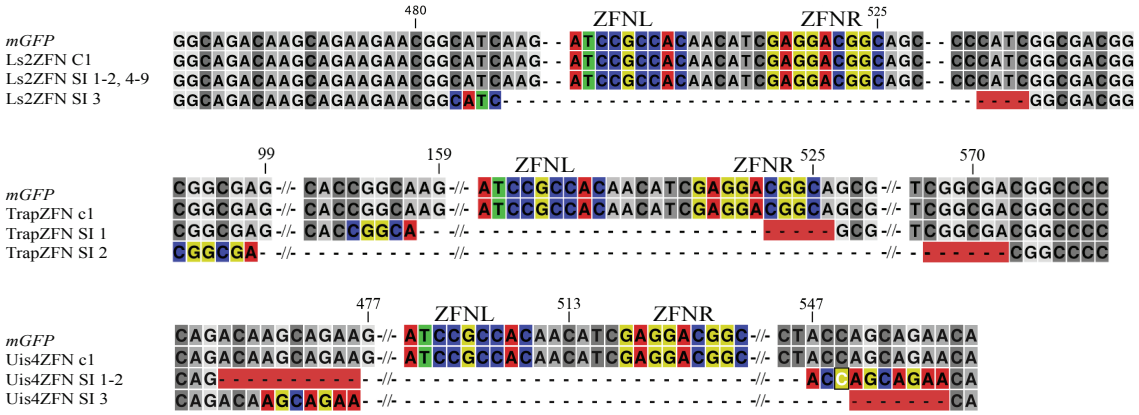

Figure 3.16: Genotyping of the *eGFP* gene of Ls2ZFN, TrapZFN and Uis4ZFN.
Figure taken from [418].

gene, many sporozoite induced clones showed more or less prominent deletions. Sequencing showed that only one out of nine breakthrough parasites of Ls2ZFN had a deletion, resulting in loss of both ZFN binding sites which was originally flanked by a microhomology of four bases. All other SI parasites of Ls2ZFN potentially repaired a DSB by HR or did not induce a DSB.

Both breakthrough parasites of TrapZFN showed huge deletions within the *eGFP* gene (369 bp and 474 bp) originally flanked by a microhomology of 5 bp and 6 bp respectively. The *eGFP* gene of Uis4ZFN SI 1-3 showed a deletion of 81 bp, originally flanked by a microhomology of 10 bp showing a single mismatch. Of these 10 bp of microhomology, Uis4ZFN SI 1-2 retained the one version of the single mismatch, whereas Uis4ZFN SI 3 retained the other version of the 10 bp microhomology. As all three breakthrough parasites are derived from the same dissection of sporozoites and have

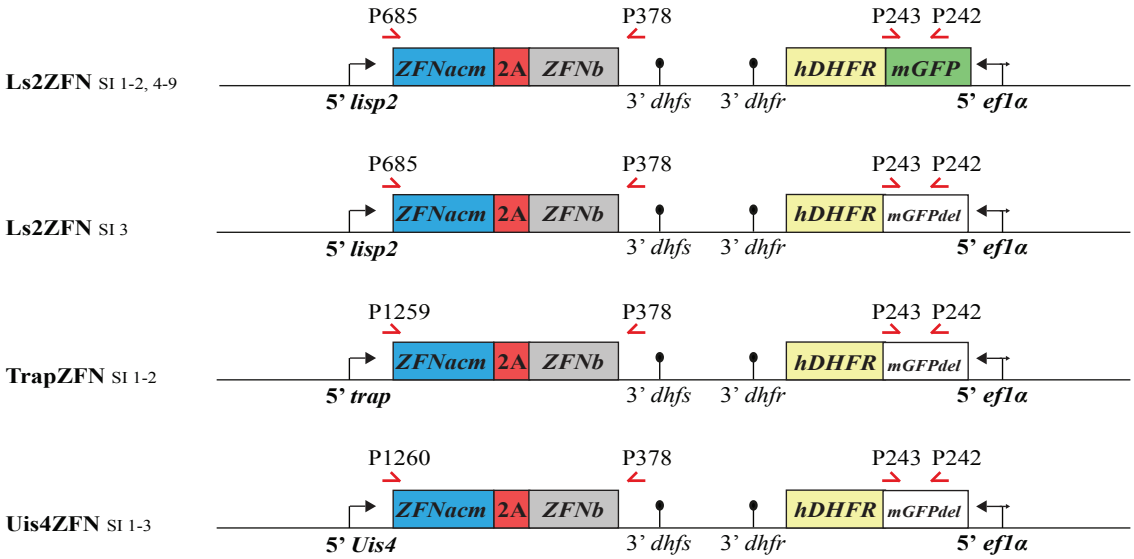

Figure 3.17: Genomic loci of Ls2ZFN, TrapZFN and Uis4ZFN after breakthrough
Overview of the plasmid integration site of all sporozoite induced clones. Primers used for genotyping are indicated. Figure taken from [418].

been injected at the same time, it seems likely that all three parasites are derived from the same oocyst and at least two subsequent genome duplications occurred after the DSB was repaired. Schematics of genomic loci of all sporozoite induced parasites are shown (**Figure 3.17**).

Comparative analysis of all repair events shows that 4-10 bp are used as microhomology (with a single missmatch in case of Uis4ZFN SI 1-3) (**Figure 3.18**). A deletion between 75-474 bp occured, ending exactly with the microhomology region on either side. However, after repair, only one of the two microhomologies is retained as it is used during repair. In all cases, the binding sites of both ZFNs are lost with the deletion. The CG content of the microhomologies is 67%, 43%, 50%, 80%, 83%, 40% and 50%, averaging to 66%. Although this is significantly higher than the average of the *P.berghei* genome, it is not far off from the 62% of the *egfp* coding region.

Genetic analysis of breakthrough parasites gives insight into the rate at which parasites are able to repair the DSB and the mode of repair. Looking at the relationship between breakthrough rates dependent on parasite inoculum for each clone (**Table 3.1**), it is difficult to estimate the type of relationship as mice numbers are limited. However if the values are blotted (**Figure 3.19**), there seems to be almost no positive correlation between sporozoite dose and breakthrough rate. However the DSB repair rate of the parasite should be independent of sporozoite dose. This suggests that in infections with higher sporozoite doses the mouse immune system is eliminating most parasites that repair the DSB. This would result in an underestimation of the DSB repair rate that is

SpZFN	CTATATCATG	**GCCGAC**	AAGCAGAAGA	-/	/-	CGTGCAGCTC	**GCCGAC**	CACTACCAGC
SpZFN SI 1-4	CTATATCATG	**GCC**		-/75 bp/-			**GAC**	CACTACCAGC
SpZFN	ATGGCCGACA	**AGCAGAA**	GAACGGCATC	-/	/-	GACCACTACC	**AGCAGAA**	CACCCCCATC
SpZFN SI 8c1	ATGGCCGACA	**AGCA**		-/81 bp/-			**GAA**	CACCCCCATC
LsZFN	AGAAGAACGG	**CATC**	AAGGTGAACT	-/	/-	AGAACACCCC	**CATC**	GGCGACGGCC
LsZFN SI 3	AGAAGAACGG	**CA**		-/81 bp/-			**TC**	GGCGACGGCC
TrapZFN	TCTGCACCAC	**CGGCA**	AGCTGCCCGT	-/	/-	ACATCGAGGA	**CGGCA**	GCGTGCAGCT
TrapZFN SI 1	TCTGCACCAC	**CGG**		-/369 bp/-			**GCA**	GCGTGCAGCT
TrapZFN	TCAGGGTGTC	**CGGCGA**	GGGCGAGGGC	-/	/-	ACACCCCCAT	**CGGCGA**	CGGCCCCGTG
TrapZFN SI 2	TCAGGGTGTC	**CGG**		-/474 bp/-			**CGA**	CGGCCCCGTG
Uis4ZFN	ATCATGGCAG	**ACAAGCAGAA**	GAACGGCATC	-/	/-	GCCGACCACT	**ACCAGCAGAA**	CACCCCCATC
Uis4ZFN SI 1-2	ATCATGGCAG			-/81 bp/-			**ACCAGCAGAA**	CACCCCCATC
Uis4ZFN SI 3	ATCATGGCAG	**ACA**		-/81 bp/-			**AGCAGAA**	CACCCCCATC

Figure 3.18: Overview of all microhomology sequences used by SI parasites to repair DSBs
Microhomology sequences are shown in **bold**. Ten base pairs flanking each homology region are shown prior to the DSB break and the remaining bases in the SI parasites. The number of base pairs lost after repair is indicated. The mismatch in the microhomology sequence used for repair of Uis4ZFN SI 1-3 is highlighted in **orange**. Figure taken from [418].

more prominent for higher parasite doses.

Analysis of genome integrity at the ZFN target site

As the majority of parasites die soon orlater after the DSB and are therefore excluded from genetic analysis in the blood stage, a more direct analysis of the ZFN target site was performed. DNA fluorescence in situ hybridisation (FISH) was attempted, labeling about 10 kb upstream and downstream of the ZFN target sites. This would be expected to colocalize before the DSB but loose colocalization after failed DSB repair. Despite several attempts, only labeling of the 2,3 kb repeat [421] was consistently achieved (data not shown).

As a consequence, I attempted an alternative approach to quantify subtelomeric copy numbers via gDNA quantitative PCR (qPCR). To this end, sets of primer pairs were designed to amplify over the cutting site (C1), two on the left side of the cutting site

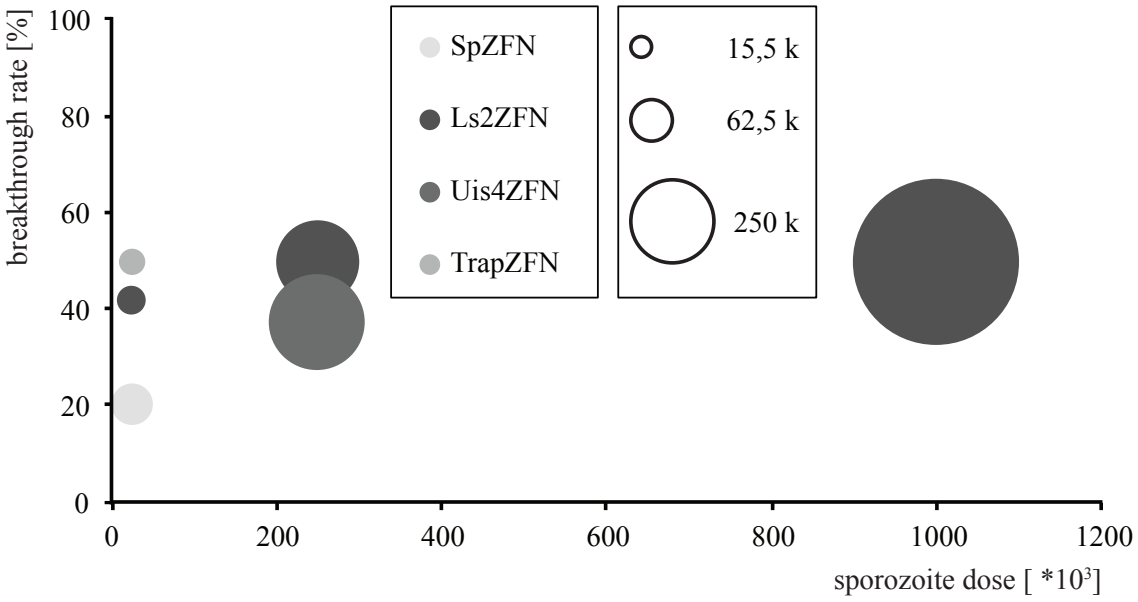

Figure 3.19: No correlation between sporozoite dose and breakthrough rate
Shown is the relationship between breakthrough rate after IV injection of sporozoites for all parasite lines where infections with different doses have been performed. Data from **Table 3.2** was blotted for all parasite lines. Experiments resulting in 0% or 100% breakthrough rate were excluded. Sporozoite dose was blotted on the x-axis, the breakthrough rate on the y-axis. The area of the circle represents the estimated dose to cause a 50% infection rate. The legend indicates which area correlates to estimated doses in thousand (k) parasites. This was individually calculated for each parasite dose assuming a linear relation ship between sporozoite dose and breakthrough rate.

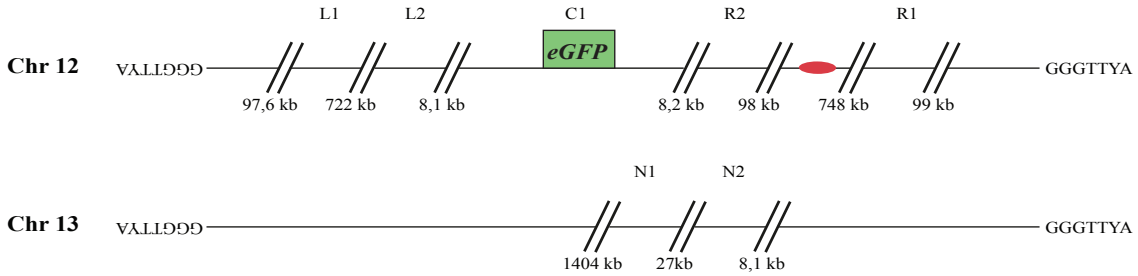

Figure 3.20: Chromosomal location of qPCR probes
Schematic overview of chromosomes 12 and 13. The centromere of chromosome 12 is shown in **red**. Binding sites for primer pairs used for qPCR are shown. Primer pair C1 amplifies the product over the cutting site of the ZFNs, while primer pairs L1 and R1 bind approximately 100 kb away from the telomeres on the left and right arm of chromosome 12, respectively. L2 and R2 bind around 8 kb away from the cutting site. N1 and N2 bind on the control chromosome 13 and are used for normalization. Figure taken from [418].

facing away from the centromere (L1 (100 kb downstream of the telomere) and L2 (8133 bp upstream of cut site)), and two on the right side towards the centromere (R1 (100 kb upstream of the telomere) and R2 (8240 bp downstream of cut site). Two probes on the unaffected chromosome 13 were generated for normalization, N1 and N2. Primers used were P1134 P1135 (C1), P1174 P1175 (L1), PP1136 P1137 (L2), P1176

P1177 (R1), P1138 P1139 (R2), P1140 P1141 (N1), P1142 P1143 (N2). Location of the probes in relation to the ZFN binding sites and in respect to the centromere are shown (**Figure 3.20**).

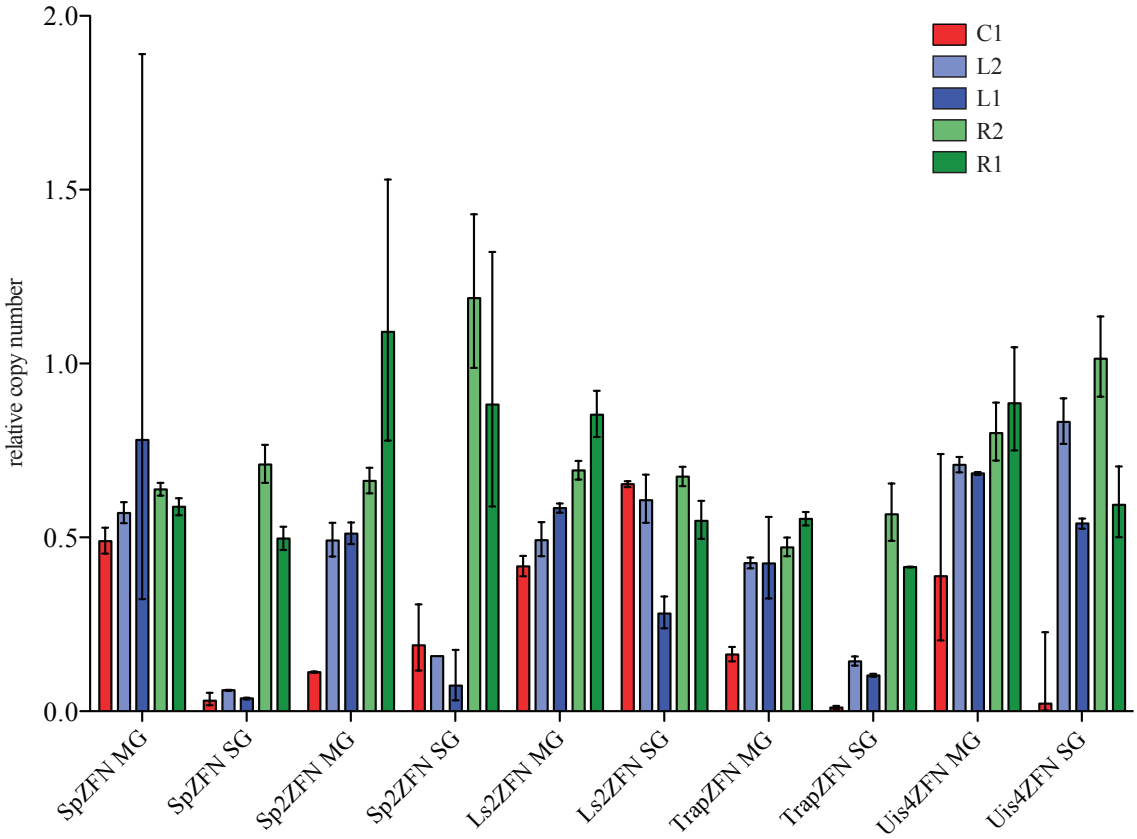

Figure 3.21: Results of qPCR on gDNA
Relative copy number of probes of chromosome 12 is shown for samples from salivary gland sporozoites (SGS) and midgut sporozoites (MGS). Values were normalised to N1 and N2 on chromosome 13 and to results from blood-stage gDNA amplification. Positive and negative error is calculated from standard error of the mean from technical duplicates. Figure taken from [418].

Next, gDNA was prepared form blood stages, as well as MGS 10 days post infection and SGS 17 days post infection. Whenever possible, at least 200.000 sporozoites were used. Using qPCR, I measured the relative copy number of each probe in both sporozoite samples relative to the presence in blood stages (**Figure 3.21**). When combining both probes upstream and both probes downstream of the ZFN target site and comparing the relative presence of both in SGS relative to MGS, all parasite lines with expected expression in the oocyst show a reduction for the left chromosomal arm (**Figure 3.22 A**). This is true from SpZFN, SP2ZFN and to a lesser extent for TrapZFN. Uis4ZFN and Ls2ZFN, both without expected expression of the ZFNs in the oocyst stage show no reduction of the either side of chromosome 12 in SGS compared to MGS. If the DSB occurs before the nuclear division of the forming sporozoite is finalized, it is expected

that the part of the chromosome lacking the centromere is not pulled into the sporozoite and remains in the residual body of the oocyst.

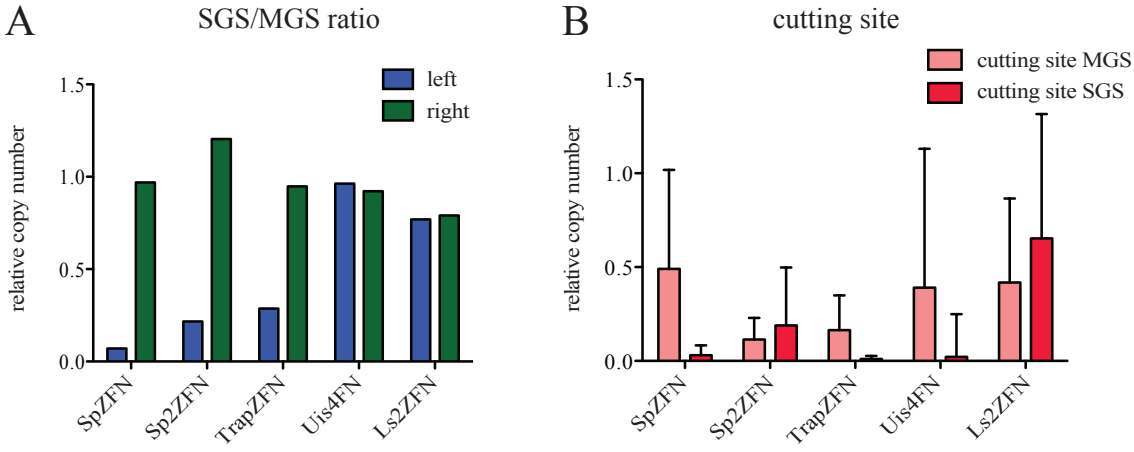

Figure 3.22: Copy number analysis by qPCR on genomic DNA
A The ratio of the relative copy number of amplicons from both sides of the break point on chromosome 12 (L1 and L2 on left of break; R1 and R2 on right of break) is shown for parasites isolated from mosquito salivary glands (SGS) compared with parasites isolated from midguts (MGS). The copy number of the left side of chromosome 12 is strongly reduced in the SG sample for parasites expressing ZFNs in the midgut, whereas the right side containing the centromere is not affected. All individual values, including errors, are shown in (**Figure 3.21**). **B** The relative copy number of PCR products amplified over the break point shown for genomic DNA isolated from midgut sporozoites (MGS) and from salivary gland sporozoites (SGS). Note the near absence of product in salivary glands from parasites where ZFNs are expressed before (SpZFN, TrapZFN) or during (Uis4ZFN) sporozoite entry into salivary glands. Positive and negative error is calculated from standard error of the mean from technical duplicates. Figure taken from [418].

If the probe over the cutting site (**Figure 3.22 B**) is analyzed, the relative copy numbers over the cutting site is reduced for the SGS sample only. As both sides of the chromosome are equally present in salivary gland sporozoites, that implies that not the DSB, but the following mitosis causes the loss of the chromosomal arm lacking the centromere. As expected, the cutting site of the Ls2ZFN parasite is present in both the MGS and the SGS sample.

In vivo development of ZFN expressing parasites

To test if the expression of ZFNs during the sporozoite stage has any negative off-target effects despite the DSB break induced in the target site, I reinfected SpZFN SI 2 (**Figure 3.11**) to mosquitoes and performed infections of C57BL/6 mice IV and BB (**Figure 3.23**). Both IV and BB resulted in infections comparable with WT parasites, concerning prepatency, development of BS parasites and time of death. In contrast, IV injections of SpZFN remained BS negative.

Additionally, the timing of the developmental arrest of the ZFN expressing para-

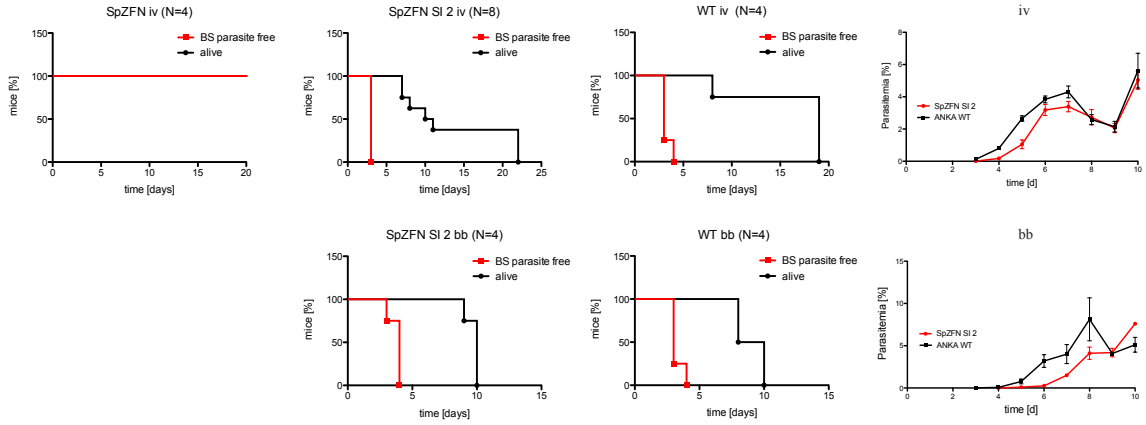

Figure 3.23: Characterisation of SpZFN SI 2
C57BL/6 mice were challenged with 10.000 sporozoites intraveously (iv) or by the bites of ten infected *A. stephensi* mosquitoes (bb). Peripheral blood parasitaemia was monitored by Giemsa-stained blood smears from three days post-infection. Percentage of mice that are blood stage (BS) parasite free and percentage of mice alive is shown over time. Parasitaemia over the course of the experiments is shown as growth curves. Control infections with SpZFN resulted in no blood stage parasitaemia. Figure taken from [418].

sites within the liver was analyzed. HepG2 cells were infected with ZFN parasites and immunofluorescence analysis (IFA). Parasite development and expression of *mGFP* was analyzed 24 and 48 h post infection (**Figure 3.24**). Sporozoites of Sp2ZFN, which are also severely reduced in salivary gland numbers (**Table 3.1**), caused a reduced amount of liver stages (not quantified). These are severely reduced in size already 24 h post infection and do not increase in size 48 h post infection.

TrapZFN parasites appeared to consist of two separate populations 48 h post infection. There was a small population that did not seem to have increased in size since the 24 h time point, similar to the whole population of Sp2ZFN. These might represent parasites where the DSB had occurred early during development before sporozoite formation, resulting in loss of the chr12 fragment during sporozoite formation. A second subset of parasites

increased in size significantly between 24 h and 48 h post infection. Uis4ZFN parasites also seemed to develop in two separate populations, although the amount of DSBs prior to sporozoite formation is expected to be minimal.

In contrast to all other parasites, liver stages of Ls2ZFN did show sizes 24 h and 48 h post infection that are expected for WT parasites and GFP was still present in the parasite. This is in striking contrast to the developmental arrest this parasite is expected to undergo only shortly after the 48 h time point, as virtually all parasites will fail to develop into replicating blood stage parasites (**Table 3.2**).

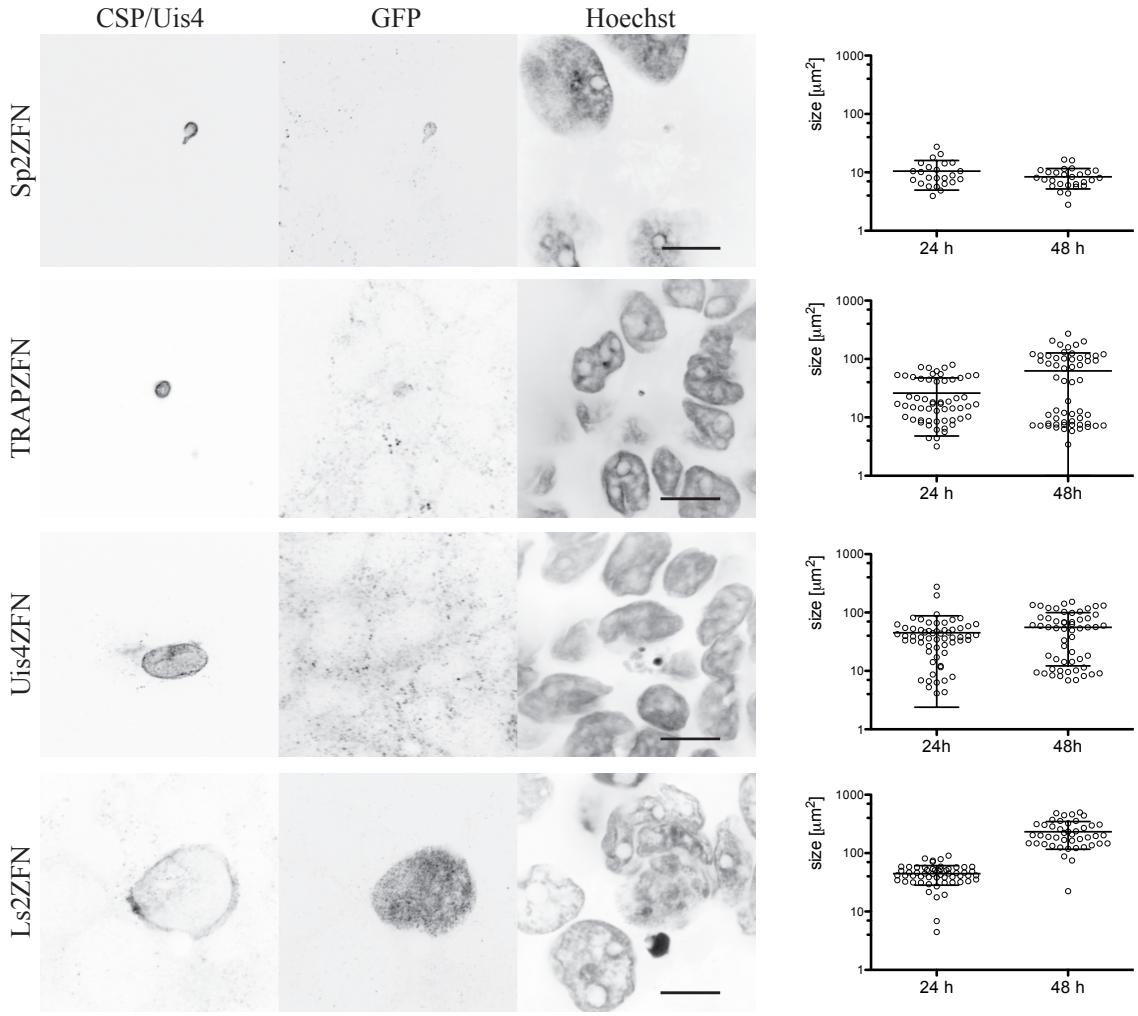

Figure 3.24: Liver stage development of ZFN parasites
Liver stages of parasites in HepG2 cells 48 h after sporozoite invasion are shown. α-CSP or αUis4 staining shows the plasma membrane / PVM of the parasite within the hepatocyte. Staining with α-GFP antibody shows residual mGFP-hDHFR fusion protein. Sizes of liver stages from single slice images were measured 24 h and 48 h post-sporozoite invasion. Error shown is mean with standard deviation. Figure taken from [418].

Sterile protection through ZFN expressing parasites

As sufficient numbers of mice remained negative after sporozoite challenge (**Table 3.2**), C57BL/6 mice were immunized with a prime two boost regimen. Mice were primed on day zero and boosted with the same number of sporozoites IV on day 14 and 21 post boost. Challenge was performed on day 28 for all SpZFN immunized with 10.000 sporozoite and for 13 mice immunized with 25.000 SpZFN. All other mice were challenged 14 days after the last boost, on day 35. Mice which became positive after priming were identified on day 13 post prime, excluded from the immunization and are included within the breakthrough parasites described earlier (**Table 3.2**).

After challenge with 10.000 *Pb* ANKA WT sporozoites, all mice immunized with

Table 3.3: Protection of immunized mice against *P. berghei* ANKA WT challenge

Parasite line	*Sporozoite dose IV for immunisation*	*Number of boosts*	*Mice positive after WT challenge*	*Prepatency after challenge (days)*
SpZFN	10.000	2	0/4	NA
SpZFN	25.000	2	0/18	NA
Sp2ZFN	25.000	2	2/4	5,5
Sp2ZFN	10.000	2	1/4	7
Ls2ZFN	25.000	2	0/7	NA
Ls2ZFN	250.000	0	4/4	5.5

Table taken from [418].

SpZFN and Ls2ZFN remained negative (**Table 3.3**). Of those mice immunized with Sp2ZFN, three became BS positive. This is most likely due to the strong impairment of liver stage development of this parasite line (**Figure 3.24**). All four mice immunized with a single prime of 250.000 Ls2ZFN sporozoites became positive after challenge with WT sporozoites.

Additionally, it was tested if protection after immunization can be transferred by adoptive transfer of total splenocytes as well as liver resident CD8+ T-cells. All mice which were transferred became positive after challenge with WT sporozoites with no delay compared to not immunized controls, including those transferred from genetically attenuated parasite (GAP) immunized control mice. Therefore the whole experiment was excluded from analysis and not repeated due to ethical concerns.

3.1.4 Self-excising selection marker through mosquito passage

The following project was initiated before selection marker recycling via *yFCU/hDHFR* was routinely used and was a main driver to explore ZFNs in *P. berghei*. The goal was to generate a selection marker that is automatically lost upon mosquito passage, using the stage specific expression of ZFNs during the oocyst stage. A big portion of the experimental work has been performed by Olivia Ramsey (generation of SpZFNe) and Jennifer Marshall under my supervision (generation of SpZFNsilence and SpZFNY66H, as well as experiments performed).

In contrast to parasites that are expected to arrest due to a DSB they cannot resolve, a parasite that is supposed to auto-recycle its selection marker requires an efficient DSB repair. As the inherent inability of *Plasmodium* to perform NHEJ is not straight forward to address, parasites were provided homology regions to repair the DSB.

SpZFNe was generated from SpZFN. To introduce the homology region used to excise

the selection marker, the 3'UTR of DHFR and part of the 3'UTR of DHFS was amplified from SpZFN with P512 P513 and cloned with PmeI into SpZFN to result in SpZFNe (**Figure 3.25**).

To generate SpZFNsilence and SpZFNY66H, *eGFP* - *hDHFR* - dhfr 3'UTR was amplified from SpZFN with P577 P578 and ligated into pGEM. The *hDHFR* coding sequence was removed with NheI AgeI restriction digest, incubated with the Klenow fragment to fill up the overhangs and religated. Subsequently the ZFN binding sites were silenced by introduction of two point mutations on either side, using P579 P580 in a mutagenesis PCR. To yield SpZFNsilence the insert was now ligated into SpZFN via EcoRV. To generate SpZFNY66H, a second mutagenesis PCR was performed on the last pGEM clone with P581 P582, introducing a Y66H mutation into the coding sequence of *eGFP*, mutating it to *BFP* [422]. The product was ligated with EcoRV into SpZFN, resulting in SpZFNY66H. The design of SpZFNe, SpZFNsilence and SpZFNY66H is shown in (**Figure 3.25**).

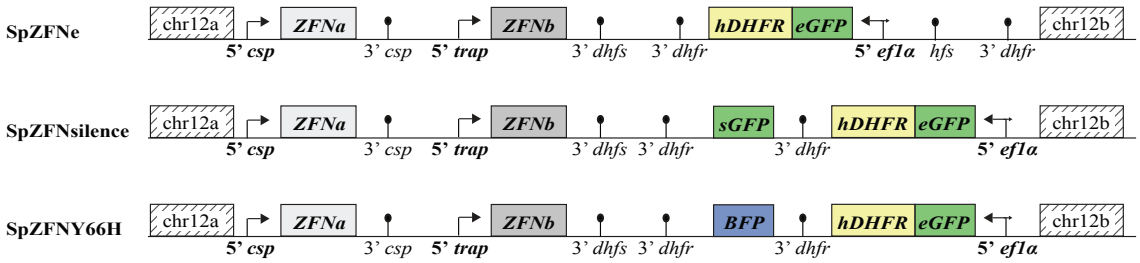

Figure 3.25: Vector design of SpZFNe, SpZFNsilence and SpZFNY66H
The arrangement of integrated DNA fragments is shown. The binding site of the dimer of ZFNa and ZFNb is located within the *eGFP* coding region, but silently mutated in *sGFP* and *BFP*. Chr12a and chr12b indicate the left and right homology arm. Coding regions are shown with boxes, 5'UTRs and 3'UTRs are indicated. **SpZFNe** has a region with perfect homology flanking the selection marker, composed of a duplicated *3' dhfs* and part of the *3' dhfs* (*hfs*). **SpZFNsilence** has the *GFP* coding region as homology, containing four shielding mutations within the ZFN binding sites. **SpZFNY66H** has the homology between *eGFP* and *BFP* with the four shielding mutations and an additional mutated basepair (Y66H) resulting in the shift from green to blue fluoresence.

Clonal lines were established and mosquitos infected. No obvious developmental phenotype was observed in mosquitoes. C57BL/6 mice were infected with 10.000 sporozoite IV and BS parasitemia was monitored daily from day three on. For each parasite, all four mice developed blood stage parasitemia (**Table 3.4**). Blood stage parasites of SpZFNe parasites after mosquito passage did not show green fluorescence, in contrast to the original parasites prior to mosquito passage. However, they showed a four day delay after IV injection compared to WT parasites, which corresponds to roughly a 10^4 fold reduction of parasite load. This indicates an extremely poor efficiency of DNA repair

Table 3.4: Mice infected with self-excising selelction marker

Parasite line	*Sporozoite dose IV*	*Mice positive*	*Prepatency (days)*
SpZFNe	10.000	4/4	7
SpZFNsilence	10.000	4/4	4
SpZFNY66H	10.000	4/4	4,25

Table generated by Jennifer Marshall.

after DSB. Thus the use of this excision strategy as selection marker recyclying would be limited to phenotypical characterizations until the oocyst stage. Additionally, at repair events at such a low rate, it cannot formally be excluded that excision of the selection marker took place prior to expression of the ZFNs in the mosquito stage. A random double strand break within the homology region can initiate excision of the selection marker during BS growth, exactly in the same way as is relied on for *yFCU-hDHFR* excision events. The only difference is that for *yFCU-hDHFR* 5-FC is used for negative selection whereas in the case of SpZFNe the DSB is selecting the desired event.

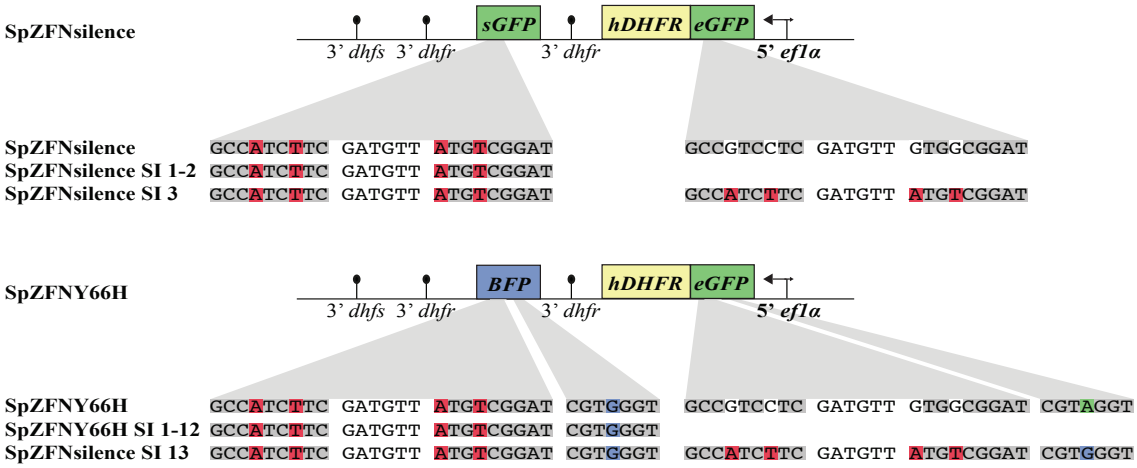

Figure 3.26: Sequencing of SpZFNsilence and SpZFNY66H after mosquito passage
The whole selection marker cassette of polyclonal sporozoite induced blood stages was amplified via PCR, inserted into a vector and individual clones sequenced. SpZFNsilence SI 1-2 and SpZFNY66H SI 1-12 have all excised the sequence previously flanked by both fluorescent proteins (*FP*) coding regions including the *hDHFR* gene. Of these all contain the shielding mutations of sGFP / BFP. One clone each did retain both *FPs* including the sequence in between (not shown). In this case all four shielding mutations are introduced into the eGFP, as well as the Y66H mutation for SpZFNY66H. Figure designed by Jennifer Marshall.

Parasites after mosquito challenge with SpZFNsilence and SpZFNY66H only showed around one day delay in BS development, representing a ten-fold reduction in infectivity compared to WT. This suggests that all sporozoite induced populations of these two parasite lines are polyclonal. Therefore, the genomic region comprising both homology regions was amplified via PCR using P233 P387 and sub-cloned into pGEM. The complete PCR amplicon of individual clones was sequenced and alined to the orig-

inal sequence. Both clones that had excised the selection marker and clones that kept both homologies could be identified (**Figure 3.26**). However in both cases that both homologies (and accordingly the flanked selection marker) remained the shielding mutations were present in both homologies as well as the neighboring Y66H mutation. This suggests that synthesis dependent strand annealing took place.

All excised clones of SpZFNY66H retained the Y66H mutation in the remaining *FP*. The site of Y66H is 315 bp away from the DSB, suggesting that after single strand annealing more than 315 bp were synthesized by polymerase δ. It should be noted that the number of clones sequenced that excised (14 in total) and had not excised (2 in total) is not representative on a population level. This is partly due to the low numbers, but mainly caused by the fact that the small PCR products are preferentially amplified, and that the excised locus is almost 2000 bp shorter that the complete one.

Additionally fluorescence microscopy was performed of mixed blood stages after mosquito passage. The SpZFNY66H samples only contained green or non-fluorescent parasites, and no blue fluorescence could be detected (data not shown). The BFP which was generated after excision represents a very poor fluorophore compared to eGFP, and the amount of fluorescence might not be detectable with the filters used for excitation of BFP. The presence of parasites within the bulk population that are still expressing the *hDHFR* resistance makes it impossible to directly transfect into the mosquito passaged bulk population without a limiting dilution in between.

3.2 Visualization of proteins involved in gliding motility

In an attempt to understand gliding motility in more detail, the visualization of proteins involved in gliding was performed. Many of these proteins had previously been localized via antibody staining of fixed cells. However observation of proteins in living cells allows to visualize the dynamics of a protein while the cell is moving. Additionally these tagged parasite lines might represent a resource that can be used to analyze and better understand mutants that show a phenotype in gliding motility.

Some of these parasite lines are already published or will be included in future publications, and are not discussed in this thesis. These are the N-terminally GFP tagged TRAP (SS:GFP:TRAP) [29, 290], the N-terminally tagged TRAP with rhomboid cleavage mutations as published in [215] as TRAP replacements, as well as a N-terminally GFP tagged TRAP wt replacement (unpublished data, Miriam Ester and Mirko Singer).

Also, N-terminally tagged TLP and S6, C-terminal endogenous tags of TRAP, TLP and S6 as well as an additional copy C-terminal tag of TRAP (unpublished data, Katharina Quadt, Jessica Kehrer and Mirko Singer). An N-terminal endogenous GFP tag of CTRP was also generated (unpublished data, Gunnar Mair and Mirko Singer). Furthermore endogenously tagged Formin 1 and Formin 2 (unpublished data, Ross Douglas and Mirko Singer) as well as a C-terminal tag of an extra copy of GAP45 with mcherry (unpublished data, Mirko Singer).

Other work on gliding motility was the trans-stage comparison of CTRP and TRAP in ookinete and sporozoite motility using an artificial promotor sequence (submitted manuscript, Dennis Klug, Jessica Kehrer, Friedrich Frischknecht and Mirko Singer); detailed in the PhD thesis of Dennis Klug.

3.3 The role of the circumsporozoite protein on sporozoite formation

CSP is one of the best studied proteins of *Plasmodium*, but its function is still not understood. As parasites lacking CSP or expressing less do not develop sporozoites [25], interdomain tagging of CSP was performed to gain insight into protein function. Using published data from important domains of CSP (**Figure 1.7**), GFP was positioned after the signal peptide (CS I), directly following the repeat region (CS II) and directly preceding the GPI-anchor (CS III) (**Figure 3.27**). For exact amino acid positions see (**Figure 1.5**), (**Figure 1.6**) and (**Figure 1.8**). In order to avoid strong developmental phenotypes at least in some of the parasite lines, the interdomain tagging mutants were designed to integrate via single crossover integration as additional copies with expression at lower levels than WT CSP (**Figure 3.28**).

Additionally, parasites lacking full length CSP were generated, where CSP was either replaced with the CS I (CS I repl), replaced with a GFP (using the signal peptide and GPI-anchor addition sequence of CSP) (GFP:GPI repl) or a α-TSR domain with GFP at its N-terminus (using the signal peptide and GPI-anchor addition sequence of CSP) (GFP:TSR:GPI) (**Figure 3.27** and **Figure 3.28**). Additionally, a parasite line was generated that expressed GPI-anchored GFP in the chr12 locus as an extra copy (**Figure 3.28**).

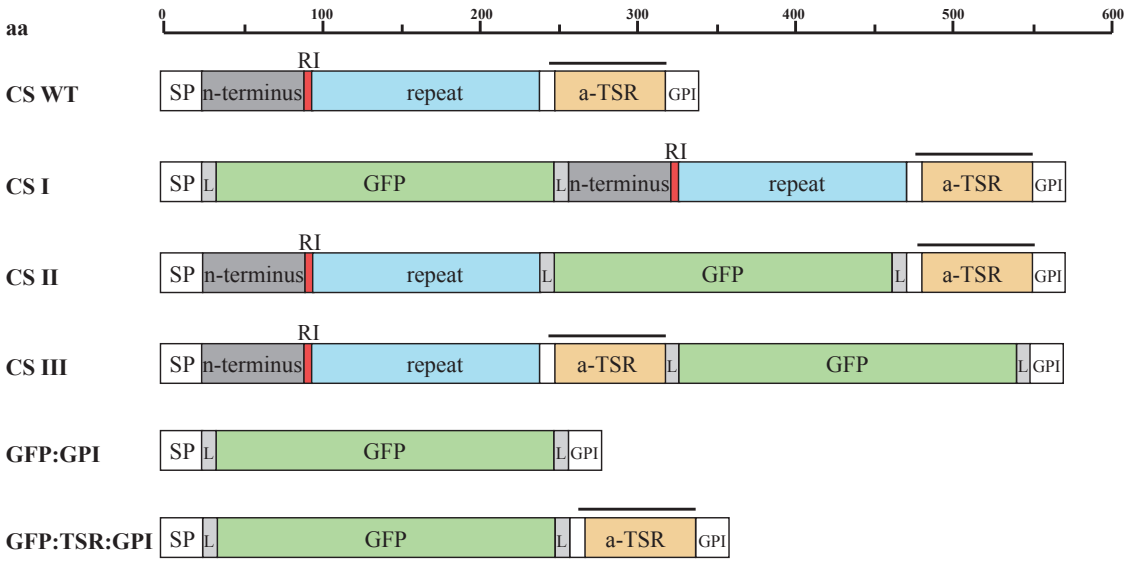

Figure 3.27: CSP domain structure
Shown is the respective size of all parts of the circumsporozoite protein (CS) and of all interdomain GFP tags generated. Sizes of respective parts of the protein are indicated. GFP is directly flanked with a glycin linker. The sequence of the peptide used to generate the C-terminal antibody used in this study is highlighted by a black line [387].

3.3.1 Generation of CSP mutants

All sequences used to generate the following vectors were amplified from gDNA of PBANKA WT blood stages. After each ligation step the correct sequence was verified by sequencing. To generate the control parasites expressing an GPI-anchored GFP (GFP:GPI) from the chr12 locus, the promoter region of CSP including the SP was amplified with P208 P268, digested with EcoRI and NdeI and ligated into Pb238. Then the GPI-anchor as well as a short 3'UTR was amplified with P274 and P270, digested with KasI and EcoRV. The resulting vector was linearized with PvuI and integrated via double crossover into the chr12 locus.

Interdomain tagging constructs were generated in the vector Pb238. The promoter region including the short or long beginning of the CSP coding region was amplified with P208 vs P268 for CS I, P208 vs P271 for CS II and P208 vs P273 for CS III. The PCR product was digested with EcoRI and NdeI and ligated into Pb238. The remaining part of CSP including the 3'UTR was amplified using P269 for CS I, P272 for CS II and P 274 for CS III all with reverse primer P270, and digested using KasI and EcoRV. The resulting end of the PCR product after the restriction digest ends at the naturally occuring EcoRV site of the 3'UTR of CSP. All PCR products were ligated into the vectors from the first step, sequenced and linearized before transfection with PacI for CS I, and PmlI for CS II and CS III.

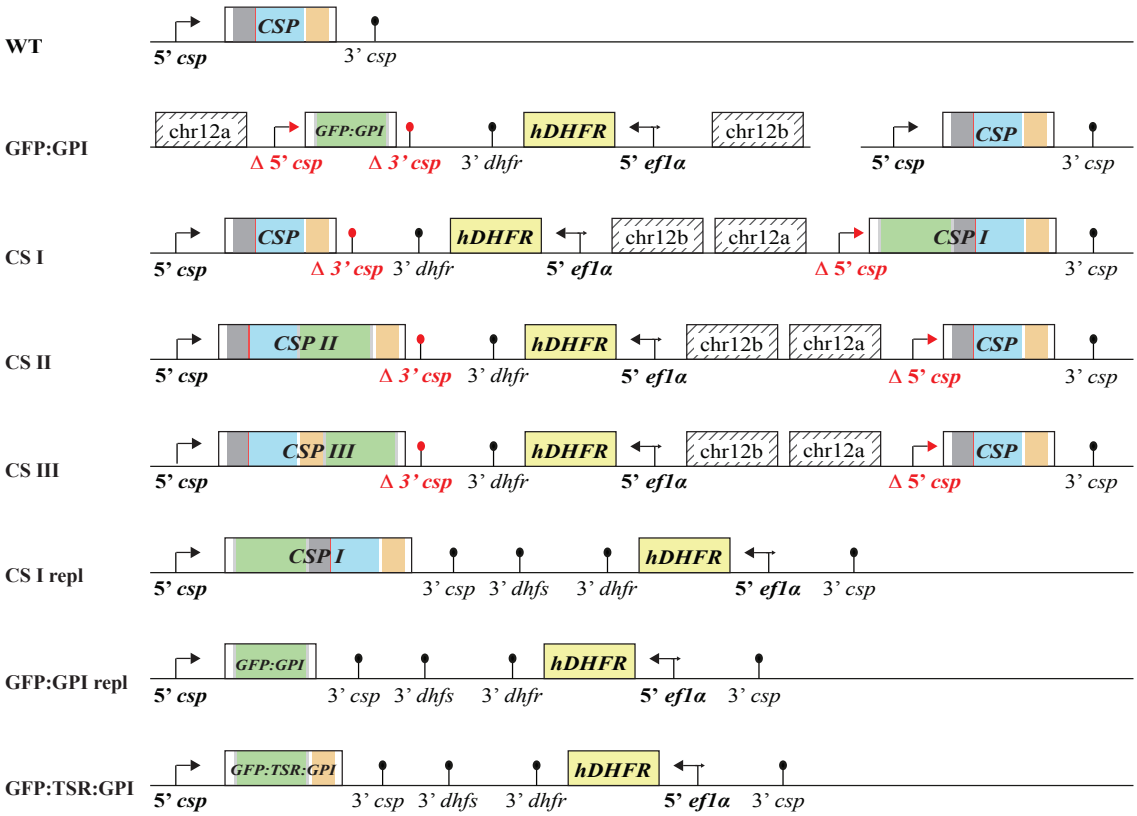

Figure 3.28: Gene model of all CSP mutants generated
The locus of CSP is indicated for all parasite lines that were generated. For **GFP:GPI**, the CSP locus is unchanged as the expressed construct in integrated in the chr12 locus. Note that for **GFP:GPI**, both the promoter region Δ ***5' csp*** as well as Δ ***3' csp*** are truncated for the GPI-anchored GFP. Also for **CS I**, the Δ ***3' csp*** of CSP and the promoter region Δ ***5' csp*** of the CS I construct are truncated, as well as for **CS II** and **CS III** the promoter region Δ ***5' csp*** of CSP and the Δ ***3' csp*** of the CS II and CS III construct. All replacements of CSP, **CS I repl**, **GFP:GPI repl** and **GFP:TSR:GPI** have the untruncated promoter region ***5' csp*** as well as ***3' csp***.

To generate the vector for GFP:GPI repl, the 3'UTR of CSP used for integration was amplified with P278 P279, digested with HindIII KpnI and cloned into Pb238. The promoter region of CSP including the SP was amplified with P208 P268, digested with EcoRI and PshAI and ligated into the vector. Then the GPI-anchor sequence including the 3'UTR was amplified with P274 P576, digested with KasI BamHI and ligated into the vector. The vector was linearized using PmeI EcoRI.

To generate the vector for GFP:TSR:GPI, the 3'UTR of CSP used for integration was amplified with P278 P279, digested with HindIII KpnI and cloned into Pb238. Note that the actual integrated 3'UTR is truncated by 228 bp due to an internal HindIII site. The promoter region of CSP including the SP was amplified with P267 P268, digested with EcoRI and PshAI and ligated into the vector. Then the GPI-anchor sequence including the 3'UTR was amplified with P272 P576, digested with KasI BamHI and ligated into the vector. The vector was linearized prior to transfection using PmeI EcoRI.

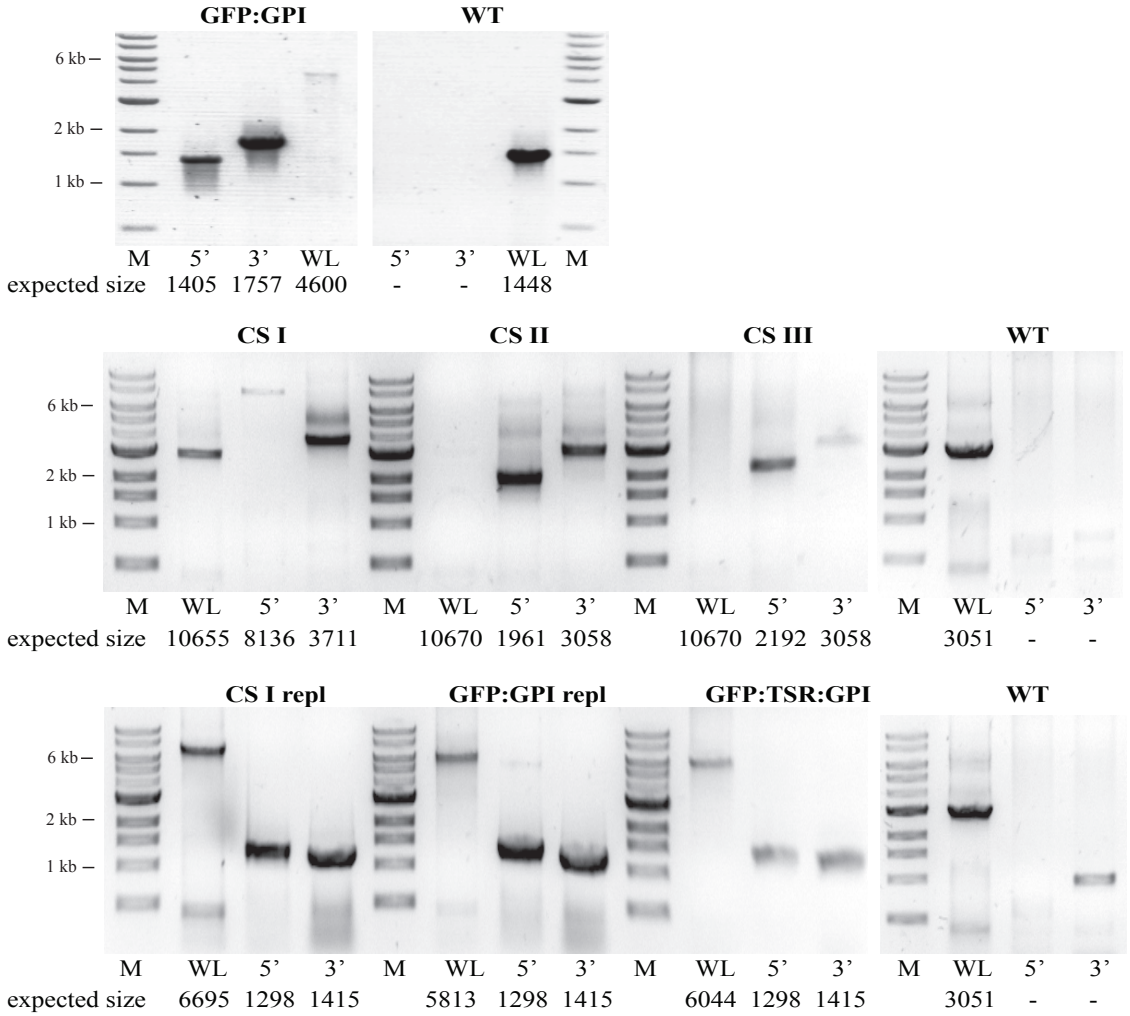

Figure 3.29: Genotyping of all CSP mutants
Genotyping of gDNA was performed for all CSP mutants as well as ANKA WT gDNA. **GFP:GPI** as well as **CS I** parasites are uncloned and may contain some WT. **CS II** clone III/2, **CS III** clone#3, **CS I repl** clone #*2, **GFP:GPI repl** clone #3 and **GFP:TSR:GPI** clone #1* are shown. Expected sizes for 5' integration, 3' integration and whole locus PCR (WL) are indicated. WL PCR products of **CS I**, **CS II** and **CS III** could not be amplified due to size.

To generate CSI repl, the vector of CS I and GFP:TSR:GPI were both digested with BmgBI and KpnI, and the 5800 bp fragment of CS I was ligated with the 3599 bp fragment of GFP:TSR:GPI, effectively extending the 3'UTR of CS I. Prior to transfection, the vector was linearized prior to transfection using PmeI EcoRI.

For genotyping of GFP:GPI, 5' integration was performed with P134 P210, resulting in 1405 bp, 3' integration with P137 P99 resulting in 1757 bp and whole locus PCR with P134 P137 resulting in 4600 bp for GFP:GPI extra and 1448 bp for WT (**Figure 3.29**).

For genotyping of CS I, CS II and CS III, 5' integration was performed with P267 P210 resulting in 1298 bp, 1961 bp and 2192 bp respectively, 3' integration with P893 P882 resulting in 3711 bp, 3058 bp and 3058 bp respectively, and whole locus PCR with

P267 P882 resulting in 10655 bp, 10670 bp and 10670 bp respectively and 3051 bp for WT.

For genotyping of CS I repl, GFP:GPI and GFP:TSR:GPI, 5' integration was tested with P267 P210 resulting in 1298 bp, 3' integration with P234 P882 resulting in 1187 bp and whole locus PCR resulting in 6695 bp, 5813 bp and 6044 bp respectively as well as 3051 bp for WT. In case the selection marker is removed by the parasite by looping out via the vector internal homology conferred by the 3'UTR of CSP, the 3' integration product would be lost and the whole locus PCR would reduce to 4524, 3642 or 3872 bp for CS I replacement, GFP:GPI or GFP:TSR:GPI respectively.

3.3.2 Basic biology of CSP mutants

Mosquito infection of CSP mutants

All CSP parasites developed normally during blood stage development. Several cages of mosquitoes were infected with each parasite line and sporozoite numbers within the midgut and salivary gland were determined (**Table 3.5**). All CSP mutants except the expression of additional copy CS I have a more or less severe salivary gland invasion phenotype, including the expression of GFP:GPI as an extra copy. Salivary gland invasion of CS II was virtually never observed as well as for CS I replacement. All CS II, CS III and CS I replacement lines had a strong egress phenotype from the oocyst and CS III might have a fairly normal salivary gland invasion capacity masked by the low numbers of haemolymph sporozoites blocked by deficient oocyst egress. Replacement mutants of CSP with GFP:GPI or GFP:TSR:GPI completely failed to produce sporozoites, as was expected [27].

Gliding motility of CSP mutants

As haemolymph and salivary gland numbers of most CSP mutants were extremely low, gliding motility of midgut derived sporozoites was assessed at days 18-25 post infection (**Figure 3.30**). This showed 2,0%, 8,9% and 4,1% motile sporozoites for WT, GFP:GPI extra and CS I extra. CS II shows 31,8% motile sporozoites, whereas CS III has 12,6%, CS I replacement 5,5% and trp1 (-) 22,7%. If this is compared with the SG/MG ratio or the HL/MG ration (**Table 3.5**), a correlation between failure to egress and motility of MG sporozoites can be observed. This is also true for trp1 (-), a parasite line that also fails to egress oocysts and additionally shows an salivary gland invasion phenotype [29]. It should be noted that GFP:GPI and CS I sporozoites showed increased numbers of

Table 3.5: Infectivity of CSP mutants in *Anopheles stephensi*

Parasite line	*MGS / mosquito*	*HLS / mosquito*	*SGS / mosquito*	*HLS / MGS*	*SGS / MGS*	*Number of infected mosquitoes analyzed*
WT	77.000	3400	18.000	0,031	0,23	68 (23)
GFP:GPI	46.000	490	2.500	0,009	0,05	160 (97)
CS I	11.000	239	4.400	0,037	0,39	154 (119)
CS II	29.000	92	0,90	0,003	0,00003	97 (97)
CS III	21.000	220	200	0,007	0,0095	108 (58)
CS I repl	120.000	190	12	0,005	0,00007	62 ** (36)
GFP:GPI repl	0	NA	NA	NA	NA	50
GFP:TSR:GPI	0	NA	NA	NA	NA	50

Number of mosquitoes analyzed represent midgut and salivary gland sporozoites, number in parenthesis represents mosquitoes analyzed for hemolymph. Countings were generated from at least three countings between day 15 to day 20 post infection of multiple infected cages. * To calculate the ration of HLS / MGS, only MGS countings were used from the same mosquitoes used to generate HLS countings. ** For this samples number of salivary gland sporozoites counted was only 38, thus the SGS / MGS ratio was only calculated from these countings.

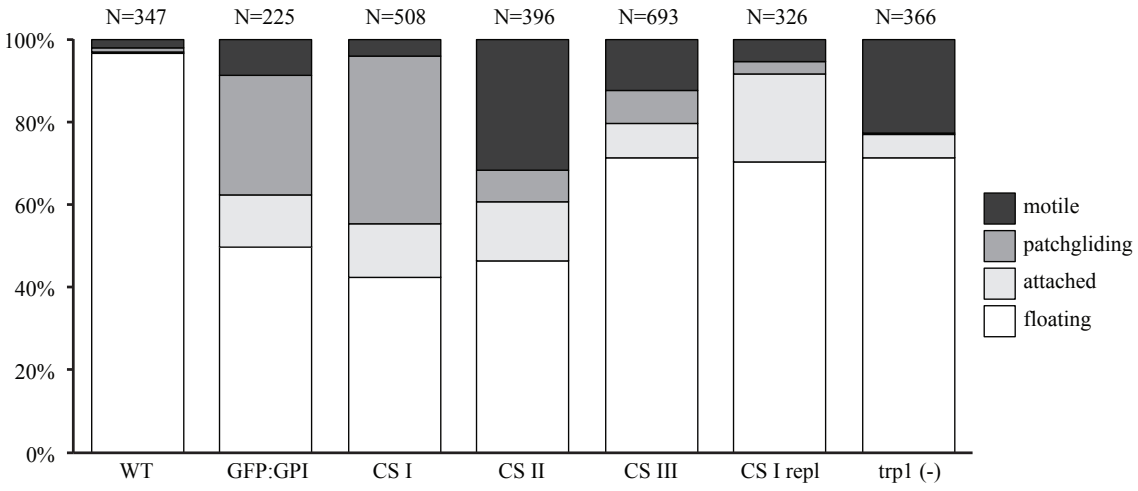

Figure 3.30: Gliding motility of midgut derived CSP mutants
Midgut derived sporozoites were analyzed for gliding motility and classified into motile (distance traveled within 180 seconds of more that 30 μm), patchgliding (back and forward motion over a single attachment site), attached or floating. Numbers on top of the graph describe the number of sporozoites analyzed. Parasites lacking TRP1 (**trp1 (-)**) also do not egress the oocyst and were analyzed for comparison [29]. Samples were derived from mosquito midguts day 25 post infection and imaged after Accudenz purification. CS I repl was derived day 18 post infection and CS III contains data with and without Accudenz purification.

patchgliding sporozoites (**Figure 3.30**). Also the CS I replacement line showed higher numbers of attached MG and HL sporozoites, a phenotype that was also observed in haemolymph sporozoites of CS I replacement (**Figure 3.30**).

Table 3.6: Mice challenged with CSP mutants

Parasite line	*sporozoite dose injected IV*	*infected mice / total mice*
WT	500.000 MGS	3/4
CS I repl	1.000.000 MGS	0/2
CS I repl	500.000 MGS	0/2
CS II	500.000 MGS	0/4

Midgut sporozoites were dissected on day 22/23 post infection and injected i.v. into C57BL/6 mice. Parasitemia was monitored from day 3 until day 20.

Mouse challenge of CSP mutants

Considering the very low numbers of salivary gland sporozoites, mice challenges were performed with midgut derived sporozoites (**Table 3.6**). While 3 of 4 mice became blood stage positive after IV injection with WT sporozoites, both CS I replacement and CS II caused no infection, despite the high ratio of motile sporozoites for CS II.

3.3.3 Oocyst development of CSP mutants

Electron microscopy

Electron microscopy of midguts infected with CSP mutants was performed. Oocysts 7 days after the bloodmeal never showed sporozoite formation. All other timepoints fixed, 10, 12 and 17 days post infection showed a relatively unsynchronous development of individual oocysts with a greater abundance of degenerative oocysts on day 17. For each parasite line as many oocysts as possible were imaged in low and high magnification. Roughly 20 to 200 oocysts were imaged for each parasite line, thus rare events might have been missed in some parasites lines.

Overview images of sporozoite development were generated for all parasite strains imaged (**Figure 3.31** and **Figure 3.32**). Imaging of WT oocysts was difficult as pre-selection of highly infected midguts was challenging, therefore the R/G parasite line (expressing a selection marker free version of Pb262) was also used as WT control. As can be seen in (**Figure 3.31**), during the initial growth of oocysts the PM directly contacts the oocyst wall. Nuclei are large and evenly dispersed throughout the oocyst.

Big patches of ER are present, as well as many mitochondria (**A**). Then the PM starts to retract from the oocyst wall and invaginates towards the center of the oocyst, resulting in sporoblast formation (**B**). The PM of neighbouring sporoblasts can be in tight contact or separated by extracellular space. Also sporoblasts can be in contact with each other by cytoplasmic bridges. If this invagination is always initiated at the

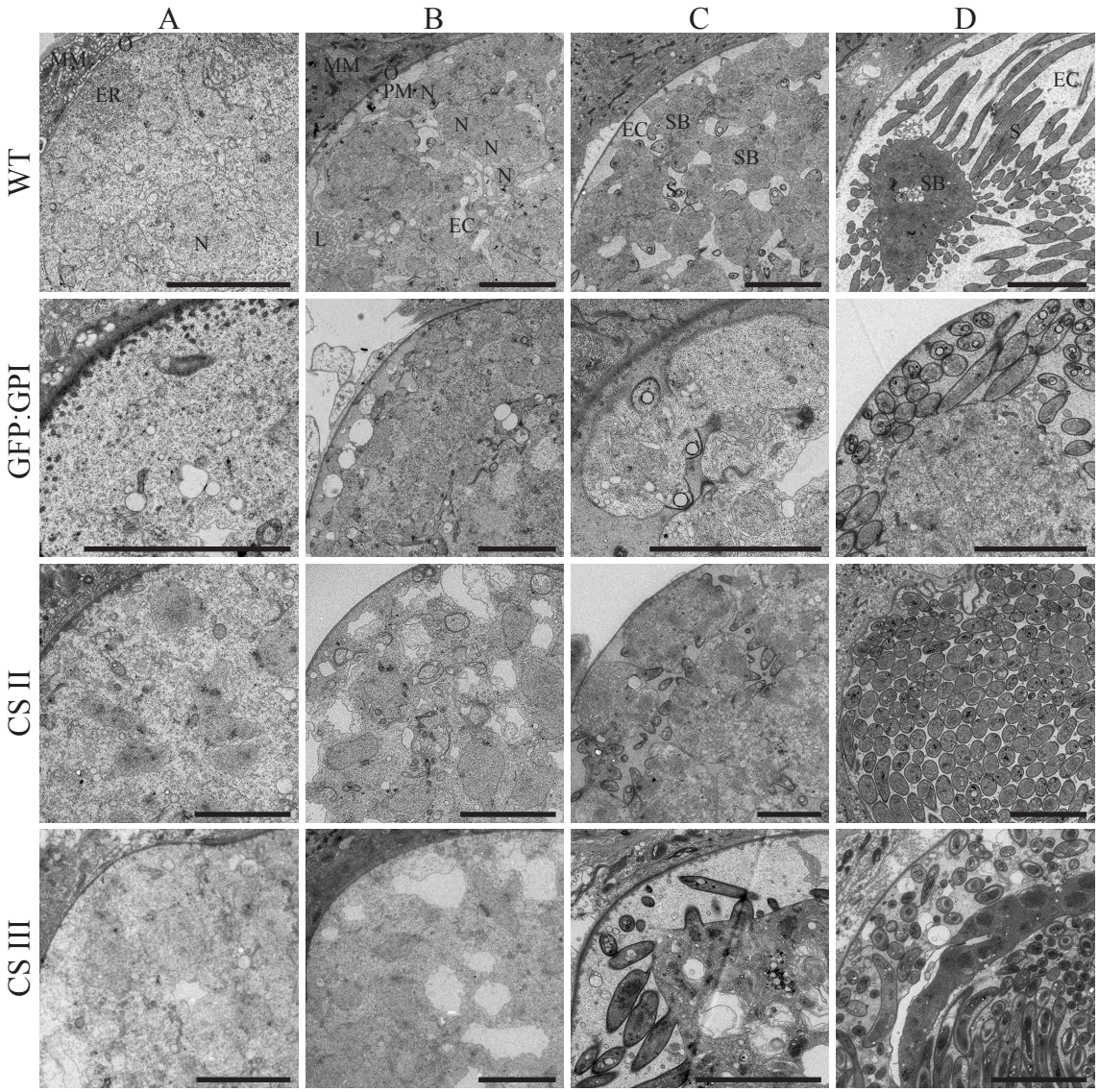

Figure 3.31: Transmission electron microscopy of oocysts of WT and additional copy mutants
Oocysts are shown as quarters from oocyst wall to oocyst center to optimize the overview while preserving some detail. Early to late oocyst are shown from **A** to **D** , images were acquired between 10 to 12 days after bloodmeal. Small nuclei appear closed to the plasma membrane (PM) while the PM starts to retract from the oocyst wall. The invagination of the PM reaches the centre of the oocyst while the PM can be separated by a gap or not, resulting in formation of sporoblasts. Sporozoite formation is initiated at the PM of the entire sporoblasts. Oocysts with mature sporozoites are more frequently observed in mutants that fail to egress the oocyst but are otherwise indistinguishable from WT. PM = plasma membrane, EC = extra cellular, ER = endoplasmic reticulum, N = nulceus, O = oocyst wall, L = labyrinthine structure, S = sporozoite or sporozoite buds, MM = mosquito midgut. Scale bars: 5 μm.

oocyst wall or can also occur by fusion of secretory vesicles is not clear. At this time labyrinthine structures can be observed at the edge of sporoblasts (**Figure 3.31 B** of WT). The initiation of sporozoite formation (**C**) preferentially starts at contact sites of several sporoblasts. It is indicated by the closed association of small nuclei with the

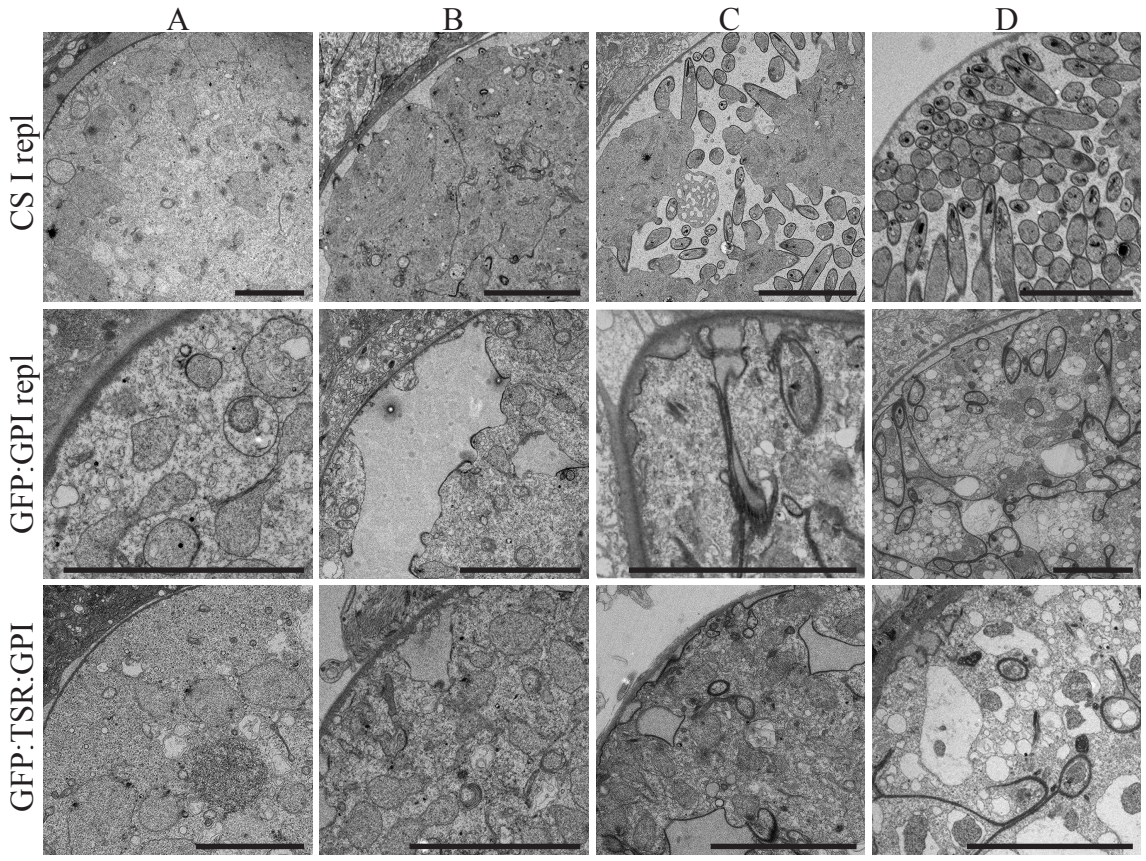

Figure 3.32: Transmission electron microscopy of replacement mutants
Oocysts are shown as quarters from oocyst wall to oocyst center to optimize overview while preserving some detail. Early to late oocyst are shown from **A** to **D**. Oocysts of CS I replacement show the same appearance as WT oocyst. Both oocysts of GFP:GPI repl and GFP:TSR:GPI repl fail to form sporozoites. Invagination is observed in relatively small oocysts frequently as wide invaginations from the oocyst wall which rarely reach the center of the oocyst. Once sporozoite formation is initiated IMC formation occurs in big areas of the plasma membrane. During later invagination the plasma membranes stay in closed contact and are underlined by IMC (darker appearance). Scale bars: 5 μm.

PM, the darkening of the PM at low magnifications caused by the formation of IMC and the formation of a single light appearing vesicle, the prerhoptry. During sporozoite elongation (**D**) the sporoblasts shrink in size and the sporozoites become longer, as the PM of the sporoblast in between the emerging sporozoites retracts. The nuclei of forming sporozoites elongate, and micronemes are formed. As fully formed sporozoites within oocysts are rarely observed for WT parasites, it can be assumed that sporozoites egress shortly after they are matured.

Sporozoite formation of parasites expressing an additional copy of GFP:GPI appears similar to WT. CS II and CS III show a higher number of oocysts where sporozoite formation arrested half way, are full of mature sporozoites or are filled with degrading sporozoites or mature sporozoites and degrading sporoblasts (**Figure 3.31**). If this is

only a cause of their failure to egress the oocysts or an additional developmental defect is not possible to judge from EM in the absense of comparable EM data from other non-egressing mutants such as SERA(-) or TRP1(-) [29, 274].

Oocysts of CS I replacement show normal sporozoite development (**Figure 3.32**). Most oocysts imaged that are invaginating or are beginning to form sporozoites (**B**) show sporoblasts in direct contact with each other. If this is a slight phenotypic difference in contrast to WT development or not is not clear. In contrast to CS II and CS III, all oocysts with mature sporozoites appeared still completely viable, even though all three parasite strains have an egress phenotype.

Oocysts of GFP:GPI replacement and GFP:TSR:GPI replacement both completely failed to develop mature sporozoites (**Figure 3.32**). Generally the invagination of the PM never reaches the center of the oocyst prior to IMC formation. Also, first formation of IMC and microtubule formation occurs at smaller oocyst sizes that for the other CSP mutants and WT. Oocyst development always ends in all PM fully underlined with IMC, with multiple stacks and structures reaching from the oocyst wall to the center of the oocyst (**C** and **D**). Finally oocysts become vacuolated and nuclei start to condense.

Plasma membrane details of CSP mutants The dynamics of the oocyst plasma membrane appears to be variable to a certain degree. In WT oocysts several structures can be observed which might coexists within a single oocyst throughout its development (**Figure 3.33**). In oocysts that have not initiated invagination yet the PM is in close contact with the oocyst wall (**A**). However even at that state the oocyst wall is thicker in certain areas, and these irregularities remain present once the PM has separated. Invagination of the PM can occur in wider areas (**B**, **E**) or in smaller areas (**C**). Occasionally small vesicles are observed closed to the PM (**B** and **P**).

The invaginating PM can invaginate by staying in closed contact with itself in a sheet-like fashion (**D**, **E**, **F**, **G** and **H**) or be separated from the other PM, resulting in a vesicular or tubular appearance in 3D (**G**) (compare with **Figure 3.39**). The labyrinthine structures are most frequently observed in areas of invagination, resulting in them being located mostly peripherally in between forming sporoblasts (**D**, **H**, **I**, **J**, **K** and **N**).

Sporozoite budding is initiated most frequently at sites of invagination in close contact of two or more sporoblasts (**E**, **F**, **G**, **H**, **I** and **L**). After the nucleus is in close contact with the PM, the IMC is formed, subpellicular microtubules appear and a prerhoptry becomes visible. This can occur at sites where the PM has close contact the

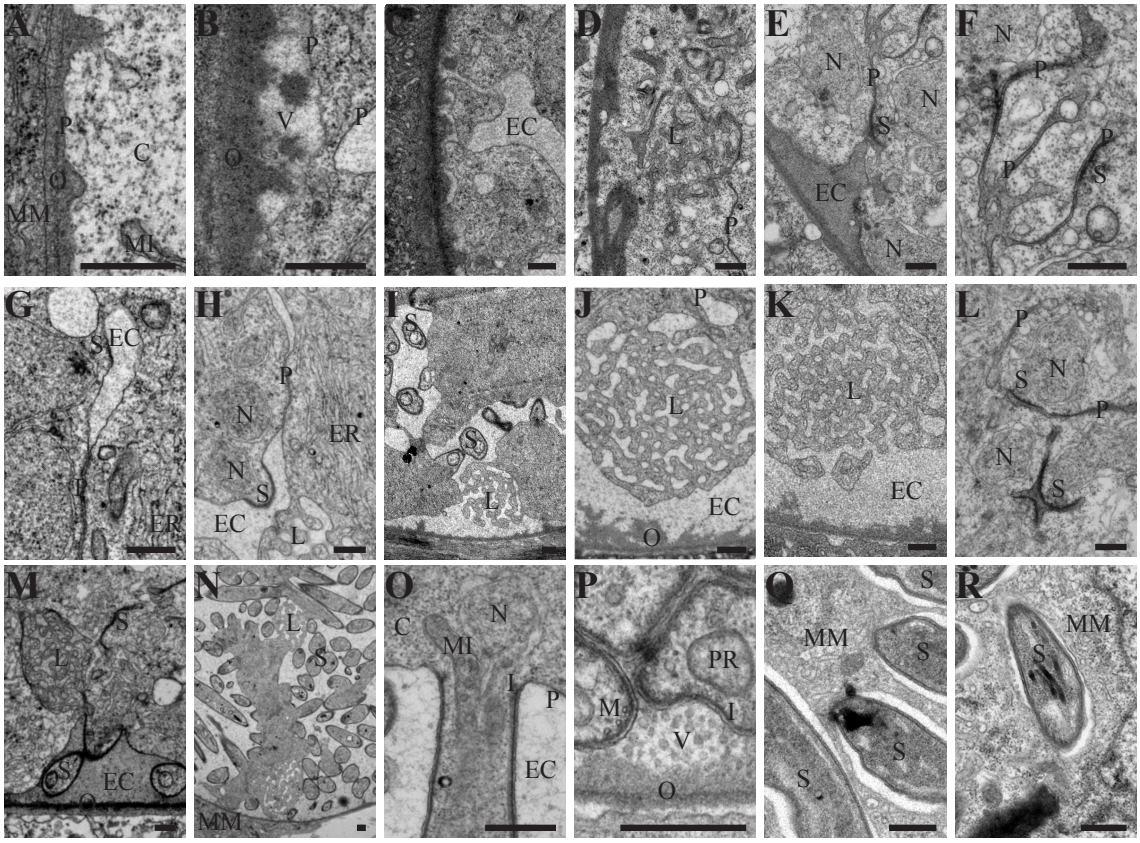

Figure 3.33: Detailed of the oocyst plasma membrane during invagination
Detail views of WT and R/G oocysts. Images **A** to **R** are roughly ordered in order of appearance. It is not known if the initial invagination of the plasma membrane (PM) is always initiated at the oocyst wall as in **B** - **E** or can also be initiated by internal fusion of secretory vesicles as might be suggested by **G**. During invagination, the PM can be in closed contact to other PMs (**D**, **E**, **F**, **G** and **H**) or separated from other PMs (**B**, **C**, **E**, **F**, **G**, **H**). It is not clear how the labyrinthine structures observed (**D**, **I**, **J** and **K**) are initially formed. Note that oocysts contain internal membrane structures in addition to the complex arrangement of the PM. Free sporozoites in midgut tissue (**O** and **R**) are surrounded by some free space, but enclosed by a membrane. P = plasma membrane, EC = extra cellular, C = cytoplasm, ER = endoplasmic reticulum, N = nucleus, O = oocyst wall, MI= mitochondrium, L = labyrinthine structure, PR = prerhoptry, I = inner membrane complex, S = sporozoite or sporozoite buds, V = vesicles, M = microtubuli, MM = mosquito midgut. Scale bars: 500 nm.

the opposing PM (**E** and **F**) or is surrounded by extracellular space (**G** and **I**). During sporozoite elongation the length of the sporozoite extending from the sporoblast is always delimited by the length of the IMC in microtubules (**O**). Elongation of sporozoites can occur with plenty of extracellular space in between (**N** and **O**) or with sporozoites in closed contact to each other (**P**).

In CSP mutants, some additional membrane dynamics are observed (**Figure 3.34**). Occasionally, big vesicular internal structures are observed that are not in visible contact with the extracellular space and might represent fusion products of internal vesicles or artifacts derived from cutting ER stacks in an unfortunate angle (**F**, **I**, **M** and **Q**).

For both GFP:GPI replacement and GFP:TSR:GPI replacement invagination deep

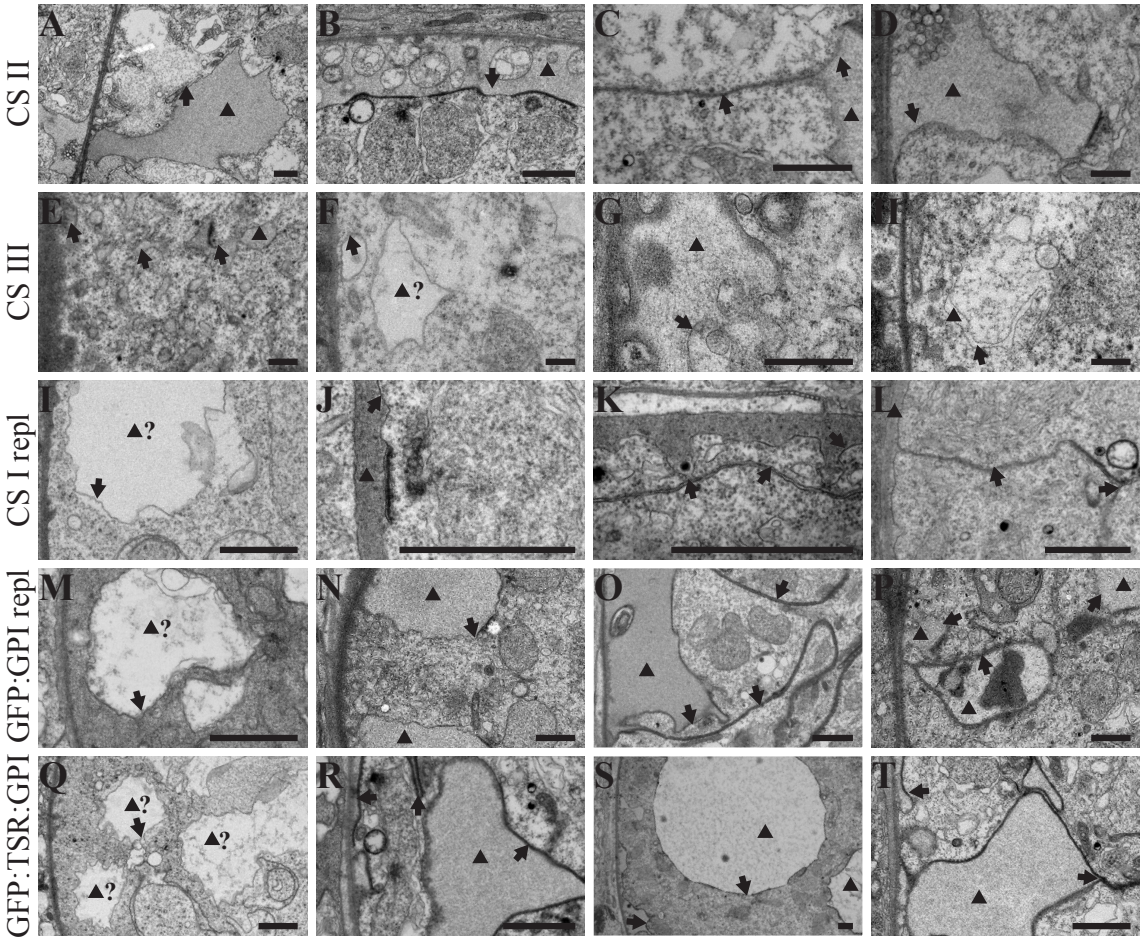

Figure 3.34: Plasma membrane invagination of all CSP mutants
Extracellular space is indicated with an arrowhead, plasma membrane with an arrow. Uncertain areas without contact to the oocyst wall that might result from ER that was partially degraded during EM processing are marked with arrowhead and a "**?**". Scale bars: 500 nm.

into the oocysts that are not yet underlined with IMC are never observed. Bigger bubble-like retractions from the oocyst wall where sporozoite initiation takes place ooccur frequently (**N** and **S**). Invaginations within the oocyst are normally completely underlined with IMC and microtubules and the PM is either at nearly round extracellular spaces (**N**, **O**, **R**, **S** and **T**) or in tight contact with itself (**O**, **R** and **T**).

The distance of closely associated PMs during invagination was measured from electron microscopic images of 8.000 x to 15.000 x magnification (**Figure 3.35**). Distances pre and post IMC formation were analyzed separately. Initial PM distances (pre IMC formation) appear to be somewhat tighter for WT and CS I replacement that for all other mutants analyzed. Once the IMC is underlining the PM the distances in between two associated PMs are generally smaller. The lowest distance is observed in GFP:GPI replacement. As this parasite does only express the GPI-anchor of CSP, an active role of CSP in the tight PM associations seems unlikely.

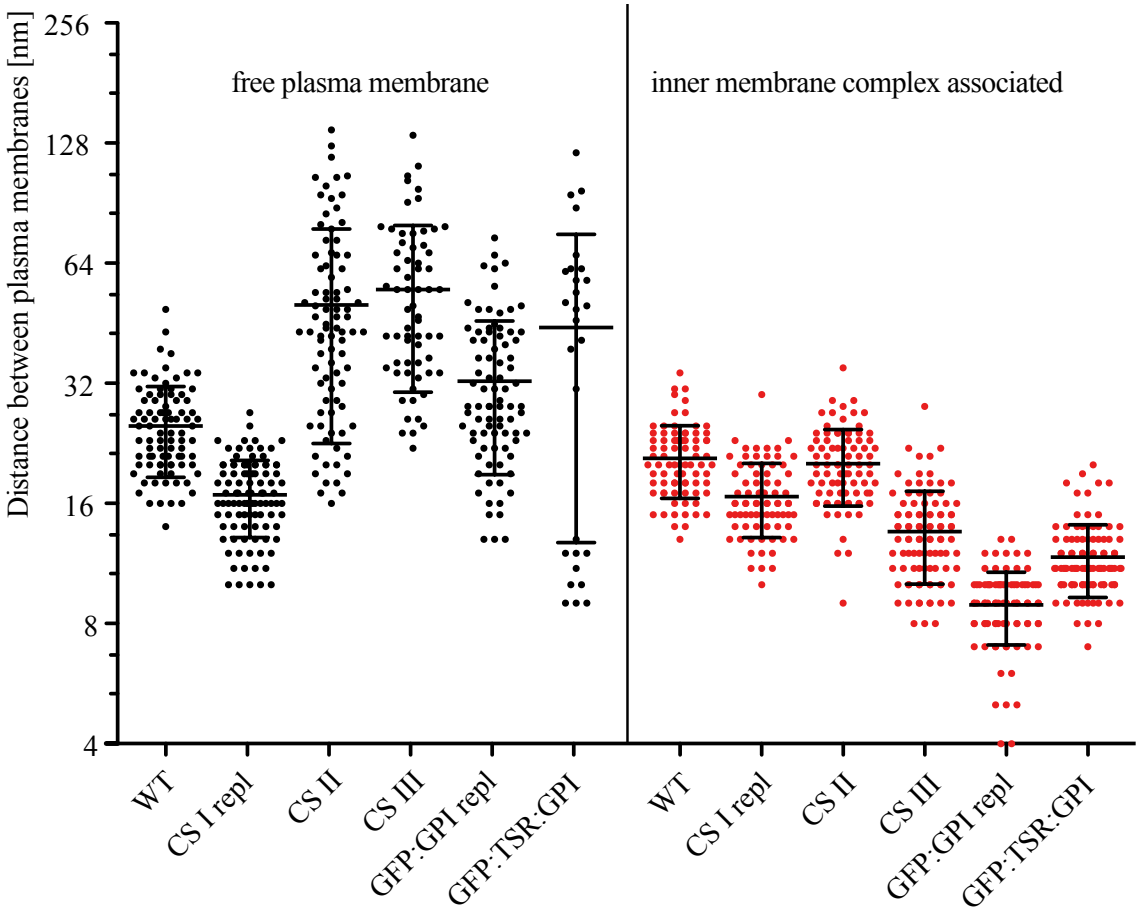

Figure 3.35: Plasma membrane distances of CSP mutants
The distance of two neighboring plasma membranes (PM) during invagination was measured for all membranes in closed contact from high magnification electron microscopic images. Free plasma membrane on the left is the distance of PMs not yet underlined by inner membrane complex (IMC), on the right the distance of PMs of IMC-underlined PMs is shown. Several measurements were obtained from a single image at different locations. Error bars are mean with standard deviation.

Labyrinthine structures In most sections of oocysts labyrinthine structure are observed (**Figure 3.36**). Neither their composition nor their function is known. They tend to appear at the periphery of sporoblasts, frequently connecting two neighboring sporoblasts with cytoplasmic bridges. Many are in closed proximity of the oocyst wall, but some appear more central (**Figure 3.33 N**). Labyrinthine structures are relatively ordered arrays of membranes (**Figure 3.33 K** and **Figure 3.36 E**) that are delimited by PM and contain additional internal membrane structures. The origin of the internal membrane that is not always visible is not known.

Sporozoite development of CSP mutants Oocysts of CS II, CS III and CS I replacement generate normal number of oocysts. Initial sporozoite formation by EM is not distinguishable from WT oocysts (**Figure 3.37**). However more oocysts with many

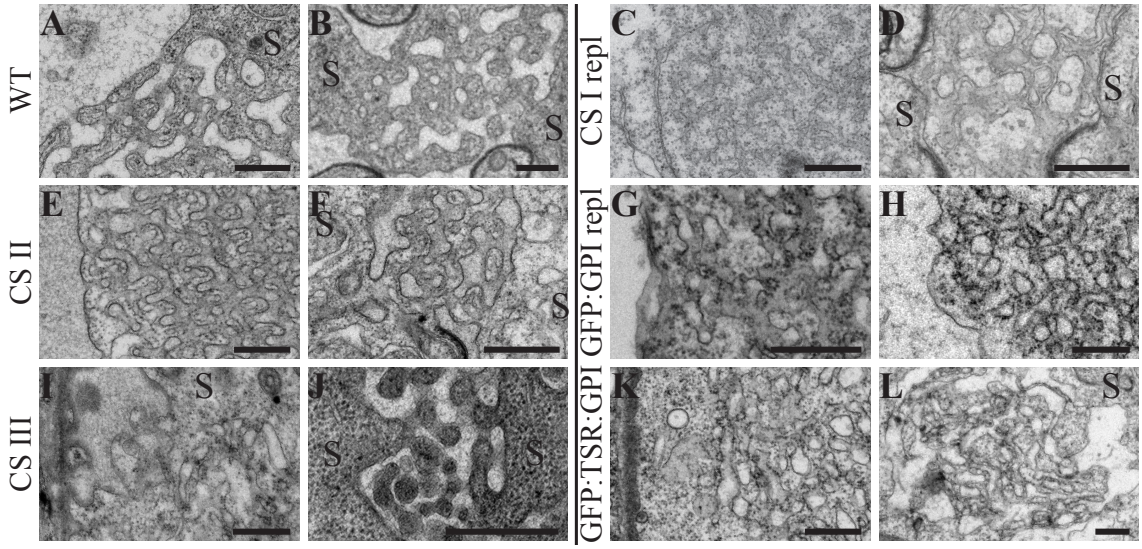

Figure 3.36: Labyrinthine structures in all CSP mutants
Labyrinthine structures as observed in all parasite lines. Mature labyrinthine structures were frequently observed in WT, CS II and CS I replacement, but not in oocysts of CS III, GFP:GPI replacement and GFP:TSR:GPI replacement. As the origin of labyrinthine structures is not known, it is not clear if the structures observed for these parasites are arrested during formation, malformed structures or missformed endoplasmatic reticulum. Structures shown in (**J**) are also observed in fully budded WT oocysts and are most like old and degraded labyrinthine structures. Labyrinthine structures are not only covered with plasma membrane, but also contain internal membranes (see **A**, **D**, **E**, and **F**). S = sporoblast, scale bars are 500 nm.

dark-staining micronemes are observed in CS II and CS III (**H**, **I**, **N** and **O**). Additionally, more oocysts which are only partially filled with mature sporozoites and also contain degraded sporozoites and or degraded sporoblasts were observed for CS II and CS III (**Figure 3.38 D - K**). Both has not been observed for CS I replacement via EM, but the number of oocysts observed that were fully filled with mature CS I replacement sporozoites was quite low.

Both GFP:GPI replacement and GFP:TSR:GPI replacement fail very early during sporozoite formation. In both parasites invagination is never completed before IMC formation starts. Rarely initial sporozoite buds are observed, but in most oocysts the complete PM is underlined with IMC and microtubules (**Figure 3.37 E, F, J, K, L, W** and **X**). Arragements of multiple layers of two tightly associated PMs, but underlined with IMC and microtubules, which are in turn again in contact with IMC underlining the next PM are observed (**F**, **J**, **K** and **X**). Even at later timepoints at least partially formed sporozoites are observed (**E**, **V** and **W**), but these are always internal and never without the direct contact of another PM. Many oocysts also seem to degrade faster than the oocysts of CS I replacement, CS II and CS III that are filled with sporozoites, while in GFP:GPI replacement and GFP:TSR:GPI replacement show strong vacularization and condensing nuclei (**Figure 3.38 L - S**).

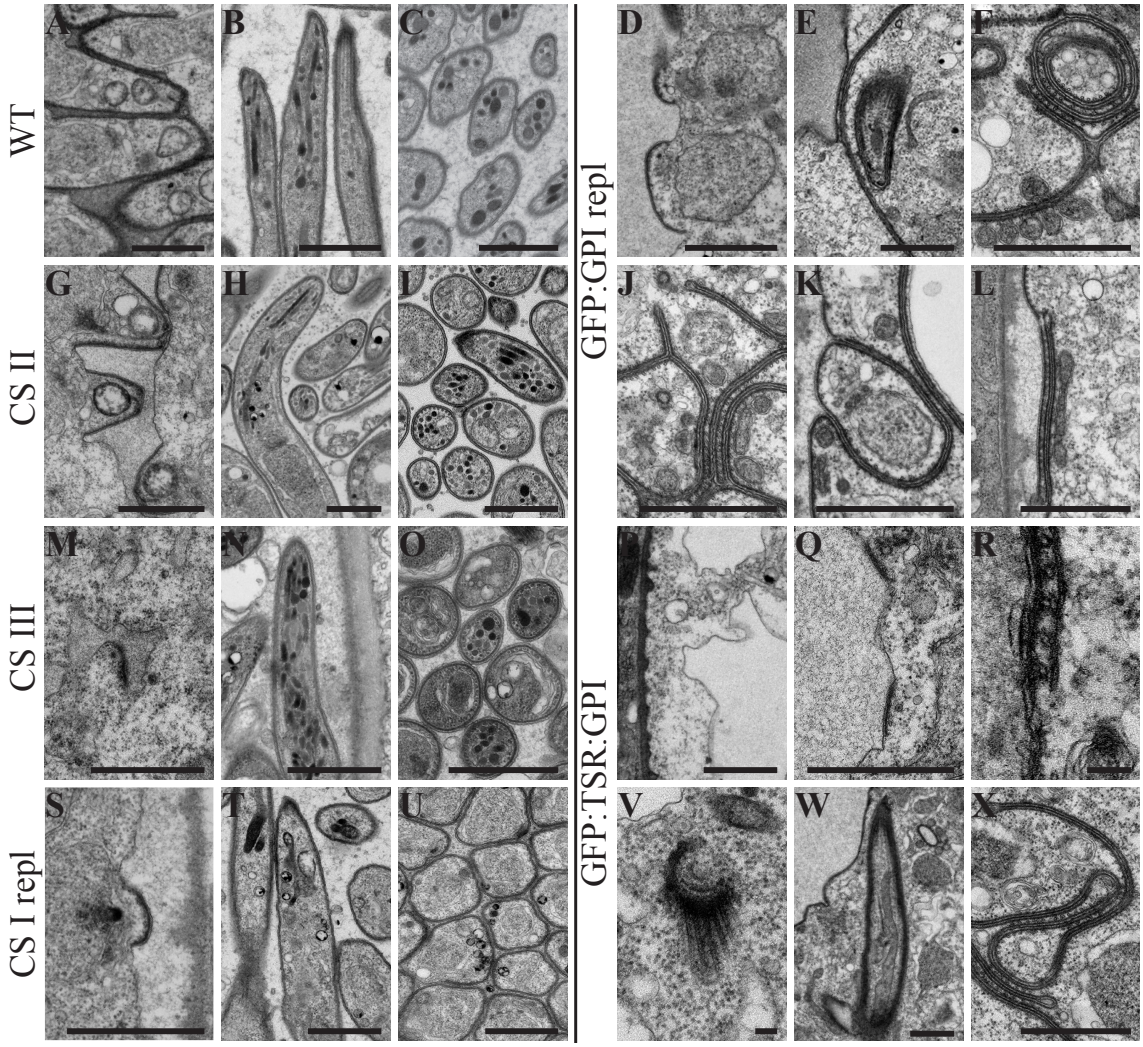

Figure 3.37: Detail of sporozoite formation of all CSP mutants
More oocysts with mature sporozoites of CS II and CS III are observed, which have numerous dark micronemes (**H**, **I**, **N**, **O**). Sporozoite formation of CS I replacement appears like in WT oocysts. Sporozoite formation in GFP:GPI replacement and GFP:TSR:GPI replacement is initiated but stops early (**D**, **E**, **Q**, **V**). Longer sporozoite-like structures in these two parasite lines are always observed budding within a sporoblast with the plasma membranes (PM) in tight contact (**E** and **W**). Stacks of multiple PM - inner membrane complex (IMC) - microtubules (MI) - IMC - PM are observed, with PMs always in tight contact and MI flanked by IMC on both sides (**F**, **J**, **K**, **L**, **R**, **W** and **X**). Nuclei become unusally small and are all in close association with this arrangement (**F** and **J**). Scale bars of **R** and **V**: 100 nm, all others: 1 μm.

Localization of interdomain GFP tags of CSP during sporozoite formation

The main reason for the generation of all interdomain GFP tags of CSP was to understand CSP localization during sporozoite formation. The timing and strength of expression depends on the length of the respective 5'UTR and 3'UTR flanking the GFP tag (**Figure 3.28**). Additionally, depending on the position of the GFP within the CSP gene the strength of fluorescence can differ significantly, suggesting that the various tags might have a varying half-life at the PM. From the following data, a considerable amount

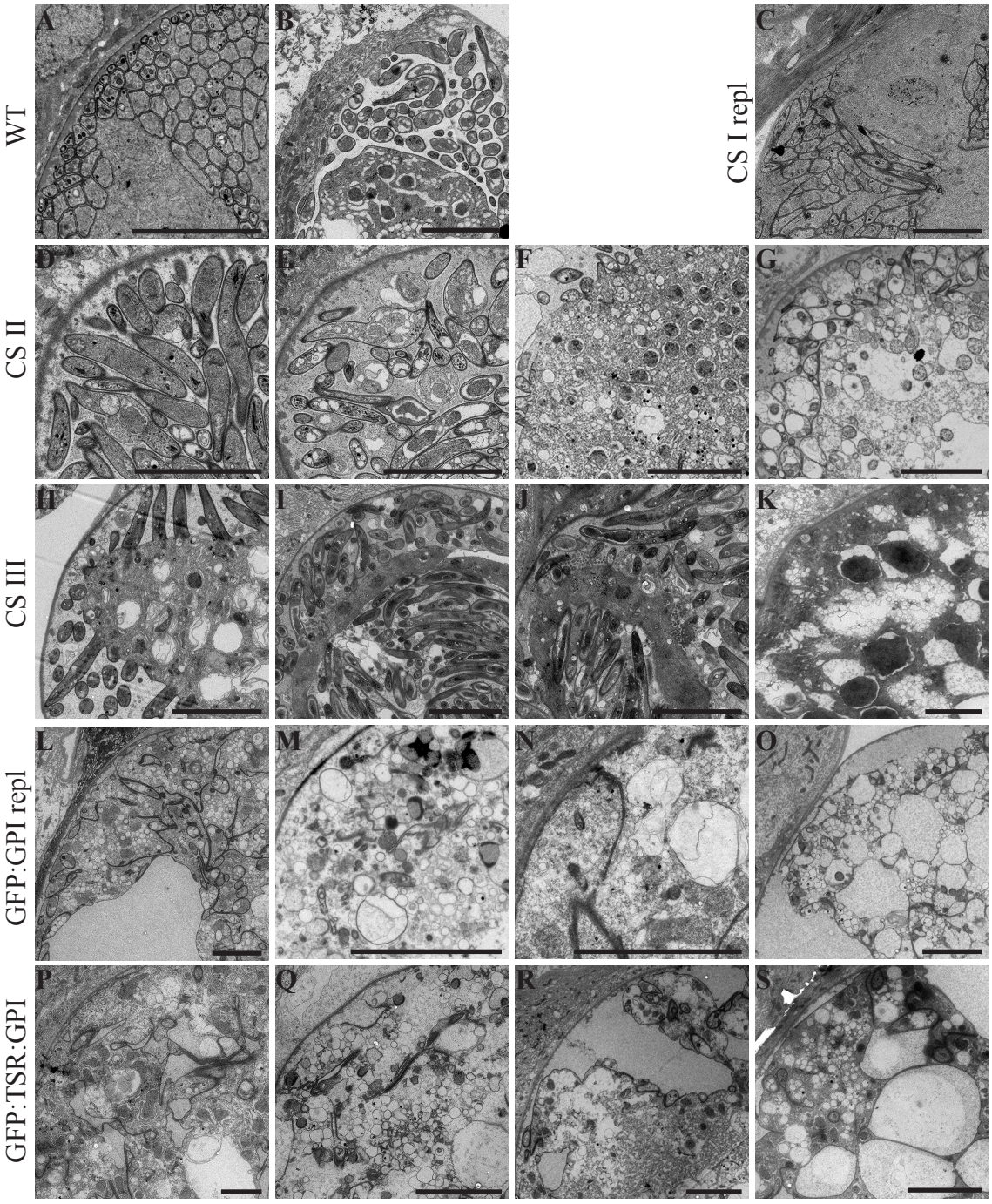

Figure 3.38: Overaged oocysts and failed sporozoite formation of all CSP mutants
All phenotypes observed in oocysts observed of WT and all CSP mutants. WT and CS I repl oocysts appear normal. For CS II and CS III, oocysts with partially degraded sporozoites, oocysts that did not fully form or failed completely to form sporozoites were observed. For GFP:GPI repl and GFP:TSR:GPI repl, many oocysts with big vacuoles and condensed and degraded nuclei were observed. Scale bars: 5 μm.

of the oocyst microscopy using SIR-Tubulin has been performed by Jannik Traut under my supervision.

Localization of GFP:GPI additional copy Oocysts expressing GFP:GPI as an additional copy most likely represent the WT development closest as they have normal MG sporozoite numbers and the expression level of GFP:GPI is significantly lower that all other CSP mutants. GFP:GPI can be observed throughout oocyst development (**Figure 3.39**).

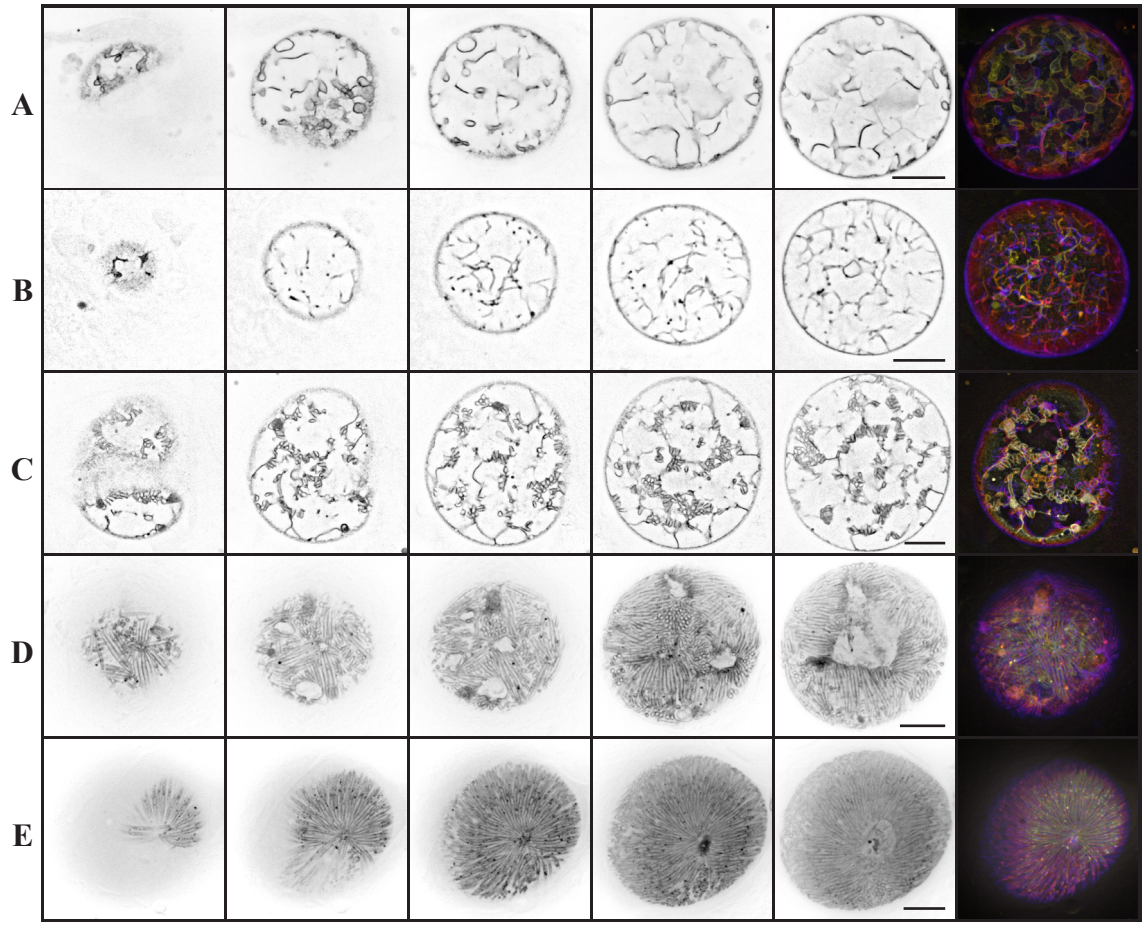

Figure 3.39: Development of oocysts expressing GFP:GPI
Live oocysts expressing GFP:GPI as an additional copy. Several representative z-layers of the oocyst from periphery to the center are displayed from left to right. A depth color-coded z-stack is shown on the right. Oocysts are ordered by developmental stage from **A** to **E**. **A** Sheet-like invagination of the plasma membrane (PM). **B** Tubular invagination of the PM. **C** Initialization of sporozoite formation. **D** and **E** Sporozoite elongation. Scale bars: 10 μm.

Invagination of the PM can be observed in a sheet like fashion (**Figure 3.39 A**), with strongly varying fluorescent signals due to z-stacking if membranes are perpendicular to the focal layer and very faint signals if they are near parallel. In contrast the more tubular invagination observed in (**B**) shows a more even intensity distribution.

Sporozoite formation is already initiated in (**C**). Most sporozoite formation events are initialized internally in between sporoblasts. Several evenly fluorescent patches in between sporoblasts in (**C** and (**D**) most likely represent the labyrinthine structures also

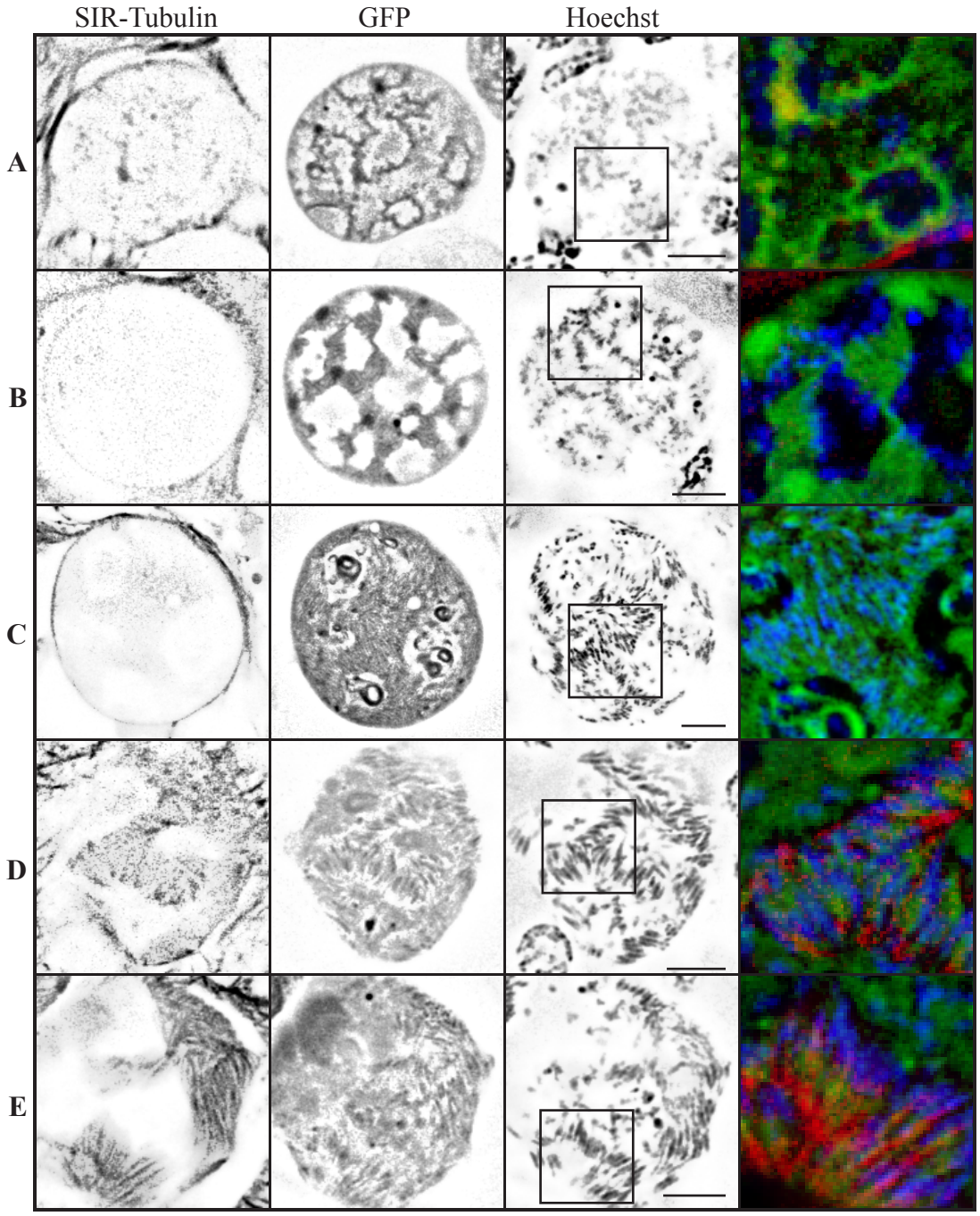

Figure 3.40: Development of oocysts expressing GFP:GPI
Live oocysts expressing GFP:GPI as an additional copy. Microtubules labeled with SIR-Tubulin and DNA labeled with Hoechst. Oocysts are ordered by developmental stage from **A** to **E**. **A** Transition from sheet-like invagination to sporozoite formation. **B** Early sporozoite formation. Note the labyrinthine structures showing a strong GFP signal. **C**, **D** and **E** Sporozoite elongation with elongated nuclei. All have a strong GFP signal within the sporoblast ER. Note that absence of SIR-Tubulin staining as in B and C does not imply absence of microtubules. Scale bars: 10 μm.

observed via EM. In (**D** and (**E**) the fluorescent signal at the oocyst wall is no longer present, indicating that there is no PM associated. The sporoblast appears to contain

relatively little GFP in (**D**), in contrast to (**E**). Also note that the PM signal of fully formed sporozoites appears somewhat weaker than during early sporozoite formation. This might be caused by increased protease activity within the oocyst. Additionally in (**E**) the fluorescence is not exclusively localized at the PM, but also partially at the nuclear envelope and potentially at the Golgi.

Additionally to direct live cell microscopy, live midguts were stained with SIR-Tubulin for microtubules and with Hoechst to localize DNA. Generally immature oocysts stain infrequently, and broken and degraded oocysts stain more frequently then intact ones with these dyes. However in some instances, all three signals could be detected in intact oocysts. In (**Figure 3.40 A**), the initiation of sporozoite formation can be observed. While the GFP signal alone appears to show a somewhat irregular invagination, the little dots of the SIR-Tubulin colocalizing with the site of invagination indicate that microtubules are already formed at the very tip. In (**B**) sporozoites are already elongated. Here staining of microtubules failed. The already elongated nuclei are about to be pulled into the forming sporozoites. The round structures with strong GFP signal represent the labyrinthine structures.

In (**C**) sporozoite formation is almost complete. The elongated nuclei are already within the sporozoites. While microtubule staining is extremely weak, it is clearly excluding the sporoblasts, which contain large ER structures strongly labeled with GFP. In (**D** and **E**), the membrane associated signal of GFP:GPI is weaker than in previous developmental stages. Nuclei are now fully elongated, and microtubules are formed throughout the whole length of sporozoites.

Localization of CS II additional copy Sporozoite development in oocysts expressing CS II as an additional copy coincides with very strong GFP expression (**Figure 3.41**). Initial localization at the oocyst wall appears to label a rough (in contrast to smooth) structure (**A**). The round structures with the strongest fluorescence observed in (**B**, **C** and **D**) are the labyrinthine structures. Virtually no fluorescent signal is observed internally at the ER, indicating a fast trafficking and / or a high stability at the surface. In addition to events occurring during sporozoite formation, several oocysts with spaghetti-like arrangement of sporozoites were observed (**E**), indicating that sporozoite are free to move in respect to each other, actively or passively. Active motility as in [29] was not observed. Also, several oocysts could be observed that show aberrant sporozoite formation (**F**). Several times while imaging mature oocysts, leaking of fluorescence from the oocyst was observed, negatively staining the entire midgut tissue (**Figure 3.52 A**).

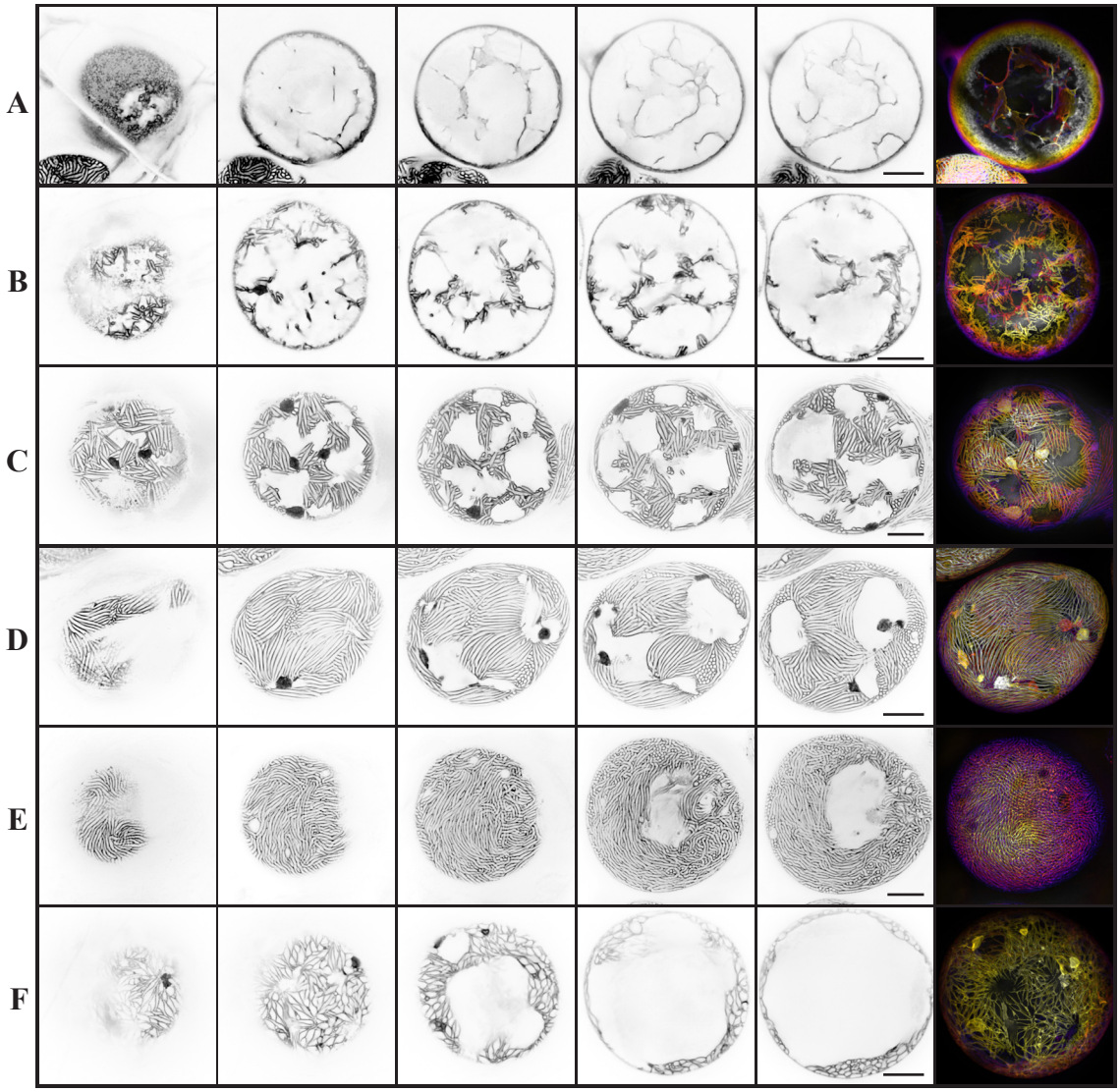

Figure 3.41: Development of oocysts expressing CS II
Live oocysts expressing CS II as an additional copy. Several representative z-layers of the oocyst from periphery to the center are display from left to right. A depth color-coded z-stack is shown on the right. Oocysts are ordered by developmental stage from **A** to **F**. **A** Sheet-like invagination of the plasma membrane. **B** Initialization of sporozoite formation. **C** and **D** Sporozoite elongation. Note the labyrinthine structures showing a strong GFP signal and absence of ER labeling in the sporoblasts. **E** Sporozoite formation completed as indicated by the unordered arrangement of sporozoite. **F** Failed sporozoite formation. Scale bars: 10 μm.

This implies that the strong surface signal of mature sporozoites within oocysts might be partly due to negative staining of the sporozoite surface by soluble protein within the tight space in between sporozoites within the oocyst.

Visualizing microtubules, CS II and DNA simultaneously shows CS II-GFP appears as expected for normal sporozoite development (**Figure 3.42**). Invagination of the PM in a sheet-like fashion prior to sporozoite formation shows that nuclei are already PM associated (**A**). In (**B** and (**C**) sporozoite formation is initiated. The sporoblasts are indicated by an absence of nuclei and weak staining of SIR-Tubulin and CS II.

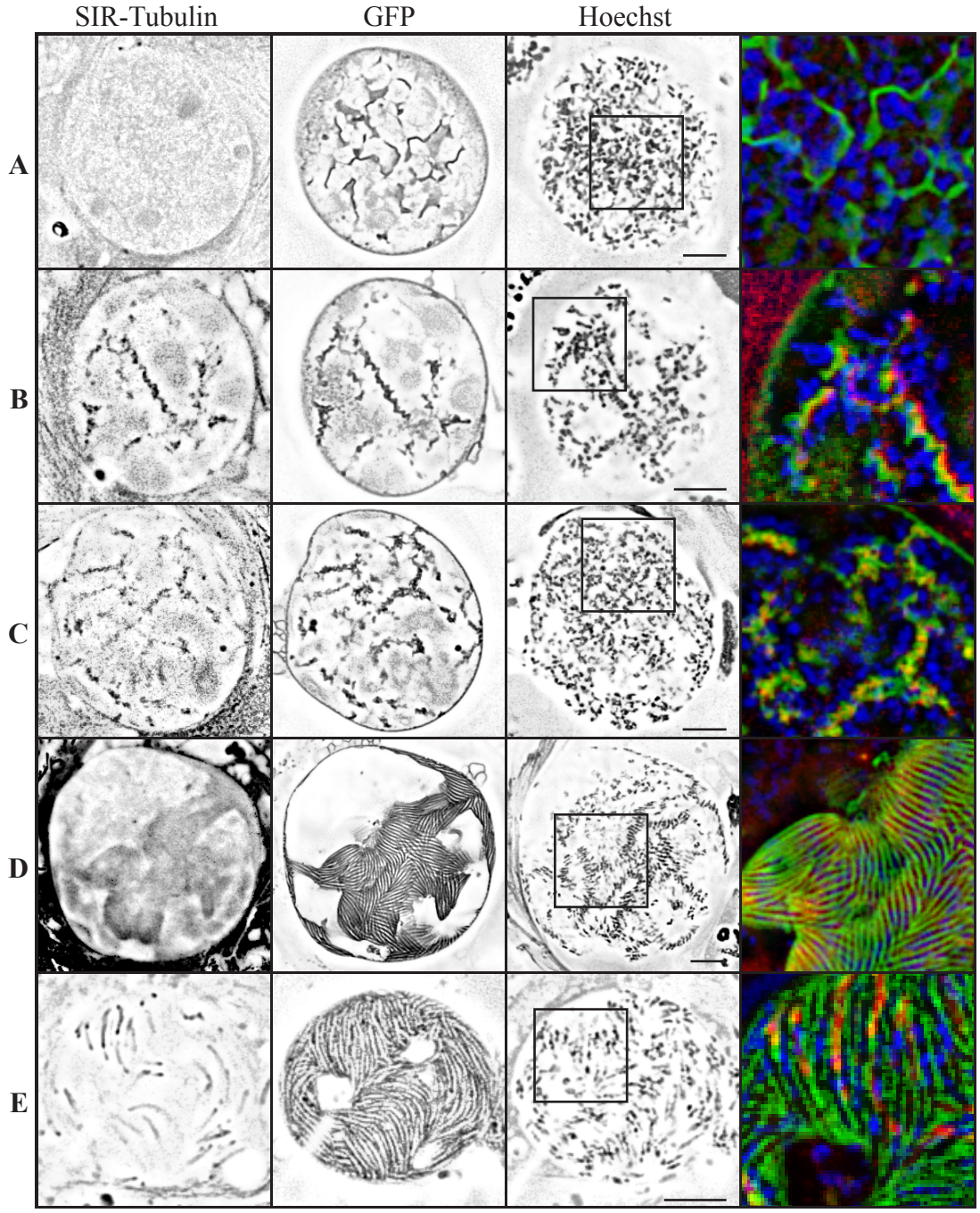

Figure 3.42: Development of oocysts expressing CS II
Live oocysts expressing CS II as an additional copy. Microtubules labeled with SIR-Tubulin and DNA labeled with Hoechst. Oocysts are ordered by developmental stage from **A** to **E**. **A** Sheet-like invagination. **B** and **C** Initiation of sporozoite formation. Sporoblast ER with weak GFP signal. **D** and **E** Sporozoite elongation with elongated nuclei and no GFP signal within the sporoblast. Note that partial absence of SIR-Tubulin staining as in D and E does not imply absence of microtubules. Scale bars: 10 μm.

In (**D**) the nuclei are already contained within the elongated sporozoites. The labeling of microtubules of only a subset of mature sporozoites (**E**) might be a sign that these sporozoites are partially degraded. Indeed, if immature oocysts were crushed

during imaging these tended to show much stronger signal with SIR-Tubulin than free mature sporozoites (data not shown).

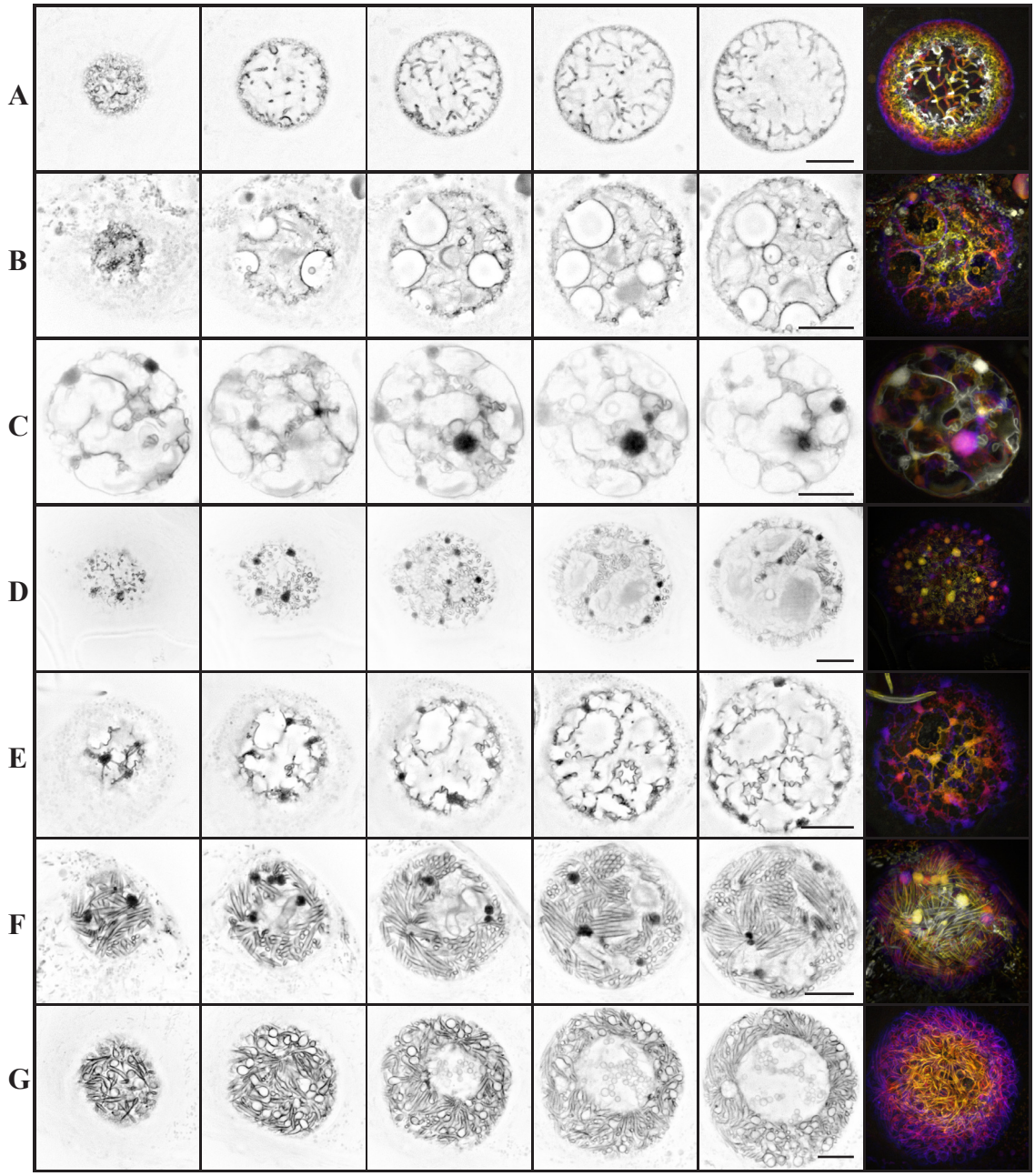

Figure 3.43: Development of oocysts expressing CS III
Live oocysts expressing CS III as an additional copy. Several representative z-layers of the oocyst from periphery to the center are display from left to right. A depth color-coded z-stack is shown on the right. Oocysts are ordered by developmental stage from **A** to **G**. **A** Tubular invagination of plasma membrane (PM). **B** Blubble-like invagination of the PM. **C** Sheet-like invagination of the PM transitioning to sporozoite formation. **D** and **E** Initialization of sporozoite formation. Note that in **E** sporozoite formation occurs also at the PM of large bubble-like invaginations. **F** Sporozoite elongation. **G** Failed sporozoite formation with GFP signal within the nuclear envelope in the sporoblast (round structures). Compare (**Figure 3.38**). Note the labyrinthine structures showing a strong GFP signal and presence of ER labeling in the sporoblasts of **B**, **D** and **F**. **F** Sporozoite formation completed indicated by the unordered arrangement of sporozoite. **G** Failed sporozoite formation. Scale bars: 10 μm.

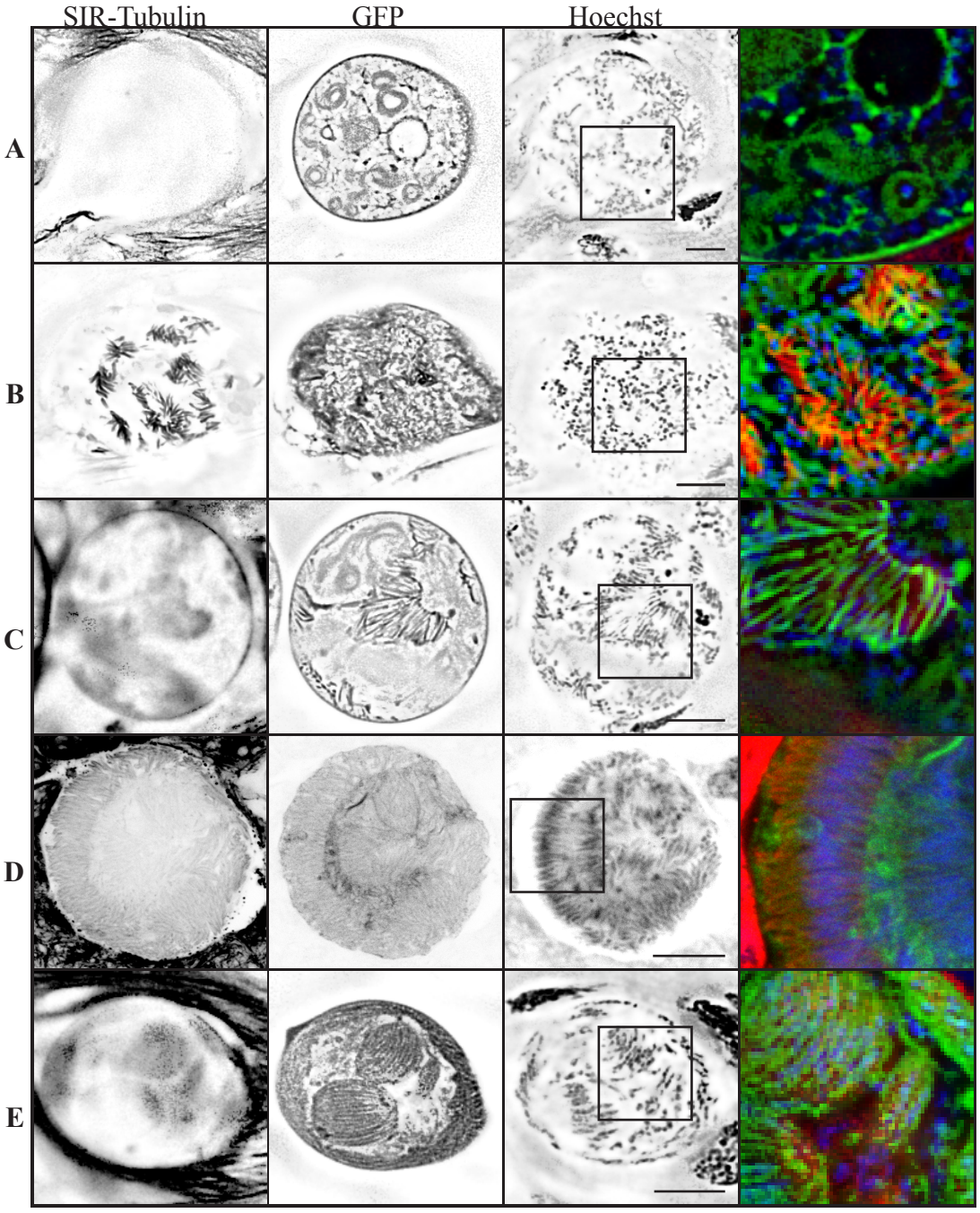

Figure 3.44: Development of oocysts expressing CS III
Live oocysts expressing CS III as an additional copy. Microtubules labeled with SIR-Tubulin and DNA labeled with Hoechst. Oocysts are ordered by developmental stage from **A** to **E**. **A** Initiation of sporozoite formation. **B**, **C**, **D** and **E** Elongation of sporozoites. Within all oocysts GFP signal is also present in the ER of the sporoblasts. Note that absence of SIR-Tubulin staining as in A does not imply absence of microtubules. Oocyst in **D** is fixed and was stained with anti-α-tubulin antibody and Draq5 for DNA. Scale bars: 10 μm.

Localization of CS III additional copy Sporozoite development in oocysts expressing CS III as an additional copy appears similar but not exactly as in CS II (**Figure 3.43**). Generally the GFP fluorescence is less concentrated to the PM and stronger in internal membranous structures, mainly the ER (**B**, **D** and **E**). Labyrinthine structures are also

labeled (**C**, **D**, **E** and **F**). In **E**, sporozoite formation occurs at the complete surface of the bubble-like invaginations, whereas in (**C** and **D**) forming sporozoites have direct contact to the sporozoites budding from the neighboring sporoblast. Several oocysts with partially budded malformed sporozoites can be observed (**G**) (compare **Figure 3.38 E** and **G**). Labeling microtubules and DNA shows the same results (**Figure 3.44**). In rare events while imaging mature oocysts, leaking of fluorescence from the oocyst was observed, negatively staining the entire midgut tissue (**Figure 3.52 A**).

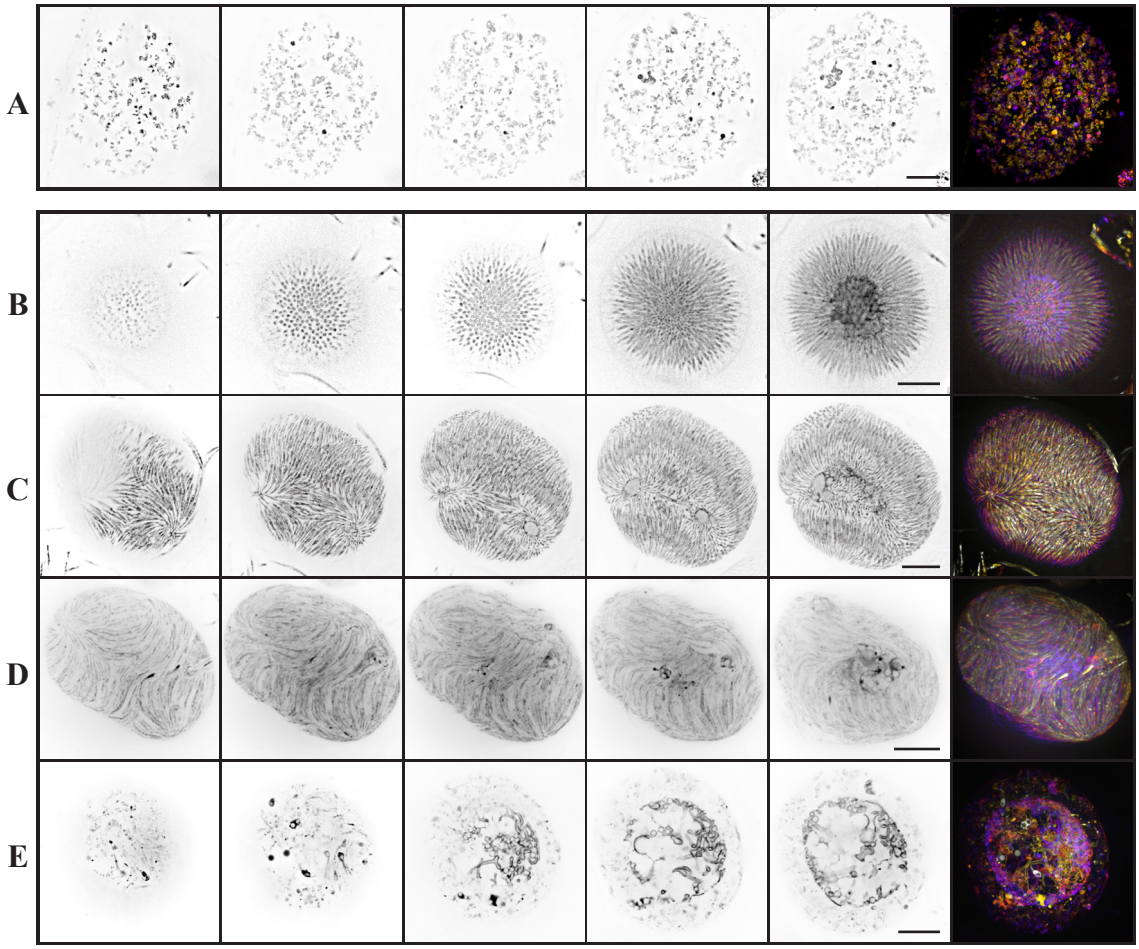

Figure 3.45: Development of oocysts expressing CS I
Live oocysts expressing CS I as an additional copy. Several representative z-layers of oocysts from periphery to the center are displayed from left to right. A depth color-coded z-stack is shown on the right. Oocysts are ordered by developmental stage from **A** to **E**. **A** CS I is not yet expressed, therefore nuclear staining using Hoechst is shown. Indication of sheet-like invagination of the plasma membrane by the arrangement of nuclei. **B** Sporozoite formation from a single central sporoblast. **C** and **D** Sporozoite elongation. **E** Failed sporozoite formation into a single central bubble-like invagination. Note the labeling of the nuclear envelope of single sporozoites in **B** and **C** whereas sporozoites in **D** show a more irregular possibly vesicular staining. Scale bars: 10 μm.

Localization of CS I additional copy Sporozoites develop normally in oocysts expressing an additional copy of CS I. These oocysts show much weaker GFP fluorescence that

CS II and CS III, mainly do to the short 5'UTR driving expression. Additionally CS I is never visible at the PM but only at internal structures, mainly ER and nuclear envelope (**Figure 3.45 B - E**). The more irregular localization observed in (**D**) as well as the apical localization in (**C**) suggests partial misstrafficking of CS I to secretory organelles.

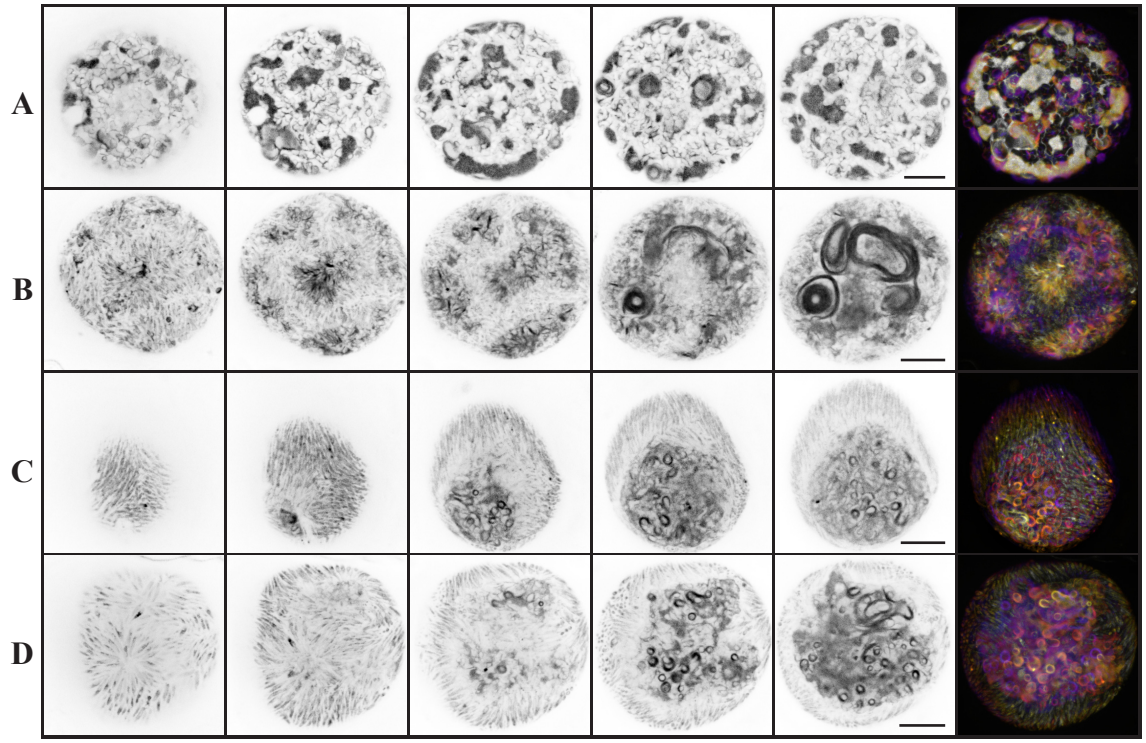

Figure 3.46: Development of oocysts of CS I replacement
Live oocysts expressing CS I replacing CSP. Several representative z-layers of the oocyst from periphery to the center are displayed from left to right. A depth color-coded z-stack is shown on the right. Oocysts are ordered by developmental stage from **A** to **D**. **A** CS I is localized with ER and the nuclear envelopes (weaker signal). **B**, **C** and **D** Sporozoite formation. CS I is localized within the ER and nuclear envelope of sporoblast and forming sporozoites. Note the relative strength of ER localization and the absence of sporozoite surface labeling. Scale bars: 10 μm.

Localization of CS I replacement Oocysts expressing CS I replacing CSP appear very different to CS II and CS III (**Figure 3.46**). Very strong fluorescence as in CS II and CS III can be observed, but no fluorescence is observed at the PM. The fluorescence is only observed within the ER and nuclear envelope of the oocyst (**A**), as well as the nuclear envelope of forming sporozoites (**B**, **C** and **D**). This is supported by staining microtubules and DNA (**Figure 3.47**). Here also all strong signals of GFP can be associated to the ER of the sporoblast and not extracellular space, indicating that the GFP never accesses the PM. No labeling of labyrinthine structures could be observed for CS I.

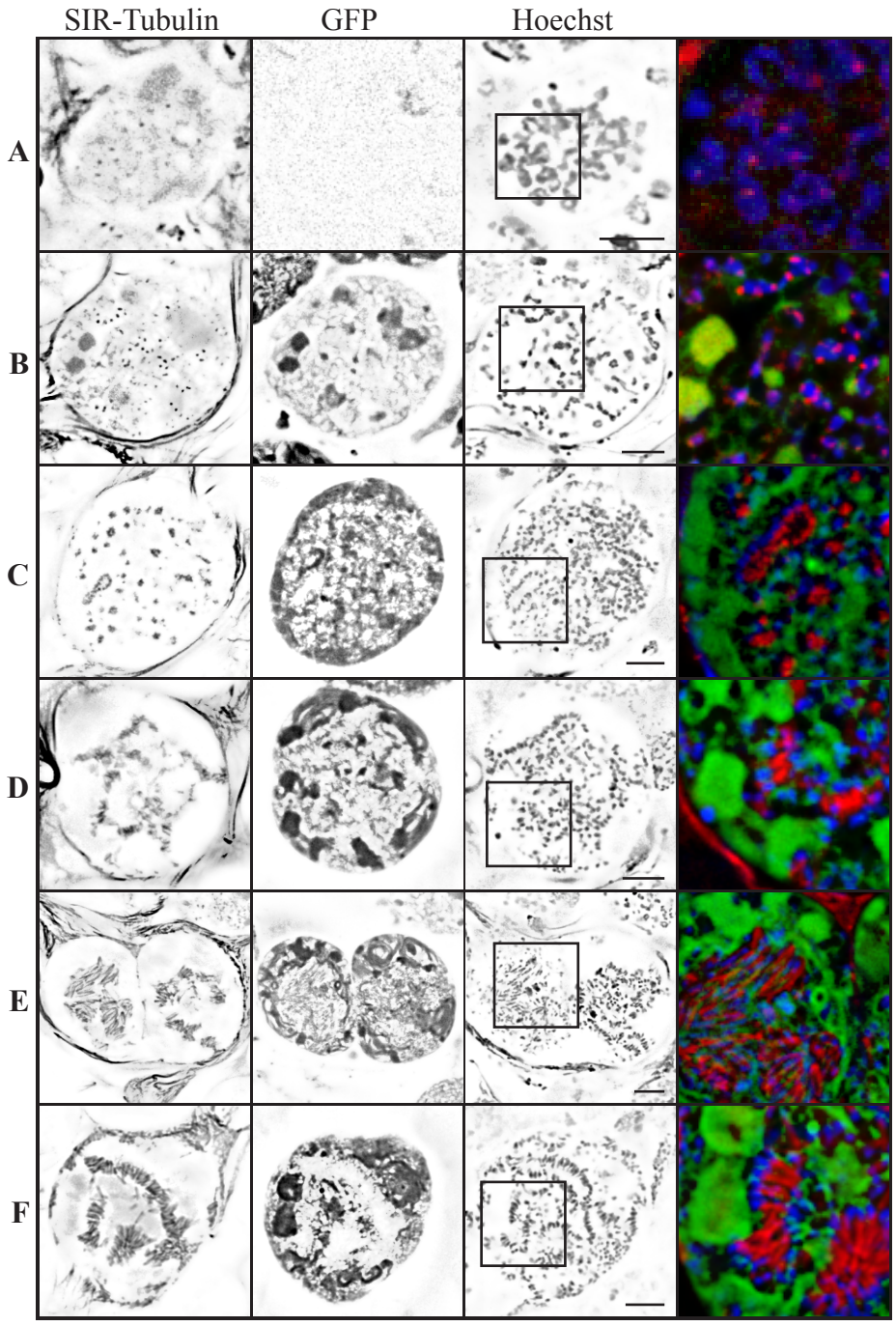

Figure 3.47: Development of oocysts of CS I replacement
Live oocysts expressing CS I replacing CSP. Microtubules labeled with SIR-Tubulin and DNA labeled with Hoechst. Oocysts are ordered by developmental stage from **A** to **F**. **A** Nuclear division as indicated by the spindle pole staining of SIR-Tubulin at the periphery of the still large central nuclei. CS I is not yet expressed. **B** Nuclear division is finalizing, nuclei are starting to localize to the periphery. Invagination might be initiated. CS I is expressed and localized within ER and nuclear envelope. **C** Sporozoite formation initiating. **D**, **E** and **F** Sporozoite elongation. CS I is still mainly localized within the ER of the sporoblasts, but also visible within the nuclear envelope of forming sporozoites and absent from all plasma membranes. Scale bars: 10 μm.

Localization of GFP:GPI replacement Oocysts lacking CSP and expressing GFP:GPI always fail to form sporozoites and show strong fluorescence (**Figure 3.48**). Localization

at early oocysts can be highly patchy and irregular (**A**). GFP:GPI is localized to the PM, the nuclear envelope and strongly labels large internal ER stacks (**B** and **C**). During later timepoints in oocysts showing invagination of the PM, the main fluorescence is observed at the PM (**D**, **E** and **F**) and at the nuclear envelope (**E**). If mechanical pressure is applied to infected midguts, the oocyst material is pushed out, leaving a fluorescent oocyst wall behind (**Figure 3.52 B**).

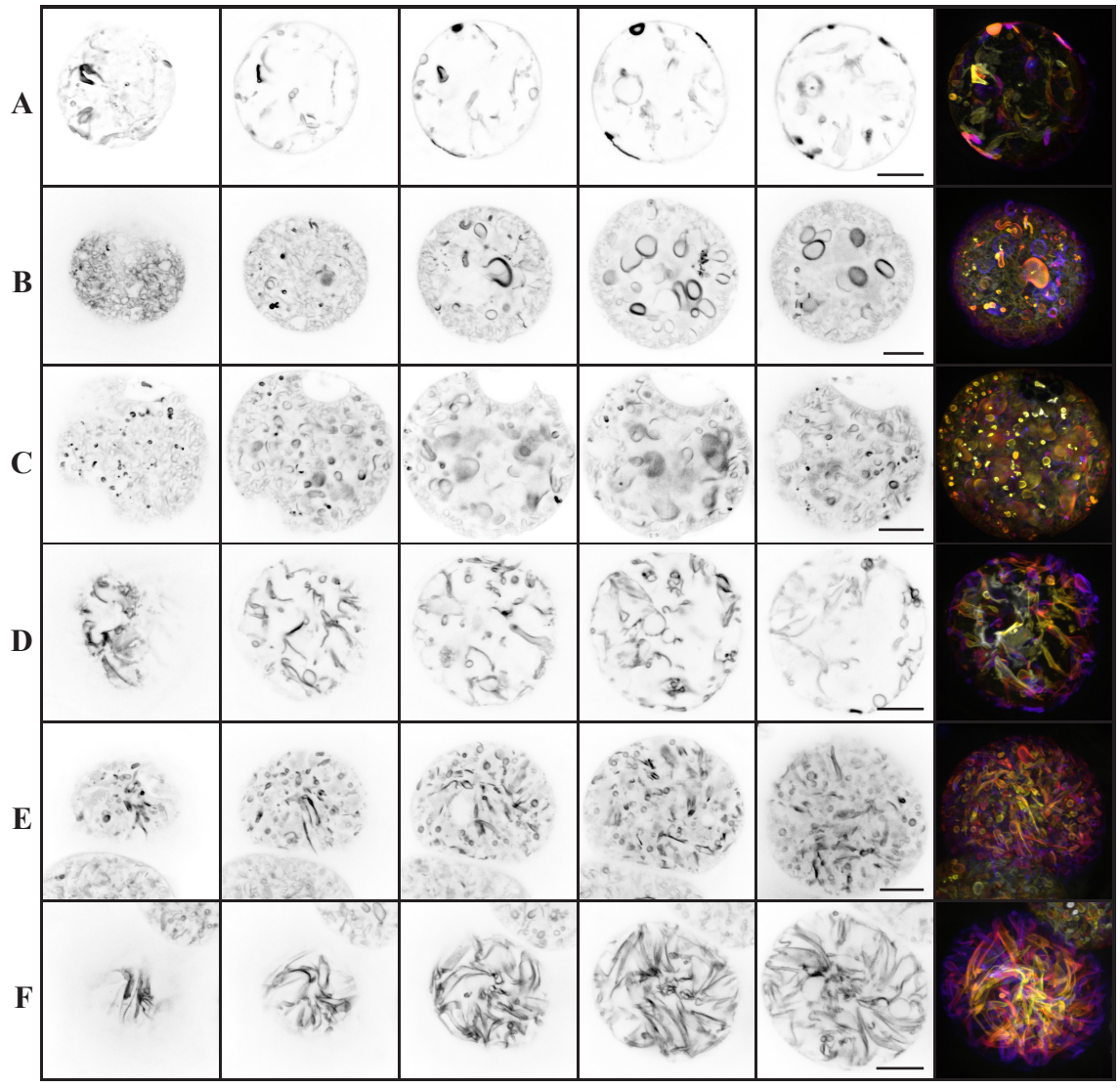

Figure 3.48: Development of oocysts of GFP:GPI replacement
Live oocysts expressing GFP:GPI replacing CSP. Several representative z-layers of the oocyst from periphery to the center are displayed from left to right. A depth color-coded z-stack is shown on the right. Oocysts are ordered by developmental stage from **A** to **F**. **A** GFP is localized at the plasma membrane (PM) and the ER in an irregular distribution. **B** GFP is localized with PM, ER and the nuclear envelope. **C** Bubble-like invaginations with nuclei nicely aligning at the PM (compare with **Figure 3.32**). GFP is localized with PM, ER and the nuclear envelope. **D**, **E** and **F**. Deep invaginations of the PM which are expected to be underlined with inner membrane complex and microtubules, compare with **Figure 3.32** and **Figure 3.34**. Note the absence of ER and nuclear envelope localization in **F**. Scale bars: 10 μm.

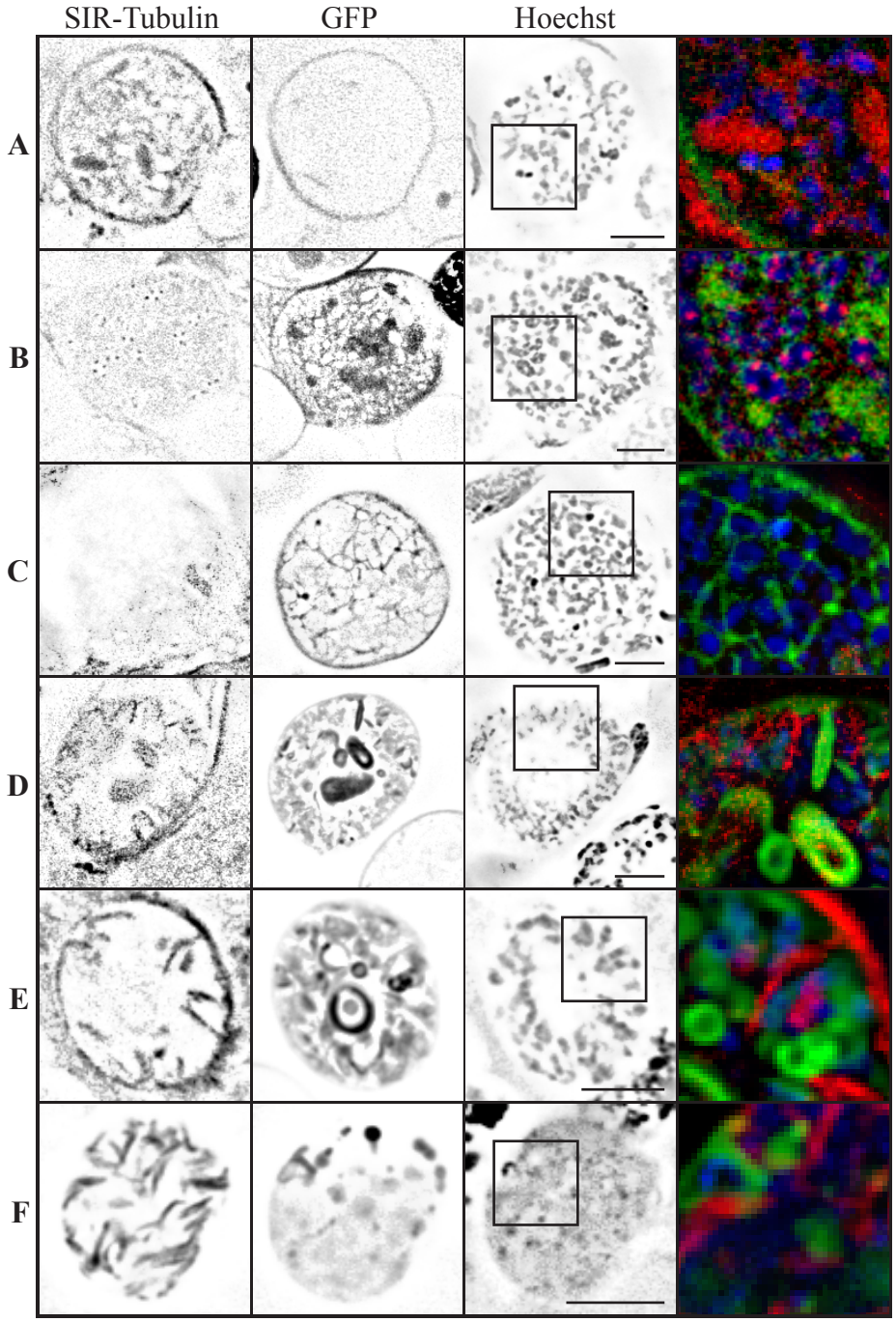

Figure 3.49: Development of oocysts of GFP:GPI replacement
Live oocysts expressing GFP:GPI replacing CSP. Microtubules labeled with SIR-Tubulin and DNA labeled with Hoechst. Oocysts are ordered by developmental stage from **A** to **F**. **A** GFP is only weakly expressed and localized at the PM. **B** Nuclear division still taking place. GFP is localized at the plasma membrane (PM) and the ER as well as the nuclear envelope. **C** GFP is localized at the PM during initial invagination and at the nuclear envelope. **D** and **E** Invagination of the PM which are underlined with microtubules. GFP is also present within the central ER. **F** Very deep invaginations of the PM underlined by microtubules. GFP is mainly localized with stacks of ER. Note that absence of SIR-Tubulin staining as in **C** does not imply absence of microtubules. Scale bars: 10 μm.

Visualization of microtubules and DNA shows that GFP:GPI can already be expressed while nuclear division is still going on (**Figure 3.49 B**). Generally invagination

of the PM does not reach the very center of the oocyst, resulting in a single interconnected sporoblast (**C** - **F**).

Localization of GFP:TSR:GPI replacement Oocysts lacking CSP and expressing GFP:TSR:GPI as a replacement develop similar to oocysts with GFP:GPI replacement.

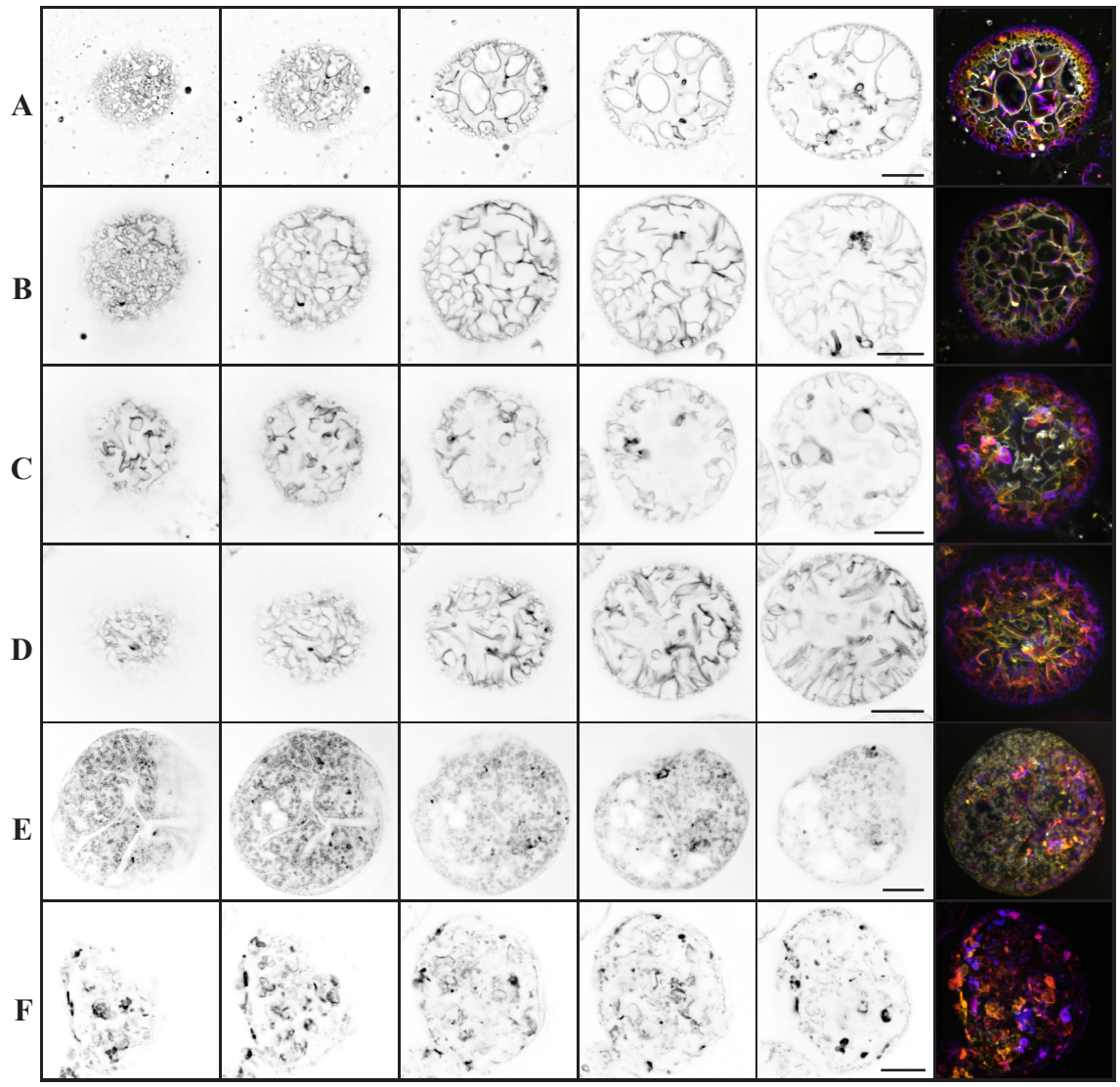

Figure 3.50: Development of oocysts of GFP:TSR:GPI replacement
Live oocysts expressing GFP:TSR:GPI replacing CSP. Several representative z-layers of the oocyst from periphery to the center are display from left to right. A depth color-coded z-stack is shown on the right. Oocysts are ordered by developmental stage from **A** to **F**. **A** Bubble-like invaginations and initiation of sporozoite formation. GFP is lolcalized at the plasma membrane (PM) and the oocyst wall. **B** and **C** Invagination of PM. GFP is localized at the PM and oocyst wall. **D** Deep invagination of the PM which are expected to be underlined with inner membrane complex and microtubules, compare with **Figure 3.32** and **Figure 3.34**. **E** and **F** Failed sporozoite formation. Compare GFP localization in **E** at the oocyst wall and nuclear envelop with highly irregular patchy localization in **F**. Scale bars: 10 μm.

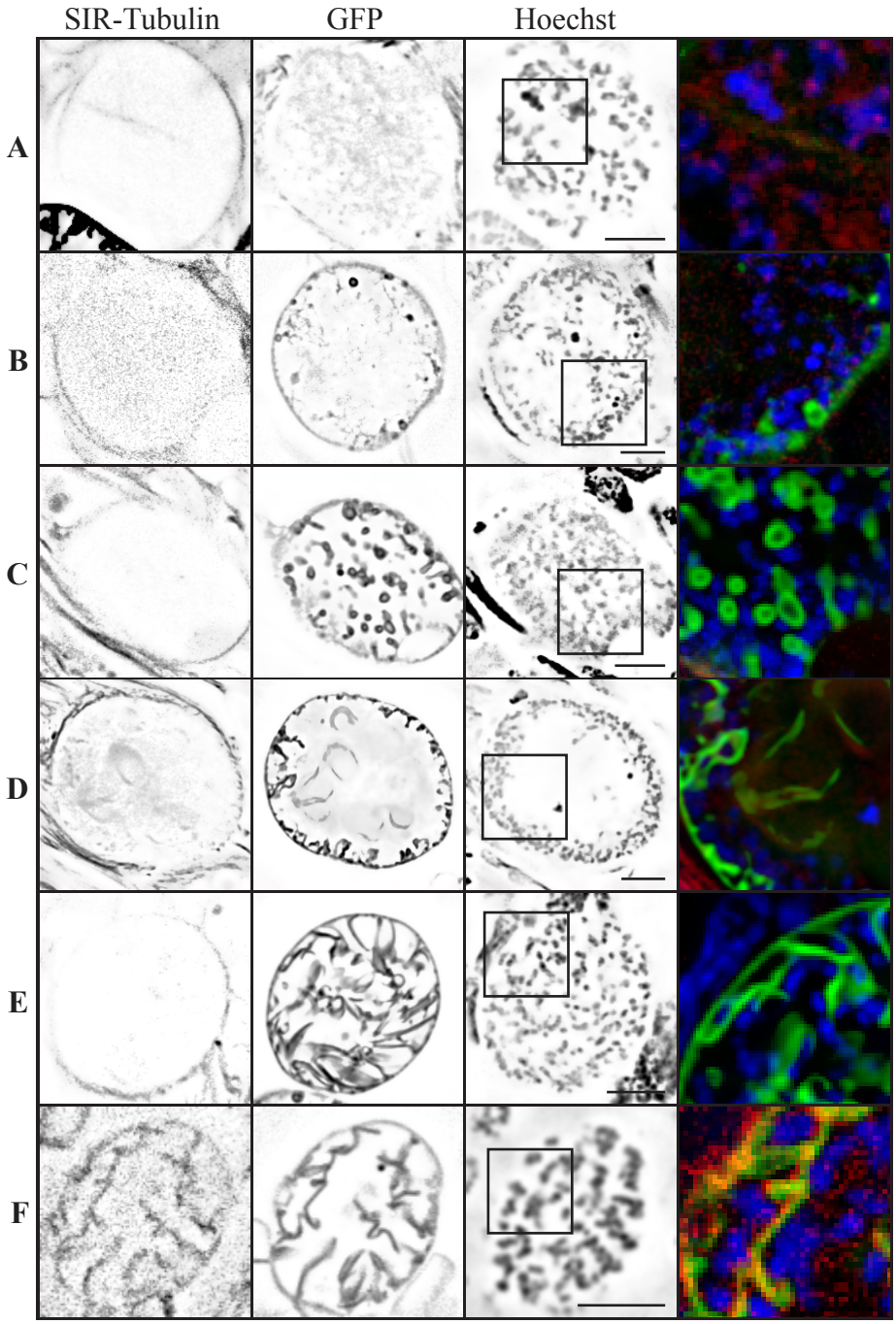

Figure 3.51: Development of oocysts of GFP:TSR:GPI replacement
Live oocysts expressing GFP:TSR:GPI replacing CSP. Microtubules labeled with SIR-Tubulin and DNA labeled with Hoechst. Oocysts are ordered by developmental stage from **A** to **F**. **A** Expression of GFP is starting. **B** GFP is localized at the plasma membrane (PM) and ER. **C** Combination of bubble-like invagination with tubular invaginations which are expected to be underlined by inner membrane complex (IMC) and microtubules. GFP is localized at the PM and oocyst wall. **D**, **E** and **F** Deep invaginations of PM underlined with IMC and micotubules. The oocyst in **F** does not show new expression of GFP at the ER. Note that absence of SIR-Tubulin staining as in **A** - **E** does not imply absence of microtubules. Scale bars: 10 μm.

Localization of GFP:TSR:GPI is mostly at the PM (**Figure 3.50 A - D**) but can also be at the nuclear envelope (**E**) or more irregular. Invagination of the PM rarely reaches the center of the oocyst (**Figure 3.51 C**, **D** and **F**). Mechanical pressure on

infected midguts results in release of the oocyst material, leaving a fluorescent oocyst wall behind (**Figure 3.52 B**).

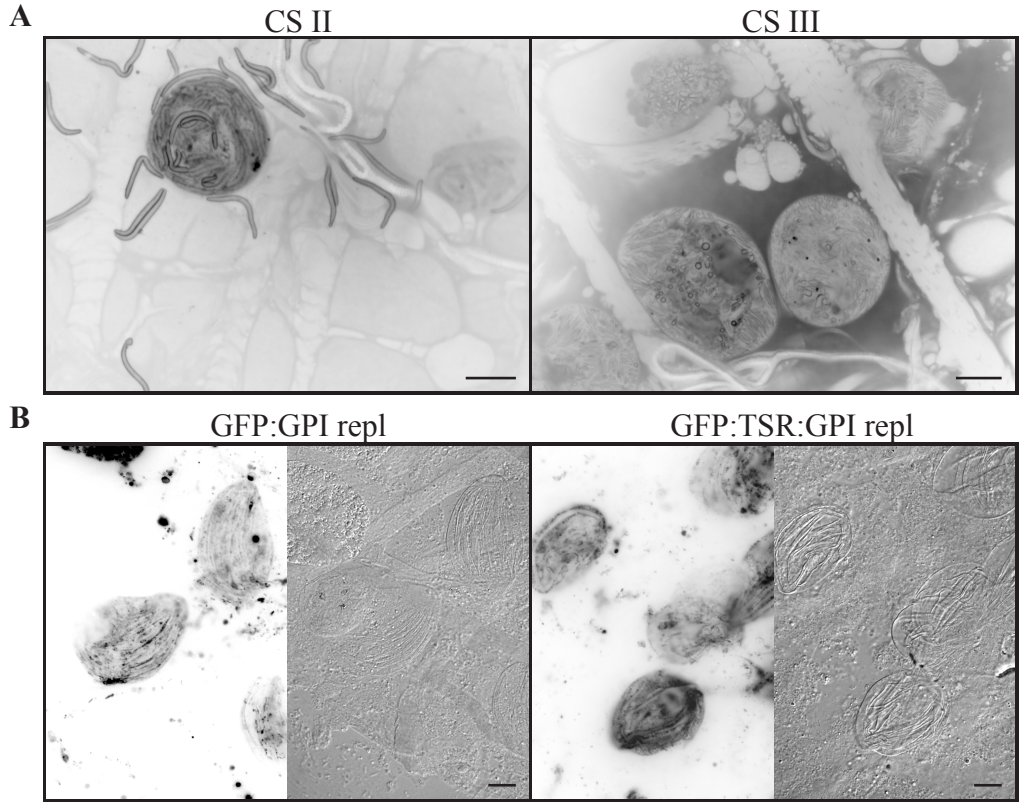

Figure 3.52: Fate of GFP in oocysts of CSP mutants
A Occasionally mechanical stress during live cell microscopy results in release of soluble fluorescent molecules from CS II / CS III oocysts into the midgut tissue. This was never observed for CS I or GFP:GPI parasites. **B** Active mechanical rupture of midguts infected with GFP:GPI replacement and GFP:TSR:GPI replacement results in release of fluorescent material from the oocyst and an a remaining fluorescent oocyst wall. This was not observed for any of the other CSP parasites. Scale bars: 10 μm.

Localization of CSP within the salivary gland All CSP mutants that productively invade the salivary gland were also imaged within salivary glands. Parasites expressing an extra copy of GFP:GPI as well as the very few observed CS III parasites inside salivary glands showed only fluorescence at the PM of the sporozoite. CS I extra copy showed a weak vesicular localization, but intriguingly, the invaded acinar cells showed cytoplasmic and nuclear GFP fluorescence (**Figure 3.53 A**).

As this observation might be due to alternative trafficking or cleavage of CS I, it was attempted to localize WT CSP in infected salivary glands. Immunofluoresence analysis was performed on salivary glands invaded with sporozoites expressing cytoplasmic GFP (CS GFP) (**Figure 3.53 B**). Multiple permeabilization attempts failed to permeabilize the SG sufficiently and CSP on the PM of the sporozoites was not detected by the

antibody staining. Thus absence of CSP detection within the acinar cells does not imply that WT CSP does not enter the acinar cells. However, a strong signal was detected at the basal lamina of invaded salivary glands which was locally restricted to sporozoite proximity in weakly infected SG and absent from uninfected sporozoites.

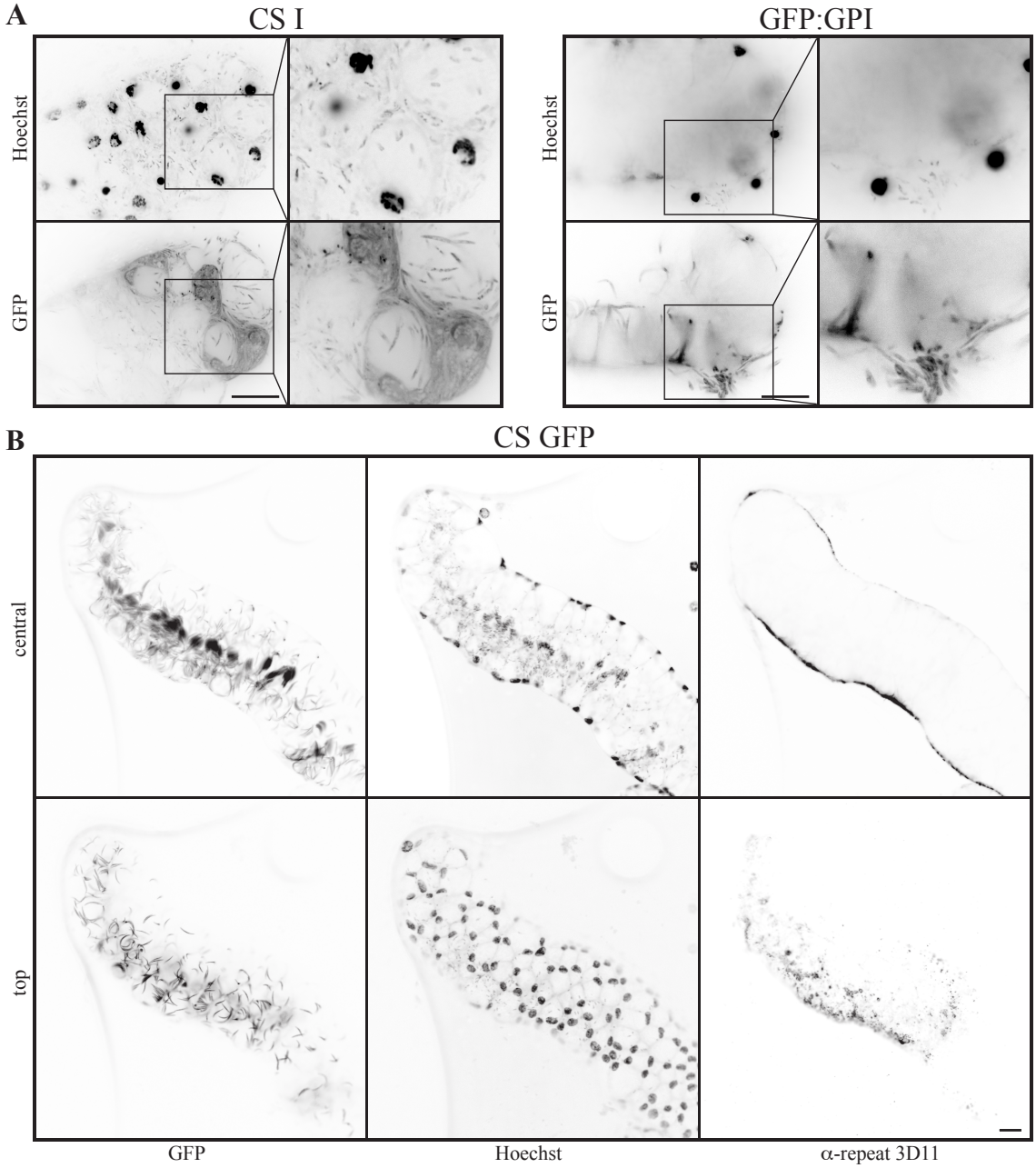

Figure 3.53: Fate of CSP within salivary glands
A Life imaging of infected salivary glands day 14 post infection of CS I additional copy and GFP:GPI additional copy. Boxes indicate the area of the zoom in on the right. **B** Immuno fluorescence analysis of PFA fixed and Triton-X-100 permeabilized salivary glands infected with WT sporozoites expressing cytoplasmic GFP under the CSP promotor. The repeat region of CSP was detected with 3D11 antibody. Central and top z-slices are shown. Scale bars: 20 μm.

Localization of tagged CSP within free sporozoites In free sporozoites, the distribution of fluorescence of all CSP mutants was also investigated (**Figure 3.54**). GFP:GPI extra copy shows mainly a surface localization of the GPI-anchored GFP, although some sporozoites show vesicular staining which is distinct from micronemal staining and might partially include Golgi localization. Generally the fluorescence intensity observed is much weaker than CS II and CS III, which appear extremely bright at the PM and rarely show weak internal fluorescence.

In contrast, both CS I extra copy and CS I replacement show virtually no surface localization and a vesicular labeling that appears similar to the micronemal localization of TRAP [290]. Additionally, midgut sporozoites of CS I replacement can show localization at the nuclear envelope, which is lost in salivary gland sporozoites. Otherwise localizations in MG and SG sporozoites is identical for all mutants, and for CS II and CS I replacement no salivary gland sporozoites were imaged due to low SGS numbers.

Attempts to specifically label internal CSP fractions by sequential protease treatment with Trypsin, followed by fixation and IFA were unsuccessful (due to residual surface staining after protease treatment), while life cell microscopy during addition of Proteinase K resulted in complete loss of fluorescence for CS III, resulting in sporozoites clumping to each other and patchgliding respective to each other (data not shown).

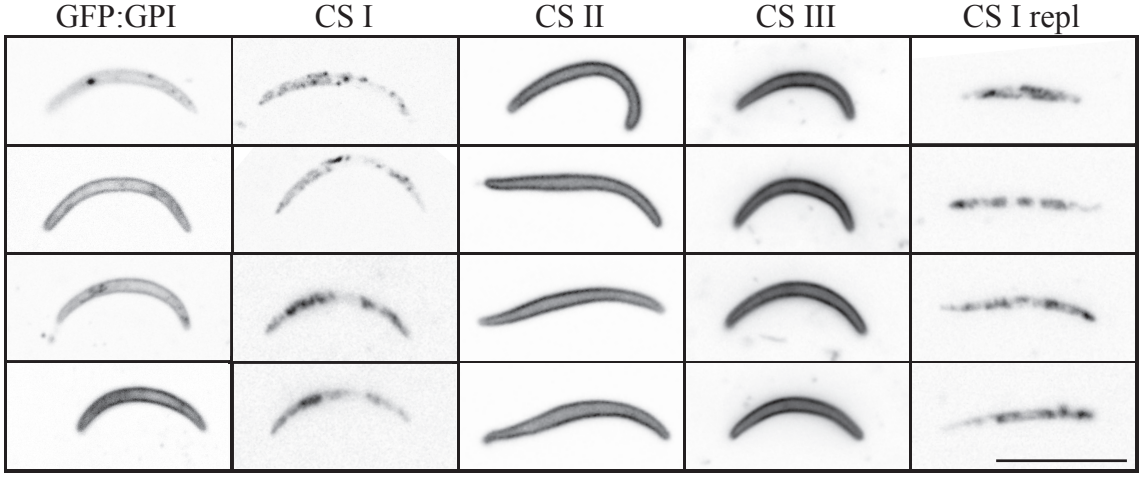

Figure 3.54: Localization of CSP within free sporozoites
Localization of fluorescence within free CSP mutant sporozoites is shown. For GFP:GPI extra copy, CS I extra copy and CS III sporozoites, salivary gland sporozoites are shown. The apical end of the sporozoite always points to the left. For CS II and CS I replacement, midgut sporozoites are shown. Scale bar is 10 μm.

Adhesion site dynamics and trail formation Originally, one of the main motivations in generating the CSP mutants was to produce a sporozoite with a bright label at

the surface. Initial attempts to use total internal fluorescence microscopy (TIRF-M) to visualize adhesion sites were only of limited success. TIRF-M fluorescence is a specialized illumination with such a strong incident angle that the complete excitation light is totally reflected and never enters the sample. During this process an evanescent field, a standing light wave is formed directly above the glass cover slide [423–425]. This evanescent wave reaches about 60 -100 nm into the sample and exponentially decreases with distance. The TIR angle required depends on the refractive index of both the glass slide and the sample itself. Fluorescent molecules within the evanescent wave can be exited and emit fluorescence. Artifacts that are not completely understood resulted in increased intensity in all sporozoites at two sites of the circle of the sporozoite for sporozoites expressing cytoplasmic GFP (unpublished data, Sylvia Münter and Mirko Singer).

The position of these points is always the same for all sporozoites and is related to the angle of the TIR excitation. It was modeled that changes in membrane thickness and protein content can influence light-scattering of membranes [426]. We speculated that a certain angle of the sporozoite in respect to the excitation light might result in angle dependent scattering of light within the sporozoite due to the high changes of refractive index within the sporozoite. As the pellicle of the sporozoite is made up of three lipid bilayers followed by the protein rich subpellicular network, the local refractive index of the sporozoite pellicle might be sufficiently high in variation to cause this process in sporozoites expressing cytoplasmic GFP [427]. The newly formed light would bridge the gap of the medium via the evanescent wave and follow in the same angle of the excitation light, illuminating the cytoplasm of the sporozoite. I assumed that a surface labeling of the sporozoite might circumvent or minimize the appearance of this artifact.

TIRF-M was performed with sporozoites from all CSP mutants. This resulted in the first direct observation of trail formation in motile sporozoites, especially frequent in midgut derived sporozoites (**Figure 3.55 A**). Due to the local proximity of the trail to the substrate, the respective illumination compared to the sporozoite is increased, reducing the difference in relative fluorescence. Also, the strong surface labeling of CS II and CS III, but also GFP:GPI allows observation of trails during and after formation, in contrast to expression of cytoplasmic GFP. This is due also due two the cubed relationship of the cytoplasmic volume within the trails in contrast to the sporozoites, whereas the increased surface of the sporozoite in respect to the trail is only squared (ignoring the thickness in z). In case of the sporozoite shown in (**A**), the adhesion site of the trail is disassembled and the trail rejoins with the moving sporozoite. In other cases a second

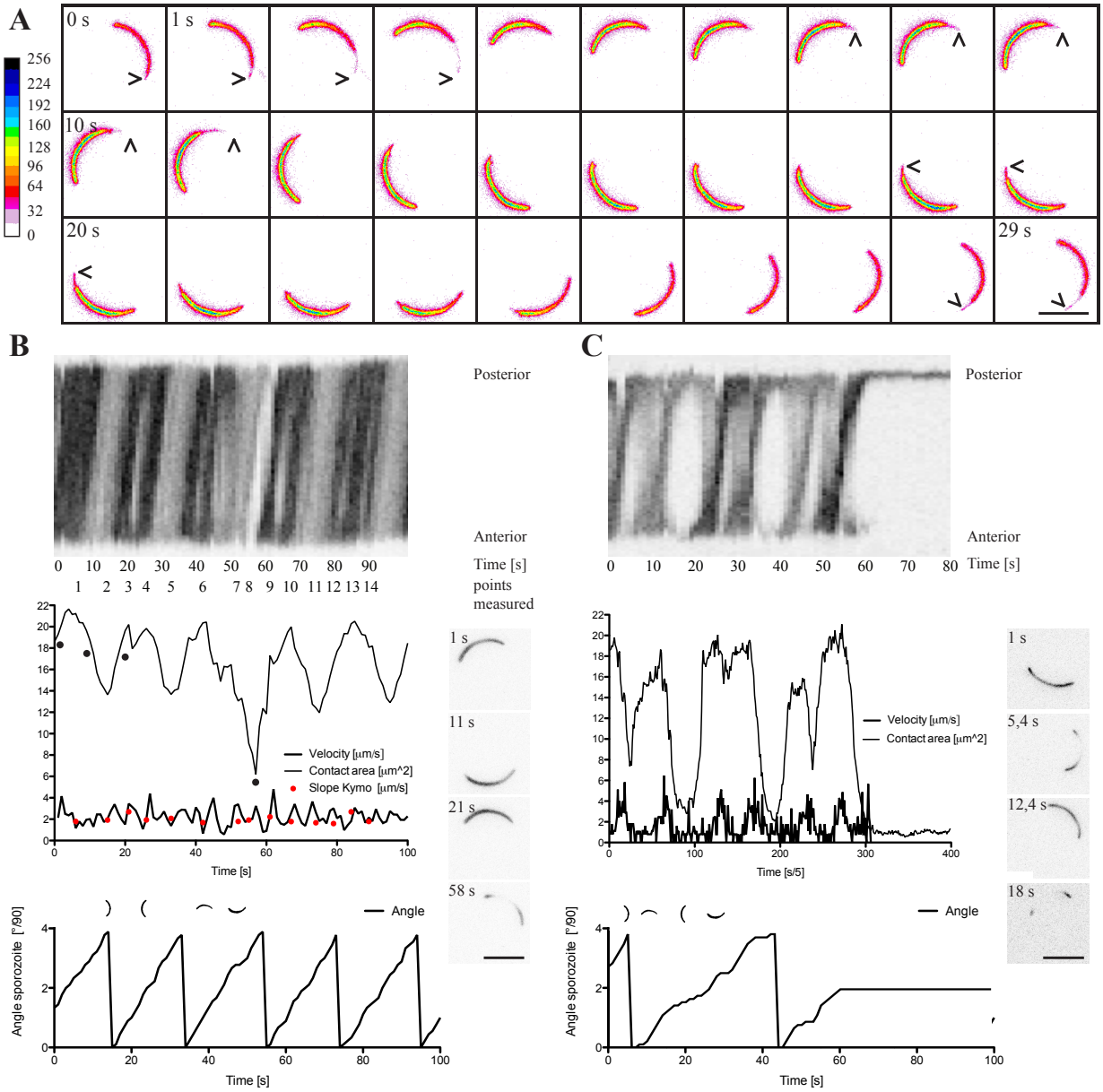

Figure 3.55: TIRF microscopy of CS III sporozoites
A Total internal reflection fluorescence microscopy (TIRF-M) was performed on a midgut sporozoite of CS III with 1 frame per second (fps). False color image shows relative intensity. Arrowheads depict identical position from beginning of trail formation until the trail is retracted. **B** and **C** TIRF-M microscopy of CS III salivary gland sporozoites in full contact with the substrate **B** and loose contact with the substrate **C**. On top the kymograph of the respective sporozoite is blotted. For this a curved line was drawn from anterior to posterior throughout the sporozoites, intensities averaged over a width of 5 pixels, straightened and blotted for every second. The image is inverted, so darker areas show higher fluorescence intensity, resembling closed contact to the substrate and lighter areas represent greater distance. Below contact area and velocity of the sporozoite are blotted. For **B** the speed was also calculated from the slope of the kymograph for 14 points indicated and is blotted with red dots within the graph. Black dots represent time points shown to the right as microscopic images for reference. Below the angle of the sporozoites is blotted for each frame (note little sporozoite cartoons above to indicate orientation). Please note that the broader changes in fluorescence intensity visible in both kymographs represent relative differences in the TIRF field and correlate with the relative angle of the sporozoite. Scale bars: 10 μm.

adhesion site is formed prior to disassembly of the first one, resulting in the trail being attached to the substrate via both adhesion sites while the sporozoites disengages from the trail and the adhesion sites and continues to glide (data not shown).

During gliding motility, two kind of adhesion site dynamics can be observed via TIRF-M, partially contradicting published data using reflection interference contrast microscopy (RICM) [285]. These are sporozoites with complete substrate proximity (**B**) and sporozoites with sporozoites with more distant and dynamic contact (**C**). Both sporozoites show comparative gliding speed, whereas the sporozoite with complete substrate proximity is rather continuous in speed and the sporozoite with dynamic contact also shows more dynamic speed. Kymographs of two sporozoites were generated using one frame per second. This shows the relative proximity of each part of the sporozoite over time by fluorescent changes from left to right and relative changes of one spot on the substrate following a line from the bottom upwards with a slight angle to the right. This indicates that the relative TIRF intensity is much more dependent on the substrate and completely dynamic in respect to the sporozoite. At the same time the angle of the kymograph allows to determine the apparent speed of the sporozoite, and this correlates with the speed of the sporozoite determined via regular manual tracking.

What is striking is that regular fluctuations of the appearet contact area are visible in the kymograph of both (**B**) and (**C**) that are also observed by analyzing the apparent contact area (which was done by automatically measuring the size of the sporozoite, see methods for details) and correlate with the angle of the sporozoite in respect to the circle it is moving in. If the sporozoite is on the left side of the microscopic image the fluorescence is stronger that on the right side. This is most likely caused by the TIR field and superimposes with the real proximity of the sporozoite to the substrate.

Surface dynamics of CSP mutants It was long proposed that CSP plays an active role in gliding motility, and is apically secreted and deposited on the substrate [401]. Recently there has been the discussion that membrane flow might contribute to gliding motility [286]. Retrograde flow is able to traverse beads with hight speed to the back of the sporozoite even in the presence of cyto D [428]. In oder to test the relevance of broad membrane flow for gliding motility in contrast to strong concentration gradients of single transmembrane molecules leading to directed diffusion and to test the mobility of the CSP mutants on the surface of sporozoite, fluorescence recovery after photobleacing (FRAP) was performed (**Figure 3.56**).

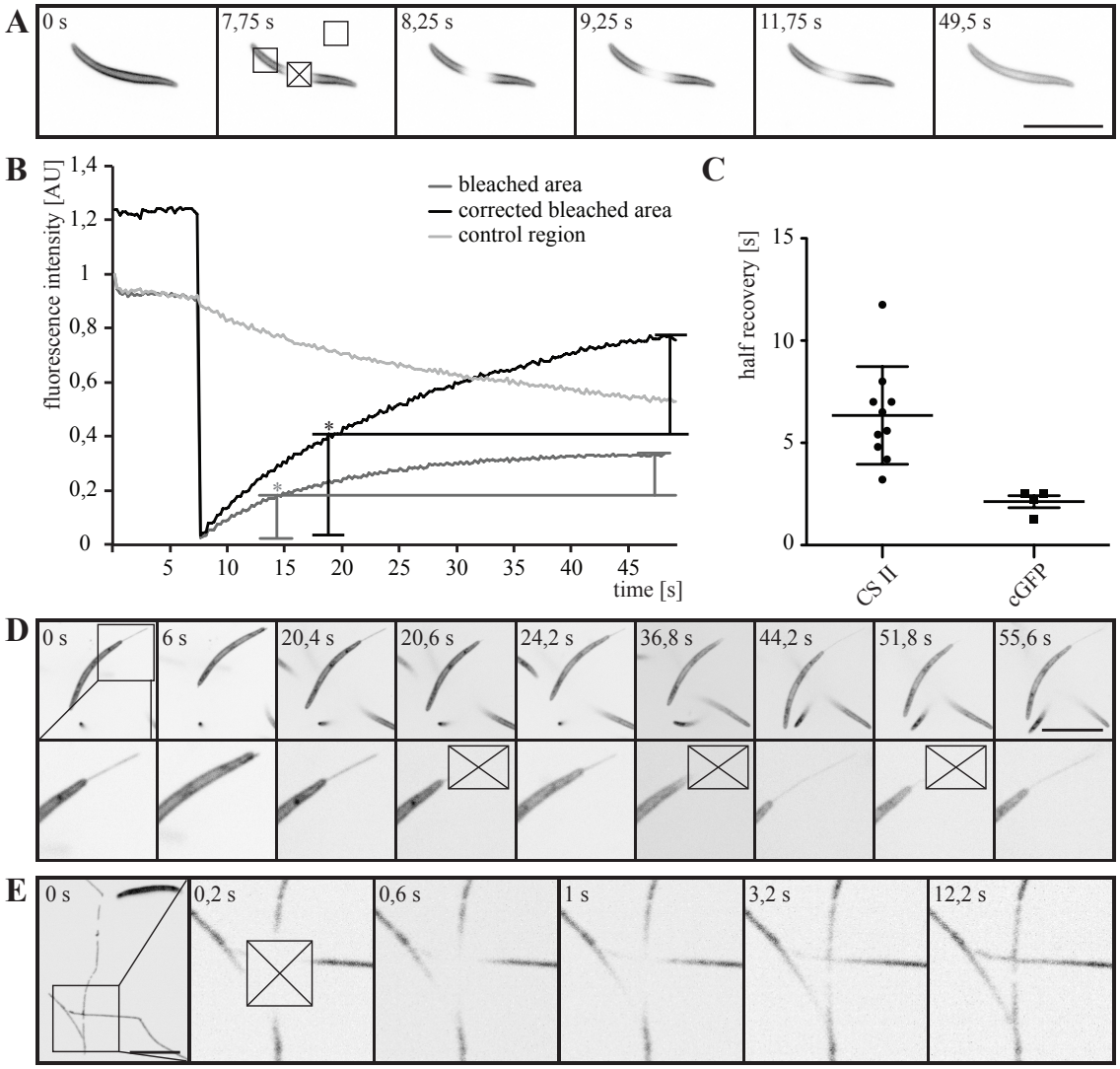

Figure 3.56: FRAP of CSP mutants
Fluorescent recovery after photobleaching (FRAP) was performed on CSP mutants. **A** Single frames of a time series of a CSP II midgut sporozoite day 20 post infection. Crossed box represents FRAP area (b), left hand box control area (c) and top right box background area (n). Note that fluorescence recovers from all directions. **B** Analysis of sporozoite shown in A. Mean fluorescent intensity was measured for all areas and background corrected fluorescence normalized to t=0 is blotted. Corrected bleach area is normalized to control region to correct for photobleaching during imaging and FRAP pulse. Point of half recovery indicated with a *. **C** Half recovery times of CS II sporozoites and sporozoites expressing cytosolic GFP (262 line). Values for individual sporozoites are blotted, standard deviation is shown. **D** Single frames of a time series of a midgut sporozoite of GFP:GPI day 15 post infection. Box indicates zoom in of lower row. Crossed boxes indicate FRAP area and events. The sporozoite is moving forward while forming a trail, moving backwards retracting into the trail multiple times. The trail recovers independent of back movement and the adhesion site of the trail remains throughout the whole movie. **E** An Accudenz purified midgut sporozoite of CS III day 26 post infection. Zoom in shows trails on the substrate of the region surrounding the FRAP area (crossed box). Scale bars: 10 μm.

In all FRAP events performed, on midgut sporozoites of CS II, CS III and GFP:GPI, fluorescence recovery always appeared equally from all directions, as in (**A**). To compare the diffusion rate of the membrane bound CS II with cytoplasmic GFP expressed in the

262 line, FRAP was performed for sporozoites of both under identical conditions. Note that while CS II can diffuse on the PM in all directions, cytosolic GFP, as well as the cytosolic mcherry expressed in 262 (data not shown) have a major diffusion obstacle, the nucleus. Thus diffusion to recover the fluorescence after photobleaching is a two order process, with local diffusion on the bleached side of the nucleus being faster than diffusion from the other side. Even though, half recovery times for cytosolic GFP where strikingly faster that CS II, which also had a relatively low half recovery time of about 6 seconds (**B** and **C**), which is also much slower than recovery rates of the actin binding protein coronin in sporozoites [289].

Additionally, FRAP was also performed on trails observed in actively or previously motile sporozoites. The midgut sporozoite in (**D**) attempts to engage in gliding motility, but fails to dismantle the adhesion site at the back, resulting in the formation of a trail. Multiple times the sporozoite is pulled back by the trail, most likely rejoining with it. The complete trail was bleached three times, and every time fluorescence quickly recovered without the sporozoite moving backwards, suggesting that the sporozoite PM and the membrane of the trail are still in continuity at this point.

In (**E**), a sporozoite expressing CS III has deposited a whole network of trails on the substrate, which is clearly already partially fragmented. A region of the trail where the sporozoite crossed its own path was bleached and recovers fluorescence, indicating that there is still a membranous connection between large parts of the trail. Notice the small gap in the trail on top of the zoom in which the stronger fluorescence of the upper part becomes clearly visible at the 12,2 s frame.

3.3.4 Processing of CSP

To gain insight into the processing of CSP and interdomain-GFP tags of CSP, western blotting was performed for WT and all CSP mutants. Generally CSP of *P. berghei* is detected with the monoclonal antibody 3D11, binding the repeat region. This increases the sensitivity of the antibody even further as multiple epitopes of the highly abundant CSP can be detected. Additionally an antibody was used generated against a peptide of the C-terminus of CSP (kind gift of the Photini Sinnis, also see **Figure 1.8** [387]). Also GFP-tags were additionally probed for GFP.

Processing of WT CSP

To better understand processing of WT CSP, samples were prepared from different timepoints and tissues from mosquitos infected with ANKA WT (**Figure 3.57**). Samples were probed with antibodies binding the repeat region (**A** and **B**) and the the C-terminus (**C** and **D**). Samples were crushed and separated by centrifugation into (**P**) pellet and (**S)** supernatant (**compl.**), or separated via Accudenz gradient (**accud.**) into the sample on top of the gradient (**S**). Additionally the fraction pelleting below the Accudenz gradient were washed and also lysed (**P**). This results in sporozoites collecting within the supernatant of the Accudenz fraction or the pellet of the complete fraction. Soluble protein is expected to be in the supernatant of the complete fraction but lost completely from the Accudenz sample.

Samples from salivary glands probed with repeat binding antibody appear as expected from published results (**Figure 3.57 A** and **B**). Only the two prominent bands around 50 kDa are detected, and are stronger from the pellet fraction of the complete sample and the supernatant fraction of the Accudenz gradient, both expected to contain the sporozoites. The signal from midgut samples is strong for both Accudenz fractions from day 17, but very low for the complete fractions from day 17 and all day 10 samples. This suggests that the amount of the repeat region in the midgut samples is lower. Potentially lysis of the pellet fraction of the complete sample was incomplete due to too much total protein (mostly from the midgut tissue).

Probing the same samples with the C-terminal antibody shows a different picture (**Figure 3.57 C** and **D**). While the protein bands detected from the salivary gland samples are mostly the same, multiple lower molecular bands appear in the midgut sample. The most prominent are a 17 kDA and a 21 kDa band. Of those the supernatant of the complete sample only contains the 17 kDa band, suggesting that this might represent a soluble fraction. In contrast only the 21 kDa band is present in the pellet fraction of the Accudenz purification, suggesting that this fragment might be associated with parts of the oocyst that do not purify within an Accudenz gradient. The pellet sample of the complete fraction also contains a band of 12 kDa and 25 kDa. The 12 kDa band is only detected in this sample, whereas the 25 kDa is also detected within the other samples (**D**). Both the 21 kDa and the 17 kDa band are more or equally abundant than the 50 kDa band in the sporozoites purified via Accudenz from the day 17 midgut sample. This suggests that these fragments are present on mature midgut sporozoites, but not on salivary gland sporozoites.

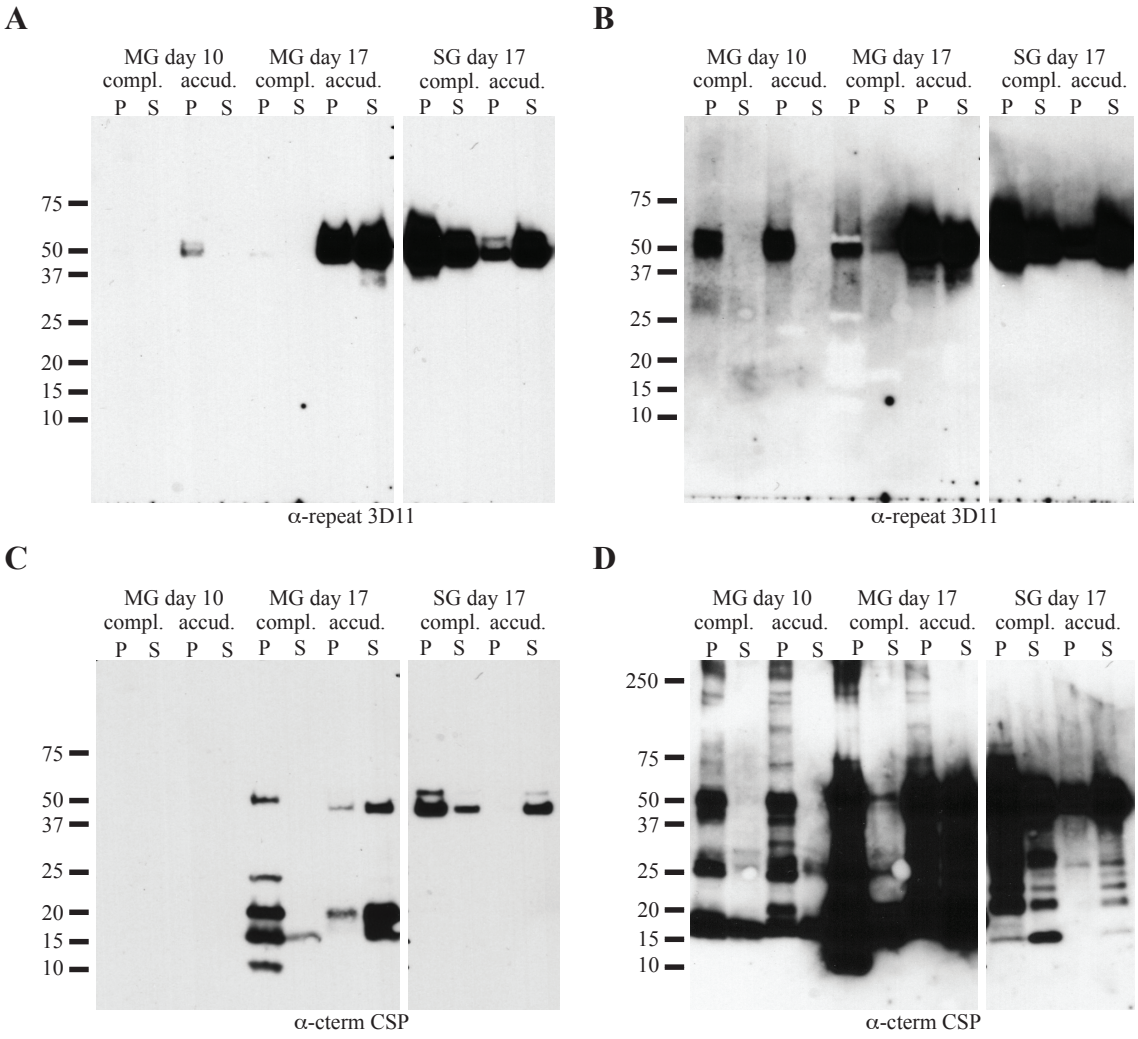

Figure 3.57: Processing of circumsporozoite protein
Midgut samples were collected from day 10 and day 17 post infections and salivary gland samples were collected day 17 post infection. **A** Short-time exposure with α-repeat antibody. **B** Long-time exposure with α-repeat antibody. **C** Short-time exposure with α-C-terminal antibody. **D** Long-time exposure with α-C-terminal antibody. The same blot was first probed with α-C-terminal antibody, exhausted and reprobed with α-repeat antibody. **comp.** Complete sample. Sample was crushed, centrifuged, separated into **P** pellet and **S** supernatant and dissolved in RIPA buffer. **accud.** Sample was crushed, diluted, underlaid with Accudenz solution and centrifuged. The gradient supernatant **S** was pelleted and dissolved in RIPA buffer. Sample passing the Accudenz layer **P** was washed, pelleted and dissolved in RIPA buffer.

The ratio of fragments found in the supernatant and pellet fraction of the Accudenz purification for midgut samples from day 10 and day 17 shifts (**Figure 3.57 C** and **D**). In the day 10 sample the 17 kDa, 21 kDa, 25 kDa and 50 kDa bands are mainly found in the pellet, while those still present at day 17 are mainly found in the supernatant fraction. This might result from different stages of oocyst development ending up in the pellet or supernatant fraction of the Accudenz purification.

Processing of CSP mutants

Given the information on sporozoite development and western blotting of WT CSP, samples of all CSP mutants were probed via western blot. This was performed for day 10 and day 17 samples, except for GFP:GPI replacement and GFP:TSR:GPI replacement which were probed only for day 10, as these parasites lines show degraded oocysts on day 17. First complete lysis samples were analyzed, where the infected midguts are crushed, pelleted and the pellet was directly dissolved in RIPA buffer (**Figure 3.58**).

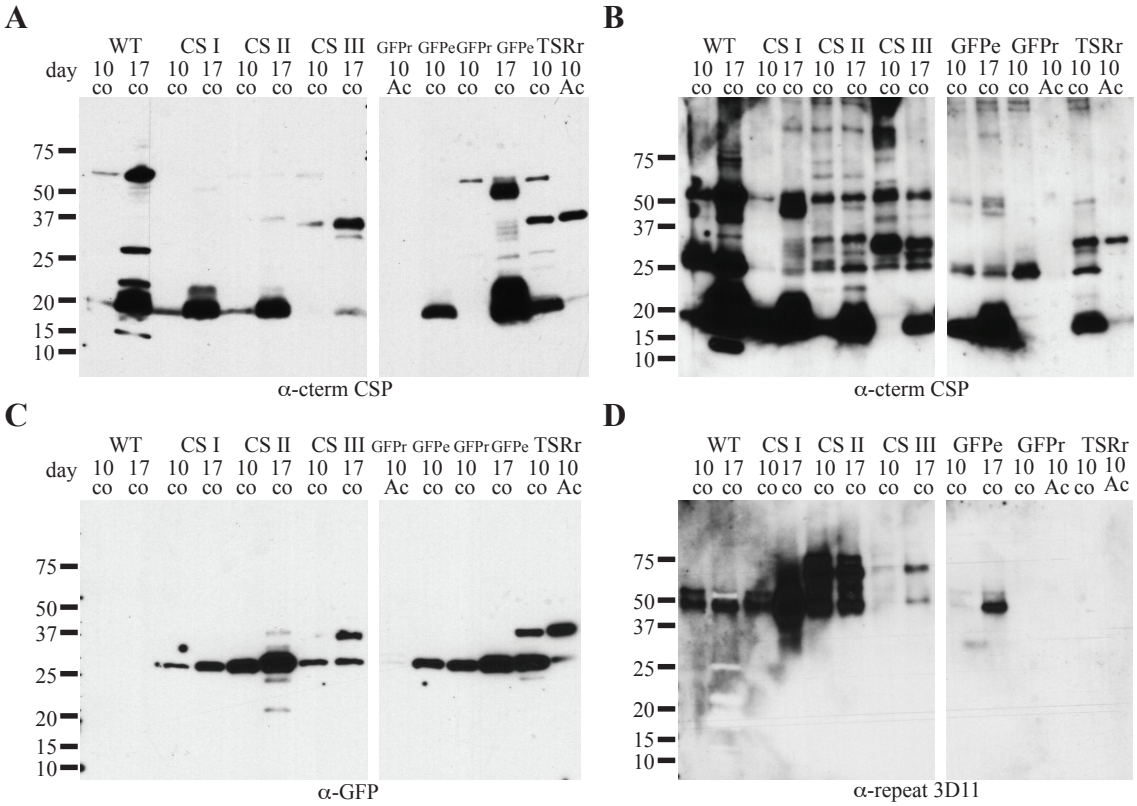

Figure 3.58: Processing of CSP mutant complete fraction
Midgut samples were collected from day 10 and day 17 post infections. **A** Short-time exposure with α-C-terminal antibody. **B** Long-time exposure with α-C-terminal antibody. **C** Probed with α-GFP antibody. **D** Probed with α-repeat antibody. **A** and **C** are two identical blots probed in parallel, **B** is a separate blot that was first probed with α-C-terminal antibody, exhausted and reprobed with α-repeat antibody (**D**). **co** Complete sample. Sample was crushed, centrifuged, and the pellet fractions dissolved in RIPA buffer. **Ac** Sample was crushed, diluted, underlaid with Accudenz solution and centrifuged. The gradient supernatant was pelleted and dissolved in RIPA buffer. GFPe is GFP:GPI, GFPr is GFP:GPI replacement, TSRr is GFP:TSR:GPI replacement.

It should be noted that the C-terminal antibody as well as the repeat antibody detects tagged and untagged CSP alike, while the antibody detecting GFP will detect free GFP as well as tagged protein. Also, Accudenz purified samples of all CSP mutants were analyzed (**Figure 3.59**). Additionally, all CSP mutants were individually analyzed at greater detail (**Figure 3.60**), including SG samples. These blots were also reprobed with

α-C-terminal antibody, α-α-Tubulin antibody or α-HSP70 antibody (data not shown).

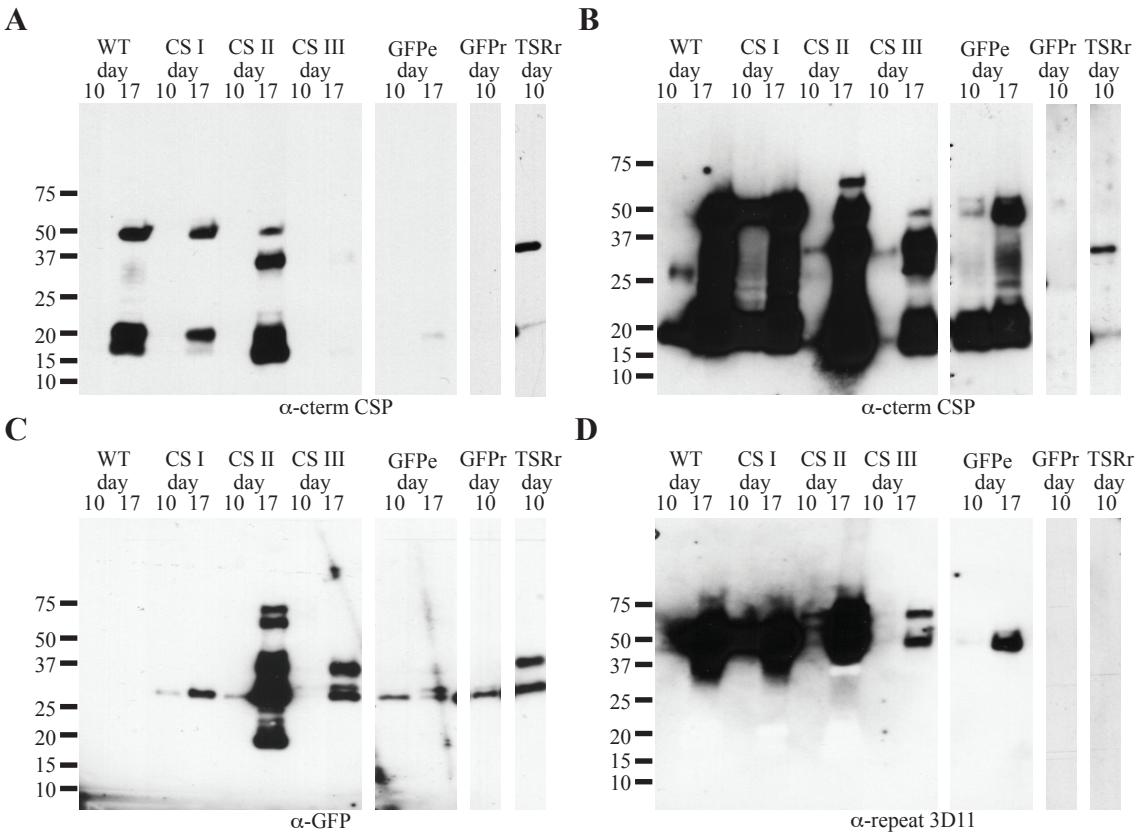

Figure 3.59: Processing of CSP mutant Accudenz fraction
Midgut samples were collected from day 10 and day 17 post infections. **A** Short-time exposure with α-C-terminal antibody. **B** Long-time exposure with α-C-terminal antibody. **C** Probed with α-GFP antibody. **D** Probed with α-repeat antibody. Samples of GFPr and TSRr of **A** and **B** and **D** are copied for (**Figure 3.58**) and only included for completeness. Blot **A** and **B** are different exposures of the same blot probed with α-C-terminal antibody, exhausted and reprobed with α-repeat antibody **D**. Blot **C** was performed separately and probed with α-GFP antibody. All sample was crushed, diluted, underlaid with Accudenz solution and centrifuged. The gradient supernatant was pelleted and dissolved in RIPA buffer. GFPe is GFP:GPI, GFPr is GFP:GPI replacement, TSRr is GFP:TSR:GPI replacement.

Having a closer look at the blots with as CSP mutants allows to evaluate the specificity of the antibodies used. The WT samples do not contain any GFP, and the blot here remains empty (**Figure 3.58** and **Figure 3.59**). GFP:GPI replacement and GFP:TSR:GPI replacement does not contain the repeat region, and no signal is detected for these samples using the 3D11 repeat binding antibody. Lastly the GFP:GPI replacement parasite does not contain the C-terminus. However here a band at 25 kDa is detected as well as a band around 55 kDa. This 55 kDa band is also detected in the GFP:TSR:GPI samples, where the full length protein is expected (and also detected) to run at around 35 kDa (**Figure 3.58**). Both of these bands appear enriched in the complete lysis fraction and are not detected in the Accudenz purified fraction. Having a

look at (**Figure 3.57 C**) shows that both bands are detected in the day 17 sample and the bands runs slightly higher that the band detected in the Accudenz purified samples. This suggest that the 25 kDa band and the 55 kDa detected with the C-terminal antibody are not CSP. In the following paragraphs the mutants will be discussed one by one.

Processing of GFP:GPI extra copy In the parasite expressing GFP:GPI as an extra copy CSP is expressed as in WT and low levels of GPI-anchored GFP are also expressed. Based on molecular weight predictions GFP:GPI should run at 29 kDa. It should be noted that GFP is detected as two bands that run as 27 kDa and around 29 kDa (**Figure 3.60**). The lower fragment most likely represents GFP only, and this is the only one found within the MG fractions representing complete lysis. The 29 kDa band is present in all salivary gland samples and in the Accudenz fractions of the midgut samples. Most likely the free GFP is removed during the Accudenz purification, as only the pellet fractions after the gradient are loaded onto the gel. However the salivary gland samples only contain the 29 kDa band independent of preparation method, indicating that the removal of the GFP anchor itself by a phospholipase C or proteases only occurs within the oocyst.

Processing of CS II In the parasite expressing CS II, WT CSP is expressed together with CS II. Both proteins are present at similar ratios as detected with the repeat binding antibody (**Figure 3.60**). However, most of the GFP detected at day 10 is GFP only, whereas at day 17, a band around 35 kDa is also detected. As this band is enriched in the Accudenz purified samples, it is suggested that this represents CS II that was cleaved just before the GFP tag, close to the repeat region but still GPI-anchored (**Figure 1.6 Figure 3.28**). This band is also detected in (**Figure 3.59**) using C-terminal and GFP binding antibodies. Having a look at samples from MG and SG shows that CS II parasites fail to invade the salivary gland (**Figure 3.60**). However in the long exposed SG samples a faint band of CSP can be detected with the repeat binding antibody. This could be free full length CSP or sporozoites attached to the SG.

Processing of CS III In the parasite expressing CS III, WT CSP is expressed together with CS III. Both proteins are present at similar rations as detected with the repeat binding antibody (**Figure 3.60**). As or CS II, most of the GFP detected at day 10 in CS III is GFP only, whereas at day 17 a 35 kDa band is also detected. Comparing the

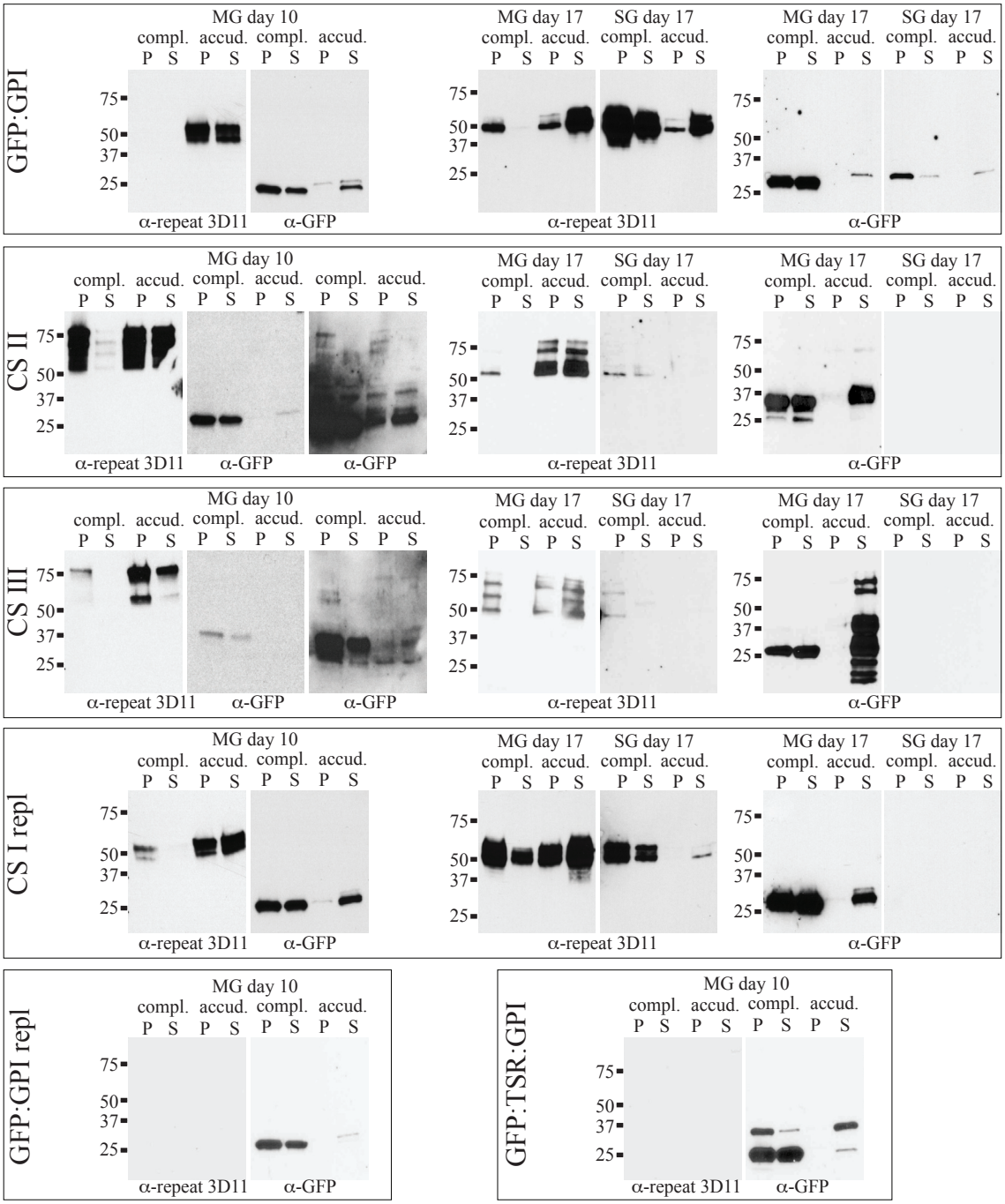

Figure 3.60: Processing of CSP mutants
CSP mutants were collected on day 10 from midgut (MG) and on day 17 from MG and salivary gland (SG). The same samples were probed with α-repeat and α-GFP antibody on separate blots. Exposure times of blots were selected to show the most detail and not relative amounts. SG samples of CS II, CS III and CS I replacement are significantly weaker than day 17 MG samples. Empty blots shown remained empty at longest exposure times. **comp.** Complete sample. Sample was crushed, centrifuged, separated into **P** pellet and **S** supernatant and dissolved in RIPA buffer. **accud.** Sample was crushed, diluted, underlaid with Accudenz solution and centrifuged. The gradient supernatant **S** was pelleted and dissolved in RIPA buffer. Sample passing the Accudenz layer **P** was washed, pelleted and dissolved in RIPA buffer.

complete samples of CS II and CS III shows that this 35 kDa is more abundant in

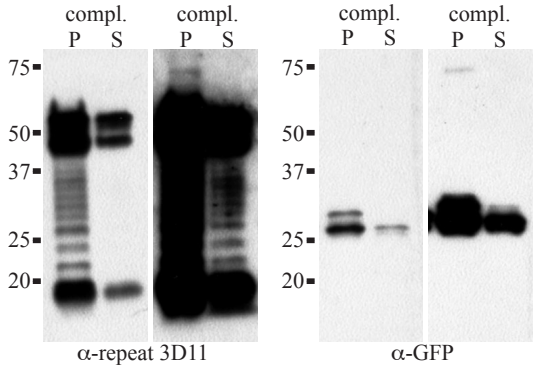

Figure 3.61: Processing of CS I replacement
CS I replacement parasites were collected on day 16 from midgut (MG) samples. The same sample was loaded twice and was probed with α-C-terminal or α-GFP antibody. Exposure times of blots were selected to show the most detail and not relative amounts. **comp.** Complete sample. Sample was crushed, centrifuged, separated into **P** pellet and **S** supernatant and dissolved in RIPA buffer.

CS III than in CS II (**Figure 3.58**). Using the C-terminal antibody also shows that the 17 kDa band is much lower in CS III and the 21 kDa band is not present al all, but the 35 kDa is enriched and also detected with the α-GFP antibody. In the Accudenz purified fraction, both the 17 kDa and the 21 kDa band are present at day 17 (**Figure 3.59**). It is expected that all bands observed in WT can be found in CS III, as these parasites also express sufficient quantities of WT CSP. However due to the modified 5'UTR and 3'UTR of WT and tagged CSP, it is possible that expression of the tagged CSP precedes WT CSP expression. The exact size of the 35 kDa fragment as well as the relative abundance for CS II and CS III in contrast to free GFP and the 17 kDa fragment might indicate that there are at least two cleavage sites on either side of the GFP in CS II, which are then both on the N-terminal side of GFP for CS III (**Figure 1.6 and Figure 3.28**). These might result in the 17 kDa and 22 kDa fragment in WT CSP (**Figure 3.58**).

Processing of CS I replacement In the parasite where WT CSP was replaced with CS I, the GFP tagged version represents the only CSP present. The GFP is at the very N-terminus after signal peptide cleavage (**Figure 1.6**). Judging from western blotting, this CSP mutant is almost identical to the parasite expressing an extra copy of GFP:GPI (**Figure 3.60**). CSP as detected by repeat binding antibody appears like WT CSP, and only free GFP is detected. Additionally in the Accudenz supernatant fraction a small band at around 29 kDa appears directly on top of the 27 kDa free GFP band. The amount of salivary gland sporozoites for CS I is strongly reduced. While some CSP can be detected with long exposures with the repeat binding antibody, this is not possible with the GFP antibody (**Figure 3.60**). Under optimal conditions it was possible to

detect some full length CS I with both the C-terminal and the GFP binding antibody (**Figure 3.61**). This represents a tiny fraction of the full length protein. This makes it most likely that the GFP is cleaved of in the CS I mutant almost immediately after signal peptide cleavage.

Processing of GFP:GPI replacement and GFP:TSR:GPI replacement In the parasite with GFP:GPI replacement no visible processing occurs, due to the lack of CSP and the fact that only GPI-anchored GFP is expressed. It is however useful to asses the specificity of the antibodies used as discussed above. GFP:TSR:GPI is a truncated version of CS II, lacking the C-terminus and the repeat region (**Figure 3.28**). On western blot, a free GFP and a full length protein fraction is visible, the latter being enriched in the Accudenz supernatant fraction (**Figure 3.60**). Using the antibody binding the C-terminus of CSP, the 35 kDa band as well as the 17 kDa bands are detected, but not the 22 kDa band (**Figure 3.58 Figure 3.59**). This supports the finding from CS II and CS III processing, that two cleavage sites are present in WT CSP, of which only one is found in GFP:TSR:GPI, directly after the GFP. It is not possible to interpret why the 35 kDa band is enriched over the cleavage products for the Accudenz sample, as the Accudenz purification of GFP:TSR:GPI was not microscopically analyzed. As Accudenz purification normally enriches sporozoites, it is unclear to what extend oocysts material of GFP:TSR:GPI is enriched. It seems likely that free GFP would mainly be removed during this process, but the TSR:GPI fraction should remain membrane bound unless the gpi-anchor is lost. This seems unlikely, given the calculated molecular weight of only 11 kDa, which suggests that the apparent 17 kDa on the western blot are the result of GPI-anchor presence.

Chapter

4

Discussion

4.1 Genetic manipulation of Plasmodium

4.1.1 Plasmid unfolding

In the pre-Cas9 area of *Plasmodium*, there was a striking difference between transfection efficiency between the rodent species *P. berghei* and *P. yoelii* and transfection efficiency in *P. falciparum*. Deleting a gene in the rodent species results in a semi-uniform parasite population after around seven days, the same process in *Pf* might take one to three months, with a lower rate of success. The main reason for that, apart from the slower growth rate of *Pf*, is the transfection of circular DNA in *Pf*. While the linear DNA transfected in *Pb* directly signals an apparent DSB in the parasite and induces its integration into the genome, the circular plasmid transfected into *Pf* requires a random DSB to occur within one of the homology regions of the plasmid within the genome. The sole reason for this detour required in *Pf* transfection is the fact that linear DNA was degraded after a few days whereas circular DNA is retained in the parasite [429]. This suggests that linear DNA in *Pf* cannot induce HR (and is slowly degraded). Why this is the case is unclear. The exact differences between *Pb* and *Pf* leading to this effect are still debated. Direct transfection of purified merozoites as performed in *Pb* is possible [430], but this has not been combined with the transfection of linear DNA.

I designed the plasmid unfolding strategy as an easy experiment to test if plasmids can be transfected in a circular state and then linearized once they are in the parasite. This has the great advantage that the same nuclease and nuclease target site can be used independent of the homology region used to target the DNA into the genome, as the nuclease targeting site is flanked by both homology regions in the vector (**Figure 3.3**).

The experiments showed that self-linearization can result in double crossover integration in *Pb* using ZFNs. The time after transfection was increased five days compared to the other constructs not resulting in double crossover integration, suggesting that the integration rate after unfolding was lower as reported for direct transfection of linear DNA [165]. The unfolding experiment has only been performed once, and the increased time after transfection might just be caused by experimental variation. The TALEN construct was not successful, and it is not clear why this was the case. Potentially the internal homology of the TALE-repeats, which is between 98-102 bp of the 102 bp long repeat might result in removal of most of the repeats as occurred in the parasite line with the unoptimized ZFNs of SpZFN (**Figure 3.10** and discussion below). As the ZFNs of the unfolding vectors were not yet codon-deoptimized to avoid HR, the amount of remaining episomal vector after transfection might be reduced if this is also modified.

If this plasmid unfolding also works in *Pf* should be evaluated. It might be possible that even after DSB within the parasite, *Pf* can discriminate foreign DNA and choose not to integrate it. However this is unlikely. I performed experiments using self-unfolding transfection vectors in *Pf* prior to the experiments in *Pb* only using the TALEN *samd4* (data not shown). We could never observe integration of these vectors, which is not surprising given the results obtained with the TALEN vector in *Pb*.

It was recently reported that transfection of linear DNA is possible, using a Cas9 induced DSB within the genome [170]. Even the use of directly synthesized end-modified dsDNA has been reported. However the increase in integration efficiency with and without DNA induced DSB break within the genome has not been assessed. After all this might be identical, but given the lack of NHEJ, result in a negative selection of all parasites that fail to integrate the linear DNA such providing a strong selection of integration events. Recently, marker free transfection has been reported in *Pf* [431]. To achieve this with plasmid unfolding would require a plasmid to self-cleave at two sites, and also require that the homology regions are not arranged back to back, but sequentially. Thus the only way plasmid unfolding might provide an improvement would be the use of plasmid linearization as a tool to eliminate residual circular DNA after an integration event.

4.1.2 Attenuation by double strand break

As this work has been already published, the following discussion will be as brief as possible. It could be shown that it is possible to completely block parasite development

with a single DSB induced by the well-timed expression of a pair of ZFNs, targeting a pair of binding sites previously integrated into the genome. These parasites lost the centromere-lacking part of the chromosome in the next nuclear division and subsequently died due to the loss of more than 200 genes. Depending on the expression timing of the ZFNs, sporozoites were still infective to hepatocytes and could develop for some time. I assume that the Uis4ZFN parasite has the most favorable expression timing with the majority of DSB occurring within the SG. This results in complete absence of HR due to a genome copy number of one and a sporozoite that still has all genes, able to develop well into the liver stage.

We could also show that mice immunized with these parasites are protected from WT sporozoite challenge, indicating that the protection of GAPs is generally independent from the cause of arrest, as has been suggested before for radiation attenuated parasites (RAS) and genetically attenuated parasites (GAP) [432]. Due to an internal cause of arrest for the ZFN based parasites, it should be expected that this methods is easily transferable to other plasmodium species. This has not been the case for many GAPs [433]. Additionally, in contrast to GAPs, where breakthrough events can be observed and generally leave the researcher puzzled about what happened and improvement can only be performed by combining multiple gene deletions which improves safety but can reduce protectivity [119, 434], we could sequence our breakthrough parasites and improve the system. However, without deleting components of the DNA repair pathway required for MMEJ, which are expected to result in reduced fitness, residual MMEJ activity is expected to remain.

DNA repair other than the frequently observed HR and the never observed NHEJ has been reported once and described as alternative end-joining in *Pf* [151]. The repair profiles where similar to those observed here, although the micro-homologies used were not that clear and insertion of several base pairs were observed within the cutting site. The nuclease used in this study produced overhanging ends, in contrast to the blunt ends resulting from the FokI cleavage of ZFNs. In the *Pf* study, repair events were extremely rare. When we tried to map repair frequency of the parasite lines generated, we realized that breakthrough rates are not correlated with sporozoite dose (**Figure 3.19**). This suggests that there are immunological effects that depend on sporozoite dose which are masking the repair event frequency. We would expect that the repair frequency itself is parasite load independent, resulting in more breakthrough events with higher parasite doses. Thus a direct estimate of MMEJ rate is not possible in this context.

The reduction of ZFN copy number from two to one observed due to HR that resulted in failure to induce a DSB was interesting by itself. This was surprising, as multiple genes in *Plasmodium* contain repeat regions that are stable without selection pressure. However, copy number variations above two that are observed under selection pressure can also be expected to result from HR [435]. As these are generally flanked by AT repeats in *Pf*, it seems feasible that the initial duplication from one to two might involve MMEJ. These observations provided some useful guidelines to improve genetic stability of engineered parasites especially in the case if negative selection events.

So far we assessed attenuation efficiency only in a parasite attenuating from a single cause. In the future this methods can easily be combined with other methods (**Figure 4.1**). Combining ZFN parasites with a gene deletion causing arrest in late liver stage development could be performed in a single transfection step. What would be also ideal, if more flexible nucleases like Cas9 are utilized, is to target blood stage essential genes in a way that a predicted MMEJ will result in a loss of function of this particular gene via deletion or frameshift mutation (**Figure 4.1 D**). Prediction of MMEJ repair was successfully applied in *T. cruzi* [152]. Additionally, targeting multiple homology region would also result in a safe way to cause 100% attenuation. A good target might be conserved sites in subtelomeric multi-gene families, which should result in a delayed death phenotype (**Figure 4.1 E**) due to lost telomeres. However this would have to be tested, as there are indication for alternative DSB repair near telomeres [436].

4.1.3 Auto-recycling of selection marker during mosquito passage

We could show that auto-recycling of a selection marker during mosquito passage is possible. In the best case prepatency after sporozoite injection was one day delayed compared to WT (**Table 3.4**). However this mixed population contained still resistant parasites, as not all parasites excised the selection marker (**Figure 3.26**). The DSB target site within the eGFP was modified in these parasites and contained the shielding mutations present in the homologous sGFP, most likely caused by DSB repair via synthesis dependent strand annealing.

What could be done in the future is to sort the parasites for fluorescence after mosquito passage using fluorescence activated cell sorting (FACS). However this would increase the amount of work required in a setup designed to work on its own. Additionally, a second target site of the ZFN could be introduced within the selection marker itself in a region lacking homology with any other region. This would result in all para-

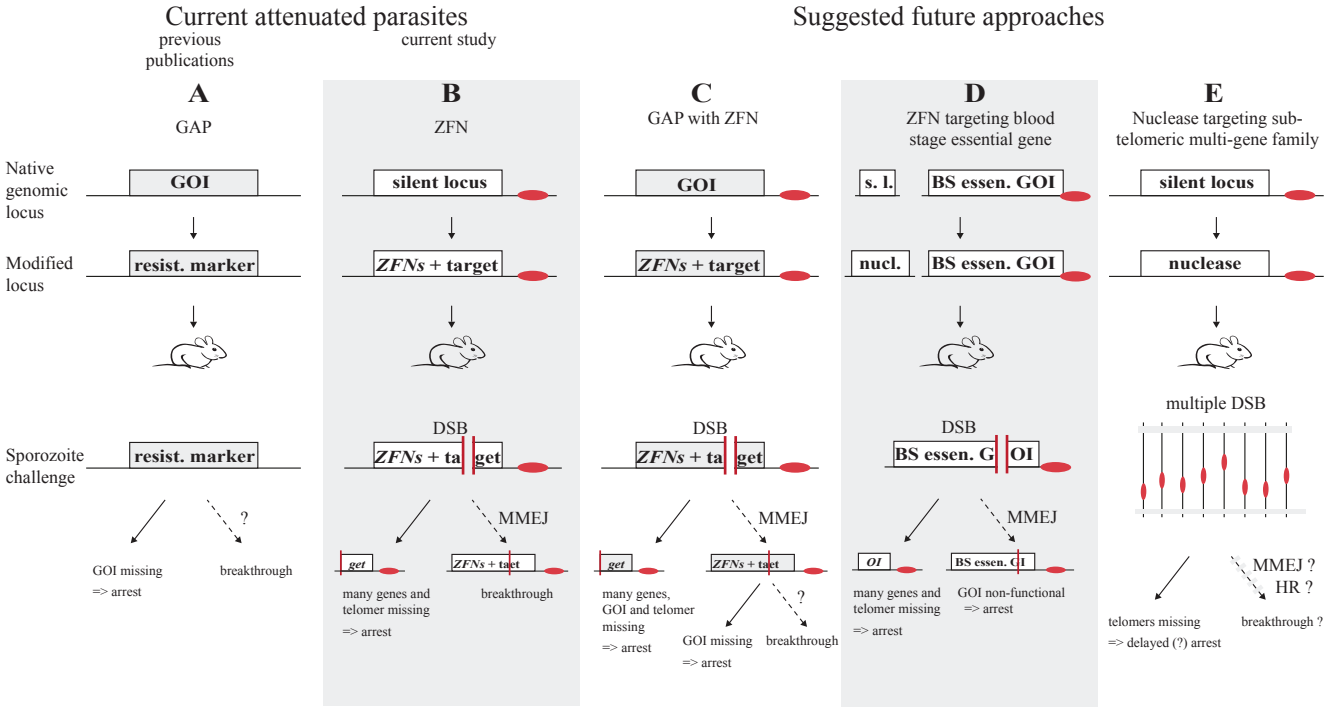

Figure 4.1: Attenuated parasites using nucleases
A Current genetically attenuated parasites (GAP) are generated by removal of an liver stage essential gene. After sporozoite challenge these parasites arrest in the liver and in some rare instances cause a bloodstage infection (breakthrough). **B** A single well-timed double strand break (DSB) can cause the same phenotype due to loss of parts of a chromosome harbouring many genes. Breakthrough can be caused by repair by microhomology mediated end-joining (MMEJ). **C** Combination of A and B is possible with a single genetic modification. **D** Nucleases that are more flexible in target sites can be used to induce the single DSB in a way that causes a blood stage essential gene do become non-functional in case of MMEJ **E** Targeting conserved sites within subtelomeric gene families could result in many DSBs. Potentially these would result in a delayed death phenotype due to lacking telomeres. Multiple repair events would be required to rescue the parasite. Centromeres are depicted in red, DSBs with a GAP, dashed arrows mark rare events. Figure modified from [418].

sites that fail to excise the selection marker to be lost from the population (**Figure 4.2 C**). Alternatively, the homology could only be provided at the outer side of the nuclease target site (**Figure 4.2 D**), only allowing the desired repair product.

The findings made with the auto-recycling parasites can also be transferred to other methods that have been used. Methods used to remove genes in an inducible or stage specific manner using recombinases always suffered from failure to excise in a small population [168, 195, 201]. The same was also observed in the auto-recycling of the selection marker. Thus the potential solutions are the same. Negative selection on those individual parasites that fail to excise can be performed with the induction of a single DSB within the region that is supposed to be excised [88].

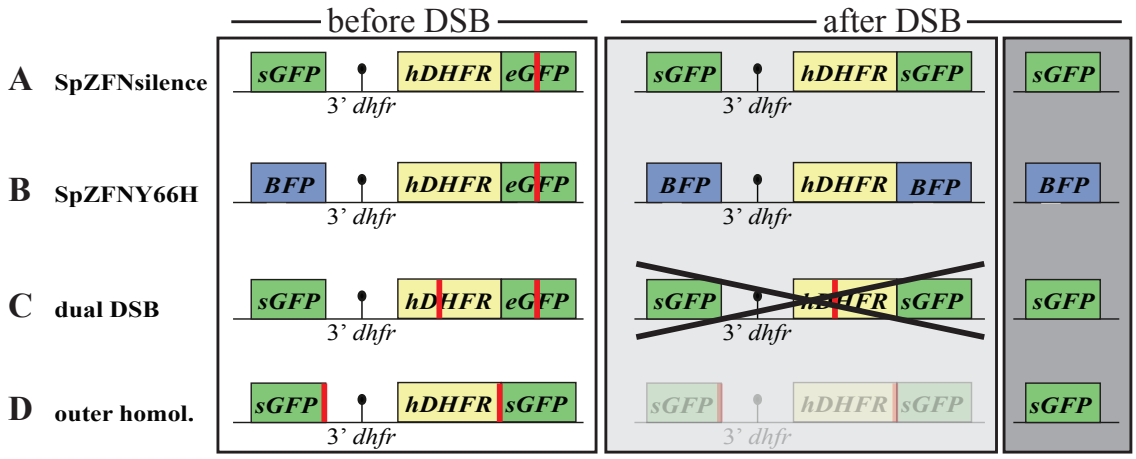

Figure 4.2: Model of nuclease induced auto-recycling
A and **B** Genetic context of parasites generated in this study before and after double strand break (DSB). Note that two separate outcomes after DSB are possible, shown in light and dark grew. **C** Design of a auto-recycling selection marker with a second internal DSB site lacking homology regions. The first repair product (light grew) will suffer from DSB within the selection marker and be lost from the population. **D** Optimization of the exact DSB site in respect to the homology. One of the two DSB sites indicated is sufficient. The faded-out repair product (in the light grew box) cannot occur due to placement of homologies. Nuclease target sites are indicated with a red line.

4.2 The circumsporozoite protein

A vast number of studies have been performed to understand the function of the circumsporozoite protein. The main motivation for thesewas its immunodominant role in early liver stage immunity. If this makes it a particular good or bad vaccine candidate is still highly debated. An open scientific discussion about this topic is rather complicated, given the vast number of people involved in and thus biased about studies on RTS/S, the main vaccine candidate based on CSP [437, 438]. Considering the importance of the liver stage itself for the development of liver stage immunity, sporozoite blocking antibodies, if utilized, have to result in a life-long sterile protection. As this is currently not achieved with RTS/S even in the short term, the number of liver stage exposure is reduced through blocking antibodies. The effect on naturally acquired immunity of this is unclear. It is currently also not clear how long this reduction lasts, but for this time window RTS/S immunization will reduce the efficiency of a real liver stage attenuated vaccine which could offer complete protective efficacy.

Despite the vast abundance of findings about CSP, its role in *Plasmodium* biology is only partially understood. This is mainly caused by the complete block of sporozoite development in parasites lacking CSP [400]. The regulation of protein expression within the mosquito stage is not yet possible and the understanding of promotors in *Plasmodium* is still in its infancy. Otherwise a manipulation of the CSP promotor to turn protein

expression off after sporozoite formation would make it much easier to study its function in later stages.

These circumstances were the main reason that inspired the generation of interdomain GFP tags of CSP. The multiple GFP insertion sites were chosen to minimize disturbance of the functional units of CSP and at first expressed additionally to CSP to disturb sporozoite formation as little as possible. The main findings from my interdomain tagging of CSP for sporozoite formation are two fold, the alternative processing of CSP within the oocyst **Section 4.2.1** and insights into membrane dynamics during sporozoite formation **Section 4.2.2**.

4.2.1 The processing of circumsporozoite protein within the oocyst

Processing at Region I

The processing of CSP is still very poorly understood. Generally the repeat binding antibody 3D11 is used to detect CSP, and results in two main bands in a western blot, running at around 52 and 48 kDa. These are the full length protein and the cleavage product after cleavage near Region I [214].

Using an antibody binding the C-terminus the major two bands can also be detected. With an antibody binding the N-terminus only the full length band can be detected [27]. The cleaved N-terminus is never visible in western blot, probably due to its small size or due to complete degradation. In this study tests with a new batch of the N-terminal antibody showed cross-reactivity with uninfected salivary glands and where therefore excluded from the analysis (data not shown). The working batch published was almost entirely destroyed during a freezer breakdown (personal communications, Photini Sinnis).

It is not know what protease confers N-terminal processing, where the processing occurs exactly within CSP and where on the sporozoite and what happens with the N-terminus after processing. However it is generally assumed that the processing occurs at the plasma membrane of the sporozoites constitutively all the time and is stimulated if sporozoites come in contact with hepatocytes [214].

The main idea is that this regulates invasive capacity of sporozoites. Is has been shown that the C-terminus of CSP is not accessible on non-activated sporozoites [214]. It was proposed that the N-terminus might sterically block the C-terminus from interacting with potential binding partners. An intriguing idea is that the N-terminus of one CSP molecule binds the hydrophobic pocket of the α-TSR domain of another CSP

molecule [391]. This could result in an L-like configuration of CSP on the membrane with the repeat regions creating a dense sheet, and possibly even result in transient protein retention at the PM after C-terminal of GPI-anchor cleavage. However these interactions can only be weak, as CSP does not form stable dimers or higher order polymers in biological samples but tends to partially form dimers if expressed in vitro [399]. Additionally, the FRAP experiments in this study indicate that CSP is diffusing relatively freely at the plasma membrane (**Figure 3.56**). However FRAP of CS II and CS III would appear freely diffusing as observed if the N-terminus is already cleaved off thus restricting interaction or if CS II and CS III do not interact with WT CSP molecules. If this is the case then WT CSP is not self-interacting strongly enough to exclude CS II or CS III into separate membrane patches.

The localization of CS I challenges the believe that the majority of surface CSP is full length CSP. CS I is never surface localized, not if expressed as additional copy nor as replacement (**Figure 3.54**). While processing of CSP within the oocyst will be discussed below, at least salivary gland sporozoites of CS I should be expected to show some GFP signal at the plasma membrane. However fluorescence is mainly detected at the ER or within internal vesicles. This might indicate that CS I is misstrafficked within SG sporozoites or that the N-terminus in cleaved off during trafficking and then degraded and that the GFP tag resists degradation for some time. This is supported by the fact that full length CS I is detected at very low levels but free GFP is easily visible via western blot **Figure 3.60**. However it cannot be excluded that CS I is processed differently that WT CSP. This is further complicated by the fact that after N-terminal cleavage of CS I, the residual repeat region and N-terminus are indistinguishable from WT CSP.

Sporozoites infected with CS I sporozoites show cytoplasmic and nuclear GFP signal within the acinar cells (**Figure 3.53 A**). This is not the case if sporozoites are expressing an extra copy of GFP:GPI. There is no data if this also occurs for full length CSP or the N-terminus only, if cleavage occurs within the sporozoite or at the surface or if this occurs also for WT CSP. Export of CSP into the acinar cell cytoplasm and nucleus would be the first relevant in vivo evidence of an biological purpose of the nuclear localization. The published work [374] concerning the nuclear localization of CSP within the hepatocyte could not be confirmed by anyone so far and has several functional flaws. There it was shown that CSP contains two PEXEL motives used to export proteins beyond the PM via the PTEX translocon and that the C-terminus of CSP contains a nuclear localization

signal. While this is true, it does not necessitate the export of CSP into the hepatocyte nucleus. PTEX export seems to be absent within hepatocytes as HSP101 is not expressed but not all options have been fully explored as *T. gondii* exports proteins into the host cell with only a partial PTEX [382, 383, 439]. In the SG it would also be easier to explain how CSP reaches the host cell cytoplasm in the first place as sporozoites are suggested to be transiently free within the cytoplasm during SG invasion [30, 31]. Given the fact that the proposed nuclear localization signal is within the C-terminus of CSP, the localization of GFP within the nucleus would require the presence of full length CSP. As the full length CS I is not observed at the sporozoite surface, this is hard to explain. However it also possible that the GFP enters the acinar cell nucleus unspecifically. Alternative cleavage of CSP in salivary gland resident sporozoites is unlikely, as the full length CS I was also very rare in the salivary gland sporozoite pellet and supernatant of CS I additional copy parasites (data not shown). Attempts to test for WT CSP localization within intact infected salivary glands proved extremely difficult **Figure 3.53 B**. Antibody signal was only detected at the surface of the salivary gland where it was previously detected and most likely localizes at the basal membrane [440]. Since internal sporozoites were hardly stained with the antibodies used this is hard to interpret as permeabilization was most likely insufficient.

The suggested model of Region I cleavage, to allow the C-terminus to become accessible includes that the C-terminus itself then confers binding to the substrate or hepatocyte [214, 387]. This is strongly supported by the fact the sporozoites expressing CSP lacking the N-terminus stick to all mosquito tissues and invade the first cells they encounter in the mammalian skin. However these results are no formal proof that the C-terminus itself is binding anything. They could also indicate that full length CSP can act as a shield, inhibiting any strong interaction of sporozoites. Once this shield is lowered by removal of the N-terminus, stronger interactions can occur. This does not have to be the C-terminus itself, it could also be other surface proteins shielded by the full length CSP that are shorter. Also this process could be a two step process, that CSP is shielding a signaling molecule that can only bind substrates after CSP processing and then in turn results in the secretion of adhesive proteins. The fact that CS III sporozoites treated with Proteinase K loose all surface fluorescence (indicating the loss of CS III including the C-terminus), but are attaching to each other and producing patchgliding motility in respect to each other might indicate that some unspecific binding and force transmission occurs in a protein-independent way or by protease resistant transmembrane proteins.

The way the sporozoite recognizes the presence of the hepatocyte to induce cleavage at Region I [387] is not known. However recently it was suggested that the N-terminus of CSP itself could fulfill this role, as it is binding hepatocytes directly [396]. This study could not confirm binding of the C-terminus of CSP to hepatocytes, as had been suggested before [441]. The fact that CS I replacement and CS II did not cause infections in vivo (**Table 3.6**) despite both showing Region I cleavage on western blot suggests that unprocessed WT CSP sterically blocks interactions of other proteins on the sporozoite surface. After Region I cleavage, CS II is bulkier that WT CSP due to the presence of the GFP tag and might appear more like unprocessed WT CSP. In contrast, CS I is indistinguishable from WT CSP on western blot after cleavage. But since it appears to be cleaved prematurely, possibly at an alternative cleavage site, processing of CS I most likely does not occur on the PM. If binding and processing of CSP on the PM results in a broader signal than just cleavage of CSP itself, CS I replacement parasites might be incapable to do so and thus lack other prerequisites for invasion.

Processing at the C-terminal region

Western blotting of CS II and CS III with antibodies detecting GFP revealed more bands than expected, while the repeat binding antibody only detected the expected bands (**Figure 3.60**). At first these unexpected bands were considered unspecific cleavage products, but some of them did remain despite vigorous sample processing. With the help of two additional antibodies (kind gift of Photini Sinnis) binding the N-terminus and the C-terminus of CSP, the presence of alternative cleavage products could be confirmed for WT CSP using the C-terminal antibody (**Figure 3.57**).

A careful analysis was performed with alternatively generated samples from early MG samples as well as day 17 MG and SG samples. The repeat binding antibody only detected the two known forms of CSP. However with the C-terminal antibody, four additional bands could be detected, which were only present in the the MG derived samples. Of these, two at 17 and 21 kDa were the most abundant, and were also the main CSP fraction present on accudenz purified midgut sporozoites. All of these protein fragments were virtually absent from purified salivary gland sporozoites, while the 17 kDa, 21 kDa and 25 kDa fragment was present in complete SG samples, albeit at very low concentrations. The fragment traveling at around 12 kDa was only present in the pellet of the midgut sample and absent from all other samples, including the day 10 midgut pellet sample.

To investigate the specificity of the C-terminal antibody and to understand the process in more detail, midgut samples from all CSP mutants were generated from day 10 and day 17 and probed together. This showed that the 25 kDa fragment was also observed for the GFP:GPI replacement samples which lack expression of CSP completely (**Figure 3.58**). Also a band at 55 kDa was observed in GFP:GPI replacement and GFP:TSR:GPI replacement, which runs extremely closed to the full length WT CP fragment, also absent in GFP:TSR:GPI replacement. Both of these appear to be unspecific cross-reactivity of the C-terminal antibody, either reacting with mosquito samples or other parasite proteins.

Additional insight came from the fact that for CS III, only the 17 kDa band was detected whereas the 21 kDa band is absent, and an additional band appeared at 35 kDa. This is also detected with the antibody detecting GFP and helps to map the main cleavage site to the beginning of the α-TSR domain. This would result in the loss of GFP after cleavage for CS II (making it the same length than WT), while increasing the product size for CS III. The fact that small amounts of a cleavage product around 36 kDa are also detected for CS II with both the C-terminal and the α-GFP antibody suggests that there might be alternative cleavage at the end of repeat region or within the N-terminal linker of GFP.

What is striking is the complete absence of the 17 kDa fragment on day 10 for CS III. After all this parasite line expresses WT CSP and CS III side by side. This suggests that on day 10, mainly CS III is expressed, and very little WT CSP. While the relative presence of the 17 kDa and 21 kDa bands cannot be interpreted for CS III parasites, the presence of the 17 kDa fragment for GFP:TSR:GPI replacement suggests that at least some cleavage between GFP and the C-terminus occurs. It most likely results from cleavage site extremely closed to the GPI-anchor in WT CSP or rather within the linker of GFP in CS III cannot be clearly determined.

Using the distribution of fluorescence of CS II and CS III within the oocyst to interpret the location of the observed cleavage products seems impossible. The main observed difference is that CS II is only visible at the PM whereas CS III is also visible in internal structures, mainly the ER (compare **Figure 3.41** and **Figure 3.43**). This suggests that CS III is secreted slower that CS II and WT CSP. This might be due to the fact that the GFP in CS III was introduced directly after the conserved cystein where the GPI anchor is predicted to be added (**Figure 1.8**). Running the protein sequence of CS III on the prediction software used [392] also resulted in the prediction to be GPI-anchored

to 100%. However, the actual addition process might occur slower for CS III. It has been shown that the GPI-anchor itself can act as an ER-exit signal [442], so CS III would be transiently trapped within the ER. The GPI-anchor might sterically protect the α-TSR domain in CSP, as has also been suggested for the glycosylation of the threonine within the α-TSR domain [373].

Alternatively, CSP might actually be endocytosed within the oocyst during sporozoite formation. In *Trypanosoma brucei* it has been shown that the GPI-anchored major surface molecule VSG is endocytosed and then excluded from clathrin coated vesicles budding form endosomes via negative sorting, recycled are secreted again [443]. The same might be true for CSP. Differences in sorting of CS II and CS III after C-terminally processing might account for the varying observation of internal fluorescence. However, the capability and abundance of endocytosis in *Plasmodium* is generally debated [51].

Additionally, all CSP mutants would appear to be localized at the PM of developing oocysts even when the fraction with the GFP has already been cleaved off by a protease. This is true for most of the oocysts that have very limited extracellular space. Thus, CS II might appear to localize especially strongly to forming sporozoite tips since there is more extracellular space surrounding these, filling up with cleaved off CSP. If oocysts ruptured due to mechanical stress during prolonged microscopy sessions, a negative staining of mosquito midgut tissue could be observed in midguts infected with CS II but also CS III. This suggest that the protein is at least partially cleaved from the PM. It is striking that even under this assumption, CS I replacement oocysts never appear to show surface localized fluorescence. This is another indicator that GFP in CS I never reaches the PM and is internally degraded. On option how this could occur with such an efficiency is that the PEXEL motif is active within oocysts beside or in addition to the signal peptide, thus resulting in GFP cleavage by Plasmepsin V within the ER. However generally PEXEL motives not at the N-terminus of proteins are not recognized and the protein is then not exported [444]. Yet in all studies so far cleavage was evaluated by PTEX export, which is not necessarily required for cleavage to occur. Recently it what shown that Plasmepsin VIII is required of oocyst egress and sporozoite infectivity [445]. In this study CSP processing appeared normal, but was only assessed using the repeat binding antibody 3D11.

A model giving a brief overview of CSP cleavage fragments for WT CSP was generated (**Figure 4.3**).

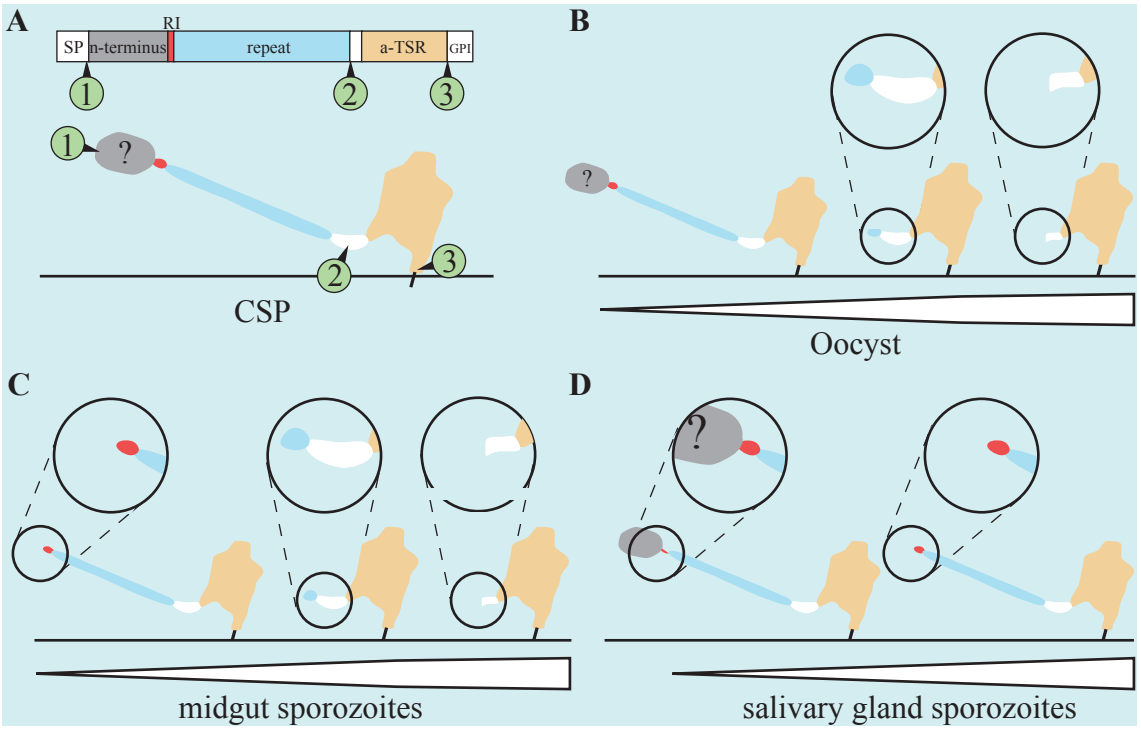

Figure 4.3: Model of CSP cleavage products
A brief summary of the presence of different CSP cleavage products during sporozoite development is depicted. **A** CSP domain architecture and potential domain organization of CSP at the plasma membrane (black line) is depicted. Note that domain organization, as well as the structure of the N-terminus is unknown. GFP insertion sites for CS I, CS II and CS III are depicted by green circles 1, 2 and 3. **B** The main CSP fragments within the oocyst are shown. The relative abundance of these fragments is indicated below. **C** The main CSP fragments of midgut sporozoites are shown. **D** The main CSP fragments of salivary gland sporozoites are shown.

Biological implications While we initially assumed that the alternative cleavage products of CSP occur somewhere within in the oocyst and are mainly important for oocyst egress, even sporozoites purified from midgut samples mainly contain the cleavage products of 17 kDa and 21 kDa and some of the 48 kDa band (**Figure 3.59**). This suggests that the PM of haemolymph sporozoites which attempt to invade the salivary gland might still be mainly filled with these cleavage products. This could result in immediate SG invasion, explaining why sporozoites with N-terminal deletion also invade SG. Alternatively, after egress, haemolymph sporozoites might take some time to resynthesize full length CSP prior to salivary gland invasion.

If CSP is or participates in some kind of receptor for activation of sporozoite for hepatocyte invasion and / or motility, this might also shed some light into CSP function. IV injection of haemolymph sporozoites is almost as efficient as IV injection of SGS. If N-terminal processing is a prerequisite for hepatocyte invasion the CSP state on purified MGS might explain this as they, in contrast to salivary gland sporozoites, do not display

full-length CSP on their surface.

It has recently been shown that several parasite mutants become activated within oocysts but fail to egress [29]. This motility was not observed in the CSP mutants generated in this study that fail to egress (CS I replacement, CS II and CS III). The easiest explanation for this would be that the mutants published are activated to egress but then fail to rupture the oocyst wall due to a missing protease or failure to traffic and secrete required proteases. In case of the CSP mutants sporozoites are never observed to be motile within the oocyst, even thought they are occasionally observed in a spaghetti-like orientation within the oocyst, suggesting they once moved. However, most oocysts are filled with ordered arrays of sporozoites, most likely still attached to a residual body. This suggests that they never get activated to egress. Potential reasons for this could be many. It seems feasible that egress occurs in a two step process. Mature oocysts increase permeability of the oocyst wall. Incoming molecules then signal to the oocyst that the oocyst wall is ready to be ruptured.

It is possible that complete processing of CSP is a 'quality control' or checkpoint mechanism of completed sporozoite formation to prevent premature egress. Incomplete processing would therefore never result in a mature oocyst. It might also be possible that sporozoites expressing mutant CSP are unable to detach from the sporoblast due to altered membrane dynamics. Alternatively, CSP has been shown to be localized at the oocyst wall [25]. Therefore CSP mutants might block oocyst wall breakdown. Lastly, activated sporozoites within oocysts do not seem to engage in normal gliding motility, rather a 'interpatching' like movement, where they patchglide in respect to each other. This might help them to detach from the sporoblast and / or produce sufficient force to rupture the oocyst wall. If this requires C-terminally cleaved CSP, CSP mutants might carry access protein on there surface, unspecifically blocking binding of the proteins involved. Thus sporozoites would be activated within the oocyst, but not be able to engage in motility and thus appear immotile.

All these options seem feasible with the observations made for CS II and CS III, but not with the observations for CS I replacement. Here, the suggested alternative N-terminal cleavage might be the reason that sporozoites are not able to egress.

Further studies of C-terminal processing of CSP should include western blotting of the CSP mutants devoid of oocyst egress that have been previously published [275, 292] using the C-terminal antibody, as well as the mutants with the same phenotype [29, 274, 445]. Additionally, and technically more challenging, would be the attempt to quantify

the amounts of C-terminally cleaved vs full length CSP within an oocyst at the PM of the sporoblast on the outside, during invagination and on the surface of forming sporozoites. To do this immuno-EM would be required using antibodies against the repeat region and the C-terminal region of CSP in the same sample. Alternatively, a two color reporter line could be generated, expression a red version of CS II and a green version of CS III simultaneously. However if cleavage or trafficking is influenced in these tagged proteins the results of the latter experiment might result in false results. Possibly such lines should be constructed with a weakened promoter to possibly only express 5% of total CSP.

4.2.2 Membrane dynamics during oocyst development

Both electron microscopy and microscopy of oocysts expressing CSP mutants resulted in a better understanding of sporozoite formation within the oocyst. Especially the initial steps, the invagination, has previously been ignored. Due to the fact that all CSP mutants are localized to the PM prior to PM invagination allows to follow this process. However, due to the requirement to image ex vivo for a limited time prior to midgut disintegration it is only possible to observe snapshots in time, much like in electron microscopy. This does not only limit the possibility to investigate if the states observed are occurring in all oocysts or only in a subset, but also does not allow to identify which of those states result in complete failure to generate sporozoites, except in those mutants where this never occurs.

What can be observed during invagination events prior to apical tip formation of sporozoites is that some oocysts show a sheet like invagination, essentially resulting in the formation of sporoblasts, whereas others show a more tubular invagination (**Figure 3.39 A** and **B**). This is best visualized in complete z-stacks (see attached movies S1-S7). The sheet-like invagination was observed in the majority of the oocysts observed. Thus the tubular invagination could be a transient state prior to the sheet-like invagination or a parallel development, result in the formation of or failure to form sporozoites. Additionally, a bubble-like or rather inverse bubble-like invagination was also observed (**Figure 3.43 B**). This is basically a local and rounded retraction of PM, resulting in huge extracellular space in between the oocyst wall and the PM. Most likely this leads to proper sporozoite formation, as apical tip formation was observed within these bubble like invaginations (**Figure 3.43 E**).

What was observed in almost every section of every oocyst observed with EM are the

labyrinthine structures, which are small prior to apical tip formation and are biggest and best defined during apical tip formation and start to disintegrate when sporozoite elongations is completed. Also using fluorescent microscopy these structures can be detected in oocysts of GFP:GPI, CS II and CS III as bright round blobs in between sporoblasts (**Figure 3.40 B**, **Figure 3.41 B - D** and **Figure 3.41 C - F**). Their size, localization at boundary sites in between sporoblasts and there absence from GFP:GPI:repl and GFP:TSR:GPI:repl correlates strongly between electron and fluorescence microscopy. The individual membranes structures are far to small to be observed in fluorescence microscopy, but their strong fluorescent intensity in contrast to the PM suggests that the main membrane component is PM. EM of some of these labyrinthine structures shows that besides the PM component, there seems to be an internal membrane network. The origin of this is completely unknown. Structures with very similar appearance have been observed previously before merozoite formation in liver schizonts, and proposed to be involved in nutrient uptake [446]. Structures which are similar to the rather degenerate labyrinthine structures observed in old oocysts of CS III have been described in oocysts of *Leucocytozoon dubreuli* as ER-associated vesicles in [266]. In the recently published CSP-repeat lacking parasites degraded labyrinthine structures can been observed, but these were not described in the publication [27].

Our first speculation about the function of these labyrinthine structures was that the increased surface area might be very suitable for nutrient uptake. Especially given the fact that during sporozoite formation including the underlying IMC, nutrient uptake via the PM of the elongating sporozoites might be limited. But then we should expect this structure during the time the oocyst is increasing in size the fastest, which is during the first days of oocyst development. At this time the PM of the developing oocyst is expected to be tightly associated with the forming oocyst wall. Although no high resolution EM is available of this time in development, we did not observe any labyrinthine structures prior to PM development. This makes the function as a general nutrient uptake area less likely. If there is endocytosis and sorting and recycling of PM components occurring in oocysts at this time similar than VSG sorting in *T. brucei* [443], this might be the place where it occurs. Additionally, this structure could represent a structure involved in the secretion of CSP itself. However CSP is secreted prior to appearance of the labyrinthine structures. Another study has recently been performed on a PM localized protein that has been tagged with GFP [447]. It should be investigated if this protein also localizes to these structure.

The observations of the fluorescence observed in CS I and CS I replacement provide the biggest challenge to interpret. Whereas CS I is expressed late in oocyst development, CS I replacement showed much earlier and stronger expression. In CS I replacement fluorescence is completely absent from the PM and strongly labels big ER structures, the nuclear envelope and big areas near the oocyst wall that are uniform in fluorescence intensity (**Figure 3.46 A**) and most likely represent the unidentified structures observed in EM (**Figure 3.34**). These could be either ER-like structures or big areas or extracellular space that are not in direct contact with the oocyst wall. Colocalization analysis with an ER marker should answer this question.

The main conclusions from the membrane dynamics for sporozoite development come from the fact that GFP:GPI replacement and GFP:TSR:GPI replacement start PM invagination at a smaller oocyst size, never completely invaginate to the central area of the oocyst prior to IMC formation and begin apical tip formation at the complete PM before invagination is completed. This suggest that IMC formation and associated apical tip formation is initiated prematurely in these parasites. The same was observed for CSP deletion, GPI-anchor removal of CSP and deletion of the repeat region and reduction of CSP to the C-terminus [25, 27, 349]. This suggests that somehow CSP restricts IMC formation to the forming apical tips. How this could be achieved is unknown. The C-terminal processing might be involved in this process. The C-terminally cleaved product (as in GFP:TSR:GPI replacement or the ΔN Δ rep from [27]) does not block IMC formation. Potentially the C-terminally uncleaved CSP recruits IMC formation to the apical tips which occurs everywhere in its absence. The opposite, that C-terminally uncleaved CSP blocks IMC formation seems unlikely, as this would postulate that C-terminally uncleaved CSP is excluded from the forming sporozoite.

However it remains an open question how any cleavage product of CSP would itself be limited to the forming apical tip. Homodimerization of CSP or the formation of whole polymer-like structures via the N-terminus or the repeat region could explain how different subsets of CSP can exclude others on the PM. However the homodimerisation-rate of soluble CSP is low. Membrane microdomains that enrich GPI-anchored proteins have been suggested [356] but their existence is still debated [448] and their size would be several orders of magnitude smaller than whole sporozoites. However the recruitment of CSP and forming IMC could be a two-way enrichment. GPI-anchored proteins have by default difficulties to interact with components of the other side of the membrane. It has been shown that the distance between the GPI-anchored protein and the underlying

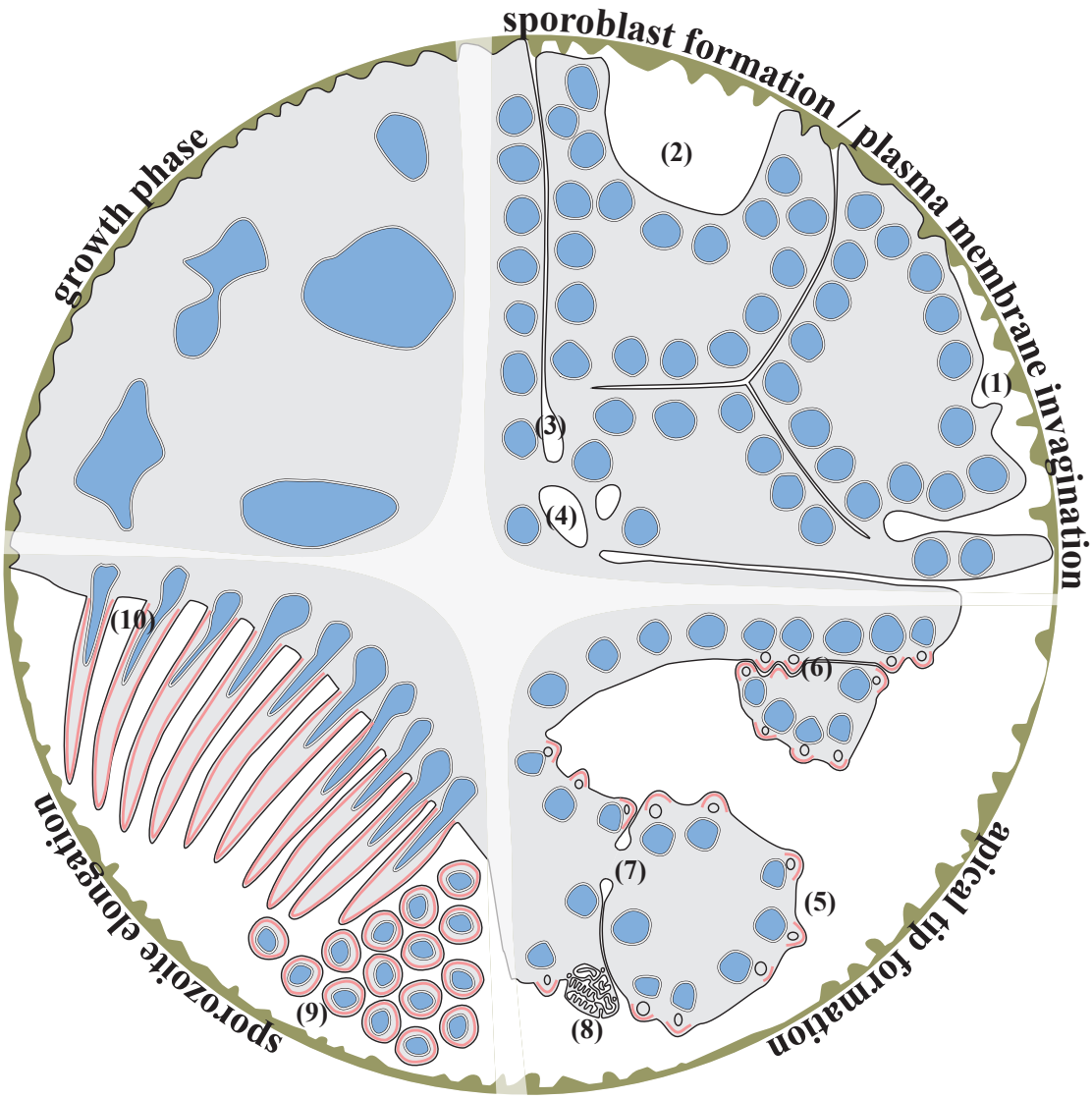

Figure 4.4: Model of sporozoite development
Oocyst development is separated into four seperate stages. **Growth phase** After rounding up of the ookinete several processes occur during the longest phase of oocyst development which is the least studied. This includes nutrient uptake, the strong increase in cell size and nuclear division, as well as oocyst wall (brown) formation and the utilization of the cristalloid. **Sporoblast formation / plasma membrane invagination** During this time nuclear division causes a reduction of the size of individual nuclei (blue). It coincides with the retraction of the plasma membrane (PM) (black) from the oocyst wall (1 and 2) and deep invaginations of the PM (3). Also internal membrane structures are observed which could potentially spread towards and fuse with the PM (4). The nuclei collect underneath the PM. **Apical tip formation** In between the PM and the underlying nuclei the apical tip of forming sporozoites is initiated, visible by formation of inner membrane complex (IMC) (red), the appearance of the praerhoptry (circle) and a bulging PM. This can occur everywhere at the PM, outside of sporoblasts (5) as well as in between sporoblasts (6). Additionally cytoplasmic bridges in between sporoblasts are occurring(7), questioning if they completely separate. Also, labyrinthine structures are observed at the periphery of sporoblasts, frequently located in between them (8). **Sporozoite elongation** During the last stage of sporozoite development prior to egress, sporozoites elongate by uniform retraction of the PM. At this time sporozoites are in similar orientation than sporozoites in their local environment (9 and 10) until they separate from the remaining sporoblast.

membrane can be as low as 1 nm [449]. Thus it it would be possible that structural changes in CSP, for example the proposed mode of dimerization via the hydrophobic core of the C-terminus [391], could result in structural changes occurring directly at the PM. The perfect interaction partner would be GAP45, as it links the PM and the IMC. CSP directly interacting with GAP45 seems unlikely, as GAP45 is N-terminal palmitoylated and myristoylated [303] and lacks an extracellular portion, but a clustering in microdomains by enchrichment of CSP via the GPI-anchor and GAP45 via the N-terminal palmitoylation and myristoylation seems possible. Enrichment of proteins via palmitoylation has been observed in many cases [450] and has been implicated in leukocyte signalling [451]. The initiation of this interaction could actually be locally restricted within the oocyst by the localization of the palmitoyl transferase of GAP45. Given its expression timing and localization within the oocyst, DHHC3 could potentially serve this role [452]. Of course the association could also occur via an third protein linking CSP and GAP45 or via another protein directly linking CSP and the forming IMC.

A model was generated from all those intermediate events frequently observed in CSP mutants and WT oocysts that are expected to results in normal sporozoite formation (**Figure 4.4**). The oocyst development and sporozoite formation was separated into four phases, (1) the growth phase, (2) the sporoblast formation and plasma membrane invagination, (3) apical tip formation and (4) sporozoite elongation. Both ookinete to oocyst transformation and oocyst egress have been excluded from the model, the later being recently investigated [29]. In the model, the various observations of PM invagination are depicted as they would be observed in 2D, as well as the dynamic interplay of sporoblast bodies observed and the labyrinthine structures.

4.2.3 The role of the circumsporozoite protein in salivary gland invasion

CSP has been implicated in salivary gland invasion, although not as stringent as an active participant as shown for TRAP [28, 328]. However, sporozoites lacking the complete N-terminus adhere unspecifically to all mosquito tissues resulting in a reduced salivary gland invasion rate [214] as well as SG invasion in mosquitoes with reduced CSP binding protein [394]. In the study about CSP binding protein, binding of soluble CSP on salivary gland was shown to occur and to be CSP binding protein dependent. I tested if this process also occurs in vivo. CSP was detectable on the surface of invaded salivary glands using a repeat-binding antibody (**Figure 3.53**). Direct observation of any of the CSP mutants generated on the surface of the salivary gland was not possible. The

fact that both CS II and CS I replacement most likely have a salivary gland invasion phenotype additionally to their strong egress phenotypes supports the suggestion that CSP is involved in salivary gland invasion. However, it cannot be excluded that this is solely based on the anti-adhesive effect of WT CSP, which was most likely the main reason for the salivary gland invasion phenotype of the N-terminal deletion mutant [214]. Other work suggested that an active binding of the N-terminus might be a part of salivary gland invasion [397]. The N-terminus blocking unspecific binding would explain the phenotype observed for the CS I replacement mutant, which also appeared to show increased unspecific adhesion. Unfortunately, due to the reduced oocyst egress, an in-mosquito off-target adhesion-analysis as performed for the N-terminal deletion mutant [214] could not be performed for CS I replacement.

Even more striking was the observation of GFP in the CS I mutant in the cytoplasm and nucleus of the acinar cells of the salivary gland as discussed above (**Section 4.2.1**). It should be further tested if WT CSP is also localized there, and if so, the role of CSP in the hierarchic invasion of outer lobes of the salivary gland should be investigated. The fact that low level infections result in reduced salivary gland invasion and sporozoite infectivity per sporozoite increases with salivary gland load [453] suggests that initial salivary gland invasion is most likely less efficient and comes with a price for those sporozoites that succeed. These then might modulate the salivary gland in such a way that following sporozoites have a better chance to successfully invade the salivary gland.

4.2.4 The circumsporozoite protein and gliding motility

The formal proof that CSP is not actively required for gliding motility is still pending, and most likely requires rapid protein depletion following salivary gland invasion. However, there are multiple indications that CSP is passively required for gliding motility for example by reducing unwanted adhesion.

Of those CSP mutants generated, CSP II and partially also CS III show enriched gliding motility of midgut derived sporozoites (**Figure 3.30**). The same is true for the already published [29] parasite lacking trp1(-), which also have an egress phenotype. Thus it is likely that the artificially increased time within the oocyst results in maturation processes normally occurring within the salivary gland, albeit at a much slower rate. The different but related phenomenon has been shown for parasites lacking the RNA binding protein Pumilio like protein (Puf2) which mature prematurely into liver stage like forms within the salivary gland [89]. Thus it is likely that also the increased motility

is independent of CSP function and just a result of the egress phenotype.

In contrast, the parasites expressing a CSP replacement with CS I show no increased gliding motility, but are relatively sticky. Given the fact that CS I is prematurely processed within region I, the expected phenotype should be similar to that of the N-terminal deletion of CSP. This has been reported to be very sticky to mosquito tissues in general, resulting in a low salivary gland invasion rate [214]. However in contrast to CS I replacement, these parasites have no egress phenotype from the oocyst and are capable of causing a blood stage infection. CS I replacement shows a strong egress phenotype from the oocyst and might also results in decreased CSP on the sporozoite surface, a phenotype alone previously linked to a complete block of invasive capability [25]. An indication for this is that CS I additional copy parasites behave indistinguishable from wild type.

The FRAP experiments performed showed that all CSP versions are freely diffusing within the PM with high speed. This suggests that there is no directed membrane flow at measurable speeds within the PM membrane as has previously been suggested [286]. This does not imply that directed diffusion caused by polar secretion of adhesion molecules within the PM occurs at high speeds, resulting in a net forward driving force without the actin-based gliding motility motor. Flow of membrane patches or the membrane as an entity is very unlikely. Additionally, the fast recovery of fluorescence after photobleaching suggests that CSP is present at the surface as a monomer or only transiently as a dimer, as has been previously suggested [396]. This conclusion requires the assumption that CS II or CS III could also participate in the dimer formation, either forming homodimers with itself given the high PM concentration or the formation of heterodimers with wild type CSP assuming that the structural differences are not significantly influencing this rate.

Adhesion site dynamics using TIRF-M

Using TIRF microscopy, two separate sets of sporozoites were identified, those showing the same TIRF signal over the length of the whole sporozoite during motility and those showing reduced and dynamic contact sites. This is not identical to the results produced with RICM of sporozoites, where a constant distance of the sporozoite to the substrate was observed at the apical and basal end of the sporozoite which was dynamic in time, while the measurements for the central parts of the sporozoite where dynamic in time and relative to the position on the sporozoite and constant to a single point on the substrate

[285]. Unlike in RICM, using TIRF-M, all signal was alway substrate-site dependent and independent to the respective site on the sporozoite. However it has to be taken into consideration that these two methods do not result in the same signals. In TIRF-M, a signal is produced if the fluorophore is close to the glass slide and deteriorates if the distance is greater than +/- 100 nm. In RICM, the internal reflexion of monochromatic light causes interference between the light reaching the sample and the light reflected of the surface of the sample [454, 455]. This results in very detailed distance measurements for objects with high and defined refractive index, and much harder to analyze data given the unknown refractive index, surface distance and membrane angles of a living cell. Local difference of refractive index of sporozoites might produce differences in signals in respect to the position on the sporozoites that are misinterpreted as differences in adhesion.

Most likely both methods result in more apparent adhesion sites than actually exist in gliding sporozoites, as they both only display proximity of the cell to the substrate. As the sporozoite is relatively stiff locally, defined small adhesion sites as they might exist will likely never be visualized as discrete spots. The dynamic interplay between force production at the front and a stalling force on the back of the sporozoite caused by delayed disassembly of adhesion sites might heavily influence the substrate proximity of the central part of the sporozoite. It might even be possible that the adhesion site itself is not necessarily as closed to the substrate as expected. In a single sporozoite observed patch gliding using TIRF-M (see attached movie S8), the exact patching spot did not produce any TIRF signal. This of course might be due to its distance from the substrate or alternatively CSP might be excluded from the adhesion site itself in patchgliding.

Ultimately what should be done in the future is to study adhesion dynamics of sporozoites in their natural environment. Gliding motility on a semi-flat substrate occurs in vivo only in very limited oocasions. This is potentially the initiation of salivary gland invasion after initial attachment of the sporozoite as well as the "arrival" of the sporozoite in the liver, when it switches from passive dissemination via the blood flow to actively enter the liver sinusoid. Only the latter has been observed [39, 405]. Gliding motility within 3-D environments like the skin and the liver are ultimately what should be focused on. Both RICM and TIRF-M are not suitable to study adhesion dynamics in 3-D environments. To do so other methods are more useful. One possibility are force sensors, which have been used to visualize adhesion dynamics and forces within adhesion sites generated in bigger and slower cells [456]. Force sensors use a two fluorophores acting

as Förster resonance energy transfer (FRET) pair or as a fluorophore and a quencher, connected with a flexible linker made from DNA or protein. While DNA based force sensors have to be artifically produced, protein based FRET sensors can be expressed from the cell measured.

Another potentially easier option is to perform FRET from certain substrates within the 3-D environment directly, like components of the extracellular matrix or PM proteins of the cells within the skin or liver. The FRET partner would be located on the surface of the sporozoite, either generally within the PM or directly within molecules involved in adhesion like TRAP. All attempts to visualize surface TRAP on live cells by N-terminally tagging it with GFP were not successful (data not shown). The large amounts of micronemal TRAP in contrast to the few molecules on the surface did not allow to see TRAP on the surface at all. Even in TIRF microscopy the weak signal observed was localized to the micronemes. Using mutated motives of the rhomboid cleavage sites [215] in the GFP tagged TRAP resulted in accumulation of fluorescence at the back of the sporozoite, which in amount correlated with their inability to continue gliding motility. The biggest potential problem of FRET to visualize adhesion dynamics in vivo is the distance limitation of FRET, which occurs most efficiently in a low nm range. However it has recently be shown that excitation can occur by excitation - emission wavelength pairs even over longer distances [457].

Trail formation

Trail formation so far has been described as an active process of the sporozoite to leave CSP protein on the substrate [403]. Shortly after it was realized that the trail is actually membraneous, and at least after preparation for EM is mostly vesicular in nature [401]. Other surface molecules than CSP have also been observed in trails in a more or less continuous pattern [215, 402]. Of these TRAP is expected to be substrate bound and membrane bound if not cleaved by a rhomboid protease, CELTOS might be secreted and directly deposited on the substrate [215, 402]. However, even today protein presence detected via IFA is still interpreted on the basis that all proteins are shed and deposited on the substrate on their own, and not together with small vesicles of PM and accompanied proteins [458].

Trail formation has since then been utilized in countless studies to assess the motility of sporozoites and tachyzoites in a so called "trail assay". In this assay, the substate is normally coated with CSP repeat-binding antibody (or simply fetal bovine serum

(FBS) in the case of *T. gondii* tachyzoites). Then the motile cells are allowed to glide (unobserved), fixed and the "trail" is visualized with CSP or SAG-1 specific antibodies. The dynamics of gliding motility in time are completely lost in this end-point assay. The dynamics of trail formation itself has not really been a subject of studies.

Imaging sporozoites of the CSP mutants during gliding motility, we realized that they produce a trail during motility on an uncoated glass slide in the presence of BSA. This appeared more frequently in midgut sporozoites and haemolymph sporozoites than in salivary gland sporozoites. Initially the trail is still connected with the sporozoite, shown by the ability of the sporozoite to move back into the trail, correlating with its disappearance, and the ability of the trail to recover fluorescence after photobleaching. Also, trails were observed that lost contact to the substrate during motility of the sporozoite, which then directly recombined again with the sporozoite PM. In contrast, trails forming two or more adhesion sites normally dislodged form the sporozoite and remained on the substrate spanning the two adhesion sites. Over time trails attached to the substrate in this manner frequently fragmented into smaller pieces, which could remain on the substrate or, lacking their own adhesion site, float away.

All these observations result in the interpretation that trail formation, besides the artificial induction via antibodies binding surface molecules, is initiated when a sporozoite is moving faster than the cleavage site can be dislodged by rhomboid protease activity. Very strong trails have also been observed in TRAP cleavage mutants using a standard trail assay [215]. As long as sufficient PM is available, the trail can be elongated. In events where the sporozoite dislodges from the trail, the membrane has to reseal on both sides. If this process is passive or active in nature is not known. It could however explain the observation of cytoplasmic proteins in surface enriched samples observed using mass spectrometry [373] (however not their confirmation via immunoflourescence analysis of fixed cells).

The diameter of the trails is well below the resolution limit of the microscopy techniques used. The vesicular structures observed in EM resembling the trails were reported to be roughly 70 nm in diameter [401]. Assuming equal distribution of the CSP mutants within the PM of the sporozoite and the trail a rough estimation of their diameter could be attempted using fluorescence intensity during TIRF-M.

What is still unresolved is the biological relevance of trail formation. After all it is not know if trails are formed in vivo. Given the fact that CSP was easily detected at the surface of salivary glands, it seems likely that trails are formed at the basal lamina of the

salivary glands (**Figure 3.53**). In the skin and liver there have been only speculation that big amounts of CSP in the traversed tissue results in an immunological cloak screen for liver stage development. However even if true this might be completely independent from trail formation and occur during cell traversal. On the other hand, trail formation could explain how sporozoites can "back up" if they hit a spot in the tissue they cannot traverse. Using in vivo imaging sporozoites are observed to move backwards for a short distance to then take another path. How this might occur is difficult to explain with a directed motor alone and trails resulting in backwards pulling of the sporozoite might explain this phenomenon. The parasites expressing additionally GPI-anchored GFP might be suitable for observation of trail formation using in vivo imaging. Potentially, preincubation of sporozoites with a strong membrane label might also be suitable to probe if trails are formed during tissue traversal in the skin and liver.

Bibliography

[1] Leander BS and Keeling PJ (2003) Morphostasis in alveolate evolution. *Trends in Ecology and Evolution* 18(8), 395–402

[2] Simpson A and Roger AJ (2004) The real 'kingdoms' of eukaryotes. *Current Biology* 14(17), R693–R696

[3] Woo YH, Ansari H, Otto TD, Klinger CM, Kolisko M *et al.* (2015) Chromerid genomes reveal the evolutionary path from photosynthetic algae to obligate intracellular parasites. *Elife* 4, e06974

[4] Morrison DA (2009) Evolution of the Apicomplexa: where are we now? *Trends in Parasitology* 25(8), 375–382

[5] Adl SM, Leander BS, Simpson AGB, Archibald JM, Anderson OR *et al.* (2007) Diversity, nomenclature, and taxonomy of protists. *Systematic Biology* 56(4), 684–689

[6] Morrissette N (2015) Targeting Toxoplasma tubules: tubulin, microtubules, and associated proteins in a human pathogen. *Eukaryotic Cell* 14(1), 2–12

[7] Klinger CM, Nisbet RE, Ouologuem DT, Roos DS, and Dacks JB (2013) Cryptic organelle homology in apicomplexan parasites: insights from evolutionary cell biology. *Current Opinion in Microbiology* 16(4), 424–431

[8] Harding CR, Egarter S, Gow M, Jimenez-Ruiz E, Ferguson DJP *et al.* (2016) Gliding Associated Proteins Play Essential Roles during the Formation of the Inner Membrane Complex of Toxoplasma gondii. *PLoS Pathogens* 12(2), e1005403

[9] Kono M, Heincke D, Wilcke L, Wong TWY, Bruns C *et al.* (2016) Pellicle formation in the malaria parasite. *Journal of Cell Science* 129(4), 673–680

[10] Janouškovec J, Horák A, Oborník M, Lukeš J, and Keeling PJ (2010) A common red algal origin of the apicomplexan, dinoflagellate, and heterokont plastids. *Proceedings of the National Academy of Sciences of the United States of America* 107(24), 10949–10954

[11] Abrahamsen MS, Templeton TJ, Enomoto S, Abrahante JE, Zhu G *et al.* (2004) Complete genome sequence of the apicomplexan, Cryptosporidium parvum. *Science* 304(5669), 441–445

[12] Templeton TJ and Pain A (2016) Diversity of extracellular proteins during the transition from the 'proto-apicomplexan' alveolates to the apicomplexan obligate parasites. *Parasitology* 143(1), 1–17

[13] Clode PL, Koh WH, and Thompson RCA (2015) Life without a Host Cell: What is Cryptosporidium? *Trends in Parasitology* 31(12), 614–624

[14] Lee JJ, Leedale GF, and Bradbury P (2000) *An illustrated guide to the protozoa. Organisms traditionnally referred to as protozoa, or newly discovered groups, Vol. II.* Society of Protozoologists

[15] Cavalier-Smith T (2014) Gregarine site-heterogeneous 18S rDNA trees, revision of gregarine higher classification, and the evolutionary diversification of Sporozoa. *European Journal of Protistology* 50(5), 472–495

[16] Borner J, Pick C, Thiede J, Kolawole OM, Kingsley MT *et al.* (2016) Phylogeny of haemosporidian blood parasites revealed by a multi-gene approach. *Molecular Phylogenetics and Evolution* 94, 221–231

[17] Otto TD, Gilabert A, Crellen T, Böhme U, and Arnathau C (2016) Genomes of an entire Plasmodium subgenus reveal paths to virulent human malaria. *bioRxiv* doi:10.1101-095679

[18] Billker O, Dechamps S, Tewari R, Wenig G, Franke-Fayard B *et al.* (2004) Calcium and a calcium-dependent protein kinase regulate gamete formation and mosquito transmission in a malaria parasite. *Cell* 117(4), 503–514

[19] Wirth CC and Pradel G (2012) Molecular mechanisms of host cell egress by malaria parasites. *International Journal of Medical Microbiology* 302(4-5), 172–178

[20] Kehrer J, Frischknecht F, and Mair GR (2016) Proteomic Analysis of the Plasmodium berghei Gametocyte Egressome and Vesicular bioID of Osmiophilic Body Proteins Identifies Merozoite TRAP-like Protein (MTRAP) as an Essential Factor for Parasite Transmission. *Molecular & Cellular Proteomics* 15(9), 2852–2862

[21] Sinden RE, Talman A, Marques SR, Wass MN, and Sternberg MJE (2010) The flagellum in malarial parasites. *Current Opinion in Microbiology* 13(4), 491–500

[22] Kooij TW and Matuschewski K (2007) Triggers and tricks of Plasmodium sexual development. *Current Opinion in Microbiology* 10(6), 547–553

[23] Bennink S, Kiesow MJ, and Pradel G (2016) The development of malaria parasites in the mosquito midgut. *Cellular Microbiology* 18(7), 905–918

[24] Smith RC and Barillas-Mury C (2016) Plasmodium Oocysts: Overlooked Targets of Mosquito Immunity. *Trends in Parasitology* 32(12), 979–990

[25] Thathy V, Fujioka H, Gantt S, Nussenzweig R, Nussenzweig V *et al.* (2002) Levels of circumsporozoite protein in the Plasmodium oocyst determine sporozoite morphology. *EMBO Journal* 21(7), 1586–1596

[26] Sinden RE and Strong K (1978) An ultrastructural study of the sporogonic development of Plasmodium falciparum in Anopheles gambiae. *Transactions of The Royal Society of Tropical Medicine and Hygiene* 72(5), 477–491

[27] Ferguson DJP, Balaban AE, Patzewitz EM, Wall RJ, Hopp CS *et al.* (2014) The repeat region of the circumsporozoite protein is critical for sporozoite formation and maturation in Plasmodium. *PLoS One* 9(12), e113923

[28] Sultan AA, Thathy V, Frevert U, Robson KJ, Crisanti A *et al.* (1997) TRAP is necessary for gliding motility and infectivity of plasmodium sporozoites. *Cell* 90(3), 511–522

[29] Klug D and Frischknecht F (2017) Motility precedes egress of malaria parasites from oocysts. *Elife* 6 doi:10.7554/eLife.19157

[30] Sterling CR, Aikawa M, and Vanderberg JP (1973) The passage of Plasmodium berghei sporozoites through the salivary glands of Anopheles stephensi: an electron microscope study. *The Journal of Parasitology* 59(4), 593–605

[31] Pimenta PF, Touray M, and Miller L (1994) The journey of malaria sporozoites in the mosquito salivary gland. *Journal of Eukaryotic Microbiology* 41(6), 608–624

[32] Sidjanski S and Vanderberg JP (1997) Delayed migration of Plasmodium sporozoites from the mosquito bite site to the blood. *American Journal of Tropical Medicine and Hygiene* 57(4), 426–429

[33] Vanderberg JP and Frevert U (2004) Intravital microscopy demonstrating antibody-mediated immobilisation of Plasmodium berghei sporozoites injected into skin by mosquitoes. *International Journal for Parasitology* 34(9), 991–996

[34] Amino R, Thiberge S, Martin B, Celli S, Shorte S *et al.* (2006) Quantitative imaging of Plasmodium transmission from mosquito to mammal. *Nature Medicine* 12(2), 220–224

[35] Amino R, Giovannini D, Thiberge S, Gueirard P, Boisson B *et al.* (2008) Host Cell Traversal Is Important for Progression of the Malaria Parasite through the Dermis to the Liver. *Cell Host & Microbe* 3(2), 88–96

[36] Shin SC, Vanderberg JP, and Terzakis JA (1982) Direct infection of hepatocytes by sporozoites of Plasmodium berghei. *Journal of Protozoology* 29(3), 448–454

[37] Ishino T, Yano K, Chinzei Y, and Yuda M (2004) Cell-Passage Activity Is Required for the Malarial Parasite to Cross the Liver Sinusoidal Cell Layer. *PLoS Biology* 2(1), e4

[38] Pradel G (2001) Malaria sporozoites actively enter and pass through rat Kupffer cells prior to hepatocyte invasion. *Hepatology* 33(5), 1154–1165

[39] Tavares J, Formaglio P, and Thiberge S (2013) Role of host cell traversal by the malaria sporozoite during liver infection. *Journal of Experimental Medicine* 210(5), 905–915

[40] Kappe SHI, Kaiser K, and Matuschewski K (2003) The Plasmodium sporozoite journey: a rite of passage. *Trends in Parasitology* 19(3), 135–143

[41] Mota MM (2001) Migration of Plasmodium Sporozoites Through Cells Before Infection. *Science* 291(5501), 141–144

[42] White NJ (2016) Why Do Some Primate Malarias Relapse? *Trends in Parasitology* 32(12), 918–920

[43] Baer K, Klotz C, Kappe SHI, Schnieder T, and Frevert U (2007) Release of hepatic Plasmodium yoelii merozoites into the pulmonary microvasculature. *PLoS Pathogens* 3(11), e171

[44] Graewe S, Rankin KE, Lehmann C, Deschermeier C, Hecht L *et al.* (2011) Hostile takeover by Plasmodium: reorganization of parasite and host cell membranes during liver stage egress. *PLoS Pathogens* 7(9), e1002224

[45] Kaushansky A and Kappe SH (2015) Selection and refinement: the malaria parasite's infection and exploitation of host hepatocytes. *Current Opinion in Microbiology* 26, 71–78

[46] Sturm A, Amino R, van de Sand C, Regen T, Retzlaff S *et al.* (2006) Manipulation of host hepatocytes by the malaria parasite for delivery into liver sinusoids. *Science* 313(5791), 1287–1290

[47] Paul AS, Egan ES, and Duraisingh MT (2015) Host-parasite interactions that guide red blood cell invasion by malaria parasites. *Current Opinion in Hematology* 22(3), 220–226

[48] Borrmann S and Matuschewski K (2011) Targeting Plasmodium liver stages: better late than never. *Trends in Molecular Medicine* 17(9), 527–536

[49] Josling GA and Llinas M (2015) Sexual development in Plasmodium parasites: knowing when it's time to commit. *Nature reviews. Microbiology* 13(9), 573–587

[50] Francia ME and Striepen B (2014) Cell division in apicomplexan parasites. *Nature reviews. Microbiology* 12(2), 125–136

[51] Tomavo S, Slomianny C, Meissner M, and Carruthers VB (2013) Protein Trafficking through the Endosomal System Prepares Intracellular Parasites for a Home Invasion. *PLoS Pathogens* 9(10), e1003629

[52] Counihan NA, Kalanon M, Coppel RL, and de Koning-Ward TF (2013) Plasmodium rhoptry proteins: why order is important. *Trends in Parasitology* 29(5), 228–236

[53] Mercier C and Cesbron-Delauw MF (2015) Toxoplasma secretory granules: one population or more? *Trends in Parasitology* 31(2), 60–71

[54] Prado M, Eickel N, De Niz M, Heitmann A, Agop-Nersesian C *et al.* (2015) Long-term live imaging reveals cytosolic immune responses of host hepatocytes against Plasmodium infection and parasite escape mechanisms. *Autophagy* 11(9), 1561–1579

[55] Kremer K, Kamin D, Rittweger E, Wilkes J, Flammer H *et al.* (2013) An overexpression screen of Toxoplasma gondii Rab-GTPases reveals distinct transport routes to the micronemes. *PLoS Pathogens* 9(3), e1003213

[56] Zhu G, Marchewka MJ, Woods KM, Upton SJ, and Keithly JS (2000) Molecular analysis of a Type I fatty acid synthase in Cryptosporidium parvum. *Molecular and Biochemical Parasitology* 105(2), 253–260

[57] McFadden GI and Yeh E (2017) The apicoplast: now you see it, now you don't. *International Journal for Parasitology* 47(2-3), 137–144

[58] Ralph SA, van Dooren GG, Waller RF, Crawford MJ, Fraunholz MJ *et al.* (2004) Metabolic maps and functions of the Plasmodium falciparum apicoplast. *Nature reviews. Microbiology* 2(3), 203–216

[59] Suplick K, Akella R, Saul A, and Vaidya AB (1988) Molecular cloning and partial sequence of a 5.8 kilobase pair repetitive DNA from Plasmodium falciparum. *Molecular and Biochemical Parasitology* 30(3), 289–290

[60] Feagin JE (1992) The 6-kb element of Plasmodium falciparum encodes mitochondrial cytochrome genes. *Molecular and Biochemical Parasitology* 52(1), 145–148

[61] Lemgruber L and Lupetti P (2012) Crystalloid body, refractile body and virus-like particles in Apicomplexa: what is in there? *Parasitology* 139(3), 285–293

[62] Dessens JT, Saeed S, Tremp AZ, and Carter V (2011) Malaria crystalloids: specialized-structures for parasite transmission? *Trends in Parasitology* 27(3), 106–110

[63] World Health Organization (2016) *World malaria report 2016.* Geneva: WHO

[64] Millar SB and Cox-Singh J (2015) Human infections with Plasmodium knowlesi–zoonotic malaria. *Clinical Microbiology and Infection* 21(7), 640–648

[65] Smith JD, Rowe JA, Higgins MK, and Lavstsen T (2013) Malaria's deadly grip: cytoadhesion of Plasmodium falciparum-infected erythrocytes. *Cellular Microbiology* 15(12), 1976–1983

[66] Wassmer SC, Taylor TE, Rathod PK, Mishra SK, Mohanty S *et al.* (2015) Investigating the Pathogenesis of Severe Malaria: A Multidisciplinary and Cross-Geographical Approach. *American Journal of Tropical Medicine and Hygiene* 93(3 Suppl), 42–56

[67] Langhorne J, Ndungu FM, Sponaas AM, and Marsh K (2008) Immunity to malaria: more questions than answers. *Nature Immunology* 9(7), 725–732

[68] Osier FHA, Fegan G, Polley SD, Murungi L, Verra F *et al.* (2008) Breadth and magnitude of antibody responses to multiple Plasmodium falciparum merozoite antigens are associated with protection from clinical malaria. *Infection and Immunity* 76(5), 2240–2248

[69] Orjih AU and Nussenzweig RS (1979) Plasmodium berghei: suppression of antibody response to sporozoite stage by acute blood stage infection. *Clinical and Experimental Immunology* 38(1), 1–8

[70] Orjih AU, Cochrane AH, and Nussenzweig RS (1982) Comparative studies on the immunogenicity of infective and attenuated sporozoites of Plasmodium berghei. *Transactions of The Royal Society of Tropical Medicine and Hygiene* 76(1), 57–61

[71] Ocana-Morgner C, Mota MM, and Rodriguez A (2003) Malaria blood stage suppression of liver stage immunity by dendritic cells. *Journal of Experimental Medicine* 197(2), 143–151

[72] Butler NS, Vaughan AM, Harty JT, and Kappe SH (2012) Whole parasite vaccination approaches for prevention of malaria infection. *Trends in Immunology* 33(5), 247–254

[73] Illingworth J, Butler NS, Roetynck S, Mwacharo J, Pierce SK *et al.* (2013) Chronic exposure to Plasmodium falciparum is associated with phenotypic evidence of B and T cell exhaustion. *Journal of Immunology* 190(3), 1038–1047

[74] Keitany GJ, Kim KS, Krishnamurty AT, Hondowicz BD, Hahn WO *et al.* (2016) Blood Stage Malaria Disrupts Humoral Immunity to the Pre-erythrocytic Stage Circumsporozoite Protein. *Cell Reports* 17(12), 3193–3205

[75] Ryg-Cornejo V, Ioannidis LJ, Ly A, Chiu CY, Tellier J *et al.* (2016) Severe Malaria Infections Impair Germinal Center Responses by Inhibiting T Follicular Helper Cell Differentiation. *Cell Reports* 14(1), 68–81

[76] Ting LM, Gissot M, Coppi A, Sinnis P, and Kim K (2008) Attenuated Plasmodium yoelii lacking purine nucleoside phosphorylase confer protective immunity. *Nature Medicine* 14(9), 954–958

[77] Demarta-Gatsi C, Smith L, Thiberge S, Peronet R, Commere PH *et al.* (2016) Protection against malaria in mice is induced by blood stage-arresting histamine-releasing factor (HRF)-deficient parasites. *Journal of Experimental Medicine* 213(8), 1419–1428

[78] Raja AI, Cai Y, Reiman JM, Groves P, Chakravarty S *et al.* (2016) Chemically Attenuated Blood-Stage Plasmodium yoelii Parasites Induce Long-Lived and Strain-Transcending Protection. *Infection and Immunity* 84(8), 2274–2288

[79] De SL, Stanisic DI, van Breda K, Bellete B, Harris I *et al.* (2016) Persistence and immunogenicity of chemically attenuated blood stage Plasmodium falciparum in Aotus monkeys. *International Journal for Parasitology* 46(9), 581–591

[80] Doolan DL and Hoffman SL (2000) The complexity of protective immunity against liver-stage malaria. *Journal of Immunology* 165(3), 1453–1462

[81] Schmidt NW, Butler NS, and Harty JT (2011) Plasmodium-host interactions directly influence the threshold of memory CD8 T cells required for protective immunity. *Journal of Immunology* 186(10), 5873–5884

[82] Nussenzweig RS, Vanderberg J, Most H, and Orton C (1967) Protective immunity produced by the injection of x-irradiated sporozoites of plasmodium berghei. *Nature* 216(5111), 160–162

[83] Labaied M, Harupa A, Dumpit RF, Coppens I, Mikolajczak SA *et al.* (2007) Plasmodium yoelii Sporozoites with Simultaneous Deletion of P52 and P36 Are Completely Attenuated and Confer Sterile Immunity against Infection. *Infection and Immunity* 75(8), 3758–3768

[84] Borrmann S and Matuschewski K (2011) Protective immunity against malaria by 'natural immunization': a question of dose, parasite diversity, or both? *Current Opinion in Immunology* 23(4), 500–508

[85] Silvie O, Semblat JP, Franetich JF, Hannoun L, Eling W *et al.* (2002) Effects of irradiation on Plasmodium falciparum sporozoite hepatic development: implications for the design of pre-erythrocytic malaria vaccines. *Parasite Immunology* 24(4), 221–223

[86] Byrne M, Wray J, Reinert B, Wu Y, Nickoloff J *et al.* (2014) Mechanisms of oncogenic chromosomal translocations. *Annals of the New York Academy of Sciences* 1310, 89–97

[87] Lobrich M, Rydberg B, and Cooper PK (1995) Repair of x-ray-induced DNA double-strand breaks in specific Not I restriction fragments in human fibroblasts: joining of correct and incorrect ends. *Proceedings of the National Academy of Sciences of the United States of America* 92(26), 12050–12054

[88] Singer M and Frischknecht F (2016) Time for Genome Editing: Next-Generation Attenuated Malaria Parasites. *Trends in Parasitology* 33(3), 202–213

[89] Gomes-Santos CS, Braks J, Prudencio M, Carret C, Gomes AR *et al.* (2011) Transition of Plasmodium sporozoites into liver stage-like forms is regulated by the RNA binding protein Pumilio. *PLoS Pathogens* 7(5), e1002046

[90] Seder RA, Chang LJ, Enama ME, Zephir KL, Sarwar UN *et al.* (2013) Protection against malaria by intravenous immunization with a nonreplicating sporozoite vaccine. *Science* 341(6152), 1359–1365

[91] Hoffman SL, Goh LML, Luke TC, Schneider I, Le TP *et al.* (2002) Protection of humans against malaria by immunization with radiation-attenuated Plasmodium falciparum sporozoites. *Journal of Infectious Diseases* 185(8), 1155–1164

[92] Tarun AS, Dumpit RF, Camargo N, Labaied M, Liu P *et al.* (2007) Protracted sterile protection with Plasmodium yoelii pre-erythrocytic genetically attenuated parasite malaria vaccines is independent of significant liver-stage persistence and is mediated by CD8+ T cells. *Journal of Infectious Diseases* 196(4), 608–616

[93] Schmidt NW, Podyminogin RL, Butler NS, Badovinac VP, Tucker BJ *et al.* (2008) Memory CD8 T cell responses exceeding a large but definable threshold provide long-term immunity to malaria. *Proceedings of the National Academy of Sciences of the United States of America* 105(37), 14017–14022

[94] Schmidt NW, Butler NS, Badovinac VP, and Harty JT (2010) Extreme CD8 T cell requirements for anti-malarial liver-stage immunity following immunization with radiation attenuated sporozoites. *PLoS Pathogens* 6(7), e1000998

[95] Jobe O, Lumsden J, Mueller AK, Williams J, Silva-Rivera H *et al.* (2007) Genetically attenuated Plasmodium berghei liver stages induce sterile protracted protection that is mediated by major histocompatibility complex Class I-dependent interferon-gamma-producing CD8+ T cells. *Journal of Infectious Diseases* 196(4), 599–607

[96] Beaudoin RL, Strome CP, Mitchell F, and Tubergen TA (1977) Plasmodium berghei: immunization of mice against the ANKA strain using the unaltered sporozoite as an antigen. *Experimental Parasitology* 42(1), 1–5

[97] Belnoue E, Costa FT, Frankenberg T, Vigario AM, Voza T *et al.* (2004) Protective T cell immunity against malaria liver stage after vaccination with live sporozoites under chloroquine treatment. *Journal of Immunology* 172(4), 2487–2495

[98] Friesen J and Matuschewski K (2011) Comparative efficacy of pre-erythrocytic whole organism vaccine strategies against the malaria parasite. *Vaccine* 29(40), 7002–7008

[99] Friesen J, Silvie O, Putrianti ED, Hafalla JC, Matuschewski K *et al.* (2010) Natural immunization against malaria: causal prophylaxis with antibiotics. *Science Translational Medicine* 2(40), 40ra49

[100] Roestenberg M, McCall M, Hopman J, Wiersma J, Luty AJ *et al.* (2009) Protection against a malaria challenge by sporozoite inoculation. *New England Journal of Medicine* 361(5), 468–477

[101] Pfeil J, Sepp KJ, Heiss K, Meister M, Mueller AK *et al.* (2014) Protection against malaria by immunization with non-attenuated sporozoites under single-dose piperaquine-tetraphosphate chemoprophylaxis. *Vaccine* 32(45), 6005–6011

[102] Thieleke-Matos C, Lopes da Silva M, Cabrita-Santos L, Portal MD, Rodrigues IP *et al.* (2016) Host cell autophagy contributes to Plasmodium liver development. *Cellular Microbiology* 18(3), 437–450

[103] Gomes-Santos CSS, Itoe MA, Afonso C, Henriques R, Gardner R *et al.* (2012) Highly Dynamic Host Actin Reorganization around Developing Plasmodium Inside Hepatocytes. *PLoS One* 7(1), e29408

[104] Leirião P, Mota MM, and Rodriguez A (2005) Apoptotic Plasmodium-infected hepatocytes provide antigens to liver dendritic cells. *Journal of Infectious Diseases* 191(10), 1576–1581

[105] van de Sand C, Horstmann S, Schmidt A, Sturm A, Bolte S *et al.* (2005) The liver stage of Plasmodium berghei inhibits host cell apoptosis. *Molecular Microbiology* 58(3), 731–742

[106] Pichugin A, Steers N, De La Vega P, Zarling S, Chalom I *et al.* (2016) TAP-mediated processing of exoerythrocytic antigens is essential for protection induced with radiation-attenuated Plasmodium sporozoites. *European Journal of Immunology* 46(4), 885–896

[107] Doll KL, Pewe LL, Kurup SP, and Harty JT (2016) Discriminating Protective from Non-protective Plasmodium-Specific CD8+ T Cell Responses. *Journal of Immunology* 196(10), 4253–4262

[108] Gruner AC, Mauduit M, Tewari R, Romero JF, Depinay N *et al.* (2007) Sterile protection against malaria is independent of immune responses to the circumsporozoite protein. *PLoS One* 2(12), e1371

[109] Longley RJ, Salman AM, Cottingham MG, Ewer K, Janse CJ *et al.* (2015) Comparative assessment of vaccine vectors encoding ten malaria antigens identifies two protective liver-stage candidates. *Scientific Reports* 5, 11820

[110] McMurtrey C, Trolle T, Sansom T, Remesh SG, Kaever T *et al.* (2016) Toxoplasma gondii peptide ligands open the gate of the HLA class I binding groove. *Elife* 5, e12556

[111] Mueller AK, Labaied M, Kappe SH, and Matuschewski K (2005) Genetically modified Plasmodium parasites as a protective experimental malaria vaccine. *Nature* 433(7022), 164–167

[112] Mueller AK, Camargo N, Kaiser K, Andorfer C, Frevert U *et al.* (2005) Plasmodium liver stage developmental arrest by depletion of a protein at the parasite-host interface. *Proceedings of the National Academy of Sciences of the United States of America* 102(8), 3022–3027

[113] van Dijk MR, Douradinha B, Franke-Fayard B, Heussler V, van Dooren MW *et al.* (2005) Genetically attenuated, P36p-deficient malarial sporozoites induce protective immunity and apoptosis of infected liver cells. *Proceedings of the National Academy of Sciences of the United States of America* 102(34), 12194–12199

[114] Silvie O, Goetz K, and Matuschewski K (2008) A Sporozoite Asparagine-Rich Protein Controls Initiation of Plasmodium Liver Stage Development. *PLoS Pathogens* 4(6), e1000086

[115] Orito Y, Ishino T, Iwanaga S, Kaneko I, Kato T *et al.* (2013) Liver-specific protein 2: a Plasmodium protein exported to the hepatocyte cytoplasm and required for merozoite formation. *Molecular Microbiology* 87(1), 66–79

[116] Keitany GJ, Sack B, Smithers H, Chen L, Jang IK *et al.* (2014) Immunization of Mice with Live-Attenuated Late Liver Stage-Arresting Plasmodium yoelii Parasites Generates Protective Antibody Responses to Preerythrocytic Stages of Malaria. *Infection and Immunity* 82(12), 5143–5153

[117] Butler NS, Schmidt NW, Vaughan AM, Aly AS, Kappe SHI *et al.* (2011) Superior Antimalarial Immunity after Vaccination with Late Liver Stage-Arresting Genetically Attenuated Parasites. *Cell Host & Microbe* 9(6), 451–462

[118] Nganou-Makamdop K and Sauerwein RW (2013) Liver or blood-stage arrest during malaria sporozoite immunization: the later the better? *Trends in Parasitology* 29(6), 304–310

[119] Kumar H, Sattler JM, Singer M, Heiss K, Reinig M *et al.* (2016) Protective efficacy and safety of liver stage attenuated malaria parasites. *Scientific Reports* 6, 26824

[120] Bessho K, Iwasa Y, and Day T (2015) The evolutionary advantage of haploid versus diploid microbes in nutrient-poor environments. *Journal of Theoretical Biology* 383, 116–129

[121] Otto SP and Gerstein AC (2008) The evolution of haploidy and diploidy. *Current Biology* 18(24), R1121–R1124

[122] Vaidya AB and Arasu P (1987) Tandemly arranged gene clusters of malarial parasites that are highly conserved and transcribed. *Molecular and Biochemical Parasitology* 22(2-3), 249–257

[123] Wilson RJ and Williamson DH (1997) Extrachromosomal DNA in the Apicomplexa. *Microbiology and Molecular Biology Reviews* 61(1), 1–16

[124] Gardner MJ, Hall N, Fung E, White O, Berriman M *et al.* (2002) Genome sequence of the human malaria parasite Plasmodium falciparum. *Nature* 419(6906), 498–511

[125] Auburn S, Böhme U, Steinbiss S, Trimarsanto H, Hostetler J *et al.* (2016) A new Plasmodium vivax reference sequence with improved assembly of the subtelomeres reveals an abundance of pir genes. *Wellcome Open Research* 1, 4

[126] Rutledge GG, Böhme U, Sanders M, Reid AJ, Cotton JA *et al.* (2017) Plasmodium malariae and P. ovale genomes provide insights into malaria parasite evolution. *Nature* 542(7639), 101–104

[127] Boehme U, Otto TD, Cotton J, Steinbiss S, and Sanders M (2016) Complete avian malaria parasite genomes reveal host-specific parasite evolution in birds and mammals. *bioRxiv* doi:10.1101-086504

[128] Otto TD, Böhme U, Jackson AP, Hunt M, Franke-Fayard B *et al.* (2014) A comprehensive evaluation of rodent malaria parasite genomes and gene expression. *BMC Biology* 12, 86

[129] DeBarry JD and Kissinger JC (2011) Jumbled genomes: missing Apicomplexan synteny. *Molecular Biology and Evolution* 28(10), 2855–2871

[130] Haltiwanger BM, Matsumoto Y, Nicolas E, Dianov GL, Bohr VA *et al.* (2000) DNA base excision repair in human malaria parasites is predominantly by a long-patch pathway. *Biochemistry* 39(4), 763–772

[131] Szafranski K, Lehmann R, Parra G, Guigo R, and Glöckner G (2005) Gene organization features in A/T-rich organisms. *Journal of Molecular Evolution* 60(1), 90–98

[132] Yadav MK and Swati D (2012) Comparative genome analysis of six malarial parasites using codon usage bias based tools. *Bioinformation* 8(24), 1230–1239

[133] Balaji S, Babu MM, Iyer LM, and Aravind L (2005) Discovery of the principal specific transcription factors of Apicomplexa and their implication for the evolution of the AP2-integrase DNA binding domains. *Nucleic Acids Research* 33(13), 3994–4006

[134] Modrzynska K, Pfander C, Chappell L, Yu L, Suarez C *et al.* (2017) A Knockout Screen of ApiAP2 Genes Reveals Networks of Interacting Transcriptional Regulators Controlling the Plasmodium Life Cycle. *Cell Host & Microbe* 21(1), 11–22

[135] Adjalley SH, Chabbert CD, Klaus B, Pelechano V, and Steinmetz LM (2016) Landscape and Dynamics of Transcription Initiation in the Malaria Parasite Plasmodium falciparum. *Cell Reports* 14(10), 2463–2475

[136] Zhu L, Mok S, Imwong M, Jaidee A, Russell B *et al.* (2016) New insights into the Plasmodium vivax transcriptome using RNA-Seq. *Scientific Reports* 6, 20498

[137] Yamauchi K (1991) The sequence flanking translational initiation site in protozoa. *Nucleic Acids Research* 19(10), 2715–2720

[138] Guizetti J and Scherf A (2013) Silence, activate, poise and switch! Mechanisms of antigenic variation in Plasmodium falciparum. *Cellular Microbiology* 15(5), 718–726

[139] Sfeir A and Symington LS (2015) Microhomology-Mediated End Joining: A Back-up Survival Mechanism or Dedicated Pathway? *Trends in Biochemical Sciences* 40(11), 701–714

[140] Paquet F, Boudvillain M, Lancelot G, and Leng M (1999) NMR solution structure of a DNA dodecamer containing a transplatin interstrand GN7-CN3 cross-link. *Nucleic Acids Research* 27(21), 4261–4268

[141] Kunkel TA and Erie DA (2005) DNA MISMATCH REPAIR. *Annual Review of Biochemistry* 74(1), 681–710

[142] Spampinato CP (2017) Protecting DNA from errors and damage: an overview of DNA repair mechanisms in plants compared to mammals. *Cellular and Molecular Life Sciences* 74(9), 1693–1709

[143] Mimitou EP and Symington LS (2011) DNA end resection - unraveling the tail. *DNA Repair* 10(3), 344–348

[144] Lee AH, Symington LS, and Fidock DA (2014) DNA Repair Mechanisms and Their Biological Roles in the Malaria Parasite Plasmodium falciparum. *Microbiology and Molecular Biology Reviews* 78(3), 469–486

[145] Fox BA, Ristuccia JG, Gigley JP, and Bzik DJ (2009) Efficient Gene Replacements in Toxoplasma gondii Strains Deficient for Nonhomologous End Joining. *Eukaryotic Cell* 8(4), 520–529

[146] Straimer J, Lee MCS, Lee AH, Zeitler B, Williams AE *et al.* (2012) Site-specific genome editing in Plasmodium falciparum using engineered zinc-finger nucleases. *Nature Methods* 9(10), 993–998

[147] Frit P, Barboule N, Yuan Y, Gomez D, and Calsou P (2014) Alternative end-joining pathway(s): Bricolage at DNA breaks. *DNA Repair* 17, 81–97

[148] Deriano L and Roth DB (2013) Modernizing the Nonhomologous End-Joining Repertoire: Alternative and Classical NHEJ Share the Stage. *Annual Review of Genetics* 47(1), 433–455

[149] Ceccaldi R, Liu JC, Amunugama R, Hajdu I, Primack B *et al.* (2015) Homologous-recombination-deficient tumours are dependent on Polθ-mediated repair. *Nature* 518(7538), 258–262

[150] Sharma S, Javadekar SM, Pandey M, Srivastava M, Kumari R *et al.* (2015) Homology and enzymatic requirements of microhomology-dependent alternative end joining. *Cell Death & Disease* 6(3), e1697–12

[151] Kirkman LA, Lawrence EA, and Deitsch KW (2013) Malaria parasites utilize both homologous recombination and alternative end joining pathways to maintain genome integrity. *Nucleic Acids Research* 42(1), 370–379

[152] Peng D, Kurup SP, Yao PY, Minning TA, and Tarleton RL (2014) CRISPR-Cas9-Mediated Single-Gene and Gene Family Disruption in Trypanosoma cruzi. *MBio* 6(1), e02097–14

[153] Ganter M, Goldberg JM, Dvorin JD, Paulo JA, King JG *et al.* (2017) Plasmodium falciparum CRK4 directs continuous rounds of DNA replication during schizogony. *Nature Microbiology* 2, 17017

[154] Francia ME, Dubremetz JF, and Morrissette NS (2016) Basal body structure and composition in the apicomplexans Toxoplasma and Plasmodium. *Cilia* 5:3 doi:10.1186/s13630-016-0025-5

[155] Mlambo G, Coppens I, and Kumar N (2012) Aberrant Sporogonic Development of Dmc1 (a Meiotic Recombinase) Deficient Plasmodium berghei Parasites. *PLoS One* 7(12), e52480

[156] Jiang H, Li N, and Gopalan V (2011) High recombination rates and hotspots in a Plasmodium falciparum genetic cross. *Genome Biology* 12(4), R33

[157] Spence PJ, Jarra W, Lévy P, Reid AJ, Chappell L *et al.* (2013) Vector transmission regulates immune control of Plasmodium virulence. *Nature* 498(7453), 228–231

[158] Yam XY, Brugat T, Siau A, Lawton J, Wong DS *et al.* (2016) Characterization of the Plasmodium Interspersed Repeats (PIR) proteins of Plasmodium chabaudi indicates functional diversity. *Scientific Reports* 6, 23449

[159] Taylor HM, Kyes SA, and Newbold CI (2000) Var gene diversity in Plasmodium falciparum is generated by frequent recombination events. *Molecular and Biochemical Parasitology* 110(2), 391–397

[160] Rosenberg R, Rungsiwongse J, Kangsadalampai S, Sattabongkot J, Suwanabun N *et al.* (1992) Random mating of natural Plasmodium populations demonstrated from individual oocysts. *Molecular and Biochemical Parasitology* 53(1-2), 129–133

[161] Nair S, Nash D, Sudimack D, Jaidee A, Barends M *et al.* (2007) Recurrent gene amplification and soft selective sweeps during evolution of multidrug resistance in malaria parasites. *Molecular Biology and Evolution* 24(2), 562–573

[162] Guler JL, Freeman DL, Ahyong V, Patrapuvich R, White J *et al.* (2013) Asexual Populations of the Human Malaria Parasite, Plasmodium falciparum, Use a Two-Step Genomic Strategy to Acquire Accurate, Beneficial DNA Amplifications. *PLoS Pathogens* 9(5), e1003375

[163] Tan JC, Tan A, Checkley L, Honsa CM, and Ferdig MT (2010) Variable numbers of tandem repeats in Plasmodium falciparum genes. *Journal of Molecular Evolution* 71(4), 268–278

[164] Hughes AL (2004) The Evolution of Amino Acid Repeat Arrays in Plasmodium and Other Organisms. *Journal of Molecular Evolution* 59(4), 528–535

[165] Janse CJ, Franke-Fayard B, Mair GR, Ramesar J, Thiel C *et al.* (2006) High efficiency transfection of Plasmodium berghei facilitates novel selection procedures. *Molecular and Biochemical Parasitology* 145(1), 60–70

[166] Crabb BS, Rug M, Gilberger TW, Thompson JK, Triglia T *et al.* (2004) Transfection of the human malaria parasite Plasmodium falciparum. *Methods in Molecular Biology* 270, 263–276

[167] Balu B and Adams JH (2007) Advancements in transfection technologies for Plasmodium. *International Journal for Parasitology* 37(1), 1–10

[168] de Koning-Ward TF, Gilson PR, and Crabb BS (2015) Advances in molecular genetic systems in malaria. *Nature reviews. Microbiology* 13(6), 373–387

[169] Boyle MJ, Wilson DW, and Beeson JG (2013) New approaches to studying Plasmodium falciparum merozoite invasion and insights into invasion biology. *International Journal for Parasitology* 43(1), 1–10

[170] Ghorbal M, Gorman M, Macpherson CR, Martins RM, Scherf A *et al.* (2014) Genome editing in the human malaria parasite Plasmodium falciparum using the CRISPR-Cas9 system. *Nature Biotechnology* 32(8), 819–821

[171] Wagner JC, Platt RJ, Goldfless SJ, Zhang F, and Niles JC (2014) efficient CRISPR-CAS9-mediated genome editing in. *Nature Methods* 11(9), 915–918

[172] Zhang C, Xiao B, Jiang Y, Zhao Y, Li Z *et al.* (2014) Efficient Editing of Malaria Parasite Genome Using the CRISPR/Cas9 System. *MBio* 5(4), e01414–14–e01414–14

[173] Sidik SM, Hackett CG, Tran F, Westwood NJ, and Lourido S (2014) Efficient Genome Engineering of Toxoplasma gondii Using CRISPR/Cas9. *PLoS One* 9(6), e100450

[174] van Dijk MR, Waters AP, and Janse CJ (1995) Stable transfection of malaria parasite blood stages. *Science* 268(5215), 1358–1362

[175] Mutungi JK, Yahata K, Sakaguchi M, and Kaneko O (2015) Isolation of invasive Plasmodium yoelii merozoites with a long half-life to evaluate invasion dynamics and potential invasion inhibitors. *Molecular and Biochemical Parasitology* 204(1), 26–33

[176] Ishizaki T, Sivakumar T, Hayashida K, Tuvshintulga B, Igarashi I *et al.* (2016) RBC invasion and invasion-inhibition assays using free merozoites isolated after cold treatment of Babesia bovis in vitro culture. *Experimental Parasitology* 166, 10–15

[177] Hasenkamp S, Merrick CJ, and Horrocks P (2013) A quantitative analysis of Plasmodium falciparum transfection using DNA-loaded erythrocytes. *Molecular and Biochemical Parasitology* 187(2), 117–120

[178] O'Donnell RA, Preiser PR, Williamson DH, Moore PW, Cowman AF *et al.* (2001) An alteration in concatameric structure is associated with efficient segregation of plasmids in transfected Plasmodium falciparum parasites. *Nucleic Acids Research* 29(3), 716–724

[179] Epp C, Raskolnikov D, and Deitsch KW (2008) A regulatable transgene expression system for cultured Plasmodium falciparum parasites. *Malaria Journal* 7, 86

[180] Iwanaga S, Kato T, Kaneko I, and Yuda M (2012) Centromere Plasmid: A New Genetic Tool for the Study of Plasmodium falciparum. *PLoS One* 7(3), e33326

[181] Pfander C, Anar B, Schwach F, Otto TD, Brochet M *et al.* (2011) A scalable pipeline for highly effective genetic modification of a malaria parasite. *Nature Methods* 8(12), 1078–1082

[182] Wah DA, Hirsch JA, Dorner LF, Schildkraut I, and Aggarwal AK (1997) Structure of the multimodular endonuclease FokI bound to DNA. *Nature* 388(6637), 97–100

[183] Durai S, Mani M, Kandavelou K, Wu J, Porteus MH *et al.* (2005) Zinc finger nucleases: custom-designed molecular scissors for genome engineering of plant and mammalian cells. *Nucleic Acids Research* 33(18), 5978–5990

[184] Miller JC, Holmes MC, Wang J, Guschin DY, Lee YL *et al.* (2007) An improved zinc-finger nuclease architecture for highly specific genome editing. *Nature Biotechnology* 25(7), 778–785

[185] Marraffini LA and Sontheimer EJ (2010) CRISPR interference: RNA-directed adaptive immunity in bacteria and archaea. *Nature reviews. Genetics* 11(3), 181–190

[186] Sidik SM, Huet D, Ganesan SM, Huynh MH, Wang T *et al.* (2016) A Genome-wide CRISPR Screen in Toxoplasma Identifies Essential Apicomplexan Genes. *Cell* 166(6), 1423–1435–e12.

[187] Hammond A, Galizi R, Kyrou K, Simoni A, Siniscalchi C *et al.* (2016) A CRISPR-Cas9 gene drive system targeting female reproduction in the malaria mosquito vector Anopheles gambiae. *Nature Biotechnology* 34(1), 78–83

[188] Gantz VM, Jasinskiene N, Tatarenkova O, Fazekas A, Macias VM *et al.* (2015) Highly efficient Cas9-mediated gene drive for population modification of the malaria vector mosquito Anopheles stephensi. *Proceedings of the National Academy of Sciences of the United States of America* 112(49), E6736–43

[189] Christian M, Cermak T, Doyle EL, Schmidt C, Zhang F *et al.* (2010) Targeting DNA double-strand breaks with TAL effector nucleases. *Genetics* 186(2), 757–761

[190] Boch J (2011) TALEs of genome targeting. *Nature Biotechnology* 29(2), 135–136

[191] Boch J, Scholze H, Schornack S, Landgraf A, Hahn S *et al.* (2009) Breaking the code of DNA binding specificity of TAL-type III effectors. *Science* 326(5959), 1509–1512

[192] Abremski K and Hoess R (1984) Bacteriophage P1 site-specific recombination. Purification and properties of the Cre recombinase protein. *Journal of Biological Chemistry* 259(3), 1509–1514

[193] Brecht S, Erdhart H, Soete M, and Soldati D (1999) Genome engineering of Toxoplasma gondii using the site-specific recombinase Cre. *Gene* 234(2), 239–247

[194] Jullien N, Sampieri F, and Enjalbert A (2003) Regulation of Cre recombinase by ligand-induced complementation of inactive fragments. *Nucleic Acids Research* 31(21), e131

[195] Andenmatten N, Egarter S, Jackson AJ, Jullien N, Herman JP *et al.* (2013) Conditional genome engineering in Toxoplasma gondii uncovers alternative invasion mechanisms. *Nature Methods* 10(2), 125–127

[196] Collins CR, Das S, Wong EH, Andenmatten N, Stallmach R *et al.* (2013) Robust inducible Cre recombinase activity in the human malaria parasite Plasmodium falciparum enables efficient gene deletion within a single asexual erythrocytic growth cycle. *Molecular Microbiology* 88(4), 687–701

[197] Jones ML, Das S, Belda H, Collins CR, Blackman MJ *et al.* (2016) A versatile strategy for rapid conditional genome engineering using loxP sites in a small synthetic intron in Plasmodium falciparum. *Scientific Reports* 6, 21800

[198] Zhu XD and Sadowski PD (1995) Cleavage-dependent ligation by the FLP recombinase. Characterization of a mutant FLP protein with an alteration in a catalytic amino acid. *Journal of Biological Chemistry* 270(39), 23044–23054

[199] Carvalho TG, Thiberge S, Sakamoto H, and Ménard R (2004) Conditional mutagenesis using site-specific recombination in Plasmodium berghei. *Proceedings of the National Academy of Sciences of the United States of America* 101(41), 14931–14936

[200] Combe A, Giovannini D, Carvalho TG, Spath S, Boisson B *et al.* (2009) Clonal Conditional Mutagenesis in Malaria Parasites. *Cell Host & Microbe* 5(4), 386–396

[201] Lacroix C, Giovannini D, Combe A, Bargieri DY, Spath S *et al.* (2011) FLP/FRT-mediated conditional mutagenesis in pre-erythrocytic stages of Plasmodium berghei. *Nature Protocols* 6(9), 1412–1428

[202] Kalanon M, Bargieri D, Sturm A, Matthews K, Ghosh S *et al.* (2016) The Plasmodium translocon of exported proteins component EXP2 is critical for establishing a patent malaria infection in mice. *Cellular Microbiology* 18(3), 399–412

[203] Janse CJ, Ramesar J, and Waters AP (2006) High-efficiency transfection and drug selection of genetically transformed blood stages of the rodent malaria parasite Plasmodium berghei. *Nature Protocols* 1(1), 346–356

[204] Stechmann A and Cavalier-Smith T (2002) Rooting the eukaryote tree by using a derived gene fusion. *Science* 297(5578), 89–91

[205] Clyde DF and Shute GT (1954) Resistance of East African varieties of Plasmodium falciparum to pyrimethamine. *Transactions of The Royal Society of Tropical Medicine and Hygiene* 48(6), 495–500

[206] de Koning-Ward TF, Fidock DA, Thathy V, Menard R, van Spaendonk RM *et al.* (2000) The selectable marker human dihydrofolate reductase enables sequential genetic manipulation of the Plasmodium berghei genome. *Molecular and Biochemical Parasitology* 106(2), 199–212

[207] Zhang K (2002) Divergent Regulation of Dihydrofolate Reductase Between Malaria Parasite and Human Host. *Science* 296(5567), 545–547

[208] Orr RY, Philip N, and Waters AP (2012) Improved negative selection protocol for Plasmodium berghei in the rodent malarial model. *Malaria Journal* 11(1), 103

[209] Lin JW, Annoura T, Sajid M, Chevalley-Maurel S, Ramesar J *et al.* (2011) A novel 'gene insertion/marker out' (GIMO) method for transgene expression and gene complementation in rodent malaria parasites. *PLoS One* 6(12), e29289

[210] Janse CJ, Franke-Fayard B, and Waters AP (2006) Selection by flow-sorting of genetically transformed, GFP-expressing blood stages of the rodent malaria parasite, Plasmodium berghei. *Nature Protocols* 1(2), 614–623

[211] Kenthirapalan S, Waters AP, Matuschewski K, and Kooij TW (2016) Functional profiles of orphan membrane transporters in the life cycle of the malaria parasite. *Nature Communications* 7, 10519

[212] Kudryashev M, Münter S, Lemgruber L, Montagna G, Stahlberg H *et al.* (2012) Structural basis for chirality and directional motility of Plasmodium sporozoites. *Cellular Microbiology* 14(11), 1757–1768

[213] Zhang M, Mishra S, Sakthivel R, Fontoura BM, and Nussenzweig V (2016) UIS2: A Unique Phosphatase Required for the Development of Plasmodium Liver Stages. *PLoS Pathogens* 12(1), e1005370

[214] Coppi A, Natarajan R, Pradel G, Bennett BL, James ER *et al.* (2011) The malaria circumsporozoite protein has two functional domains, each with distinct roles as sporozoites journey from mosquito to mammalian host. *Journal of Experimental Medicine* 208(2), 341–356

[215] Ejigiri I, Ragheb DRT, Pino P, Coppi A, Bennett BL *et al.* (2012) Shedding of TRAP by a rhomboid protease from the malaria sporozoite surface is essential for gliding motility and sporozoite infectivity. *PLoS Pathogens* 8(7), e1002725

[216] Hegge S, Munter S, Steinbuchel M, Heiss K, Engel U *et al.* (2010) Multistep adhesion of Plasmodium sporozoites. *FASEB Journal* 24(7), 2222–2234

[217] Steinbuechel M and Matuschewski K (2009) Role for the Plasmodiumsporozoite-specific transmembrane protein S6 in parasite motility and efficient malaria transmission. *Cellular Microbiology* 11(2), 279–288

[218] Ploemen IH, Chakravarty S, van Gemert GJJ, Annoura T, Khan SM *et al.* (2013) Plasmodium liver load following parenteral sporozoite administration in rodents. *Vaccine* 31(34), 3410–3416

[219] Mishra S, Nussenzweig RS, and Nussenzweig V (2012) Journal of Immunological Methods. *Journal of Immunological Methods* 377(1-2), 47–52

[220] Sato Y, Montagna GN, and Matuschewski K (2014) Plasmodium berghei sporozoites acquire virulence and immunogenicity during mosquito hemocoel transit. *Infection and Immunity* 82(3), 1164–1172

[221] Vanderberg J, Rdodin J, and Yoeli M (1967) Electron microscopic and histochemical studies of sporozoite formation in Plasmodium berghei. *Journal of Eukaryotic Microbiology* 14(1), 82–103

[222] Kudryashev M, Lepper S, Stanway R, Bohn S, Baumeister W *et al.* (2010) Positioning of large organelles by a membrane- associated cytoskeleton in Plasmodium sporozoites. *Cellular Microbiology* 12(3), 362–371

[223] Frischknecht F, Baldacci P, Martin B, Zimmer C, Thiberge S *et al.* (2004) Imaging movement of malaria parasites during transmission by Anopheles mosquitoes. *Cellular Microbiology* 6(7), 687–694

[224] Akaki M and Dvorak JA (2005) A chemotactic response facilitates mosquito salivary gland infection by malaria sporozoites. *Journal of Experimental Biology* 208(16), 3211–3218

[225] Battista A, Frischknecht F, and Schwarz US (2014) Geometrical model for malaria parasite migration in structured environments. *Physical Review E* 90(4), 042720

[226] Nussenzweig V and Nussenzweig RS (1985) Circumsporozoite proteins of malaria parasites. *Cell* 42(2), 401–403

[227] Shen B and Sibley LD (2014) Toxoplasma aldolase is required for metabolism but dispensable for host-cell invasion. *Proceedings of the National Academy of Sciences of the United States of America* 111(9), 3567–3572

[228] Jacot D, Tosetti N, Pires I, Stock J, Graindorge A *et al.* (2016) An Apicomplexan Actin-Binding Protein Serves as a Connector and Lipid Sensor to Coordinate Motility and Invasion. *Cell Host & Microbe* 20(6), 731–743

[229] Heintzelman MB (2015) Gliding motility in apicomplexan parasites. *Seminars in Cell and Developmental Biology* 46, 135–142

[230] Baum J, Richard D, Healer J, Rug M, Krnajski Z *et al.* (2006) A Conserved Molecular Motor Drives Cell Invasion and Gliding Motility across Malaria Life Cycle Stages and Other Apicomplexan Parasites. *Journal of Biological Chemistry* 281(8), 5197–5208

[231] Soldati-Favre D (2008) Molecular dissection of host cell invasion by the Apicomplexans: the glideosome. *Parasite* 15(3), 197–205

[232] Jacot D, Fr nal K, Marq JB, Sharma P, and Soldati-Favre D (2014) Assessment of phosphorylation in Toxoplasma glideosome assembly and function. *Cellular Microbiology* 16(10), 1518–1532

[233] Chen AL, Kim EW, Toh JY, Vashisht AA, Rashoff AQ *et al.* (2015) Novel Components of the Toxoplasma Inner Membrane Complex Revealed by BioID. *MBio* 6(1), e02357–14

[234] Chen AL, Moon AS, Bell HN, Huang AS, Vashisht AA *et al.* (2016) Novel insights into the composition and function of the Toxoplasma IMC sutures. *Cellular Microbiology* 19(4)

[235] Lentini G, Kong-Hap M, El Hajj H, Francia M, Claudet C *et al.* (2015) Identification and characterization of Toxoplasma SIP, a conserved apicomplexan cytoskeleton protein involved in maintaining the shape, motility and virulence of the parasite. *Cellular Microbiology* 17(1), 62–78

[236] Kono M, Herrmann S, Loughran NB, Cabrera A, Engelberg K *et al.* (2012) Evolution and Architecture of the Inner Membrane Complex in Asexual and Sexual Stages of the Malaria Parasite. *Molecular Biology and Evolution* 29(9), 2113–2132

[237] Beck JR, Rodriguez-Fernandez IA, Cruz de Leon J, Huynh MH, Carruthers VB *et al.* (2010) A Novel Family of Toxoplasma IMC Proteins Displays a Hierarchical Organization and Functions in Coordinating Parasite Division. *PLoS Pathogens* 6(9), e1001094

[238] Poulin B, Patzewitz EM, Brady D, Silvie O, Wright MH *et al.* (2013) Unique apicomplexan IMC sub-compartment proteins are early markers for apical polarity in the malaria parasite. *Biology Open* 2(11), 1160–1170

[239] Gould SB, Kraft LGK, van Dooren GG, Goodman CD, Ford KL *et al.* (2011) Ciliate Pellicular Proteome Identifies Novel Protein Families with Characteristic Repeat Motifs That Are Common to Alveolates. *Molecular Biology and Evolution* 28(3), 1319–1331

[240] Al-Khattaf FS, Tremp AZ, and Dessens JT (2014) Plasmodium alveolins possess distinct but structurally and functionally related multi-repeat domains. *Parasitology Research* 114(2), 631–639

[241] Mann T and Beckers C (2001) Characterization of the subpellicular network, a filamentous membrane skeletal component in the parasite Toxoplasma gondii. *Molecular and Biochemical Parasitology* 115(2), 257–268

[242] Tremp AZ, Carter V, Saeed S, and Dessens JT (2013) Morphogenesis of Plasmodium zoites is uncoupled from tensile strength. *Molecular Microbiology* 89(3), 552–564

[243] Russell DG and Burns RG (1984) The polar ring of coccidian sporozoites: a unique microtubule-organizing centre. *Journal of Cell Science* 65(1), 193–207

[244] Cyrklaff M, Kudryashev M, Leis A, Leonard K, Baumeister W *et al.* (2007) Cryoelectron tomography reveals periodic material at the inner side of subpellicular microtubules in apicomplexan parasites. *Journal of Experimental Medicine* 204(6), 1281–1287

[245] Liu J, He Y, Benmerzouga I, Sullivan WJ, Morrissette NS *et al.* (2016) An ensemble of specifically targeted proteins stabilizes cortical microtubules in the human parasite Toxoplasma gondii. *Molecular Biology of the Cell* 27(3), 549–571

[246] Patra KP and Vinetz JM (2012) New ultrastructural analysis of the invasive apparatus of the Plasmodium ookinete. *American Journal of Tropical Medicine and Hygiene* 87(3), 412–417

[247] Schrevel J, Asfaux-Foucher G, Hopkins JM, Robert V, Bourgouin C *et al.* (2007) Vesicle trafficking during sporozoite development in Plasmodium berghei: ultrastructural evidence for a novel trafficking mechanism. *Parasitology* 135(01)

[248] Paredes-Santos TC, de Souza W, and Attias M (2012) Dynamics and 3D organization of secretory organelles of Toxoplasma gondii. *Journal of Structural Biology* 177(2), 420–430

[249] Silvie O, Briquet S, Müller K, Manzoni G, and Matuschewski K (2014) Post-transcriptional silencing of UIS4 in Plasmodium berghei sporozoites is important for host switch. *Molecular Microbiology* 91(6), 1200–1213

[250] Silva PAGC, Guerreiro A, Santos JM, Braks JAM, Janse CJ *et al.* (2016) Translational Control of UIS4 Protein of the Host-Parasite Interface Is Mediated by the RNA Binding Protein Puf2 in Plasmodium berghei Sporozoites. *PLoS One* 11(1), e0147940

[251] Hager KM, Striepen B, and Tilney LG (1999) The nuclear envelope serves as an intermediary between the ER and Golgi complex in the intracellular parasite Toxoplasma gondii. *Journal of Cell Science* 112(PT 16), 2631–2638

[252] Sinden RE and Garnham PC (1973) A comparative study on the ultrastructure of Plasmodium sporozoites within the oöcyst and salivary glands, with particular reference to the incidence of the micropore. *Transactions of The Royal Society of Tropical Medicine and Hygiene* 67(5), 631–637

[253] Beier JC (1998) Malaria parasite development in mosquitoes. *Annual Review of Entomology* 43, 519–543

[254] Dessens JT, Sidén-Kiamos I, Mendoza J, Mahairaki V, Khater E *et al.* (2003) SOAP, a novel malaria ookinete protein involved in mosquito midgut invasion and oocyst development. *Molecular Microbiology* 49(2), 319–329

[255] Tomas AM, Margos G, Dimopoulos G, van Lin LH, de Koning-Ward TF *et al.* (2001) P25 and P28 proteins of the malaria ookinete surface have multiple and partially redundant functions. *EMBO Journal* 20(15), 3975–3983

[256] Mahairaki V, Voyatzi T, Sidén-Kiamos I, and Louis C (2005) The Anopheles gambiae gamma1 laminin directly binds the Plasmodium berghei circumsporozoite- and TRAP-related protein (CTRP). *Molecular and Biochemical Parasitology* 140(1), 119–121

[257] Srinivasan P, Fujioka H, and Jacobs-Lorena M (2008) PbCap380, a novel oocyst capsule protein, is essential for malaria parasite survival in the mosquito. *Cellular Microbiology* 10(6), 1304–1312

[258] Meis JF, Hollingdale MR, Verhave JP, and Aikawa M (1984) Intranuclear localization of Plasmodium berghei sporozoites. *Cell Biology International Reports* 8(12), 1016

[259] Rono MK, Whitten MMA, Oulad-Abdelghani M, Levashina EA, and Marois E (2010) The major yolk protein vitellogenin interferes with the anti-plasmodium response in the malaria mosquito Anopheles gambiae. *PLoS Biology* 8(7), e1000434

[260] Clement AN (1992) *The biology of mosquitoes. Vol. 1 Development, nutrition and reproduction.* Chapman and Hall

[261] Attardo GM, Hansen IA, and Raikhel AS (2005) Nutritional regulation of vitellogenesis in mosquitoes: implications for anautogeny. *Insect Biochemistry and Molecular Biology* 35(7), 661–675

[262] Simonetti AB, Billingsley PF, Winger LA, and Sinden RE (1993) Kinetics of expression of two major Plasmodium berghei antigens in the mosquito vector, Anopheles stephensi. *Journal of Eukaryotic Microbiology* 40(5), 569–576

[263] Chen PH, Chang S, Wu H, and Shi YL (1984) Scanning electron microscopic observations of the oocyst, sporoblast and sporozoite of Plasmodium yoelii yoelii. *The Journal of Parasitology* 70(6), 902–906

[264] Terzakis JA, Sprinz H, and Ward RA (1967) The transformation of the Plasmodium gallinaceum oocyst in Aedes aegypti mosquitoes. *The Journal of Cell Biology* 34(1), 311–326

[265] Terzakis JA, Sprinz H, and Ward RA (1966) Sporoblast and sporozoite formation in Plasmodium gallinaceum infection of Aedes aegypti. *Military Medicine* 131(9), Suppl:984–92

[266] Wong TC and Desser SS (1976) Fine structure of oocyst transformation and the sporozoites of Leucocytozoon dubreuili. *Journal of Protozoology* 23(1), 115–126

[267] Terzakis JA (1971) Transformation of the Plasmodium cynomolgi Oocyst. *Journal of Protozoology* 18(1), 62–73

[268] Francia ME, Jordan CN, Patel JD, Sheiner L, Demerly JL *et al.* (2012) Cell division in Apicomplexan parasites is organized by a homolog of the striated rootlet fiber of algal flagella. *PLoS Biology* 10(12), e1001444

[269] Frischknecht F and Matuschewski K (2017) Plasmodium Sporozoite Biology. *Cold Spring Harbor Perspectives in Medicine* 7(5), pii: a025478.

[270] Morrissette NS and Sibley LD (2002) Cytoskeleton of Apicomplexan Parasites. *Microbiology and Molecular Biology Reviews* 66(1), 21–38

[271] Read M, Sherwin T, Holloway SP, Gull K, and Hyde JE (1993) Microtubular organization visualized by immunofluorescence microscopy during erythrocytic schizogony in Plasmodium falciparum and investigation of post-translational modifications of parasite tubulin. *Parasitology* 106(Pt 3), 223–232

[272] Meis JF, Wismans PG, Jap PH, Lensen AH, and Ponnudurai T (1992) A scanning electron microscopic study of the sporogonic development of Plasmodium falciparum in Anopheles stephensi. *Acta Tropica* 50(3), 227–236

[273] Dubey JP, Lindsay DS, and Speer CA (1998) Structures of Toxoplasma gondii tachyzoites, bradyzoites, and sporozoites and biology and development of tissue cysts. *Clinical Microbiology Reviews* 11(2), 267–299

[274] Aly ASI and Matuschewski K (2005) A malarial cysteine protease is necessary for Plasmodiumsporozoite egress from oocysts. *Journal of Experimental Medicine* 202(2), 225–230

[275] Wang Q, Fujioka H, and Nussenzweig V (2005) Exit of Plasmodium Sporozoites from Oocysts Is an Active Process That Involves the Circumsporozoite Protein. *PLoS Pathogens* 1(1), 72–79

[276] Islam ST and Mignot T (2015) The mysterious nature of bacterial surface (gliding) motility: A focal adhesion-based mechanism in Myxococcus xanthus. *Seminars in Cell and Developmental Biology* 46, 143–154

[277] Garnham P, Bird RG, and Baker JR (1967) Electron microscope studies of motile stages of malaria parasites V. Exflagellation in Plasmodium, Hepatocystis and Leucocytozoon. *Transactions of The Royal Society of Tropical Medicine and Hygiene* 61(2), 58–68

[278] Kooij TWA, Franke-Fayard B, Renz J, Kroeze H, van Dooren MW *et al.* (2005) Plasmodium berghei α-tubulin II: A role in both male gamete formation and asexual blood stages. *Molecular and Biochemical Parasitology* 144(1), 16–26

[279] Deligianni E, Morgan RN, Bertuccini L, Kooij TWA, Laforge A *et al.* (2011) Critical role for a stage-specific actin in male exflagellation of the malaria parasite. *Cellular Microbiology* 13(11), 1714–1730

[280] Valigurova A, Vaskovicova N, Musilova N, and Schrevel J (2013) The enigma of eugregarine epicytic folds: where gliding motility originates? *Frontiers in Zoology* 10(1), 57

[281] Asada M, Goto Y, Yahata K, Yokoyama N, Kawai S *et al.* (2012) Gliding motility of Babesia bovis merozoites visualized by time-lapse video microscopy. *PLoS One* 7(4), e35227

[282] Hegge S, Kudryashev M, Smith A, and Frischknecht F (2009) Automated classification of Plasmodium sporozoite movement patterns reveals a shift towards productive motility during salivary gland infection. *Biotechnology Journal* 4(6), 903–913

[283] Riglar DT, Richard D, Wilson DW, Boyle MJ, Dekiwadia C *et al.* (2011) Super-Resolution Dissection of Coordinated Events during Malaria Parasite Invasion of the Human Erythrocyte. *Cell Host & Microbe* 9(1), 9–20

[284] Vanderberg JP (1974) Studies on the motility of Plasmodium sporozoites. *Journal of Protozoology* 21(4), 527–537

[285] Münter S, Sabass B, Selhuber-Unkel C, Kudryashev M, Hegge S *et al.* (2009) Plasmodium Sporozoite Motility Is Modulated by the Turnover of Discrete Adhesion Sites. *Cell Host & Microbe* 6(6), 551–562

[286] Whitelaw JA, Latorre-Barragan F, Gras S, Pall GS, Leung JM *et al.* (2017) Surface attachment, promoted by the actomyosin system of Toxoplasma gondii is important for efficient gliding motility and invasion. *BMC Biology* 15(1), 1

[287] Egarter S, Andenmatten N, Jackson AJ, Whitelaw JA, Pall G *et al.* (2014) The Toxoplasma Acto-MyoA Motor Complex Is Important but Not Essential for Gliding Motility and Host Cell Invasion. *PLoS One* 9(3), e91819

[288] Hopp CS, Chiou K, Ragheb DRT, Salman A, Khan SM *et al.* (2015) Longitudinal analysis of Plasmodium sporozoite motility in the dermis reveals component of blood vessel recognition. *Elife* 4 doi:10.7554/eLife.07789.

[289] Bane KS, Lepper S, Kehrer J, Sattler JM, Singer M *et al.* (2016) The Actin Filament-Binding Protein Coronin Regulates Motility in Plasmodium Sporozoites. *PLoS Pathogens* 12(7), e1005710

[290] Kehrer J, Singer M, Lemgruber L, Silva PAGC, Frischknecht F *et al.* (2016) A Putative Small Solute Transporter Is Responsible for the Secretion of G377 and TRAP-Containing Secretory Vesicles during Plasmodium Gamete Egress and Sporozoite Motility. *PLoS Pathogens* 12(7), e1005734

[291] Kariu T, Yuda M, Yano K, and Chinzei Y (2002) MAEBL Is Essential for Malarial Sporozoite Infection of the Mosquito Salivary Gland. *Journal of Experimental Medicine* 195(10), 1317–1323

[292] Tewari R, Spaccapelo R, Bistoni F, Holder AA, and Crisanti A (2002) Function of region I and II adhesive motifs of Plasmodium falciparum circumsporozoite protein in sporozoite motility and infectivity. *Journal of Biological Chemistry* 277(49), 47613–47618

[293] Kappe SHI, Buscaglia CA, Bergman LW, Coppens I, and Nussenzweig V (2004) Apicomplexan gliding motility and host cell invasion: overhauling the motor model. *Trends in Parasitology* 20(1), 13–16

[294] Baum J, Gilberger TW, Frischknecht F, and Meissner M (2008) Host-cell invasion by malaria parasites: insights from Plasmodium and Toxoplasma. *Trends in Parasitology* 24(12), 557–563

[295] Boucher LE and Bosch J (2015) The apicomplexan glideosome and adhesins–structures and function. *Journal of Structural Biology* 192(2), 93–114

[296] Soldati D and Meissner M (2004) Toxoplasma as a novel system for motility. *Current Opinion in Cell Biology* 16(1), 32–40

[297] Dobrowolski JM and Sibley LD (1996) Toxoplasma invasion of mammalian cells is powered by the actin cytoskeleton of the parasite. *Cell* 84(6), 933–939

[298] Wetzel DM (2002) Actin Filament Polymerization Regulates Gliding Motility by Apicomplexan Parasites. *Molecular Biology of the Cell* 14(2), 396–406

[299] Skillman KM, Diraviyam K, Khan A, Tang K, Sept D *et al.* (2011) Evolutionarily divergent, unstable filamentous actin is essential for gliding motility in apicomplexan parasites. *PLoS Pathogens* 7(10), e1002280

[300] Periz J, Whitelaw J, Harding C, Gras S, Del Rosario Minina MI *et al.* (2017) Toxoplasma gondii F-actin forms an extensive filamentous network required for material exchange and parasite maturation. *Elife* 6, e24119

[301] Sidén-Kiamos I, Ganter M, Kunze A, Hliscs M, Steinbüchel M *et al.* (2011) Stage-specific depletion of myosin A supports an essential role in motility of malarial ookinetes. *Cellular Microbiology* 13(12), 1996–2006

[302] Frénal K, Marq JB, Jacot D, Polonais V, and Soldati-Favre D (2014) Plasticity between MyoC- and MyoA-glideosomes: an example of functional compensation in Toxoplasma gondii invasion. *PLoS Pathogens* 10(10), e1004504

[303] Frénal K, Polonais V, Marq JB, Stratmann R, Limenitakis J *et al.* (2010) Functional Dissection of the Apicomplexan Glideosome Molecular Architecture. *Cell Host & Microbe* 8(4), 343–357

[304] Williams MJ, Alonso H, Enciso M, Egarter S, and Sheiner L (2015) Two Essential Light Chains Regulate the MyoA Lever Arm To Promote Toxoplasma Gliding Motility. *MBio* 15;6(5), e00845–15

[305] Ridzuan MAM, Moon RW, Knuepfer E, Black S, Holder AA *et al.* (2012) Subcellular Location, Phosphorylation and Assembly into the Motor Complex of GAP45 during Plasmodium falciparum Schizont Development. *PLoS One* 7(3), e33845

[306] Sebastian S, Brochet M, Collins MO, Schwach F, Jones ML *et al.* (2012) A Plasmodium calcium-dependent protein kinase controls zygote development and transmission by translationally activating repressed mRNAs. *Cell Host & Microbe* 12(1), 9–19

[307] Hughes KR and Waters AP (2017) Rapid inducible protein displacement in Plasmodium in vivo and in vitro using knocksideways technology. *Wellcome Open Research* 4(2), 18

[308] Agop-Nersesian C, Egarter S, Langsley G, Foth BJ, Ferguson DJP *et al.* (2010) Biogenesis of the Inner Membrane Complex Is Dependent on Vesicular Transport by the Alveolate Specific GTPase Rab11B. *PLoS Pathogens* 6(7), e1001029

[309] Dubremetz JF and Torpier G (1978) Freeze fracture study of the pellicle of an eimerian sporozoite (Protozoa, Coccidia). *Journal of Ultrastructure Research* 62(2), 94–109

[310] Ferguson DJP, Sahoo N, Pinches RA, Bumstead JM, Tomley FM *et al.* (2008) MORN1 Has a Conserved Role in Asexual and Sexual Development across the Apicomplexa. *Eukaryotic Cell* 7(4), 698–711

[311] Lorestani A, Sheiner L, Yang K, Robertson SD, Sahoo N *et al.* (2010) A Toxoplasma MORN1 null mutant undergoes repeated divisions but is defective in basal assembly, apicoplast division and cytokinesis. *PLoS One* 5(8), e12302

[312] Engelberg K, Ivey FD, Lin A, and Kono M (2016) A MORN1 associated HAD phosphatase in the basal complex is essential for Toxoplasma gondii daughter budding. *Cellular Microbiology* 18(8), 1153–1171

[313] Tremp AZ, Al-Khattaf FS, and Dessens JT (2014) Distinct temporal recruitment of Plasmodium alveolins to the subpellicular network. *Parasitology Research* 113(11), 4177–4188

[314] Khater EI, Sinden RE, and Dessens JT (2004) A malaria membrane skeletal protein is essential for normal morphogenesis, motility, and infectivity of sporozoites. *The Journal of Cell Biology* 167(3), 425–432

[315] Tremp AZ and Dessens JT (2011) Malaria IMC1 Membrane Skeleton Proteins Operate Autonomously and Participate in Motility Independently of Cell Shape. *Journal of Biological Chemistry* 286(7), 5383–5391

[316] Volkmann K, Pfander C, Burstroem C, Ahras M, Goulding D *et al.* (2012) The alveolin IMC1h is required for normal ookinete and sporozoite motility behaviour and host colonisation in Plasmodium berghei. *PLoS One* 7(7), e41409

[317] Gilk SD, Raviv Y, Hu K, Murray JM, and Beckers C (2006) Identification of PhIL1, a novel cytoskeletal protein of the Toxoplasma gondii pellicle, through photosensitized labeling with 5-[125I] iodonaphthalene-1-azide. *Eukaryotic Cell* 5(10), 1622–1634

[318] Tran JQ, Li C, Chyan A, Chung L, and Morrissette NS (2012) SPM1 stabilizes subpellicular microtubules in Toxoplasma gondii. *Eukaryotic Cell* 11(2), 206–216

[319] Liu J, Wetzel L, Zhang Y, Nagayasu E, Ems-McClung S *et al.* (2013) Novel Thioredoxin-Like Proteins Are Components of a Protein Complex Coating the Cortical Microtubules of Toxoplasma gondii. *Eukaryotic Cell* 12(12), 1588–1599

[320] Soldati D, Dubremetz JF, and Lebrun M (2001) Microneme proteins: structural and functional requirements to promote adhesion and invasion by the apicomplexan parasite Toxoplasma gondii. *International Journal for Parasitology* 31(12), 1293–1302

[321] Yeoh S, O'Donnell RA, Koussis K, Dluzewski AR, Ansell KH *et al.* (2007) Subcellular Discharge of a Serine Protease Mediates Release of Invasive Malaria Parasites from Host Erythrocytes. *Cell* 131(6), 1072–1083

[322] Striepen B, Soldati D, Garcia-Réguet N, Dubremetz JF, and Roos DS (2001) Targeting of soluble proteins to the rhoptries and micronemes in Toxoplasma gondii. *Molecular and Biochemical Parasitology* 113(1), 45–53

[323] Sangaré LO, Alayi TD, Westermann B, Hovasse A, Sindikubwabo F *et al.* (2016) Unconventional endosome-like compartment and retromer complex in Toxoplasma gondii govern parasite integrity and host infection. *Nature Communications* 7, 11191

[324] Jimenez-Ruiz E, Morlon-Guyot J, Daher W, and Meissner M (2016) Vacuolar protein sorting mechanisms in apicomplexan parasites. *Molecular and Biochemical Parasitology* 209(1-2), 18–25

[325] Voss C, Ehrenman K, Mlambo G, Mishra S, Kumar KA *et al.* (2016) Overexpression of Plasmodium berghei ATG8 by Liver Forms Leads to Cumulative Defects in Organelle Dynamics and to Generation of Noninfectious Merozoites. *MBio* 7(3)

[326] Moreira CK, Templeton TJ, Lavazec C, Hayward RE, Hobbs CV *et al.* (2008) The Plasmodium TRAP/MIC2 family member, TRAP Like Protein (TLP), is involved in tissue traversal by sporozoites. *Cellular Microbiology* 10(7), 1505–1516

[327] Di Cristina M, Spaccapelo R, Soldati D, Bistoni F, and Crisanti A (2000) Two conserved amino acid motifs mediate protein targeting to the micronemes of the apicomplexan parasite Toxoplasma gondii. *Molecular and Cellular Biology* 20(19), 7332–7341

[328] Ghosh AK, Devenport M, Jethwaney D, Kalume DE, Pandey A *et al.* (2009) Malaria Parasite Invasion of the Mosquito Salivary Gland Requires Interaction between the Plasmodium TRAP and the Anopheles Saglin Proteins. *PLoS Pathogens* 5(1), e1000265

[329] Heiss K, Nie H, Kumar S, Daly TM, Bergman LW *et al.* (2008) Functional Characterization of a Redundant Plasmodium TRAP Family Invasin, TRAP-Like Protein, by Aldolase Binding and a Genetic Complementation Test. *Eukaryotic Cell* 7(6), 1062–1070

[330] Wan KL, Carruthers VB, Sibley LD, and Ajioka JW (1997) Molecular characterisation of an expressed sequence tag locus of Toxoplasma gondii encoding the micronemal protein MIC2. *Molecular and Biochemical Parasitology* 84(2), 203–214

[331] Carruthers VB, Sherman GD, and Sibley LD (2000) The Toxoplasma adhesive protein MIC2 is proteolytically processed at multiple sites by two parasite-derived proteases. *Journal of Biological Chemistry* 275(19), 14346–14353

[332] Dessens JT, Beetsma AL, Dimopoulos G, Wengelnik K, Crisanti A *et al.* (1999) CTRP is essential for mosquito infection by malaria ookinetes. *EMBO Journal* 18(22), 6221–6227

[333] Nacer A, Underhill A, and Hurd H (2008) The microneme proteins CTRP and SOAP are not essential for Plasmodium berghei ookinete to oocyst transformation in vitro in a cell free system. *Malaria Journal* 7(1), 82

[334] Strisovsky K, Sharpe HJ, and Freeman M (2009) Sequence-specific intramembrane proteolysis: identification of a recognition motif in rhomboid substrates. *Molecular Cell* 36(6), 1048–1059

[335] Dowse TJ and Soldati D (2005) Rhomboid-like proteins in Apicomplexa: phylogeny and nomenclature. *Trends in Parasitology* 21(6), 254–258

[336] Sibley LD (2013) The roles of intramembrane proteases in protozoan parasites. *Biochimica et biophysica acta* 1828(12), 2908–2915

[337] Baker RP, Wijetilaka R, and Urban S (2006) Two Plasmodium rhomboid proteases preferentially cleave different adhesins implicated in all invasive stages of malaria. *PLoS Pathogens* 2(10), e113

[338] Rugarabamu G, Marq JB, Guérin A, Lebrun M, and Soldati-Favre D (2015) Distinct contribution of Toxoplasma gondii rhomboid proteases 4 and 5 to micronemal protein protease 1 activity during invasion. *Molecular Microbiology* 97(2), 244–262

[339] Meissner M, Schlüter D, and Soldati D (2002) Role of Toxoplasma gondii myosin A in powering parasite gliding and host cell invasion. *Science* 298(5594), 837–840

[340] Bichet M, Touquet B, Gonzalez V, Florent I, Meissner M *et al.* (2016) Genetic impairment of parasite myosin motors uncovers the contribution of host cell membrane dynamics to Toxoplasma invasion forces. *BMC Biology* 14(1), 97

[341] Baum J, Tonkin CJ, Paul AS, Rug M, Smith BJ *et al.* (2008) A Malaria Parasite Formin Regulates Actin Polymerization and Localizes to the Parasite-Erythrocyte Moving Junction during Invasion. *Cell Host & Microbe* 3(3), 188–198

[342] Singh BK, Sattler JM, Chatterjee M, Huttu J, Schüler H *et al.* (2011) Crystal structures explain functional differences in the two actin depolymerization factors of the malaria parasite. *Journal of Biological Chemistry* 286(32), 28256–28264

[343] Moreau CA, Bhargav SP, Kumar H, Quadt KA, Piirainen H *et al.* (2017) A unique profilin-actin interface is important for malaria parasite motility. *PLoS Pathogens* 13(5), e1006412

[344] Ganter M, Schüler H, and Matuschewski K (2009) Vital role for the Plasmodium actin capping protein (CP) beta-subunit in motility of malaria sporozoites. *Molecular Microbiology* 74(6), 1356–1367

[345] Manna PT, Boehm C, Leung KF, Natesan SK, and Field MC (2014) Life and times: synthesis, trafficking, and evolution of VSG. *Trends in Parasitology* 30(5), 251–258

[346] Manger ID, Hehl AB, and Boothroyd JC (1998) The surface of Toxoplasma tachyzoites is dominated by a family of glycosylphosphatidylinositol-anchored antigens related to SAG1. *Infection and Immunity* 66(5), 2237–2244

[347] Xue G, von Schubert C, Hermann P, Peyer M, Maushagen R *et al.* (2010) Characterisation of gp34, a GPI-anchored protein expressed by schizonts of Theileria parva and T. annulata. *Molecular and Biochemical Parasitology* 172(2), 113–120

[348] Gerold P, Schofield L, Blackman MJ, Holder AA, and Schwarz RT (1996) Structural analysis of the glycosyl-phosphatidylinositol membrane anchor of the merozoite surface proteins-1 and -2 of Plasmodium falciparum. *Molecular and Biochemical Parasitology* 75(2), 131–143

[349] Wang Q, Fujioka H, and Nussenzweig V (2005) Mutational analysis of the GPI-anchor addition sequence from the circumsporozoite protein of Plasmodium. *Cellular Microbiology* 7(11), 1616–1626

[350] Gruszynski AE, van Deursen FJ, Albareda MC, Best A, Chaudhary K *et al.* (2006) Regulation of surface coat exchange by differentiating African trypanosomes. *Molecular and Biochemical Parasitology* 147(2), 211–223

[351] Bütikofer P, Greganova E, Liu YC, Edwards IJ, Lehane MJ *et al.* (2010) Lipid remodelling of glycosylphosphatidylinositol (GPI) glycoconjugates in procyclic-form trypanosomes: biosynthesis and processing of GPIs revisited. *The Biochemical journal* 428(3), 409–418

[352] Medof ME, Walter EI, Roberts WL, Haas R, and Rosenberry TL (1986) Decay accelerating factor of complement is anchored to cells by a C-terminal glycolipid. *Biochemistry* 25(22), 6740–6747

[353] Hartel AJW, Glogger M, Jones NG, Abuillan W, Batram C *et al.* (2016) N-glycosylation enables high lateral mobility of GPI-anchored proteins at a molecular crowding threshold. *Nature Communications* 7, 12870

[354] Saha S, Anilkumar AA, and Mayor S (2016) GPI-anchored protein organization and dynamics at the cell surface. *Journal of Lipid Research* 57(2), 159–175

[355] Mayor S and Riezman H (2004) Sorting GPI-anchored proteins. *Nature reviews. Molecular Cell Biology* 5(2), 110–120

[356] Zurzolo C and Simons K (2016) Glycosylphosphatidylinositol-anchored proteins: Membrane organization and transport. *Biochimica et biophysica acta* 1858(4), 632–639

[357] Muñiz M and Riezman H (2016) Trafficking of glycosylphosphatidylinositol anchored proteins from the endoplasmic reticulum to the cell surface. *Journal of Lipid Research* 57(3), 352–360

[358] Müller A, Klöppel C, Smith-Valentine M, Van Houten J, and Simon M (2012) Biochimica et Biophysica Acta. *Biochimica et Biophysica Acta* 1818(1), 117–124

[359] Sunter J, Webb H, and Carrington M (2013) Determinants of GPI-PLC localisation to the flagellum and access to GPI-anchored substrates in trypanosomes. *PLoS Pathogens* 9(8), e1003566

[360] Goldston AM, Powell RR, and Temesvari LA (2012) Sink or swim: lipid rafts in parasite pathogenesis. *Trends in Parasitology* 28(10), 417–426

[361] Maeda Y and Kinoshita T (2011) Progress in Lipid Research. *Progress in Lipid Research* 50(4), 411–424

[362] Naik RS, Branch OH, Woods AS, Vijaykumar M, Perkins DJ *et al.* (2000) Glycosylphosphatidylinositol anchors of Plasmodium falciparum: molecular characterization and naturally elicited antibody response that may provide immunity to malaria pathogenesis. *Journal of Experimental Medicine* 192(11), 1563–1576

[363] Channe Gowda D (2002) Structure and activity of glycosylphosphatidylinositol anchors of Plasmodium falciparum. *Microbes and Infection* 4(9), 983–990

[364] Schofield L and Hackett F (1993) Signal transduction in host cells by a glycosylphosphatidylinositol toxin of malaria parasites. *Journal of Experimental Medicine* 177(1), 145–153

[365] Arrighi RBG and Faye I (2010) Plasmodium falciparum GPI toxin: a common foe for man and mosquito. *Acta Tropica* 114(3), 162–165

[366] Debierre-Grockiego F and Schwarz RT (2010) Immunological reactions in response to apicomplexan glycosylphosphatidylinositols. *Glycobiology* 20(7), 801–811

[367] Moran P and Caras IW (1994) Requirements for glycosylphosphatidylinositol attachment are similar but not identical in mammalian cells and parasitic protozoa. *The Journal of Cell Biology* 125(2), 333–343

[368] Kanu N, Imokawa Y, Drechsel DN, Williamson RA, Birkett CR *et al.* (2002) Transfer of scrapie prion infectivity by cell contact in culture. *Current Biology* 12(7), 523–530

[369] Lou E, Fujisawa S, Morozov A, Barlas A, Romin Y *et al.* (2012) Tunneling nanotubes provide a unique conduit for intercellular transfer of cellular contents in human malignant pleural mesothelioma. *PLoS One* 7(3), e33093

[370] Frühbeis C, Fröhlich D, Kuo WP, Amphornrat J, Thilemann S *et al.* (2013) Neurotransmitter-triggered transfer of exosomes mediates oligodendrocyte-neuron communication. *PLoS Biology* 11(7), e1001604

[371] Szempruch AJ, Sykes SE, Kieft R, Dennison L, Becker AC *et al.* (2016) Extracellular Vesicles from Trypanosoma brucei Mediate Virulence Factor Transfer and Cause Host Anemia. *Cell* 164(1-2), 246–257

[372] Yoshida N, Potocnjak P, Nussenzweig V, and Nussenzweig RS (1981) Biosynthesis of Pb44, the protective antigen of sporozoites of Plasmodium berghei. *Journal of Experimental Medicine* 154(4), 1225–1236

[373] Swearingen KE, Lindner SE, Shi LR, Shears MJ, Harupa A *et al.* (2016) Interrogating the Plasmodium Sporozoite Surface: Identification of Surface-Exposed Proteins and Demonstration of Glycosylation on CSP and TRAP by Mass Spectrometry-Based Proteomics. *PLoS Pathogens* 12(4), e1005606

[374] Singh AP, Buscaglia CA, Wang Q, Levay A, Nussenzweig DR *et al.* (2007) Plasmodium Circumsporozoite Protein Promotes the Development of the Liver Stages of the Parasite. *Cell* 131(3), 492–504

[375] Peterson DS, Gao Y, Asokan K, and Gaertig J (2002) The circumsporozoite protein of Plasmodium falciparum is expressed and localized to the cell surface in the free-living ciliate Tetrahymena thermophila. *Molecular and Biochemical Parasitology* 122(2), 119–126

[376] Aurrecoechea C, Brestelli J, Brunk BP, Dommer J, Fischer S *et al.* (2009) PlasmoDB: a functional genomic database for malaria parasites. *Nucleic Acids Research* 37(suppl 1), D539–543

[377] Tewari R, Rathore D, and Crisanti A (2005) Motility and infectivity of Plasmodium berghei sporozoites expressing avian Plasmodium gallinaceum circumsporozoite protein. *Cellular Microbiology* 7(5), 699–707

[378] Zhang M, Kaneko I, Tsao T, Mitchell R, Nardin EH *et al.* (2016) A highly infectious Plasmodium yoelii parasite, bearing Plasmodium falciparum circumsporozoite protein. *Malaria Journal* 12(15), 201

[379] Aldrich C, Magini A, Emiliani C, Dottorini T, Bistoni F *et al.* (2012) Roles of the amino terminal region and repeat region of the Plasmodium berghei circumsporozoite protein in parasite infectivity. *PLoS One* 7(2), e32524

[380] Spillman NJ, Beck JR, and Goldberg DE (2015) Protein export into malaria parasite-infected erythrocytes: mechanisms and functional consequences. *Annual Review of Biochemistry* 84, 813–841

[381] Elsworth B, Matthews K, Nie CQ, Kalanon M, Charnaud SC *et al.* (2014) PTEX is an essential nexus for protein export in malaria parasites. *Nature* 511(7511), 587–591

[382] Matz JM, Goosmann C, Brinkmann V, Grutzke J, Ingmundson A *et al.* (2015) The Plasmodium berghei translocon of exported proteins reveals spatiotemporal dynamics of tubular extensions. *Scientific Reports* 5, 12532

[383] Curt-Varesano A, Braun L, Ranquet C, Hakimi MA, and Bougdour A (2016) The aspartyl protease TgASP5 mediates the export of the Toxoplasma GRA16 and GRA24 effectors into host cells. *Cellular Microbiology* 18(2), 151–167

[384] Franco M, Panas MW, Marino ND, Lee MCW, Buchholz KR *et al.* (2016) A Novel Secreted Protein, MYR1, Is Central to Toxoplasma's Manipulation of Host Cells. *MBio* 7(1), e02231–15

[385] Gold DA, Kaplan AD, Lis A, Bett GCL, Rosowski EE *et al.* (2015) The Toxoplasma Dense Granule Proteins GRA17 and GRA23 Mediate the Movement of Small Molecules between the Host and the Parasitophorous Vacuole. *Cell Host & Microbe* 17(5), 642–652

[386] Petersen TN, Brunak S, von Heijne G, and Nielsen H (2011) SignalP 4.0: discriminating signal peptides from transmembrane regions. *Nature Methods* 8(10), 785–786

[387] Coppi A, Pinzon-Ortiz C, Hutter C, and Sinnis P (2005) The Plasmodium circumsporozoite protein is proteolytically processed during cell invasion. *Journal of Experimental Medicine* 201(1), 27–33

[388] Persson C, Oliveira GA, Sultan AA, Bhanot P, Nussenzweig V *et al.* (2002) Cutting edge: a new tool to evaluate human pre-erythrocytic malaria vaccines: rodent parasites bearing a hybrid Plasmodium falciparum circumsporozoite protein. *Journal of Immunology* 169(12), 6681–6685

[389] Espinosa DA, Yadava A, Angov E, Maurizio PL, Ockenhouse CF *et al.* (2013) Development of a chimeric Plasmodium berghei strain expressing the repeat region of the P. vivax circumsporozoite protein for in vivo evaluation of vaccine efficacy. *Infection and Immunity* 81(8), 2882–2887

[390] Gandhi K, Thera MA, Coulibaly D, Traoré K, Guindo AB *et al.* (2014) Variation in the Circumsporozoite Protein of Plasmodium falciparum: Vaccine Development Implications. *PLoS One* 9(7), e101783

[391] Doud MB, Koksal AC, Mi LZ, Song G, Lu C *et al.* (2012) Unexpected fold in the circumsporozoite protein target of malaria vaccines. *Proceedings of the National Academy of Sciences of the United States of America* 109(20), 7817–7822

[392] Pierleoni A, Martelli PL, and Casadio R (2008) PredGPI: a GPI-anchor predictor. *BMC Bioinformatics* 9, 392

[393] Lindner SE, Swearingen KE, Harupa A, Vaughan AM, Sinnis P *et al.* (2013) Total and putative surface proteomics of malaria parasite salivary gland sporozoites. *Molecular & Cellular Proteomics* 12(5), 1127–1143

[394] Wang J, Zhang Y, Zhao YO, Li MWM, Zhang L *et al.* (2013) Anopheles gambiae circumsporozoite protein-binding protein facilitates plasmodium infection of mosquito salivary glands. *Journal of Infectious Diseases* 208(7), 1161–1169

[395] Cerami C, Frevert U, Sinnis P, Takacs B, and Nussenzweig V (1994) Rapid clearance of malaria circumsporozoite protein (CS) by hepatocytes. *Journal of Experimental Medicine* 179(2), 695–701

[396] Zhao JH, Bhanot P, Hu JJ, and Wang Q (2016) A Comprehensive Analysis of Plasmodium Circumsporozoite Protein Binding to Hepatocytes. *PLoS One* 11(8), e0161607

[397] Myung JM, Marshall P, and Sinnis P (2004) The Plasmodium circumsporozoite protein is involved in mosquito salivary gland invasion by sporozoites. *Molecular and Biochemical Parasitology* 133(1), 53–59

[398] Matsushima N, Yoshida H, Kumaki Y, Kamiya M, Tanaka T *et al.* (2008) Flexible structures and ligand interactions of tandem repeats consisting of proline, glycine, asparagine, serine, and/or threonine rich oligopeptides in proteins. *Current Protein & Peptide Science* 9(6), 591–610

[399] Plassmeyer ML, Reiter K, Shimp RL, Kotova S, Smith PD *et al.* (2009) Structure of the Plasmodium falciparum Circumsporozoite Protein, a Leading Malaria Vaccine Candidate. *Journal of Biological Chemistry* 284(39), 26951–26963

[400] Menard R, Sultan AA, Cortes C, Altszuler R, van Dijk MR *et al.* (1997) Circumsporozoite protein is required for development of malaria sporozoites in mosquitoes. *Nature* 385(6614), 336–340

[401] Stewart MJ and Vanderberg JP (1992) Electron microscopic analysis of circumsporozoite protein trail formation by gliding malaria sporozoites. *Journal of Protozoology* 39(6), 663–671

[402] Kariu T, Ishino T, Yano K, Chinzei Y, and Yuda M (2006) CelTOS, a novel malarial protein that mediates transmission to mosquito and vertebrate hosts. *Molecular Microbiology* 59(5), 1369–1379

[403] Stewart MJ and Vanderberg JP (1991) Malaria Sporozoites Release Circumsporozoite Protein from Their Apical End and Translocate It along Their Surface. *Journal of Eukaryotic Microbiology* 38(4), 411–421

[404] Hügel FU, Pradel G, and Frevert U (1996) Release of malaria circumsporozoite protein into the host cell cytoplasm and interaction with ribosomes. *Molecular and Biochemical Parasitology* 81(2), 151–170

[405] Frevert U, Engelmann S, Zougbédé S, Stange J, Ng B *et al.* (2005) Intravital observation of Plasmodium berghei sporozoite infection of the liver. *PLoS Biology* 3(6), e192

[406] Mota MM, Hafalla JCR, and Rodriguez A (2002) Migration through host cells activates Plasmodium sporozoites for infection. *Nature Medicine* 8(11), 1318–1322

[407] Harupa A, Sack BK, Lakshmanan V, Arang N, Douglass AN *et al.* (2014) SSP3 Is a Novel Plasmodium yoelii Sporozoite Surface Protein with a Role in Gliding Motility. *Infection and Immunity* 82(11), 4643–4653

[408] Wiser MF and Plitt B (1987) Plasmodium berghei, P. chabaudi, and P. falciparum: similarities in phosphoproteins and protein kinase activities and their stage specific expression. *Experimental Parasitology* 64(3), 328–335

[409] Yoshida N, Nussenzweig RS, Potocnjak P, Nussenzweig V, and Aikawa M (1980) Hybridoma produces protective antibodies directed against the sporozoite stage of malaria parasite. *Science* 207(4426), 71–73

[410] Kennedy M and Fishbaugher ME (2012) A rapid and scalable density gradient purification method for Plasmodium sporozoites. *Malaria Journal* 17(11), 421

[411] Lukinavičius G, Umezawa K, Olivier N, Honigmann A, Yang G *et al.* (2013) A near-infrared fluorophore for live-cell super-resolution microscopy of cellular proteins. *Nature Chemistry* 5(2), 132–139

[412] De Niz M, Helm S, Horstmann S, Annoura T, del Portillo HA *et al.* (2015) In Vivo and In Vitro Characterization of a Plasmodium Liver Stage-Specific Promoter. *PLoS One* 10(4), e0123473

[413] Klug D, Mair GR, Frischknecht F, and Douglas RG (2016) A small mitochondrial protein present in myzozoans is essential for malaria transmission. *Open Biology* 6(4), 160034

[414] Kooij TWA, Rauch MM, and Matuschewski K (2012) Expansion of experimental genetics approaches for Plasmodium berghei with versatile transfection vectors. *Molecular and Biochemical Parasitology* 185(1), 19–26

[415] Fanucchi S, Shibayama Y, Burd S, Weinberg MS, and Mhlanga MM (2013) Chromosomal Contact Permits Transcription between Coregulated Genes. *Cell* 155(3), 606–620

[416] Donnelly ML, Hughes LE, Luke G, Mendoza H, ten Dam E *et al.* (2001) The 'cleavage' activities of foot-and-mouth disease virus 2A site-directed mutants and naturally occurring '2A-like' sequences. *Journal of General Virology* 82(Pt 5), 1027–1041

[417] Maeder ML, Thibodeau-Beganny S, Osiak A, Wright DA, Anthony RM *et al.* (2008) Rapid "Open-Source" Engineering of Customized Zinc-Finger Nucleases for Highly Efficient Gene Modification. *Molecular Cell* 31(2), 294–301

[418] Singer M, Marshall J, Heiss K, Mair GR, Grimm D *et al.* (2015) Zinc finger nuclease-based double-strand breaks attenuate malaria parasites and reveal rare microhomology-mediated end joining. *Genome Biology* 16(249), 1–18

[419] Nakamura Y, Gojobori T, and Ikemura T (2000) Codon usage tabulated from international DNA sequence databases: status for the year 2000. *Nucleic Acids Research* 28(1), 292

[420] Puigbo P, Guzman E, Romeu A, and Garcia-Vallve S (2007) OPTIMIZER: a web server for optimizing the codon usage of DNA sequences. *Nucleic Acids Research* 35(web server issue), W126–W131

[421] Pace T, Ponzi M, Dore E, and Frontali C (1987) Telomeric motifs are present in a highly repetitive element in the Plasmodium berghei genome. *Molecular and Biochemical Parasitology* 24(2), 193–202

[422] Heim R, Prasher DC, and Tsien RY (1994) Wavelength mutations and posttranslational autoxidation of green fluorescent protein. *Proceedings of the National Academy of Sciences of the United States of America* 91(26), 12501–12504

[423] Burmeister JS, Olivier LA, Reichert WM, and Truskey GA (1998) Application of total internal reflection fluorescence microscopy to study cell adhesion to biomaterials. *Biomaterials* 19(4-5), 307–325

[424] Axelrod D (2013) Evanescent excitation and emission in fluorescence microscopy. *Biophysical Journal* 104(7), 1401–1409

[425] Poulter NS, Pitkeathly WTE, Smith PJ, and Rappoport JZ (2015) The physical basis of total internal reflection fluorescence (TIRF) microscopy and its cellular applications. *Methods in Molecular Biology* 1251, 1–23

[426] Meyer RA (1979) Light scattering from biological cells: dependence of backscatter radiation on membrane thickness and refractive index. *Applied Optics* 18(5), 585–588

[427] Brunstein M, Teremetz M, Hérault K, Tourain C, and Oheim M (2014) Eliminating unwanted far-field excitation in objective-type TIRF. Part I. identifying sources of nonevanescent excitation light. *Biophysical Journal* 106(5), 1020–1032

[428] Quadt KA, Streichfuss M, Moreau CA, Spatz JP, and Frischknecht F (2016) Coupling of Retrograde Flow to Force Production During Malaria Parasite Migration. *ACS Nano* 10(2), 2091–2102

[429] Deitsch KW (2001) Transformation of malaria parasites by the spontaneous uptake and expression of DNA from human erythrocytes. *Nucleic Acids Research* 29(3), 850–853

[430] Boyle MJ, Wilson DW, Richards JS, Riglar DT, Tetteh KKA *et al.* (2010) Isolation of viable Plasmodium falciparum merozoites to define erythrocyte invasion events and advance vaccine and drug development. *Proceedings of the National Academy of Sciences of the United States of America* 107(32), 14378–14383

[431] Mogollon CM, van Pul FJA, Imai T, Ramesar J, Chevalley-Maurel S *et al.* (2016) Rapid Generation of Marker-Free P. falciparum Fluorescent Reporter Lines Using Modified CRISPR/Cas9 Constructs and Selection Protocol. *PLoS One* 11(12), e0168362

[432] Kumar KA, Baxter P, Tarun AS, Kappe SH, and Nussenzweig V (2009) Conserved protective mechanisms in radiation and genetically attenuated uis3(-) and uis4(-) Plasmodium sporozoites. *PLoS One* 4(2), e4480

[433] Khan SM, Janse CJ, Kappe SH, and Mikolajczak SA (2012) Genetic engineering of attenuated malariaparasites for vaccination. *Current Opinion in Biotechnology* 23(6), 908–916

[434] Mikolajczak SA, Lakshmanan V, Fishbaugher M, Camargo N, Harupa A *et al.* (2014) A next-generation genetically attenuated Plasmodium falciparum parasite created by triple gene deletion. *Molecular Therapy* 22(9), 1707–1715

[435] Anderson TJC, Patel J, and Ferdig MT (2009) Gene copy number and malaria biology. *Trends in Parasitology* 25(7), 336–343

[436] Calhoun SF, Reed J, Alexander N, Mason CE, Deitsch KW *et al.* (2017) Chromosome End Repair and Genome Stability in Plasmodium falciparum. *MBio* (in press)

[437] RTS SCTP (2015) Efficacy and safety of RTS,S/AS01 malaria vaccine with or without a booster dose in infants and children in Africa: final results of a phase 3, individually randomised, controlled trial - ScienceDirect. *The Lancet* 386(9988), 31–45

[438] Matuschewski K (2017) Vaccines against malaria - still a long way to go. *The FEBS journal* Epub doi:10.1111/febs.14107

[439] Fougère A, Jackson AP, Bechtsi DP, Braks JAM, Annoura T *et al.* (2016) Variant Exported Blood-Stage Proteins Encoded by Plasmodium Multigene Families Are Expressed in Liver Stages Where They Are Exported into the Parasitophorous Vacuole. *PLoS Pathogens* 12(11), e1005917

[440] Golenda CF, Starkweather WH, and Wirtz RA (1990) The distribution of circumsporozoite protein (CS) in Anopheles stephensi mosquitoes infected with Plasmodium falciparum malaria. *Journal of Histochemistry & Cytochemistry* 38(4), 475–481

[441] Cerami C, Frevert U, Sinnis P, Takacs B, Clavijo P *et al.* (1992) The basolateral domain of the hepatocyte plasma membrane bears receptors for the circumsporozoite protein of Plasmodium falciparum sporozoites. *Cell* 70(6), 1021–1033

[442] Doering TL and Schekman R (1996) GPI anchor attachment is required for Gas1p transport from the endoplasmic reticulum in COP II vesicles. *EMBO Journal* 15(1), 182–191

[443] Grünfelder CG, Engstler M, Weise F, Schwarz H, Stierhof YD *et al.* (2003) Endocytosis of a glycosylphosphatidylinositol-anchored protein via clathrin-coated vesicles, sorting by default in endosomes, and exocytosis via RAB11-positive carriers. *Molecular Biology of the Cell* 14(5), 2029–2040

[444] Boddey JA, Carvalho TG, Hodder AN, Sargeant TJ, Sleebs BE *et al.* (2013) Role of Plasmepsin V in Export of Diverse Protein Families from the Plasmodium falciparum Exportome. *Traffic* 14(5), 532–550

[445] Mastan BS, Narwal SK, Dey S, Kumar KA, and Mishra S (2017) Plasmodium berghei plasmepsin VIII is essential for sporozoite gliding motility. *International Journal for Parasitology* 47(5), 239–245

[446] Meis JF, Verhave JP, Jap PH, and Meuwissen JH (1985) Fine structure of exoerythrocytic merozoite formation of Plasmodium berghei in rat liver. *Journal of Protozoology* 32(4), 694–699

[447] Burda PC, Roelli MA, Schaffner M, Khan SM, Janse CJ *et al.* (2015) A Plasmodium phospholipase is involved in disruption of the liver stage parasitophorous vacuole membrane. *PLoS Pathogens* 11(3), e1004760

[448] Sevcsik E, Brameshuber M, Fölser M, Weghuber J, and Honigmann A (2015) GPI-anchored proteins do not reside in ordered domains in the live cell plasma membrane. *Nature Communications* 6, 6969

[449] Lehto MT and Sharom FJ (2002) Proximity of the Protein Moiety of a GPI-Anchored Protein to the Membrane Surface: a FRET Study. *Biochemistry* 41(26), 8368–8376

[450] Resh MD (2016) Fatty acylation of proteins: The long and the short of it. *Progress in Lipid Research* 63, 120–131

[451] Stepanek O, Draber P, and Horejsi V (2014) Palmitoylated transmembrane adaptor proteins in leukocyte signaling. *Cellular Signalling* 26(5), 895–902

[452] Hopp CS, Balaban AE, Bushell ESC, Billker O, Rayner JC *et al.* (2016) Palmitoyl transferases have critical roles in the development of mosquito and liver stages of Plasmodium. *Cellular Microbiology* 18(11), 1625–1641

[453] Pumpuni CB, Mendis C, and Beier JC (1997) Plasmodium yoelii sporozoite infectivity varies as a function of sporozoite loads in Anopheles stephensi mosquitoes. *The Journal of Parasitology* 83(4), 652–655

[454] Lipowsky R, Richter D, and Kremer K (1991) *The Structure and Conformation of Amphiphilic Membranes: Proceedings of the International Workshop on Amphiphilic Membranes, Jülich, Germany.* Springer-Verlag

[455] Limozin L and Sengupta K (2009) Quantitative reflection interference contrast microscopy (RICM) in soft matter and cell adhesion. *ChemPhysChem* 10(16), 2752–2768

[456] Morimatsu M, Mekhdjian AH, Adhikari AS, and Dunn AR (2013) Molecular Tension Sensors Report Forces Generated by Single Integrin Molecules in Living Cells. *Nano Letters* 13(9), 3985–3989

[457] Dragavon J, Sinow C, Holland AD, Rekiki A, Theodorou I *et al.* (2014) A step beyond BRET: Fluorescence by Unbound Excitation from Luminescence (FUEL). *Journal of Visualized Experiments* (87), e51549

[458] Santos JM, Egarter S, Zuzarte-Luis V, Kumar H, Moreau CA *et al.* (2017) Malaria parasite LIMP protein regulates sporozoite gliding motility and infectivity in mosquito and mammalian hosts. *Elife* 6, e24109.

Chapter

5

Appendix

5.1 Species

As	*Anopheles stephensi*
Hs	*Homo sapiens*
Pb	*Plasmodium berghei*
Pc	*Plasmodium chabaudii*
Pf	*Plasmodium falciparum*
Pg	*Plasmodium gallinaceum*
Pk	*Plasmodium knowlewsi*
Pm	*Plasmodium malarie*
Po	*Plasmodium ovale*
Pv	*Plasmodium vivax*
Prel	*Plasmodium relictum*
Py	*Plasmodium yoelii*
Tg	*Toxoplasma gondii*

5.2 Abbreviations

5-FC	5-fluorocytosine
A-domain	von Willenbrand factor type A-domain
ASP5	aspartyl protease 5, *Toxoplasma gondii* homolog of Plasmepsin V
AU	arbitrary units
bb	bite back
BER	base excision repair
bp	base pairs
BS	Blood stage
BSA	bovine serum albumin
CSP	circumsporozoite protein

CAS9	CRISPR associated protein 9
cDNA	complementary DNA
CIRSPR	clustered regularly interspaced short palindromic repeats
Cre	Cre recombinase
CTRP	circumsporozoite and trap related protein
Cyto D	cytochalasin D
dd H_2O	double distilled water
DG	dense granules
DHFR	dehydrofolat reductase
DHFR-TS	dehydrofolat reductase - thymidine synthase
DiCre	Dimeric Cre recombinase
DNA	Deoxyribonucleic acid
DSB	double stranded break
ER	endoplasmatic reticulum
EtOH	ethanol
EXP2	exported protein 2
FACS	fluorescence-activated cell sorting
FLP	Flippase
FP	fluorescent protein
fps	frames per second
FRET	Förster resonance energy transfer
GAP	genetically attenuated parasites
GAP40	glideosome associated protein 40
GAP45	glideosome associated protein 45
GAP50	glideosome associated protein 50
gDNA	genomic DNA
GFP	green fluorescent protein
GIMO	gene in marker out
GPI	glycosylphosphatidylinositol, anchors proteins into membranes
GRA16	dense granule protein 16
Gy	gray unit, 1 joule of radiation energy per kg of matter
HLS	haemolymph sporozoites
HR	homologous recombination
HSP70	heat shock protein 70
ID	intradermal
IFA	immunofluorescence analysis
IMC	inner membrane complex
ISP	IMC sub-compartment protein
IV	intravenous
JAS	jasplakinolide
KB	kilobase
kDa	kilo Dalton
MB	megabase
MCS	multiple cloning site
MGS	midgut sporozoites
MHC	major histocompatibility complex
min	minutes

MLC1	myosin light chain 1
MMEJ	microhomology mediated end joining
MORN1	membrane occupation and recognition nexus protein
MRX complex	complex of Mre11, Rad50 and Xrs2
MTOC	microtubule organizing center
MTRAP	merozoite TRAP-like protein
MYR1	myc regulation 1
NA	numerical aperture
NHEJ	non-homologous end joining
NLS	nuclear localization signal
ON	over night
ORF	open reading frame
PAM	protospacer adjacent motif
PAT	putative pathothenate transporter
PCR	Polymerase chain reaction
PEXEL	*Plasmodium* export element
PFA	paraformaldehyde
pir	plasmodium interspersed repeat genes
PM	plasma membrane
Puf2	mRNA binding protein Pumilio-2
prepatency	time from infection to detectability by standard methods
PTEX	*Plasmodium* transport element of exported proteins
PV	parasitophorous vacuole
PVM	parasitophorous vacuole membrane
qPCR	quantitative PCR
R I	Region I: conserved five AA of CSP following the n-terminusl
RAS	radiation attenuated sporozoites
RBC	red blood cell
rpm	rounds per minute
RT	room temperature
S6	sporozoite specific gene 6, also termed TREP, TRAP -related protein
SC	subcutaneous
SERA5	serine repeat antigen 5, a papai-like cystein protease
SGS	salivary gland sporozoites
SP	signal peptide
SPN	subpellicular network
SPM1	subpellicular microtubule binding protein 1
SSA	synthesis dependent strand annealing
TIRF-M	total internal reflection fluorescence microscopy
TLP	TRAP like protein
TRAP	thrombospondin related anonymous protein
TRP1	thrombospondin related protein 1
TSR	thrombospondin type 1 repeat
TSS	Transcription start site
UTR	untranslated region
VNTR	variable number of tandem repeats
vWF	Willebrand Factor-like A
x’	x minutes
x”	x seconds

5.3 Primers

P98	cgaccggtaaactgcatcgtcgctg
P99	ctagctagcttaatcattcttctcatatacttc
P847	ttcgagaattcgaagtacttcgtcgacgacg
P848	ttcgagaattcgaagtacttcgtcgacgacg
P849	acgggtacctatgaagcttttaactcgagaaagacttaagtagctaaaaggtgtgcaagc
P850	ttcgagaattcgtttacaatttaatattcatactttaag
P851	tgaaagctttataaaggggaccccatatatagg
P852	gatcctcgagatttaaataattgtaattgtaatttattggg
P853	ggagggccagcctccttcactggggtgtggaagcatgacatattacatgtttggggatttttg
P854	ttaaaagcttaatgcacaccatgctatagttg
P855	acgggtacctatcaaaacaaattgacagatatgtac
P856	gaaggaggctggccctccactggggtgtggaagcattgattcatcactgttttgtattcg
P893	gccgtcctcgatgttgtggcggatgacatattacatgtttggggatttttg
P894	atccgccacaacatcgaggacggctgattcatcactgttttgtattcg
P241	cttgcaccggtatggttggttcgctaaac
P233	cccagggcccaattcttttcgagctctttatgc
P234	cttgcaccggtttttataaaatttttatttatttataagc
P207	ggaattcatatgtttaaatatatgcgtgtatatatagattttg
P208	ccggaattcatgtgttggttgtaattgagg
P238	ggaattccatatggccatcatcaaggagttcatg
P232	cgcggatccttacttgtacagctcgtccatgc
P242	cttgcaccggtatggtgagcaagggcgag
P243	cttgcaccggtaccaccaccaccaccaccaccaccaccaccacctctagatccggtggatccc
P600	cccaagcttcaaaaaagcaggcttgccgc
P601	gccgatatccaagaaagctgggtggtaccc
P377	ataagaatgcggccgcatgtgttggttgtaattgagg
P378	ccggatatccgtatttaaatacggacaattgtcggggtacctttaaatatatgcgtgtatatatagattttg
P379	cggggtaccatgggccctaagaaaaagc
P380	atacggacaattgtcttaaaagttgatttcgccgttg
P381	atacggacaattgtcgtattctttaattaaataaacattacgcatg
P382	acgtatttaaatgtcatagcaagttaactacatatataataaac
P387	acgtatttaaatacggacaattgtcggggtacctagctaaaaggtgtgcaagc
P388	cgggatatcatatttgtaatgatgctttttcacg
P385	gacaattgtcatgggccctaagaaaaagc
P386	cggggtaccttaaaagttgatttcgccgttg
P383	acgtatttaaatgctcatattaatacacataatgtcttcc
P384	gacaattgtctataagggaaagggaaaatggg
P685	aaggaaaaaagcggccgcgttgcattatcgtcaaaagtg
P686	gctttttcttagggcccatttttttatgtgtaaaaaagtaaaatgattataatagaag
P687	cttctattataatcattttacttttttacacataaaaaatgggccctaagaaaaagc
P688	atacggacaattgtccctggacctggattttcttcaacatcaccacatgtaagaagtgaacctctaccttcaccaaagttgatttcgccgttg
P1168	aatctgcagaattcgaagcttgagc
P1169	gtctatatcatggcagacaagcagaagaacggc
P1170	cttctgcttgtctgccatgatatagacgttgtg
P1171	ttagatttaaatttatttttaatatttcctaaaatatatatactttgtg
P1172	attaagctttttatgtgtaaaaaagtaaaatgattataatagaag

P1173	attaagctttttaaatatatgcgtgtatatatagattttg
P685	aaggaaaaaagcggccgcgttgcattatcgtcaaaagtg
P378	ccggatatccgtatttaaatacggacaattgtcggggtacctttaaatatatgcgtgtatatatagattttg
P686	gctttttcttagggcccatttttttatgtgtaaaaaagtaaaatgattataatagaag
P243	cttgcaccggtaccaccaccaccaccaccaccaccaccaccacctctagatccggtggatccc
P384	gacaattgtctataagggaaagggaaaatggg
P1262	gggaattccatatggatatcccattgatcttccaacttttctttttcttttttggtcccattttattcagacgtaataattatgtgc
P1259	aaggaaaaaagcggccgcgctcattatagggtgaataaaaatgg
P1260	aaggaaaaaagcggccgcgctcatattaatacacataatgtcttcc
P1261	gggaattccatatggatatcccattgatcttccaacttttctttttcttttttggtcccattctataagggaaagggaaaatgg
P234	cttgcaccggtttttataaaatttttatttatttataagc
P207	ggaattcatatgtttaaatatatgcgtgtatatatagattttg
P377	ataagaatgcggccgcatgtgttggttgtaattgagg
P685	aaggaaaaaagcggccgcgttgcattatcgtcaaaagtg
P388	cgggatatcatatttgtaatgatgctttttcacg
P242	cttgcaccggtatggtgagcaagggcgag
P243	cttgcaccggtaccaccaccaccaccaccaccaccaccaccacctctagatccggtggatccc
P1134	tagtggttgtcgggcagcag
P1135	acaactacaacagccacaacgtc
P1136	acattgcaggtgggttcagag
P1137	gcaatttggttcactttcgccaatg
P1138	ggtacacctcctcaagaaattcatcc
P1139	accagttattgacccagatccaaaaac
P1140	tgtacgaaggaaatccaaattcttctactc
P1141	actatctaattcccttccataccctcc
P1142	attagctctgacttaccatcccgac
P1143	tttgcaaaaacatttctttgcatctttcc
P1144	cctaattcgaaaaataaggataatttgtgggatc
P1145	cccttcttctccagagcttacactac
P1174	Gcgttatcttctcggcgtaatacc
P1175	aatttggaattgttcaaatgctggattg
P1176	tgcttaatcaatatttttcttctatgaccagaac
P1177	aaaattatgaaagaccctactgtaaacacatc
P1178	aagcttgagctcgagatctg
P1179	tatcatggccgaccactac
P512	ctgtttaaaccatcaacattgatagcgatatagcg
P513	gagtttaaacctgtaaaaatgtgtatgttgtgtgc
P577	gatatcatggtgagcaagggcg
P578	gatatcgaaattgaaggaaaaaacatcatttgtg
P579	Cttcaagatccgacataacatcgaagatggcagcgtgc
P580	gcacgctgccatcttcgatgttatgtcggatcttgaag
P581	gaccaccctgacccacggcgtgcagtg
P582	cactgcacgccgtgggtcagggtggtc
P134	gagcatacaaaaatacatgcacac
p137	tgatttacttccatcattttgccc
P210	ttaacatcaccatctaattcaacaag
P267	ccggaattcatgagcacgcttttactttgtc
P882	aggagaattaaccaatgctgtatac

P208	ccggaattcatgtgttggttgtaattgagg
P268	gcaattccatatgtcctcctcctccttgtccatatcctggaagtagagaattaac
P269	aacggcgccggtggaggtggaggtggaggtggaaataaaagcatccaagcccaaag
P270	ccggatatccagaaatatttcaaaagcctacataac
P271	gcaattccatatgacctccacctccacctccacctccaccacctggctgtggttgtg
P272	aacggcgccggaggtggaggtggaggtggaggtaataacaataacaaaaataataataatgacg
P273	gcaattccatatgtccacctccacctccacctccacctgaacatttatccattttacaaatttcagtatc
P274	aacggcgccggaggtggaggtggaggtggaggtagtatatttaatattgtaagcaattcattagg
P275	cgcggatccgtattctttaattaaataaacattacgcatg
P278	cccaagcttctttatttttttattgtgaacttttcc
P279	cggggtaccatttatgtacacctttttgtgg
P576	acgggatccatttatgtacacctttttgtgg

Acknowledgment

First and most of all, I what to thank **Freddy** for convincing me that Plasmodium is the coolest parasite. You gave me more freedom I could have ever asked for (sometimes a bit to much), supported me when necessary and challenged me to work on my weaknesses. I learned from your direct intervention, from watching you work or lean back and let things develop on their own. Also thank you for proofreading; my thesis (Lets cleave an an c-terminus of accudenz) and countless other things I wrote.

Iris, for being by my side, always, and for making me improve by not asking me to do so. Also, for being my anchor to what is important in the real world. This is also true for **Paul** and **Emma**, you both shown me what matters in life. I also want to thank my parents, **Vienna** and **Otto** for raising the person I am today, for the unlimited support and the confidence in me.

The whole lab with all its members for making the time working not feel like work. **Simone** for directing my first little steps with a pipette and teaching me microscopy, **Sylvia** for starting my interest in genetics, **Catherine** and **Jessica** for the laughs. **Dennis**, **Markus**, **Johanna**, **Catherine** and **Jessica** for letting me know when I am a bit too far on thin ice. **Mendi** for the liver. **Kartik** for the joy in iceskating. **Marek** for the introduction into waterskiing. **Carmen**, **Olivia**, **Ulrike**, **Jennifer** and **Hirdesh**, for teaching me how to explain in a way that I am not the only one following. **Lucas**, for showing me when stop showing and **Johannes** for the microscopy. **Madlen**, **Julia**, **Julia**, **Noa**, **Marcel**, **Dennis**, **Ross**, **Miriam**, **Konrad** and **Léanne** for frequently or at least once joining our morning or afternoon runs. **Konrad** for actually making me run a few times. **Ben**, **Julia**, **Dennis**, **Markus** for being parents in science. **Katharina** for being the perfect office member with a perfect balance of talk and work. All those lab members and former lab members I forgot to mention. I also want to thank all the lunch outside members, who followed my lead also in sunny February, at least a few times.

All the current and former members of the department, especially **Sophia** for the time not in the lab. I want to apologize for all those questions I asked in the seminars (at least a little bit (for some)), and want to thank all students and group leaders who had questions and suggestions for my work.